



Abdul Shakoor
Kerry Cato *Editors*

IAEG/AEG Annual Meeting Proceedings, San Francisco, California, 2018— Volume 5

Geologic Hazards: Earthquakes, Land Subsidence,
Coastal Hazards, and Emergency Response



 Springer

IAEG/AEG Annual Meeting Proceedings,
San Francisco, California, 2018—Volume 5

Abdul Shakoor • Kerry Cato
Editors

IAEG/AEG Annual Meeting Proceedings, San Francisco, California, 2018—Volume 5

Geologic Hazards: Earthquakes, Land
Subsidence, Coastal Hazards, and Emergency
Response



 Springer

Editors

Abdul Shakoor
Department of Geology
Kent State University
Kent, OH, USA

Kerry Cato
Department of Geological Sciences
California State University
San Bernardino, CA, USA

ISBN 978-3-319-93135-7 ISBN 978-3-319-93136-4 (eBook)
<https://doi.org/10.1007/978-3-319-93136-4>

Library of Congress Control Number: 2018947486

© Springer Nature Switzerland AG 2019

This work is subject to copyright. All rights are reserved by the Publisher, whether the whole or part of the material is concerned, specifically the rights of translation, reprinting, reuse of illustrations, recitation, broadcasting, reproduction on microfilms or in any other physical way, and transmission or information storage and retrieval, electronic adaptation, computer software, or by similar or dissimilar methodology now known or hereafter developed.

The use of general descriptive names, registered names, trademarks, service marks, etc. in this publication does not imply, even in the absence of a specific statement, that such names are exempt from the relevant protective laws and regulations and therefore free for general use.

The publisher, the authors and the editors are safe to assume that the advice and information in this book are believed to be true and accurate at the date of publication. Neither the publisher nor the authors or the editors give a warranty, express or implied, with respect to the material contained herein or for any errors or omissions that may have been made. The publisher remains neutral with regard to jurisdictional claims in published maps and institutional affiliations.

Cover illustration: Golden Gate Bridge at night. Frederic Prochasson © 123rf.com

This Springer imprint is published by the registered company Springer Nature Switzerland AG
The registered company address is: Gewerbestrasse 11, 6330 Cham, Switzerland

Preface

The XIII IAEG Congress and 61st AEG Annual Meeting, San Francisco, USA, chose *Engineering Geology for a Sustainable World* as the theme for 2018. Based on the topical symposia and technical sessions, the proceedings are organized into six volumes and sub-categories as follows:

Volume 1: Slope Stability: Case Histories, Landslide Mapping, Emerging Technologies

Volume 2: Geotechnical and Environmental Site Characterization

Volume 3: Mining, Aggregates, Karst

Volume 4: Dams, Tunnels, Groundwater Resources, Climate Change

Volume 5: Geologic Hazards: Earthquakes, Land Subsidence, Coastal Hazards, and
Emergency Response

Volume 6: Advances in Engineering Geology: Education, Soil and Rock Properties, Modeling

Participants of this joint meeting had the option to submit either a full paper or only an abstract. The editors would like to thank the authors for their valuable contributions. One hundred eighty-six full papers were submitted for review, and 153 papers successfully completed the process. Each paper submitted for the proceedings was peer-reviewed by two reviewers. Authors revised their papers in accordance with reviewers' comments. The reviewers, from across the globe, included professional experts as well as authors of other papers. The editors greatly appreciate the help provided by reviewers. A list of reviewers follows.

The editors are also very grateful to Karen Smith and Paisley Cato for their assistance throughout the review process.

Kent, OH, USA
San Bernardino, CA, USA
2018

Abdul Shakoor
Kerry Cato

Organization

General Meeting Chairs

Sarah Kalika, Cornerstone Earth Group
Gary Luce, Resource Concepts, Inc.
Coralie Wilhite, United States Army Corps of Engineers

Field Course Chairs

Chase White, California Geological Survey
Drew Kennedy, Sage Engineers

IAEG Planning Committee Heads

Scott Burns, Portland State University
Jeffrey R. Keaton, Wood

Proceedings Editors

Abdul Shakoor, Kent State University
Kerry Cato, Cato Geoscience, Inc./California State University, San Bernardino

Editorial Assistants

Karen Smith, Kent State University
Paisley Cato, Cato Geoscience, Inc.

Short Course Chairs

E. Morley Beckman, Kleinfelder
Byron Anderson, Kleinfelder
Chrissey Villeneuve, Shannon & Wilson, Inc.

Technical Program Committee

Abdul Shakoor, Kent State University
Kerry Cato, Cato Geoscience, Inc./California State University, San Bernardino
William Godwin, Consulting Geologist
Sarah Kalika, Cornerstone Earth Group

Symposium Chairs

Robert E. Tepel, Retired Professional Geologist and Certified Engineering Geologist
Brian H. Greene, United States Army Corps of Engineers
Donald Bruce, Geosystems, L.P.
Holly Nichols, California Department of Water Resources
Keith Turner, Colorado School of Mines
Fred Baynes, Consulting Engineering Geologist
Kevin McCoy, Colorado Geological Survey

Hilary Whitney, Environmental Resources Management
Michelle Sneed, United States Geological Survey
Thomas Oommen, Michigan Technological University
Julien Waeber, AECOM
Ed Medley, Consulting Geological Engineer
Mark Bailey, Asbestos TEM Labs
Atiye Tugrul, Istanbul University, Avcilar Campus, Turkey
Lindsay Swain, Dudek
Ike Isaacson, Brierley Associates
Mike Piepenburg, Aldea Services, LLC
Bruce Hilton, Kleinfelder
Anne Rosinski, California Geological Survey
Steve Parry, Parry Engineering Geological Services
Jan Novotny, Ceska Geologicka Sluzba, Czech Republic
Xiaolei Liu, Shandong Provincial Key Laboratory of Marine Environment and Geological Engineering (Ocean University of China), China

Field Course Leaders and Contributors

William Godwin, Consulting Geologist
William McCormick, Kleinfelder
Bradley Erskine, Kleinfelder
Marina Mascorro, Langan
Frank Rollo, Rollo & Ridley
John Egan, Sage Engineers
Ken Johnson, WSP
John Wallace, Cotton, Shires and Associates, Inc.
Ryan Seelbach, Geosyntec
Tom Barry, California Department of Conservation, Division of Oil, Gas and Geothermal Resources
John Wakabayashi, Fresno State University
Greg Stock, Yosemite National Park
Janet Sowers, Fugro
Jim Lienkaemper, United States Geological Survey
Keith Kelson, United States Army Corps of Engineers
Carol Prentice, United States Geological Survey
Gordon Seitz, California Department of Conservation
Chris Madugo, Pacific Gas & Electric Company
Mike Jewett, Miller Pacific Engineers
Ray Sullivan, San Francisco State University
George Ford, Geosyntec
Wayne Akiyama, APTIM
Ryan Coe, Terracon
Kate Zeiger, AECOM
John Murphy, California State Water Resources Control Board
Jennifer Gomez, Syar Industries
Mike George, BGC Engineering
Nick Sitar, University of California, Berkeley
Peter Holland, California Geological Survey
Chris Hundemer, C2earth
Jake Hudson, Holdrege & Kull/NV5
Shane Cummings, Holdrege & Kull/NV5
Chris Hitchcock, InfraTerra
Roxanne Renedo, BSK Associates
Tim Dawson, California Department of Conservation

Margaret Doolittle, Kleinfelder
Kevin Clahan, Lettis Consultants
Donald Wells, AMEC/Foster Wheeler
Jennifer Dean, California State Water Resources Control Board
Felix Desperrier, Lettis Consultants
Karen Grove, San Francisco State University

Guest Tour Chairs

Alice Tepel
Linda Upp

Publicity Committee

Nathan Saraceno, DiGioia Gray & Associates
Courtney Johnson, Sage Engineers
Maggie Parks, Engeo

Sponsorship Chair

Courtney Johnson, Sage Engineers

Technical Session Editing

Bill Yu, Case Western Reserve University

Guidebook App

Clayton Johnson, Golder Associates
Nathan Saraceno, DiGioia Gray & Associates

Fed IGS

Jean-Louis Briaud, Texas A&M University

K-12 Teacher Workshop

Cynthia Pridmore, California Geological Survey

Special Event

E. Morley Beckman, Kleinfelder

AEG Meeting Manager

Heather Clark, Association of Environmental & Engineering Geologists

AEG Headquarters

AMR Management

List of Reviewers

David Abbott, USA
Biljana Abolmasov, Serbia
Okechukwu Aghamelu, Nigeria
M. Farooq Ahmed, Pakistan
Paolo Allasia, Italy
Priyanthi Amarasinghe, USA
Sofia Anagnostopoulou, Greece
Pedro Andrade, Portugal
Luis Bacellar, Brazil
Marco Baldo, Italy
Elizabeth Beckman, USA
Zbigniew Bednarczyk, Poland
Eduardo Bergillos Navarro, Spain
David Bieber, USA
Candan BiLen, Turkey
Andrée Blais-Stevens, Canada
Peter Bobrowsky, Canada
Nana Bolashvili, Georgia
James Borchers, USA
Anika Braun, Germany
Stephanie Briggs, USA
Luke Brouwers, United Arab Emirates
Brian Bruckno, USA
Matthias Brugger, Germany
Fintan Buggy, Ireland
Domenico Calcaterra, Italy
Michael Carpenter, USA
Kerry Cato, USA
Andrea Cevasco, Italy
Hannah Chapella, USA
Xiaoli Chen, China
Sibonakaliso Chiliza, South Africa
Jeff Coe, USA
Mike Collins, USA
Brian Conway, USA
Jasper Cook, UK
Isabela Coutinho, Brazil
John Cripps, UK
Balázs Czinder, Hungary
Ranjan Kumar Dahal, Nepal
Jerome De Graff, USA
Rachael Delaney, USA
Artem Demenev, Russia

Diego Di Martire, Italy
Matthys Dippenaar, South Africa
Angelo Doglioni, Italy
Anastasia Dorozhko, Russia
Peter Ellecosta, Germany
Selman Er, Turkey
Olga Eremina, Russia
Georg Erharder, Austria
Moises Failache, Brazil
Andrew Farrant, UK
Zhen Feng, China
Clark Fenton, New Zealand
Maria Ferentinou, South Africa
Kenneth Ferguson, USA
Isabel Fernandes, Portugal
Paz Fernandez, Spain
Mohammad Feruj Alam, Bangladesh
Phil Flentje, Australia
Yannis Fourniadis, UK
Edwin Friend, USA
Irina Galitskaya, Russia
George Gaprindashvili, Georgia
George Gardner, USA
Jesus Garrido Manrique, Spain
Eldon Gath, USA
Ben Gilson, UK
Daniele Giordan, Italy
William Godwin, USA
Robert Goldsmith, Australia
Dick Gray, USA
Brian Greene, USA
James Hamel, USA
Hans-Balder-Havenith, Belgium
Greg Hempen, USA
Egerton Hingston, South Africa
Peter Hudec, Canada
Matthew Huebner, USA
Maria Ingunza, Brazil
Upali De Silva Jayawardena, Sri Lanka
Filipe Jeremias, Portugal
Brendon Jones, South Africa
Frank Jordan, USA
Kumud Raj Kafle, Nepal
Sarah Kalika, USA
Efstratios Karantanellis, Greece
Ekaterina Karfidova, Russia
Hamza Karrad, Algeria
Heiko Käsling, Germany
Brian Katz, USA
Katerina Kavoura, Greece
Andrey Kazeev, Russia
Jeffrey Keaton, USA
Klaus-Peterkeilig, Germany
Alexey Kindler, Russia
Matheus Klein Flach, Brazil

Aliko Kokkala, Greece
Goh Thian Lai, Malaysia
Hana Lee, Austria
Nkopane Lefu, South Africa
Leticia Lescano, Argentina
Cheng Li, China
Wenping Li, China
Qian Liu, Austria
José Lollo, Brazil
Silvina Marfil, Argentina
Vassilis Marinos, Greece
Milos Marjanovic, Serbia
Kristofer Marsch, Germany
Pedro Martins, New Zealand
Flora Menezes, Germany
Amira Merchichi, Algeria
Olga Meshcheriakova, Russia
Stuart Millis, Hong Kong
Omar Mimouni, Algeria
Oleg Mironov, Russia
Matthew Morris, USA
Tim Mote, Australia
Elena Mraz, Germany
Marcos Musso, Uruguay
Masashi Nakaya, Japan
Arpita Nandi, USA
Marivaldo Dos Nascimento, Brazil
Monique Neves, Brazil
Holly Nichols, USA
Vanessa Noveletto, Brazil
Takehiro Ohta, Japan
Kazuhiro Onuma, Japan
Thomas Oommen, USA
Rolando Orense, New Zealand
Ibrahim Oyediran, Nigeria
George Papathanasiou, Greece
Steve Parry, UK
Darren Paul, Australia
Osni Jose Pejon, Brazil
Giacomo Pepe, Italy
Regina Pläskén, Germany
Lindsay Poluga, USA
Joaquim Pombo, Portugal
Martin Potten, Germany
Constantin Prins, Germany
Mário Quinta-Ferreira, Portugal
Rute Ramos, Portugal
Emanuele Raso, Italy
Liana Rocha, Brazil
Valéria Rodrigues, Brazil
Michael Rucker, USA
Nicholas Sabatakakis, Greece
Rosanna Saindon, USA
Mahin Salimi, Iran
Ligia Sampaio, Brazil

Paul Santi, USA
Regiane Sbroglia, Brazil
David Scarpato, USA
Malcolm Schaeffer, USA
William Schulz, USA
Jorge Sfragulla, Argentina
Sachin Shah, USA
Abdul Shakoor, USA
Timothy Shevlin, USA
Anna Shidlovskaya, Russia
Roy Shlemon, USA
Zachary Simpson, South Africa
Alessandra Siqueira, Brazil
Young-Suk Song, South Korea
Georg Stockinger, Germany
Alexander Strom, Russia
Wanghua Sui, China
Valentina Svalova, Russia
Debora Targa, Brazil
Ashley Tizzano, USA
Ákos Török, Hungary
Emil Tsereteli, Georgia
Ryosuke Tsuruta, Japan
Atiye Tugrul, Turkey
Alan Keith Turner, USA
Anatiliï Tushev, Ukraine
Resat Ulusay, Turkey
Isabella Magalhães Valadares, Brazil
Lazaro Valezuquette, Brazil
J. Louis Van Rooy, South Africa
Ioannis Vazaïos, Canada
Marlene Villeneuve, New Zealand
Nicholas Vlachopoulos, Canada
Yasuhiko Wakizaka, Japan
Chester (Skip) Watts, USA
Luke Weidner, USA
Baoping Wen, China
Charles Wilk, USA
Stephen Wilkinson, UK
John Williams, USA
Louis Wong, Hong Kong
Martin Woodard, USA
Richard Wooten, USA
Yang Yang, China
Katherine Yates, New Zealand
Julia Yeakley, USA
Murat Yilmaz, Turkey
Zelin Zhang, China

Contents

Part I Earthquakes

Surface Rupture Hazard Zonation: Lessons from Recent New Zealand Earthquakes	3
Clark Fenton, Natalie Hyland, and Blake Hoare	
Neotectonics of the Hollywood Fault, Central Hollywood District, Los Angeles, California, U.S.A.	13
Steven H. Kolthoff, Michael F. Mills, and Roy J. Shlemon	
Liquefaction Susceptibility Map of the Broader Thessaloniki Urban Area	21
George Papathanassiou and Vasilis Marinou	
Study of the Phenomenon of Quicksand in the Geotechnical Laboratory	27
Sebastião Geraldo Guimarães Júnior, Isabella Magalhães Valadares, Marcus Vinícius Araújo da Silva Mendes, and Jaqueline da Silva Feitosa	
Fault-Landslide Interactions: Examples from the 2016 M7.8 ‘Kaikōura’, New Zealand, Earthquake	33
Clark Fenton, Mark Gray, Natalie Hyland, and James Smith	

Part II Land Subsidence

Revealing Sinkholes of Karst-Suffosion Origin in Moscow	45
Irina Kozliakova, Aleksandr Anikeev, Olga Eremina, and Natalia Ustinova	
Addressing Subsidence in Bangkok, Thailand and Houston, Texas: Scientific Comparisons and Data-Driven Groundwater Policies for Coastal Land-Surface Subsidence	51
Aranya Fuangswasdi, Surin Worakijthamrong, and Sachin D. Shah	
Arizona Department of Water Resources Land Subsidence Monitoring Program	61
Brian D. Conway	
The Pixley Fissure Revisited—Understanding an Old Geohazard to Safeguard New Infrastructure	69
Michael L. Rucker, Kenneth C. Ferguson, and Danielle Smilovsky	
Mitigation Strategies and Engineering Solutions for Infrastructure at Risk from Earth Fissures	77
Kenneth C. Ferguson and Michael L. Rucker	

Earth Fissures and Infrastructure: A Case History at the Siphon Draw Detention Basin, Central Arizona	85
Kenneth C. Ferguson and Michael L. Rucker	
Part III Coastal Hazards	
A Coastal Susceptibility Index Assessment of KwaZulu-Natal, East Coast of South Africa	93
A. Shanganlall, M. Ferentinou, E. Karymbalis, and A. Smith	
Part IV Emergency Response	
Emergency Warning of Landslide Natural Hazard Using Nearly Real-Time Monitoring Data	103
Zbigniew Bednarczyk	
Flood Hazard Evaluation in Mزاب Valley (Ghardaia—Algeria)	113
Omar Mimouni, Amira Merchichi, Ghani Cheikh Lounis, Bachir Taleb, and El Hadi Tahalaitit	
Assessment of Landslides Triggered by Earthquakes Based on the Combination of Peak Ground Motion and Critical Acceleration Analysis	123
Chen Xiaoli and Liu Chunguo	
Rockfall Mitigation Practices in Nepal	131
Ranjan Kumar Dahal	
Internal Erosion in Volcanic Soils—Challenges for Infrastructure Projects in New Zealand	137
Pedro Martins	
Site-Specific Rockfall Risk Assessments and Rockfall Protection Structure Design Following the 2010/2011 Canterbury Earthquake Sequence	143
T. I. Mote, M. D. Skinner, M. L. Taylor, and C. Lyons	
Hazard Risk of Debris/Mud Flow Events in Georgia and Methodological Approaches for Management	153
Emil Tsereteli, George Gaprindashvili, Merab Gaprindashvili, Nana Bolashvili, and Merab Gongadze	
Disaster Risk Reduction and Land Use Planning: Opportunities to Improve Practice	161
J. Garrido and W. S. A. Saunders	
Author Index	167

Part I
Earthquakes

Surface Rupture Hazard Zonation: Lessons from Recent New Zealand Earthquakes

Clark Fenton, Natalie Hyland, and Blake Hoare

Abstract

Engineered structures crossing active faults are vulnerable to damage during surface faulting earthquakes. The design and location of mitigation measures to counteract fault rupture requires detailed knowledge of the location of the active fault traces, fault geometry, including the width of the fault zone at the surface, and the distribution of strain within the fault zone. The current understanding of fault geometry and displacement profiles is based on predominantly subsurface data through essentially isotropic ground conditions. Although empirical relationships among fault parameters, such as rupture length, earthquake magnitude and average or maximum displacement, can be used to characterize potential surface rupture hazard for an entire fault zone, the behavior of a fault at a specific location, as is required for engineering design, can be harder to forecast. For hazard planning and front-end engineering design, rupture zonation is a useful approach. To produce meaningful fault rupture zonation maps requires an integration of data on tectonic geomorphology, paleoseismology, and both crustal and near-surface fault geometry. The results of detailed surface rupture mapping, LiDAR image interpretation and shallow geophysical investigations following the 2016 Kaikōura earthquake are used to highlight some of the problems in determining potential fault rupture hazard zones. Existing zonation approaches are evaluated in light of this complex, multi-fault rupture. Rather than define narrow prescriptive

fault avoidance zones, a better approach is to develop a broader zonation that highlight areas where there is the need for detailed fault rupture mitigation studies to be performed for all significant developments.

1 Introduction

The 14th November 2016 M 7.8 Kaikōura earthquake provides a reminder of the potential dangers of surface fault ruptures. Fortunately, most ruptures occurred on farm land or sparsely populated areas causing little property damage and remarkably few casualties for an earthquake of this magnitude. The earthquake ruptured at least 17 faults for a distance of ~ 180 km across the New Zealand plate boundary zone in the northern South Island (Fig. 1). The faults that ruptured comprise two main sets that strike E-NE and NNW-NNE, both with mainly steep dips ($\geq 60^\circ$). The more northerly striking faults were mostly unknown prior to the earthquake and accommodated predominantly left-lateral reverse slip (Leader and Stone Jug faults with net slip of ≤ 4 and ≤ 1 m, respectively). The E-NE striking faults (The Humps and Conway-Charwell faults with net slip of ≤ 4 and ≤ 2 m, respectively) are parallel to the primary plate boundary structures and accommodated right-lateral to oblique reverse slip. Intersection of the main fault sets resulted in significant rupture complexity, the northeast transfer of slip, and northward propagation of the earthquake. Fault slip is dominantly oblique and accommodates regional right-lateral transpression consistent with the regional $\delta_H \sim 120^\circ$, the $\sim 260^\circ$ trending relative plate motion vector, and observed Quaternary bedrock deformation.

Like a number of recent surface rupturing earthquakes (e.g., 1992 Landers, 1999 Hector Mine, 2008 Wenchuan), the involvement of a number of fault structures, has led to a significant degree of complexity in the surface deformation zone (Figs. 1 and 2).

C. Fenton (✉) · N. Hyland · B. Hoare
Department of Geological Sciences, University of Canterbury,
Christchurch, New Zealand
e-mail: clark.fenton@canterbury.ac.nz

N. Hyland
e-mail: natalie.hyland@pg.canterbury.ac.nz

B. Hoare
e-mail: blh40@uclive.ac.nz

Fig. 1 Top: Fault rupture from the 2016 Kaikōura earthquake. Faults with both primary and secondary surface deformation shown in red. Other active faults shown in black. NCD: North Canterbury Domain; MFS: Marlborough Fault System. Bottom: Detail of the fault rupture in the epicentral region

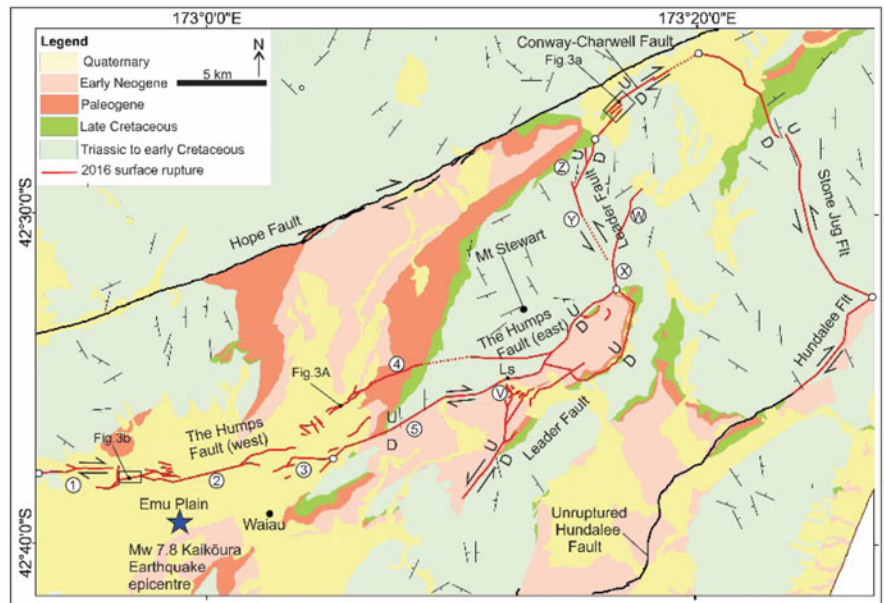
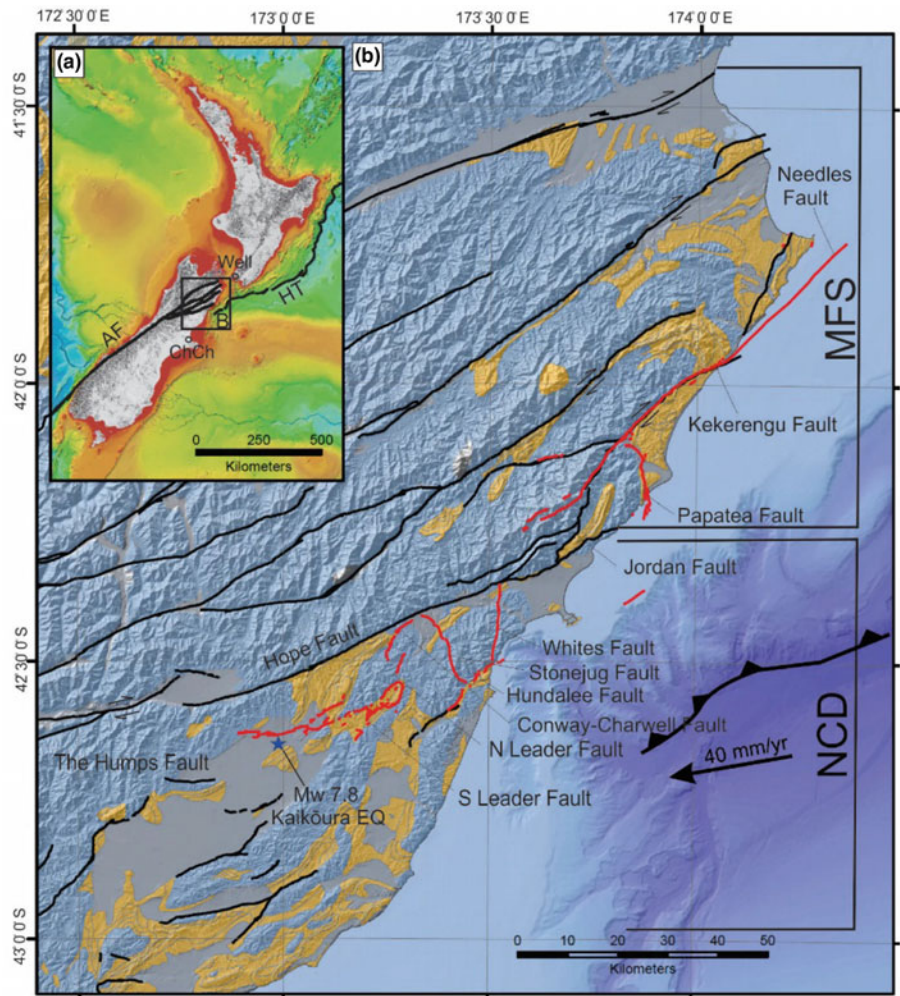
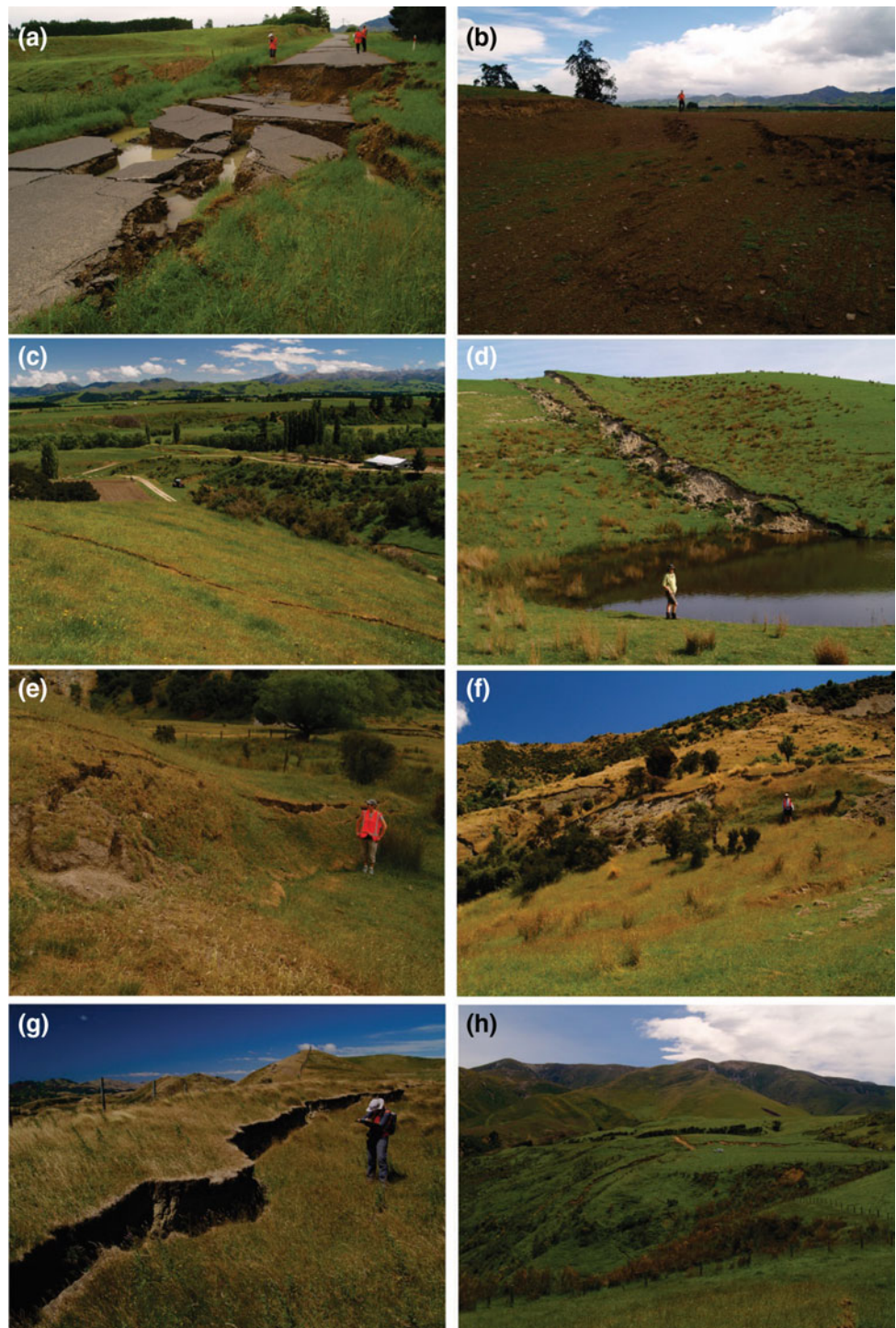


Fig. 2 Examples of differing styles of surface deformation along the Kaikōura earthquake surface rupture in the epicentral region and across the North Canterbury Domain. **a** Fault scarp enhanced by lateral spreading at Leslie Hills Road, Emu Plain. **b** Graben formed at a releasing bend at Hossack Downs. **c** Broad releasing bend at Glenbourne. **d** A normal fault scarp above a blind thrust fault, Woodchester Station. **e** Thrust fault scarp and fault bend warp with extensional cracking in the hanging wall, Woodchester Station. **f** A 4 m high warp and thrust fault scarp on Mount Stewart. **g** Secondary extensional faulting in the hanging wall of a thrust fault section, Mendip Station. **h** Right-lateral strike-slip and extensional dip-slip displacement at the western end of the Conway-Charwell fault, Conway Downs



It is not uncommon for surface faulting to occur on previously unrecognized structures (e.g., the Greendale fault in the 2010 Darfield earthquake; Villamor et al. 2012). This is often a function of low slip rates and high erosion and/or deposition rates (Fenton et al. 1999).

Blind structures can also cause significant surface deformation, akin to surface rupture, even without primary rupture/surface rupture of the causative structure (e.g., the

1980 El Asnam earthquake). This is displayed spectacularly along the South Leader section of the Kaikōura surface rupture. Here the 3.5 m high Waiiau Wall represents secondary normal dip-slip deformation in the hanging wall of a blind, west-dipping reverse fault (Fig. 2d).

Better post event investigative techniques, especially LiDAR, allows greater resolution of surface deformation and faster data acquisition, allowing even minor fault details to

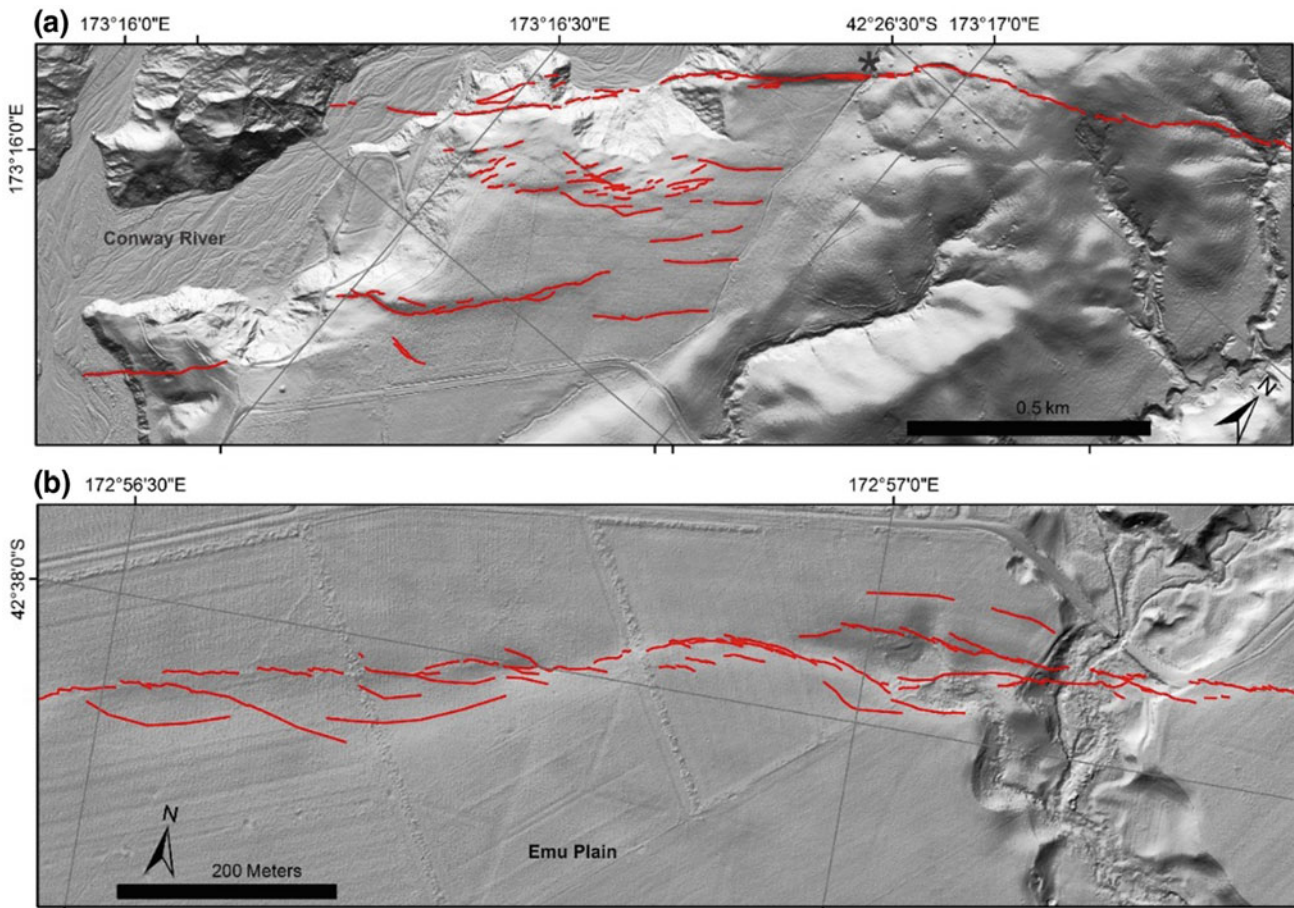


Fig. 3 Post event LiDAR imagery showing fault complexity at Conway Downs (Top) and Emu Plain (Bottom). See Fig. 1 for locations. Both locations show the fault complexity encountered at fault bends and step

be captured before they are obscured by other surface processes (Fig. 3). Differential LiDAR, InSAR, improved seismotectonic models, and high precision earthquake location allow the rapid development of a detailed regional seismotectonic framework within which predictive models of fault propagation and rupture style can direct field-based investigation. As part of field investigations, the introduction of high precision hand-held geodesy (RTK) allows the rapid determination of detailed strain profiles across complex fault rupture zones (Fig. 3). The combination of better investigative techniques and rapid post-earthquake field deployment affords us a much more detailed picture of surface faulting than was previously possible.

2 Existing Approaches to Fault Zonation

In New Zealand, current hazard mitigation efforts require a fault avoidance zone (FAZ) to be established within which new construction is regulated (Kerr et al. 2003). The FAZ is delineated using a 20 m setback distance from a recognized

over zones. The red lines show the fault traces mapped in the field. At Conway Downs the LiDAR image clearly shows other geomorphologically-recent fault traces that were not involved in the 2016 surface rupture

active fault or fault zone. In contrast California's Alquist-Priolo Earthquake Fault Zoning Act (AP Act) requires an earthquake fault zone (EFZ) up to 400 m wide to be established around a potentially hazardous fault. Within the EFZ subsurface investigation is required at each new development site to determine if the site is underlain by an active fault (one which shows evidence of Holocene displacement along a portion of its length). Structures for human occupancy are prohibited from being placed across an active fault and, unless the trench proves otherwise, a 15 m (50 foot) setback distance is enforced around the active fault based on the assumption that active branches are present within this distance (Bryant 2010). Trench investigations are not required outside an EFZ, making it possible for a structure to be placed over or near an active fault if the fault lies outside of an established EFZ. The limitations of this approach were highlighted by the 1992 Landers Earthquake, in which 45% of surface ruptures occurred outside EFZs (Hart et al. 1993).

New Zealand's Ministry for the Environment (ME) Guidelines define three parameters which can be used to take

a risk based approach to hazard assessment—fault recurrence interval, fault complexity, and building importance. Each parameter is divided into several classes. This allows buildings of a low importance class (e.g., farm buildings) to be placed adjacent to faults of a shorter return interval, while prohibiting critical infrastructure, such as hospitals, from being placed adjacent to the same fault. Unlike the AP Act, the avoidance zone (usually 20 m) is established in advance and no further investigation is required.

Little evidence is cited by either the AP Act or ME Guidelines in support of their stated setback distances. Two questions must therefore be addressed. Is this distance adequate to avoid all surface deformation? Can the width of the deformation zone (WDZ) around a surface fault rupture be anticipated accurately? If so, setback distances and EFZs can be designed to be more or less conservative as required, thus reducing the risk of ground deformations occurring outside of established avoidance zones.

The AP Act and ME Guidelines only require active faults to be zoned. The AP Act considers a fault active if it displays evidence of Holocene displacement. The ME Guidelines define six fault classes based on recurrence intervals ranging from <2000 years to $\leq 125,000$ years. This raises several further questions. What is the most appropriate definition of an active fault considering the tectonic setting of New Zealand? How best to assess the activity of a fault given an imperfect geologic record? How best to identify and define a fault in the first place? Should a minor fault with a few centimeters of offset be treated the same as one with several meters of offset?

By not allowing any hazard mitigation measures other than avoidance, the AP Act and ME Guidelines potentially limit the amount of land available for development. Allowing engineering mitigation of minor faults on which there is little displacement or of broad shear zones where discrete ruptures are not expected may be economically beneficial.

3 Geological Controls on Surface Rupture

Ideally FAZs should be established using measurable geological criteria to predict the width of the deformation zone surrounding surface fault ruptures, rather than using a pre-determined setback distance. There are six principal factors controlling the general characteristics and rupture path of surface faulting: (1) sense of fault movement (dip-slip or strike-slip); (2) geometry of the fault plane; (3) amount of fault displacement; (4) depth of overlying earth materials; (5) nature of overlying earth materials; (6) definition of the fault (recently developed or established). The effects of these factors are described herein to better understand the nature of surface faulting, aid our ability to

predict the distribution of surface deformations, and assess the appropriateness of hazard zoning. The majority of surface fault offset is typically accommodated on a central rupture zone in the order of one to tens of meters width, with secondary off-fault deformations spanning hundreds of meters to over a kilometer. Distributed, off fault deformation may account for a significant portion of the total displacement. Fault ruptures are diverse in nature and may exhibit discrete offsets on fractures or scarps, complex *en echelon* arrays, or broad, distributed shear zones.

3.1 Fault Geometry

Fault geometry is a fundamental factor in controlling surface fault rupture morphology. Each principle fault type (strike-slip, normal, and reverse) creates a different surface expression which needs to be recognized in order to establish effective FAZs.

There is a positive correlation between structural complexity and the magnitude and width of off-fault deformation (Boncio et al. 2012). In the 1992 Landers earthquake, off-fault displacement commonly reached over several hundred meters in step overs, kinks and fault bends (Milliner et al. 2015). Similar behavior is observed in the Kaikōura rupture. The greatest displacements occurred on structurally simple single-stranded sections of the fault. Slip on individual faults decreased in complex zones, as the total displacement was spread over multiple structures. Therefore it would be wise to employ very conservative FAZs around geometric complexities such as step overs where the surface damage zone is observed to broaden markedly.

Analysis of earthquakes worldwide shows ruptures do not propagate through step overs or discontinuities >3–4 km and below this distance ruptures are arrested only 40% of the time (Wesnousky 2008). Furthermore, earthquakes in which fault slip decreases abruptly towards a step over commonly re-nucleate on adjacent segments (Elliot et al. 2009). Thus, it may be prudent to consider faults that are within <3–4 km of active fault on which displacement decreases abruptly to be zoned as active.

3.2 Damage Zone

In many faults the damage zone is asymmetric. The hanging wall of dip-slip faults usually experience a wider and more severe deformation zone than the foot wall. Following the 2008 Wenchuan, China earthquake, authorities introduced an asymmetric FAZ around the causative fault which was three times wider on the hanging wall than the foot wall (Yongshuang et al. 2013). Reverse faults typically show less offset at the surface than normal faults of similar

displacement in comparable near-surface materials. In addition, surface offset increases with dip (Lade et al. 1984). A shallower dipping fault generally produces a wider rupture zone (Fenton 2001).

3.3 Near-Surface Material

Thick deposits of loose soil (e.g., alluvium) produce wide deformation zones, either as warping, broad *en echelon* arrays or multiple fault strands. In such materials, new surface ruptures may manifest over a wide zone as high angle (with respect to the orientation of the primary fault zone) *en echelon* fractures, whereas low angle fractures are older and more proximal to the pre-existing basement fault (Lin and Nishikawa 2011). Where surface materials indicate a very broad deformation zone should be expected there are two options; (1) expand the FAZ to encompass all distributed deformation (potentially hundreds of meters); or (2) allow the introduction of engineered mitigation of minor distributed deformations at a certain distance beyond the primary rupture zone.

3.4 Fault Maturity

Fault zones evolve towards geometric simplicity with cumulative slip. Riedel (R) shears form during the initial stages of fault development when resistance to shear is greatest. This behavior was observed in the Darfield earthquake when the Greendale fault ruptured after period of 20–30,000 years (Hornblow 2016). The fault rupture propagated through a significant thickness of undeformed coarse fluvial gravels. Although the rupture formed a continuous 40 km long zone of deformation, rather than forming a major through-going rupture, much of the displacement was accommodated across a broad zone of Riedel shears. As the fault zone matures movement on the R shears ceases and central principal displacement shears develop aligned to the general direction of fault movement (Tchalenko 1970). Strain is localized throughout this process and the zone of active deformation gradually simplifies and narrows such that the older peripheral faults become inactive. Structurally immature faults may manifest ~50–60% of total slip on narrow fault traces whereas structurally mature faults manifest ~85–95% (Dolan and Haravitch 2014). The missing slip is accounted for by aseismic creep or distributed off-fault deformation. Borchardt (2010) demonstrated that after 30 fault ruptures, the likelihood of a new rupture developing in a soil that shows no evidence of prior ruptures

is negligible. Evidence also suggests that faults in a low-strain setting with long recurrence intervals are prone to complex geometries.

Having an appreciation of the structural maturity of a fault gives an indication of how much off-fault deformation to expect and informs the construction of a displacement-distribution curve. The youngest faults in a fault zone should be identified as these are the most likely to be active and rupture in the future; more distal faults may be inactive.

The general location of surface ruptures is controlled in tectonically active regions by pre-existing fault zones that have either experienced surface faulting in the late Pleistocene or Holocene or are undergoing active creep (Lin and Nishikawa 2011; Fenton and Kernohan 2015). Thus, in a general sense, surface ruptures can be expected where they have been observed historically, or for where there is geomorphological evidence of prehistoric ruptures. However, this does not stop a long recurrence interval fault for which there is no existing geomorphic evidence from rupturing to the surface (e.g., the 2010 Greendale fault rupture).

The geological controls on surface rupture morphology described above suggest surface fault ruptures within New Zealand are likely to generate wide, complex patterns of ground deformation. This is because; (1) many faults are structurally complex with oblique strike-slip movements; (2) fault may be covered by loose, uncemented alluvial sediments hundreds of meters thick, moraine, till, fan deposits, or landslide debris; (3) faults may not rupture with characteristic behavior and have not matured into narrow, linear traces. While primary ruptures can be expected on identifiable pre-existing fault traces, secondary ground deformations for which there is no historic evidence may occur hundreds of meters away. For this reason, applying a 20 m setback distance around the central rupture zone of a fault is not likely to capture the full extent of deformation.

4 Creating a Predictive Model of Slip Distribution

The geologic controls on surface rupture and observations from historic events help us to predict the shape of the deformation-distribution curve for an active fault (Fenton and Kernohan 2015). This should form the basis on which FAZs are established. A fault displacement curve can be used by land-use planners and engineers to completely avoid surface ruptures, allow buildings of lesser or greater importance closer or farther from a fault zone, respectively, or design structures to withstand the expected amount of ground deformation or strain at a particular location.

5 Key Inputs for a Surface Fault Hazard Investigation

Any surface fault hazard investigation must begin with the identification and characterization of active faults. Standard geologic maps (Q Map in New Zealand) at scales of 1:250,000 are not adequate for site-specific fault location. Only primary fault traces are marked with no indication of the deformation zone width. When enlarged to the scale required by land planners (<1:10,000), faults are inaccurately portrayed and liable to misinterpretation (ME Guidelines, 2003). Large scale (<1:10,000) geomorphologic mapping must be conducted. Several remote sensing technologies may be employed including LiDAR and aerial and satellite photography as well as field mapping.

LiDAR surveys are particularly advantageous in that they can generate bare-earth topography (Fig. 3). This removes the obscuring effects of vegetation and allows the ground below heavily vegetated areas to be imaged. The effects of erosion and local environmental factors should also be recognized. Decades of agriculture are likely to diminish subtle geomorphic indicators of surface faulting. Assessment of the length of a fault beyond that which is observable is justified for faults which are thousands of years old, as the true length of the fault is unlikely to be preserved (Villamor et al. 2012).

Trench investigations are a valuable component of fault hazard studies and should be used to assess the displacement and recurrence interval of fault ruptures. However, the limitations of trenching must be recognized to avoid misinterpretation, and trenches sited in the wrong place or of

inadequate length or depth will be of little value. Bonilla and Lienkaemper (1991) found that in 45% of trenches faults appear to die-out upwards and in 30% of trenches faults appear to die-out downwards where other data showed that surface displacement had occurred. Failure to recognize that fault strands often die-out for reasons other than being covered by younger deposits may lead to an underestimation of fault activity (Bonilla and Lienkaemper 1991). The use of geophysical techniques can be extremely useful in fault zone determination (Fig. 4). Site-specific limitations, such as soil type and the presence of groundwater can limit the resolution and depth of penetration.

The spatial and temporal variation in the behavior of a fault is hard to assess from the single observation point provided by a trench. Care must be taken that the amount of displacement measured in a trench is characteristic of the entire fault. In 1979 there was a small earthquake swarm on two of the faults that ruptured in the 1992 Landers earthquake (Treiman 2010). The 1979 event generated 0.1 m of slip, yet in 1992 the same area experienced 1–2 m displacement. If a trench were dug in 1980, it may have shown a few centimeters of displacement from the 1979 event, but it may not have been possible to characterize the 1992 event beforehand (Treiman 2010). Broad shear zones and warping are also unlikely to be appreciated in trench investigations. Wells and Coppersmith (1994) found that for a single event, the average displacement on a fault is half of the maximum displacement. Empirical regressions may assist the estimation of fault rupture parameters that are hard to ascertain by field investigation.

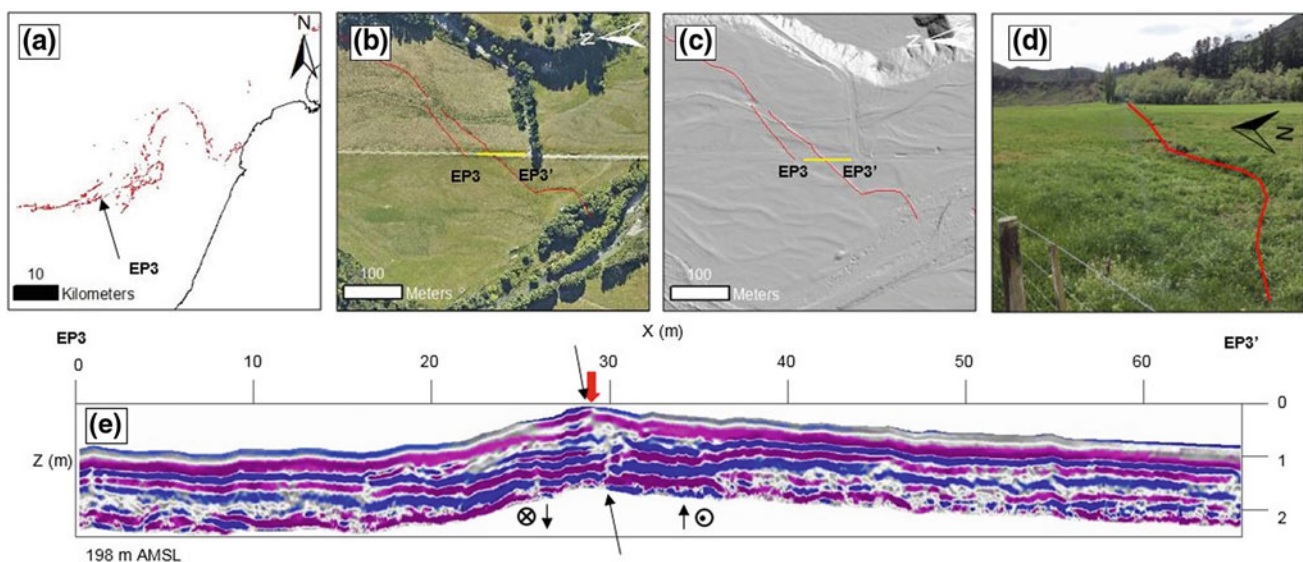


Fig. 4 A GPR profile across a 2016 Kaikōura thrust trace at Glenbourne. The near-surface materials are alluvial sands and gravels. Shallow groundwater and/or the presence of fines has reduced the depth of penetration to 1.5 m. **a** Location of Glenbourne GPR profile.

b Vertical aerial photograph of GPR profile site. Red lines show 2016 surface rupture traces. **c** LiDAR image of the GPR profile site. **d** Field photo showing the low reverse fault scarp at Glenbourne

Trenches should extend well beyond the full length of a proposed development. While there may be no evidence for faulting beneath a site, the area may be subject to secondary deformations if a large fault is discovered beyond the site. This may be hard to justify in an area of no known active faults or where there is no geomorphic evidence of faulting, however there are several cases of unknown faults rupturing (e.g. China 2008, Darfield 2010, Kaikōura 2016) which could have been recognized prior in a trench.

It is worth considering the most appropriate definition of an active fault. The six classes defined by the ME Guidelines require rupture intervals to be dated to an accuracy of up to 1500 years; a difficult task given an imperfect geological record and inaccuracies in dating. A simpler approach would be to define fault activity based on evidence for Holocene, Late Quaternary or Quaternary displacements.

6 Suggestions for Best Practice

Surface fault ruptures are often complex and appear unpredictable. While surface ruptures have occurred on unrecognized faults, there are often subtle, pre-existing geomorphic traces and evidence for prehistoric ruptures in trenches that are only recognized post-event. A 20 m setback distance may not always be an adequate. Secondary deformations should be expected to span up to hundreds of meters from the central rupture zone. An understanding of the geologic factors that control the style, location, and distribution of surface ruptures allows us to establish wider avoidance zones where necessary. Advances in LiDAR surveys and high resolution aerial photography aid the identification of active fault traces. The response of structures to historic ruptures provides guidance on how to construct surface rupture resistant buildings. This information can be used to establish robust mitigation measures.

New Zealand has a relatively low population density and a large number of active faults. It would be impractical and unnecessary to establish a non-arbitrary avoidance zone for every fault; to do so properly would require extensive geomorphic mapping, detailed trench investigations, all requiring significant capital expenditure. Major active faults in proximity to urban environments are likely to see ongoing civil engineering developments. These faults warrant investigation and the establishment of wide avoidance zones. This approach would be similar to the AP Act, which requires maps to be published showing potentially hazardous EFZs. The onus would then be on a developer to prove the lack of surface rupture hazard by carrying out the appropriate geological investigations. However, unrecognized faults have ruptured outside of EFZs, so for all critical infrastructure (e.g. hospitals, power stations), even that sited away from known active faults, some specified minimum

level of fault investigation would be prudent. For known inland faults away from major urban areas, some minimum level of engineering mitigation within a certain distance (e.g., 1 km) from known active faults would protect life-safety without the need for detailed fault investigations. The current ME Guidelines define narrow fault recurrence intervals that depend on faults having developed characteristic rupture cycles and our ability to date ruptures accurately. How sure can we be that a fault of recurrence interval 2000–3500 years is more likely to rupture than a fault of 3500–5000 years when inaccuracies in dating and an imperfect geologic record are considered? Can we be sure enough to determine the type of building that should be allowed and the potential risk to life we are willing to assume? It may be simpler to simply class faults as Holocene-active or Late Pleistocene-active.

References

- Boncio, P., Galli, P., Naso, G., Pizzi, A.: Zoning surface rupture hazard along normal faults: insight from the 2009 Mw 6.3 L'Aquila, Central Italy, earthquake and other global earthquakes. *Bull. Seismol. Soc. Am.* **102**(3), 918–935 (2012). <https://doi.org/10.1785/0120100301>
- Bonilla, M.G., Lienkaemper, J.J.: Factors affecting the recognition of faults exposed in exploratory trenches. *Bulletin Rep.* 1947, 54 p. USGS (1991)
- Borchardt, D.: Establishing appropriate setback widths for active faults. *Environ. Eng. Geosci.* **16**(1), 47–53 (2010)
- Bryant, W.A.: History of the Alquist-Priolo Earthquake Fault Zoning Act, California, USA. *Environ. Eng. Geosci.* **16**(1), 7–18 (2010)
- Dolan, J.F., Haravitch, B.D.: How well do surface slip measurements track slip at depth in large strike-slip earthquakes? The importance of fault structural maturity in controlling on-fault slip versus off-fault surface deformation. *Earth Planet. Sci. Lett.* **388**, 38–47 (2014)
- Fenton, C., & Kernohan, J.: Characterisation of surface fault rupture for civil engineering design. In: 6th International Conference on Earthquake Geotechnical Engineering, pp. 1–7. 6th International Conference on Earthquake Geotechnical Engineering, Christchurch (2015)
- Fenton, C.H.: Quantifying surface faulting hazards for lifelines crossing active faults. In: 12th European Conference on Earthquake Engineering, Paper Reference 714, pp. 1–9. Elsevier Science Ltd. (2001)
- Fenton, C.H., Charusiri, P., Hinthong, C.: Low slip rates versus high erosion rates: recognition and characterization of active faults in a tropical environment. *Seismol. Res. Lett.* **70**(2), 266 (1999)
- Hart, E.W., Bryant, W.A., Treiman, J.A.: Surface faulting associated with the June 1992 Landers earthquake, California. *Calif. Geol.* **46**(1), 10–16 (1993)
- Hornblow, S.: Paleoseismicity and rupture characteristics of the greendale fault and formation of the canterbury plains. Unpublished Ph.D. thesis, University of Canterbury, 161 p (2016)
- Kerr, J., Nathan, S., Van Dissen, R., Webb, P., Brunson, D., King, A. (2003). Planning for development of land on or close to active faults: a guideline to assist resource management planners in New Zealand. Client report 2002/124 Rep., 67 p, Institute of Geological & Nuclear Sciences
- Lade, P.V., Cole, D.A., Cummings, D.: Multiple failure surfaces over dip-slip faults. *Geotech. Eng.* **110**(5), 616–627 (1984)

- Lin, A., Nishikawa, M.: Riedel shear structures in the co-seismic surface rupture zone produced by the 2001 M 7.8 Kunlun earthquake, northern Tibetan Plateau. *J. Struct. Geol.* **33**, 1302–1311 (2011). <https://doi.org/10.1016/j.jsg.2011.07.003>
- Milliner, C.W., Dolan, J.F., Hollingsworth, J., Leprince, S., Ayoub, F., Sammis, C.G.: Quantifying near-field and off-fault deformation patterns of the 1992 M 7.3 Landers earthquake. *Geochem. Geophys. Geosyst.* **16**, 1577–1598 (2015). <https://doi.org/10.1002/2014GC005693>
- Tchalenko, J.S.: Similarities between shear zones of different magnitude. *Geol. Soc. Am. Bull.* **81**, 1625–1640 (1970)
- Treiman, J.A.: Fault rupture and surface deformation: defining the hazard. *Environ. Eng. Geosci.* **16**(1), 19–30 (2010)
- Villamor, P., Litchfield, N., Barrell, D., Van Dissen, R., Hornblow, S., Quigley, M., Levick, S., Ries, W., Duffy, B., Begg, J., Townsend, D.: Map of the 2010 Greendale Fault surface rupture, Canterbury, New Zealand: application to land use planning. *NZ J. Geol. Geophys.* **55**(3), 223–230 (2012). <https://doi.org/10.1080/00288306.2012.680473>
- Wells, D.L., Coppersmith, K.J.: New empirical relationships among magnitude, rupture length, rupture width, rupture area, and surface displacement. *Bull. Seismol. Soc. Am.* **84**(4), 974–1002 (1994)
- Wesnousky, S.G.: Displacement and geometrical characteristics of earthquake surface ruptures: issues and implications for seismic-hazard analysis and the process of earthquake rupture. *Bull. Seismol. Soc. Am.* **98**(4), 1609–1632 (2008). <https://doi.org/10.1785/0120070111>
- Yongshuang, Z., Jusong, S., Ping, S., Weimin, Y., Xin, Y., Chunshan, Z., Tanyu, X.: Surface ruptures induced by the Wenchuan earthquake: their influence widths and safety distances for construction sites. *Eng. Geol.* **166**, 245–254 (2013)

Neotectonics of the Hollywood Fault, Central Hollywood District, Los Angeles, California, U.S.A.

Steven H. Kolthoff, Michael F. Mills, and Roy J. Shlemon

Abstract

We present new data and analyses indicating that the inferred “active” Hollywood Fault is not mainly left-lateral, strike slip, as previously postulated, but rather, as now shown for the Central Hollywood District of Los Angeles, is driven mainly by crustal shortening indicated by uplift of the adjacent Santa Monica Mountains, by presence of the Hollywood Syncline and by the asymmetric (south verging), newly discovered “Yucca Street Anticline.” This crustal shortening follows a regional structural fabric developing since at least Miocene time. Evidence stems from interpretation of historic earthquake moment-tensor solutions, from regional GPS plate velocity data, and from new, site-specific engineering-geological trench exposures and related subsurface investigations. The California Geological Survey (CGS) concluded that the Hollywood Fault is “active” (surface or near-surface displacement within about the late 11,500 years). Likewise, adopted by City of Los Angeles regulations, the inferred active fault mandated site-specific, neotectonic and paleoseismic investigations for proposed construction of several sub-adjacent high-rise tower buildings. Based on exposures in approximately ~213 m long and up to 10 m deep trenches, on advancement and interpretation of 100+ cone penetrometer tests (CPT), and on excavation and collection of over 304 m of continuous cores, we conclude that—at least in the Central Hollywood area—the presumed Hollywood Fault is not an active, mainly strike-slip fault but rather is structurally expressed by several near-surface folds

indicative of compression normal to the inferred trace. Inherently, therefore, any assumed “active” Hollywood Fault in the Central Hollywood area of Los Angeles may trend outside the study area, may have slip taken up in contemporary folding, or—though less likely—be obscured by thick wedges of Holocene alluvium.

Keywords

Hollywood fault • Neotectonics • Paleoseismology

1 Introduction

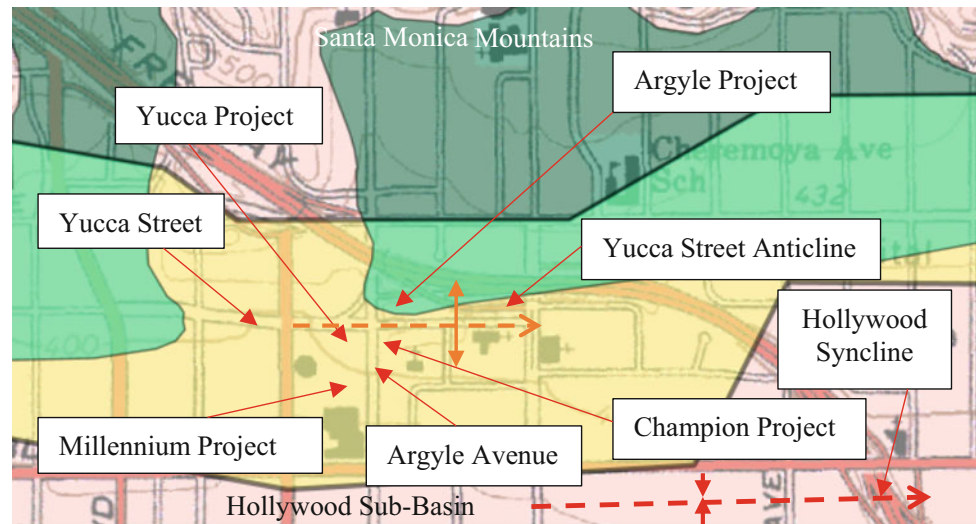
The Hollywood Fault is a much-discussed and controversial geologic feature at the southern boundary of the Eastern Santa Monica Mountains. The California Geological Survey (CGS), after compiling published data, aerial photographic interpretations and field reports, judged that the Hollywood Fault is a fault rupture hazard. Accordingly, the CGS established an “active fault zone” for much of the Hollywood Fault. The Los Angeles Department of Building and Safety then restricts development within the Zone until a paleoseismic evaluation is performed. As engineering geologists and paleoseismologist consultants to Group Delta Consultants, Inc. (Torrance, California), we evaluated four sites near the area of the intersection of Yucca Street and Argyle Avenue in the Hollywood District, Los Angeles to verify the location of the Hollywood Fault and to determine if the Hollywood Fault ruptured during the Holocene (Fig. 1). We found that the inferred “active” Hollywood Fault did not exist, but rather coincided with several discontinuous, older normal faults on the crest of an anticline. The senior author initially proposed that evolution of the Hollywood Fault and the eastern Santa Monica Mountains was not caused by Quaternary rotation with strike-slip faulting, but rather by crustal shortening. We now present regional and site-specific data supporting this hypothesis.

S. H. Kolthoff (✉)
SK Geological, Inc., San Pedro, CA, USA
e-mail: stevenk.skgeo@gmail.com

M. F. Mills
Peninsula Geologic, Inc., Torrance, CA, USA
e-mail: peninsula.mfm@gmail.com

R. J. Shlemon
Roy J. Shlemon and Associates, Newport Beach, CA, USA
e-mail: rshlemon@jps.net

Fig. 1 Earthquake zones of required investigation map (CGS 2014a) and project location map. Dark green—liquefaction hazard zones, yellow—earthquake fault zone, light green—overlap of earthquake zone and liquefaction hazard zone. The Yucca Street Anticline and Hollywood Syncline are approximate locations added to this figure



The Hollywood Fault has been postulated as having mainly left-lateral strike-slip movement with a reverse component produced by detachment of the Transverse Ranges from the southern Peninsular Ranges (Dolan et al. 1997). Ostensibly, strike-slip movement associated with the San Andreas Fault and between the Pacific and North American Plates was, and continues to be, the main driver of Los Angeles Basin tectonics. Past studies suggested that the Transverse Ranges rotated with the southern boundary movement taken up by sinistral-slip on the Hollywood fault system. This apparently continues only throughout the Holocene (Dolan et al. 1997).

In contrast, alternative models by geologists who have mapped thrust belts throughout the world indicated that the modern Southern California Transverse Ranges are actually thickening from crustal shortening, resulting in deep-seated thrusting and not strike-slip faulting (Namson and Davis 1988; Davis and Namson 1994). Our recent site-specific investigations in the Central Hollywood area now support the “deep-seated thrusting” model.

We now describe the general tectonics of the Eastern Santa Monica Mountains, Hollywood Sub-Basin and shallow geologic structures based on published data. We also provide new data stemming from paleoseismic exploration in the Yucca Street and Argyle Avenue areas (Fig. 1) showing that, throughout the Quaternary, the Hollywood Fault has been typified mainly by reverse rather than by left-lateral strike-slip offset.

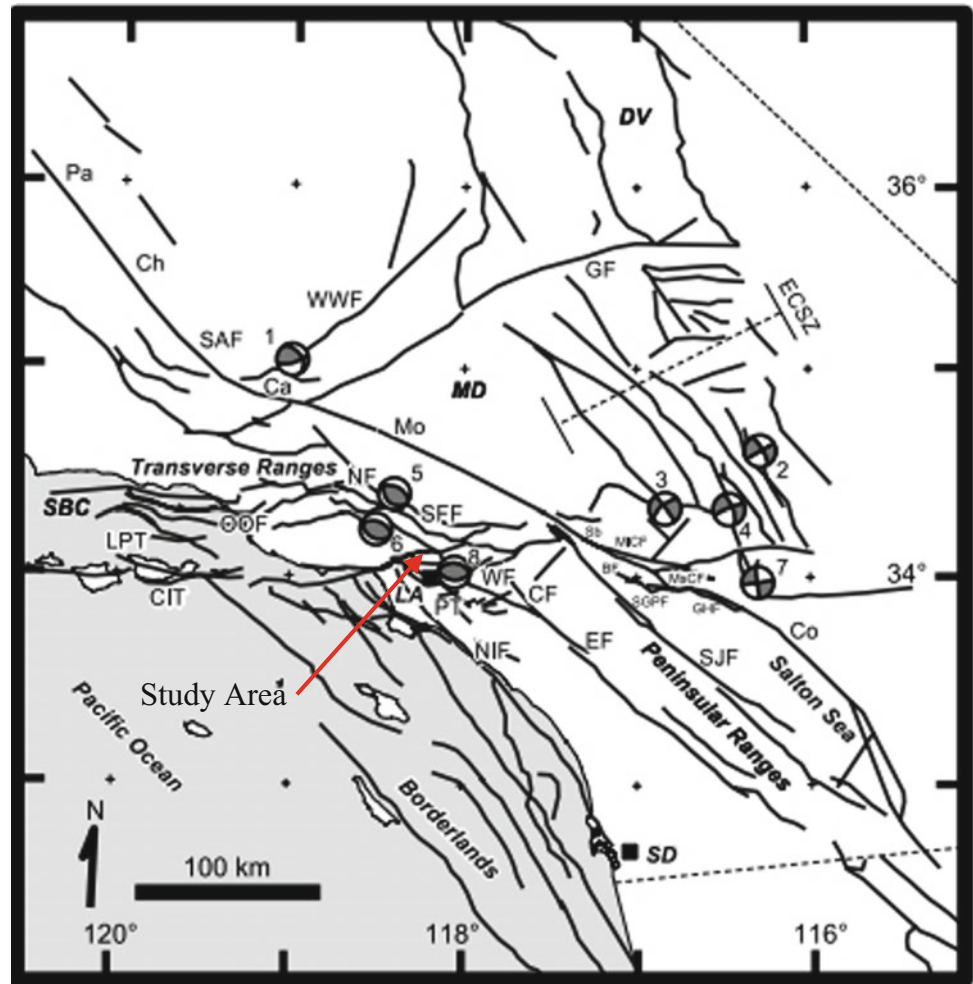
2 Tectonics of the Santa Monica Mountains, Transverse Range, Geomorphic Province of California

Between 12 and 6 Ma, the Transverse Range, Geomorphic Province of the Santa Monica Mountains, was part of the northern Peninsular Ranges. Ingersoll and Rumelhart (1999) proposed that the Los Angeles Basin went through a three-stage tectonic evolution. Initially, the Transverse Ranges rotated in a clockwise direction detaching off the Peninsular Range. During these pre-6 Ma tectonic events, the Los Angeles Basin underwent lateral translation (extension) with normal faulting and extensional basins dominating the main structures. Sub-basins and elevated (sub-marine) ridges developed where most marine Miocene sediments accumulated. Today, these marine, Miocene basin sediments deposited are inverted as outcrops in the east-west trending Santa Monica Mountains and below Quaternary sediments bordering the Santa Monica Mountains and filling the Los Angeles Basin.

The modern geologic structures of the Los Angeles Basin are still influenced by crustal shortening that started approximately 2–3 Ma, giving rise to the seismically active folding and thrust faulting documented by reverse-fault earthquakes during the last forty years (Davis and Namson 1994, 1989; Namson and Davis 1988; Plesch et al. 2007) (Fig. 2).

During strike-slip faulting, double-plunge folds, shear fractures, extension fractures and thrust faults occur as

Fig. 2 Regional fault map (after Plesch et al. 2007). The abbreviations are names of faults used in the referenced paper. Numbers for Moment Tensor Solutions refer to Plesch et al. earthquakes; bold abbreviations are specific geographic locations. The fault names and earthquake references are omitted. Earthquake solutions in the Transverse Range (Santa Monica Mountains) illustrate that the principal movement of faulting during historical earthquakes is reverse



en-echelon and oblique to the strike-slip fault zones (Sylvester 1988) not parallel or sub-parallel to the fault zone. The velocity vectors from Southern California Integrated GPS Stations (SCGIN) (Science Spotlight) show that the tectonic plate movements are perpendicular to sub-perpendicular to the Santa Monica Mountain front and the Hollywood Sub-Basin (Fig. 3). East-west normal faulting, formed by lateral translation of the Los Angeles Basin, ceased by late Miocene time.

2.1 Neotectonics of the Hollywood Area

During the Miocene, the Hollywood Fault formed the general boundary separating the Los Angeles Basin (Hollywood Sub-Basin) from the Santa Monica Mountains. The Transverse Ranges' clockwise rotation positioned the Santa Monica Mountains perpendicular to the plate movement and the extensional faulting in the Los Angeles Basin ceased about 6 Ma ago (Ingersoll and Rumelhart 1999).

By the start of the Quaternary, crustal shortening began in the Transverse Ranges and the Los Angeles Basin, but any

surface expressions of Miocene compressional folding, local thrust faults and the normal-fault tectonics would have been generally buried by continued region-wide alluviation. Major topographic relief probably characterized south-trending canyons that incised the alluvial wedge(s) exposing the pre-Miocene rocks in the Eastern Santa Monica Mountains. The canyons were then likely filled, exhumed and refilled during Quaternary climatic changes.

From the regional tectonic evolution and from our site-specific investigations, we therefore conclude that the likely surface trace of the Hollywood Fault is not along today's bedrock/alluvium contact (Dibblee and Ehrenspeck 1991) but is buried under alluvium to the south. We now propose that the Hollywood Fault, as previously mapped by Dibblee and Ehrenspeck (1991) in the Los Feliz area east of Hollywood, crosses the alluvial basin in the Central Hollywood area and then reconnects with the previously mapped Hollywood Fault in the West Hollywood area (west of Hollywood). This projection of the Hollywood Fault shows the likely location of the Miocene through Holocene Hollywood Fault in the Central Hollywood area, now inferred to trend immediately north of the Yucca Street Anticline (Fig. 4).

Fig. 3 Map of southern California showing permanent GPS stations (after Science Spotlight (undated))

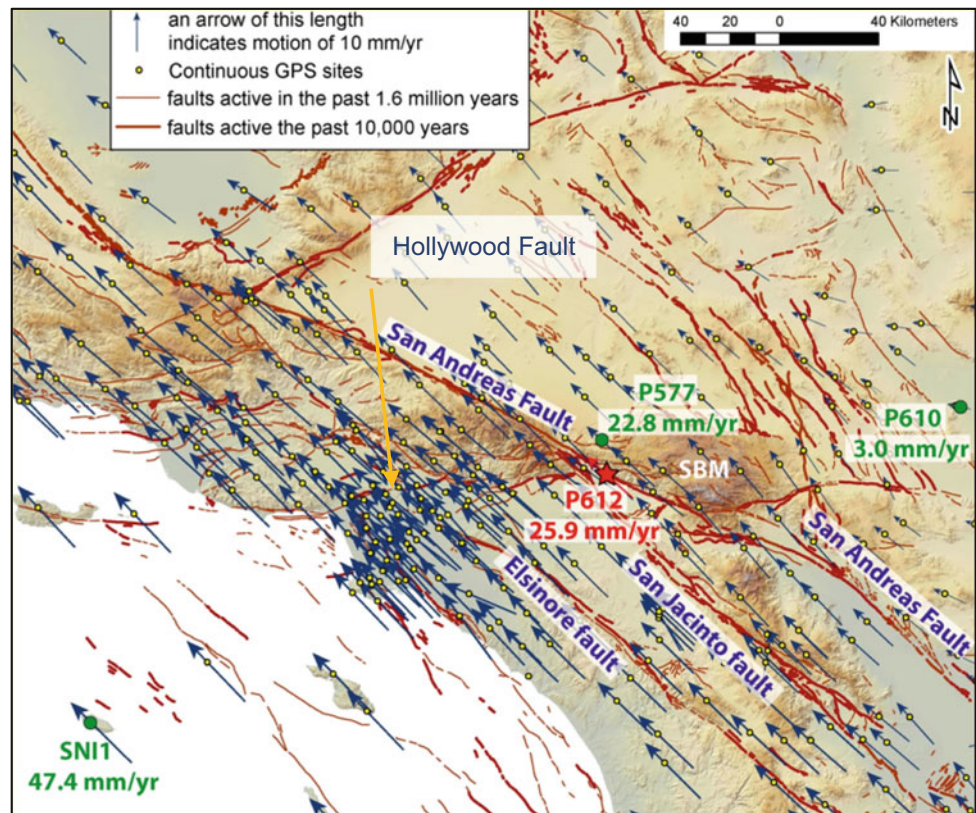


Fig. 4 Suggested trend of the Hollywood Fault following regional geomorphic features and perpendicular to the direction of crustal shortening



2.2 Strike-Slip Versus Compressional Tectonics

Specific structural and geomorphic features characteristic of southern California strike-slip faults have been well documented by Ammon (2001), Sylvester (1988) and Anderson and Nourse (2005). We specifically sought to find such strike-slip indicators in the trenches and deep cores examined during our site-specific paleoseismic investigations, but none were found.

Our inferred Hollywood Fault (Fig. 4) is perpendicular to the direction of the crustal shortening of the Santa Monica

Mountains. The Hollywood Fault mapped by Dibblee and Ehrenspeck (1991) and the California Geological Survey (2014a, b), in the Central Hollywood area, may therefore be one of many older bedrock faults generally coincident with canyon heads incised during the Pleistocene.

Our paleoseismic investigations specifically exposed structure formed by parallel anticlinal and synclinal folding with associated anticlinal crest faulting. A similar relationship between strike-slip faulting and crustal shortening tectonics was documented by Kolthoff (1994) in his investigation of the Coalinga Anticline in central California.

This relationship indicated that the Coalinga Anticline was similarly produced by crustal shortening and not by simple strike slip along the adjacent San Andreas fault system.

3 Paleoseismic Investigations of the Yucca Street and Argyle Avenue Area, Central Hollywood

Paleoseismic investigations in Central Hollywood (Fig. 1) included trench exposures ~213 m long and up to 10 m deep (Fig. 5), advancement and interpretation of 100+ cone penetrometer tests (CPT), and excavation and collection of over 304 m of continuous cores. The CPTs, in particular, showed regional continuity of stratigraphic markers throughout the investigated area (Fig. 1). Similarly, the up-to-10 m deep trenches (Fig. 5) exposed several extensive soil-stratigraphic markers useful for regional correlation and for relative dating of the underlying sediments. We found, at least in the Central

Hollywood area, the presence of an anticline (Yucca Street Anticline) with no evidence of a large magnitude strike-slip fault. This anticline deforms late Quaternary sediments and may be a low amplitude fold; alternatively, it might be the “crest” of a larger regional anticline associated with the Hollywood Syncline (California Department of Water Resources 1961, Plate 1) forming the Hollywood Sub-Basin to the south. The Yucca Street Anticline, at the southern front of the Santa Monica Mountains, parallels the south adjacent Hollywood Syncline, further evidence that the Santa Monica Mountains are now undergoing crustal shortening and thickening and hence uplift and folding.

3.1 Paleoseismicity in the Yucca Street and Argyle Avenue Area

The Yucca Street Anticline was first discovered and recognized in trenches emplaced to evaluate possible Holocene

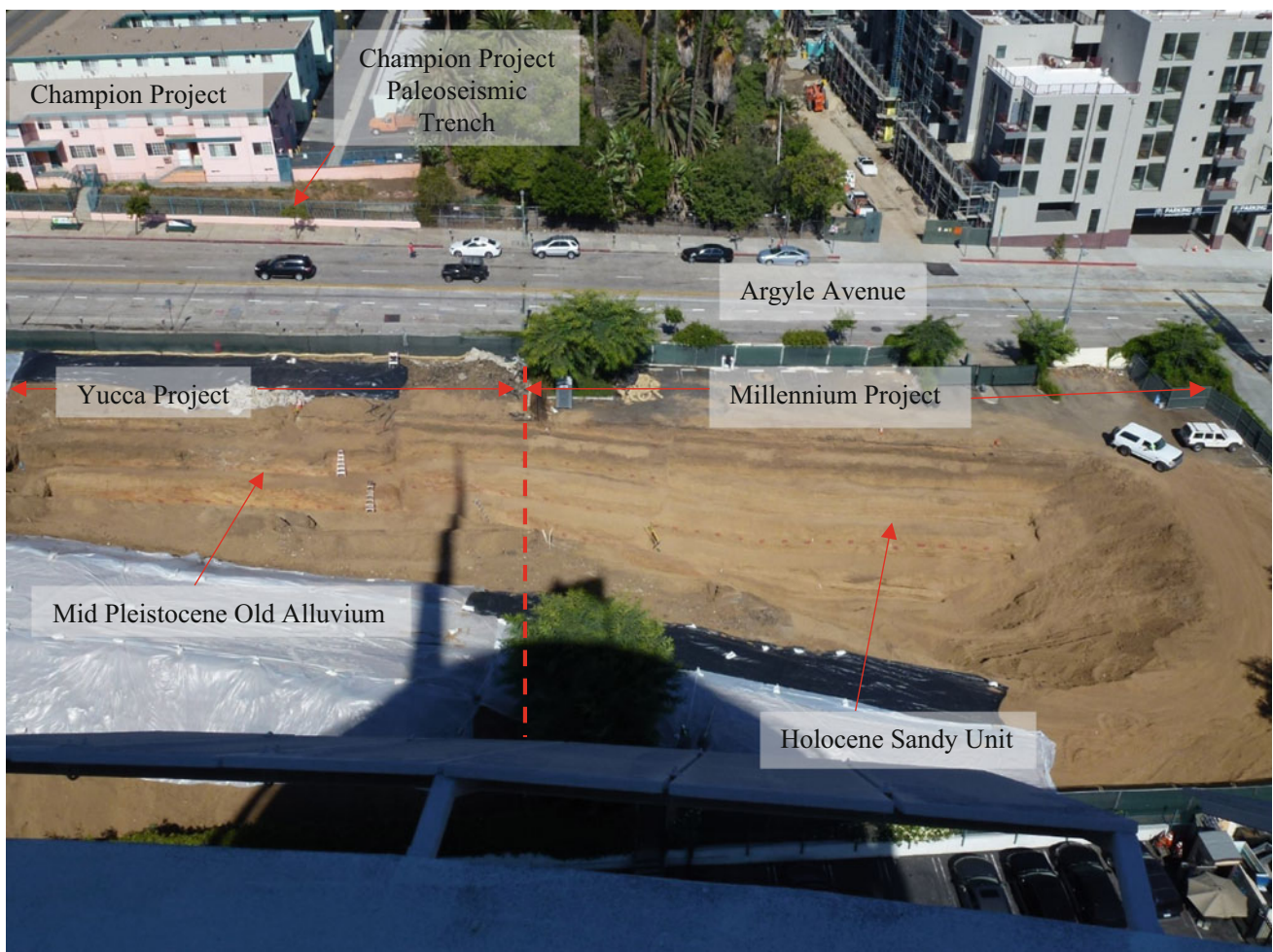


Fig. 5 A typical urban paleoseismic trench across the Yucca and Millennium Projects excavated at the Capitol Records parking lot. The Champion Project paleoseismic trench is shown at the top left corner of the photo. Photo by Steven Kolthoff

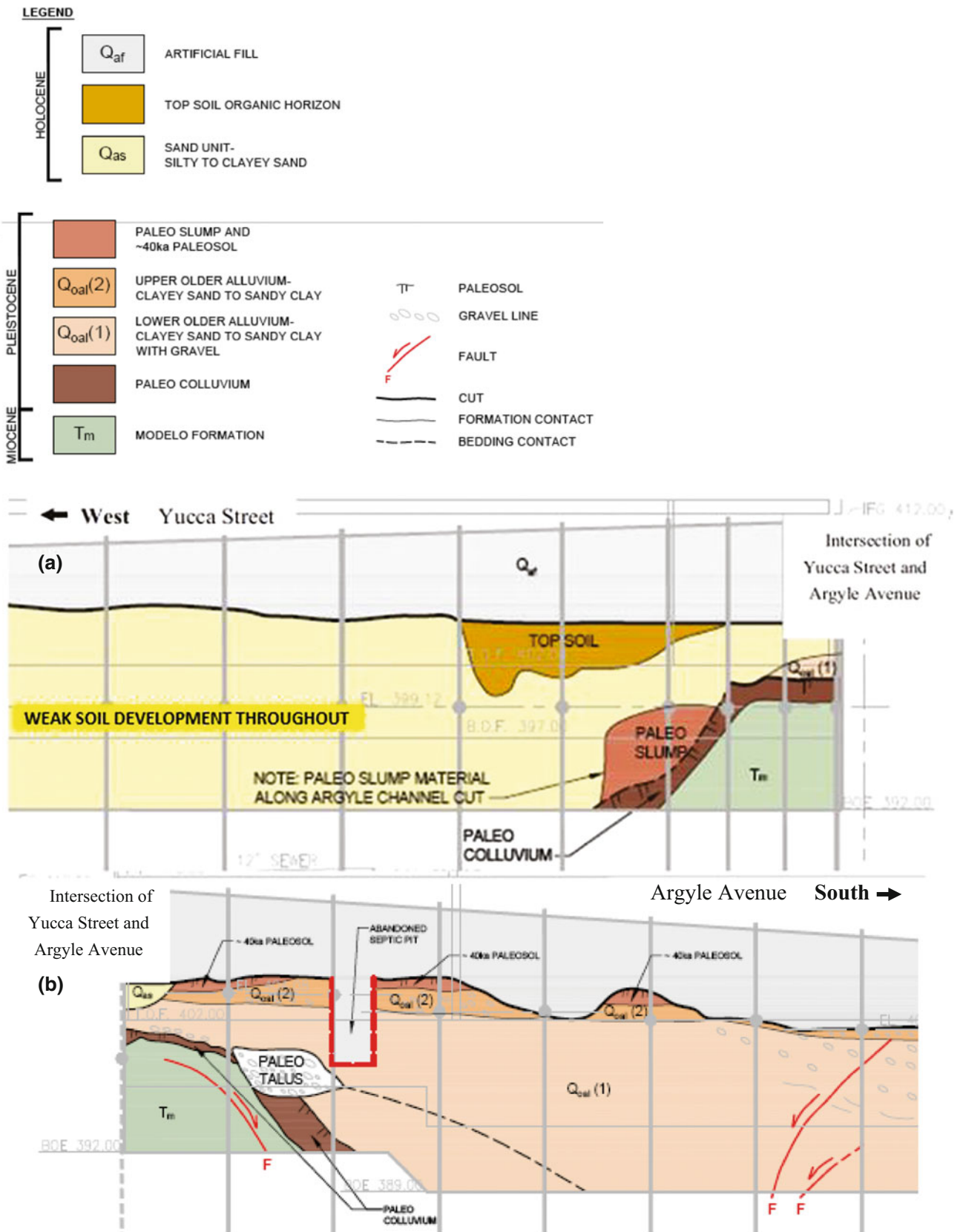


Fig. 6 Simplified trench logs of the Yucca Project showing units mapped in basement bulkhead exposures. The legend is the uppermost illustration; representative east-west and north-south cross sections given in (a) and (b), respectively. Graphics modified from Group Delta (2016)

displacement of the Hollywood Fault (Group Delta 2014a, b, c). The so-called “Champion trench” exposed near-horizontal older alluvium in the north (near Yucca Street) that increasingly dipped 15 to 30+ degrees to the south. In contrast, the nearby “Argyle trench” exposed north-dipping Pleistocene older alluvium. And north of the Argyle site, exposures revealed north-dipping older alluvium, thereby defining an anticline with a generally east-west axis. The Yucca Street Anticline was well exposed in basement bulkheads of a multi-story building scheduled for demolition. The Miocene sediments in the core of the Yucca Street Anticline are highly deformed thin shales and fine sandstones. These were covered by colluvium capped by a strongly developed buried paleosol indicating at least a ~100 ka year epoch of weathering after anticlinal folding (Group Delta 2014a, b, c).

Based on our subsurface investigations (Group Delta 2014a, b, c), we now propose a general, three-stage model to explain the late Quaternary evolution of the Central Hollywood area: First, before about 500 ka, the Santa Monica

Mountains were deeply incised by south-trending canyons carrying sediments to the adjacent Hollywood Sub-Basin. At this time, the lower “older alluvium” (Qoal(1)) overlapped the core of the Yucca Street Anticline, interfingering with local paleo-colluvium and talus (Group Delta 2016), and eventually buried most of the Miocene anticlinal structures (Figs. 6a, b and 7).

Second, regional compression re-folded Miocene sediments and deformed the Qoal(1) alluvium. The renewed folding formed discontinuous extensional normal faults along anticlinal crests. Some faults show bedding thickening in hanging walls, ostensibly due to antithetic flexure (roll-over). This period of renewed folding was after the deposition of Qoal(1) and likely not contemporary.

And third, episodic growth of the Yucca Anticline apparently ceased before ~100 ka ago, based on soil-stratigraphic dating of undeformed alluvium (Qoal(2)) overlying the core crest (Group Delta 2014a). Accordingly, the Yucca Anticline ceased before 100 ka and has remained quiescent since.



Fig. 7 Excavating the Yucca Project basement bulkhead. See Fig. 6b for a graphic illustration of this exposed section along Argyle Avenue. Photo by Steven Kolthoff

4 Conclusion

From regional structural assessments and from site-specific paleoseismic data for the Central Hollywood area, we deduce that: (1) the modern Hollywood Fault is not driven by strike-slip tectonics, as has been previously proposed; (2) in the Central Hollywood area, tectonics are mainly driven mainly by regional compression (crustal shortening) evidenced by the uplift of the Santa Monica Mountains in general and by folding of the Yucca Street Anticline and Hollywood Syncline in particular. The folding, erosion and alluviation documented in the Yucca Street and Argyle Avenue area of Central Hollywood indicate that faulting and folding is episodic with the last crustal shortening (folding and faulting) events taking place prior to at least ~ 100 ka ago.

We also propose that the Hollywood Fault, as previously mapped in the Los Feliz area, crosses the alluvial basin in the Central Hollywood area, north of the Yucca Street Anticline, then reconnects with the previously mapped Hollywood Fault in the West Hollywood area. We now conclude that “active traces” of the Hollywood Fault do not exist in the Central Hollywood area, but rather, if extant, are outside the area, are taken up by slip in contemporary folding or, less likely, covered by unusually thick wedges of Holocene alluvium.

Acknowledgements We thank Group Delta Consultants, Inc. for the opportunity to consult on the above-mentioned projects. We also thank Zach Aarons, Project Manager at Millennium Partners, for his logistical and management support throughout the investigative process. We additionally thank the City of Los Angeles Department of Building and Safety Reviewers for their time and insightful comments on the general geologic structures of the area.

References

- Ammon, C.J.: Introduction to Earthquakes (Chap. 5). In: Faults and Faulting, from Internet Class Notes EAS-A193. St. Louis University (2001). http://eqseis.geosc.psu.edu/~cammon/HTML/Classes/IntroQuakes/Notes/notes_framed.html
- Anderson, T.H., Nourse, J.A.: Pull-apart basins at releasing bends of the sinistral Late Jurassic Mojave-Sonora fault system. *Geol. Soc. Am. Spec. Pap.* **393**, 97–123 (2005)
- California Department of Water Resources: Planned Utilization of the Ground Water Basins of the Coastal Planes of Los Angeles Country, Appendix A, Ground Water Geology (1961)
- California Geological Survey: Earthquake Zones of Required Investigation, Hollywood 7.5' Quadrangle, Los Angeles County, California, Earthquake Fault Zones and Seismic Hazard Zones (2014a)
- California Geological Survey: Preliminary review earthquake zones of required investigation, Hollywood Quadrangle. Released January 2014, scale: 1:24000 (2014b)
- Davis, T.L., Namson, J.: A balanced cross-section of the 1994 Northridge Earthquake, Southern California. *Nature* **372**, 167–169 (1994)
- Davis, T.L., Namson, J., Yerkes, R.F.: A cross-section of the Los Angeles area: seismically active fold and thrust belt, the 1987 Whittier earthquake and earthquake hazard. *J. Geophys. Res.* **94** (B7), 9644–9666 (1989)
- Dibblee, T.W., Ehrenspeck, H.E. (ed.): Geologic map of the Hollywood and Burbank (south 1/2) quadrangles, Los Angeles, California. Dibblee Geological Foundation, Map DF-30, scale, 1:24000 (1991)
- Dolan, J.F., Sieh, K., Rockwell, T.K., Gupta, P., Miller, G.: Active tectonics, paleoseismology, and seismic hazards of the Hollywood Fault, northern Los Angeles Basin. *Geol. Soc. Am. Bull.* **109**, 1595–1616 (1997)
- Group Delta Consultants, Inc.: Fault Activity Investigation. Yucca-Argyle Apartments, 1756 and 1760 Argyle Avenue, Hollywood Area, City of Los Angeles, California (2014a)
- Group Delta Consultants, Inc.: Fault Activity Investigation. 1800 Argyle Avenue, Hollywood Area, City of Los Angeles, California, GDC Project no. LA-1183 A (2014b)
- Group Delta Consultants, Inc.: Fault Activity Investigation. 1800 Argyle Avenue, Hollywood Area, City of Los Angeles, California, (Supersedes Previous Version 9/3/14) GDC Project no. LA-1175 A (2014c)
- Group Delta Consultants, Inc.: Fault Verification Report. Proposed Mixed-Use Development, 6230 Yucca Street, Los Angeles, California (2016)
- Ingersoll, R.V., Rumelhart, P.E.: Three-stage evolution of the Los Angeles basin, southern, California. *Geology* **27**, 593–596 (1999)
- Kolthoff, S.H.: Tectonic and Gravity Study of the Coalinga Area, California. Requirement for CSULB Master's thesis (1994)
- McGill, S.: Science Spotlight: GPS Station P 612 (no date). <http://xenon.colorado.edu/spotlight/index.php?product=spotlight&station=p612>
- Namson, J., Davis, T.L.: Structural transect of the western Transverse Ranges, California: implication for lithospheric kinematics and seismic risk evaluation. *Geology* **16**, 675–679 (1988)
- Plesch, A., Shaw, J.H., Benson, C., Bryant, W.A., Carena, S., Cooke, M., Dolan, J., Fuis, G., Gath, E., Grant, L., Hauksson, E., Jordan, T., Kamerling, M., Legg, M., Liindvall, S., Magistrale, H., Nicholson, C., Niemi, N., Oslin, M., Perry, S., Planansky, G., Rockwell, T., Shearer, P., Sorlien, C., Suss, M., Suppe, J., Treiman, J., Yeats, R.: Community fault model (CFM) for Southern California. *Bull. Seismol. Soc. Am.* **97**(6), 1793–1802 (2007)
- Sylvester, A.G.: Strike-slip faults. *Geol. Soc. Am. Bull.* **100**, 1666–1703 (1988)

Liquefaction Susceptibility Map of the Broader Thessaloniki Urban Area

George Papathanassiou and Vasilis Marinos

Abstract

The occurrence of liquefaction and the generation of liquefaction-induced deformations can result in severe damages to the manmade environment particularly in urban areas constructed in coastal areas. The first event close to an urban environment and studied in detail, was the 1906 San Francisco earthquake while the last decade, severe structural damages were induced due to soil liquefaction (CES 2010–2011, Great East Japan 2011, Emilia Romagna 2012 and Cephalonia 2014 earthquakes). In order to prevent the occurrence of soil liquefaction and to minimize its effects to the manmade environment, studies regarding the susceptibility of the geological units should initially take place, oriented to the assessment of the depositional environment. The goal of this study is to delineate susceptible to liquefaction geological units within the broader Thessaloniki urban area. In order to achieve this, information regarding the surficial distribution of geological units was taken into account in conjunction with the historical seismicity background of the area. The result obtained by this study is that the industrialized area, located to the western edge of the urban area, is constructed upon sediments classified as high to very high liquefaction susceptibility. The outcome of this study can be used by urban planners for the future extension of the city of Thessaloniki.

Keywords

Earthquake • Thessaloniki • Liquefaction
Susceptibility

1 Introduction

It was well known that the occurrence of liquefaction and the generation of liquefaction-induced deformations have a huge economical cost particularly in urban areas constructed in coastal areas. The first event that occurred close to an urban environment and studied in detail was the 1906 San Francisco earthquake. However, the most severe liquefaction-induced damages to civil infrastructure were observed after the Niigata and Anchorage earthquakes in 1964 which helped to identify liquefaction as a major problem within an urban area (Idriss and Boulanger 2008). Other major events that provided data regarding the occurrence of liquefaction in an urban area were the 1989 Loma Prieta and the 1995 Kobe earthquakes. Other major events that provided data regarding the occurrence of liquefaction in an urban area were the 1989 Loma Prieta and the 1995 Kobe earthquakes. The latter event caused pervasive liquefaction throughout the reclaimed lands and the manmade islands in the Kobe region, causing extensive structural damages to quay walls around the port facilities and associated damage to the cranes and other supporting facilities (Idriss and Boulanger 2008).

The last decade, severe structural damages such as building settlement, lifeline failures and quay wall displacements were induced due to soil liquefaction. Such structural damages were triggered by the Canterbury Earthquake Sequence 2010–2011, Great East Japan 2011, Emilia Romagna 2012 and Cephalonia 2014 earthquakes. The most characteristic liquefaction-induced deformations were documented in the urban areas of Christchurch (New Zealand) where the cost to insurers of rebuilding has been estimated at NZ\$20–30 billion, the villages of San Carlo and Mirabello (Emilia Romagna, Italy) and the waterfront areas of Lixouri and Argostoli (Cephalonia, Greece).

Taking into account the above information, it is clearly established the necessity for compiling studies focusing on the triggering of liquefaction. The preliminary step for

G. Papathanassiou (✉) · V. Marinos
Department of Geology, Aristotle University of Thessaloniki,
Thessaloniki, Greece
e-mail: gpapatha@auth.gr

evaluating the liquefaction potential in an area, is the preparation of liquefaction susceptibility map that will be used as a base layer in order to evaluate the liquefaction hazard and manage the associated risk of foundation and structural damage.

Therefore, this study should be considered as the first step regarding the evaluation of liquefaction hazard within the broader area of Thessaloniki and it is focused on the delineation of susceptible to liquefaction geological units.

2 Assessing the Liquefaction Susceptibility on Regional Scale

In order to prevent the occurrence of soil liquefaction and to minimize its effects to the manmade environment, studies regarding the susceptibility of the geological units should initially take place. Areas susceptible to liquefaction can be identified through detailed geologic, geomorphic and hydrologic mapping (Witter et al. 2006). Afterwards, a prone to liquefaction area should be further investigated in detail in order to evaluate the liquefaction potential and the degree of ground and/or structural failure. It should be pointed out that these maps do not predict liquefaction-related ground failures, although ground failures may accompany liquefaction and are more likely to occur in areas with higher liquefaction susceptibility (Tinsley et al. 1985).

In general, the susceptibility to liquefaction of a geological unit can be evaluated based on its depositional environment; the depositional process affect the liquefaction susceptibility of sediments since fine and coarse grained soils sorted by fluvial or wave actions are more susceptible than unsorted sediments (Youd 1998). The most well-known and globally applied methodologies in order to assess the liquefaction susceptibility of the geological units at regional scale were proposed by Wakamatsu (1992) and the California Department of Conservation, Division of Mines and Geology (CDMG 1999).

Following the above regional-oriented guidelines, the liquefaction susceptibility of the sediments at the urban area of Thessaloniki, Greece was assessed.

3 Engineering Geological Settings at the Study Area

For the purposes of this study the engineering geological map (scale 1:10.000) compiled by Rozos et al. (2004) was used as a base layer. It was decided to use this map not only because it is more detailed regarding the spatial distribution of sediments but also because extra meaningful information regarding geotechnical characteristics of the geological units is also provided.

In particular, having collected and analyzed more than 1300 geotechnical boreholes, Rozos et al. (2004) distinguished thirteen engineering geological units within the broader Thessaloniki area. These units have been grouped in four lithostratigraphic units while the range of their physical and mechanical properties was also provided. This is a critical issue regarding the assessment of liquefaction susceptibility of deposits since the provided data regarding the Atterberg limits and the dominant size/type of grains within a soil unit were used in order to perform a liquefaction-oriented classification.

According to Rozos et al. (2004), four pre-Neogene basement units and one Neogene (mixed phases coded as Pl, f-c), units are mapped within the studied area. The Neogene units are mainly reported in the southern and northern part of the city while the pre-Neogene found in the semi-mountainous and mountainous zone to the north-east and east of Thessaloniki. Obviously, both geological units are considered as non liquefiable and were not further analyzed for the purposes of this study.

The rest of the examined area is covered by seven engineering geological units of Quaternary age while the historical centre of Thessaloniki is covered by earth fills (historic fills coded as Hf), mainly consists of building stones and other construction material mixed with natural soils (Rozos et al. 2004). Towards the waterfront area of Thessaloniki, these artificial fills mainly consists of clayey silts with some sand and gravels, and are grouped in the engineering geological map as recent fills, Rf. The rest of Quaternary geological units at the broader Thessaloniki area are grouped as coastal sands (Sd), torrential deposits (Rd), inland basins deposits (f,c-l), Quaternary loose sandy deposits (sd-l), Quaternary loose silty deposits (sl-l), Quaternary loose fine deposits with organics (fp-l) Quaternary scree material (Scr) and the Pleistocene cohesive sediments of mixed phases coded as f,c-cm.

Thus, as it is shown in Fig. 1, a preliminary age-based discrimination of the geological units took place for the purposes of this study in order to delineate the Quaternary and pre-Quaternary sediments. This discrimination is critical since it is well known that only Quaternary sediments should be further examined regarding the susceptibility to liquefaction. A brief liquefaction-oriented description of these units is presented in the following section.

4 Assessing the Liquefaction Susceptibility of Deposits Mapped at the Study Area

Following the brief presentation of the Quaternary deposits that were mapped at the study area, it can be clearly demonstrated that likely to liquefaction zones exist. Thus, the goal of this study, which is mainly presented in this

Fig. 1 Engineering geological map of Thessaloniki (modified by Rozos et al. (2004)). Coastal sands (sd), torrential deposits (Rd), inland basins deposits (f,c-l), Quaternary loose sandy deposits (sd-l), Quaternary loose silty deposits (sl-l), Quaternary loose fine deposits with organics (fp-l) Quaternary scree material (Scr) and the Pleistocene cohesive sediments of mixed phases coded as f,c-cm



section, is to analyze and classify these deposits based on their level of susceptibility to liquefaction and to compile a relevant map for the entire urban area of Thessaloniki.

In particular, starting from the younger manmade unit, which is described with the general term of “Artificial fill”, it was decided to classify the area covered by this unit as high susceptible to liquefaction zone. For this classification we took into account the outcome of a research conducted by Anastasiadis et al. (2001) and Senetakis et al. (2008), concluding that soil layers of high potential to liquefaction are encountered at the waterfront of Thessaloniki, and the conclusion of a relevant research by Kiratzi et al. (2014), indicating that likely to liquefaction subsoil layers are encountered in this area. Both analyses were based on data provided by in situ tests (SPT) performed at the waterfront area of the city of Thessaloniki and its suburbs.

The unit that covers the historical center of Thessaloniki, coded as “historical fill” it was decided to be classified as

non susceptible by taking into account the general structure of this unit and the fact that the level of ground water table is deeper than 3 m. However, it should be pointed out that within this zone, sites or “spots” can be existed where the deposited soil layers could be liquefied under saturated conditions.

Regarding the Quaternary age deposits, the most likely to liquefaction unit that is classified as very high susceptible is correlated to the mapped coastal sands sd with thickness up to 3 m. A geological unit of similar susceptibility class (high to very high) is the one mapped as Quaternary loose sandy deposits sd-l. On a qualitative-base approach, this unit contains soils that fulfill two basic criteria regarding the occurrence of liquefaction: the loose state and the sandy gradation with fines content (silt and clay size particles) less than 20%. In addition, this sandy loose material though t it shows a large variation in Atterberg limits, in most cases show no plasticity (Andronopoulos et al. 1991).

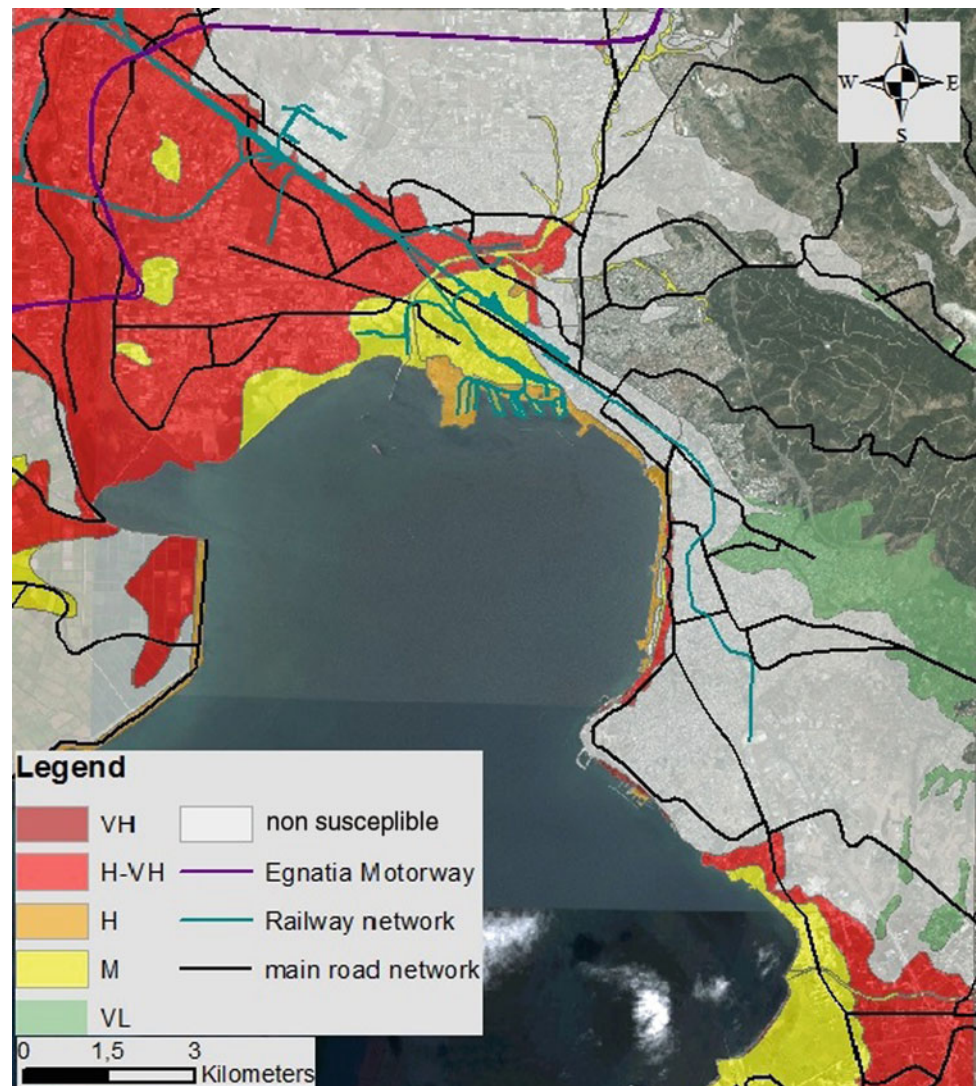
As moderate susceptible to liquefaction were classified the units mapped as fluvio-torrential deposits Rd and Quaternary loose silty deposits (sl-l). According to Rozos et al. (2004), the Atterberg limits of the latter formation show a small variation with ranges equal to 28 (21–49%) for the liquid limit and 14.7 (17–32%) for the plastic limit. Thus, and by taking into account the fact that the plastic index ranges equal to 13, it cannot be excluded that likely to liquefaction sites exist. However, based on the previously mentioned physical parameters, the level of liquefaction susceptibility is considered as moderate.

The formation mapped as Quaternary loose fine deposits with organics (fp-l) consists of a black to black-grey silty clay with organics. This horizon includes scattered sandy intercalations with a thickness not exceeding 1.0 m. According to Rozos et al. (2004), the Atterberg limits show a large range of plasticity values from low in sandy intercalations to high for the silty clay-based sites. Thus, this unit is

classified as non-susceptible to liquefaction with the exception of sandy spots. Within the same group of non susceptible to liquefaction units, are classified the mapped as Loose Quaternary deposits, with predominance of coarse grained material Scr and the inland basin deposits f,c-l. The former has been formed by scree material and accordingly is not liquefiable and the latter is mainly consist by sandy clay soil that is also considered as non susceptible to liquefaction. Finally, although the fact that liquefaction phenomena are not expected within the area covered by the Pleistocene cohesive sediments, this zone is classified as very low susceptibility to liquefaction in order to maintain the consistency with the accepted discrimination of Quaternary and pre-Quaternary sediments.

Having assessed the liquefaction susceptibility of the sediments, the future step of this research deals with the evaluation of the liquefaction potential of the soil layers based on data provided by geotechnical boreholes with SPT

Fig. 2 Liquefaction susceptibility map of the broader Thessaloniki urban area, VH: very high susceptibility, H: high susceptibility, M: moderate susceptibility, VL: very low susceptibility



and in situ tests e.g. CPT. Up to date, more than 200 profiles of boreholes that were performed from 1963 to 2006, were collected. These in situ tests were drilled for various purposes such as the construction of Thessaloniki metro, the extension of coastal part and the construction of buildings such as schools, hospitals, museums, town halls, gyms, apartment buildings etc. (Fig. 2).

5 Conclusions

The goal of this study was the compilation of a liquefaction susceptibility map of the broader Thessaloniki area. In order to achieve this, the engineering geological map that was compiled by Rozos et al. (2004) was used as a base layer while additional information obtained by published articles and reports were also taken into account.

As a result, a map is developed where the mapped formations are delineated based on the assessed susceptibility to liquefaction level. This map clearly indicates that the waterfront area of Thessaloniki is covered by high susceptibility to liquefaction units while at the historical centre of the city the hazard due to soil liquefaction can be neglected with the exception of “spots” where the subsoil layers under condition are likely to liquefaction.

The most meaningful outcome of this study deals with the spatial distribution of high to very high susceptible to liquefaction at the western part of the city; an area that is crossed by the train network and Egnatia motorway, and where the industrialized zone of the city is located. At this area, it was concluded that the soil layers are likely to liquefaction and accordingly further investigation e.g. geotechnical boreholes should be performed in order to quantitatively evaluate the liquefaction potential. Furthermore, this conclusion should also be taken into consideration by urban planners and decision makers regarding the extension of the urban area of Thessaloniki.

References

- Anastasiadis, A., Raptakis, D., Pitilakis, K.: Thessaloniki's detailed microzoning: subsurface structure as basis for site response analysis. *Pure Appl. Geophys.-PAGEOPH* **158**(12), 2597–2633 (2001)
- Andronopoulos, V., Rozos, D., Hadzinakos, I.: Subsidence phenomena in the Industrial Area of Thessaloniki, Greece. In: Johnson, A. (ed.) *Land Subsidence*, vol. 200, pp. 59–69. IAHS Publ. (1991)
- CDMG: Guidelines for analyzing and mitigating liquefaction hazards in California. California Department of Conservation, Division of Mines and Geology, Special Publication 117, p. 63 (1999)
- Idriss, I.M., Boulanger, R.W.: *Soil Liquefaction During Earthquakes*, MNO-12, p. 242. Earthquake Engineering Research Institute, Oakland, CA (2008)
- Kiratzí, A., Roumelioti, Z., Chatzipetros, A., Papathanassiou, G.: Simulation of off-fault surface effects from historical earthquakes: the case of the city of Thessaloniki (Northern Greece), *Engineering Geology for Society and Territory*, vol. 5, pp. 957–963 (2014)
- Rozos, D., Apostolidis, E., Xatzinakos, I.: Engineering-geological map of the wider Thessaloniki area, Greece. *Bull. Eng. Geol. Environ.* **63**, 103–108 (2004)
- Senetakis, K., Anastasiadis, A., Pitilakis, K.: Liquefaction risk in Thessaloniki. In: *Proceedings, 3rd Hellenic Conference on Engineering Seismology and Earthquake Engineering*, November 5–7, Athens, Greece (2008). (in Greek)
- Tinsley, J.C., Youd, T.L., Perkins, D.M., Chen, A.T.F.: Evaluating liquefaction potential. In: Ziony, J.I. (ed.) *Evaluating earthquake hazards in the Los Angeles Region—An Earth Science Perspective*, pp. 263–316. U.S. Geological Survey Professional Paper 1360 (1985)
- Wakamatsu, K.: Evaluation of liquefaction susceptibility based on detailed geomorphological classification. In: *Proceedings of the Technical Papers of Annual Meeting Architectural Institute of Japan*, pp. 1443–1444 (1992). (in Japanese)
- Witter, C.R., Knudsen, L.K., Sowers, M.J., Wentworth, M.C., Koehler, D.R., Randolph, C.E.: Maps of quaternary deposits and liquefaction susceptibility in the Central San Francisco Bay Region, California, p. 43. Open file report 2006-1037, USGS (2006)
- Youd, T.L.: Screening guide for rapid assessment of liquefaction hazard at highway bridge site. Technical report MCEER-98-0005, 58 p (1998)

Study of the Phenomenon of Quicksand in the Geotechnical Laboratory

Sebastião Geraldo Guimarães Júnior, Isabella Magalhães Valadares,
Marcus Vinícius Araújo da Silva Mendes,
and Jaquelline da Silva Feitosa

Abstract

The quicksand phenomenon occurs when the sand particles are saturated by an upward flow of an aqueous fluid and microscopically the particles of the mineral lose contact. Thus, the tension of the soil weight equals the water pressure value making the effective tension of the soil null. The sandy soil does not present plasticity and cohesion, when saturated the sand loses its mechanical characteristics and acts like a liquid. The objective of this paper is the elaboration of a didactic physical model, in laboratory, that simulates the phenomenon of quicksand and the development of a better understanding of its occurrence operations and characteristics. The methodologies used were quantitative and qualitative. The quantitative methods were geotechnical characterization tests, such as the classification of sands in terms of granulometry (ABNT NBR 7181: 2016), specific mass test and the development of a permeameter capable of determining the permeability coefficient in a BMA (system that is composed of gravel, geodrenant mesh and sand). The methods of quantitative character were the analyses of the phenomena in reduced scale and the behavior of the sands in the BMA system. The results found coincide with the expected physical properties. This was possible due to the fact that the glass apparatus was adequate to promote and watch the quicksand

phenomenon, besides, the BMA system was important to maintain the permeability constant in all the simulations carried out in the laboratory.

Keywords

Quicksand • Sand • Permeability

1 Introduction

There is a great diversity of soils in the world, there are clay soils, silty soils, sandy soils, loam soils, among others. The combination and configuration of the soil branch out in several aspects. In the city of Natal- Rio Grande do Norte, on the northeastern coast of Brazil, there is a formation of dunes (sand hill) that can be prone to the phenomenon of quicksand if there were to be a cut in the dunes or increase of water table or environment, however, before knowing about this phenomenon it is necessary to understand soil science.

Soil Mechanics studies the behavior of each soil under stress. For Campos (2012) the Mechanics of the Soils divides the materials that cover the earth in 4 groups: rocks (rocky terrain); sandy soils; silt soils and clay soils. The Campos division (2012) is initially simplistic, but is primarily a soil classification method.

The ABNT NBR 6502: 1995 classifies sand as fine sand (0.06–0.2 mm), medium sand (0.2–0.6 mm) and coarse sand (0.6–2.0 mm). Thus, a sandy soil is composed of mineral particles of granulometry between 0.06 and 2.0 mm visible to the naked eye. One of the main characteristics is the lack of cohesion between the grains, that is, their grains are easily separated from each other allowing a great permeability in these types of soils allowing water ease circulation under this condition. According to Caputo (1988), permeability is the capacity of soil to allow water to flow through it and the permeability coefficient quantifies this property.

The quicksand phenomenon occurs when a large stream of water fills the voids of the sand, canceling the friction

S. G. G. Júnior (✉) · I. M. Valadares · M. V. A. da Silva Mendes
Instituto Federal de Educação, Ciência e Tecnologia de Goiás,
Câmpus Formosa, São Paulo, Brazil
e-mail: sebastiaooggj@gmail.com

I. M. Valadares
e-mail: isabellamv.civil@gmail.com

M. V. A. da Silva Mendes
e-mail: mvasmendes.ifg@gmail.com

J. da Silva Feitosa
Instituto Federal de Educação, Ciência e Tecnologia de São Paulo,
Câmpus Itapetininga, Itapetininga, Brazil
e-mail: jaquellinef@gmail.com

between the grains (Freitas 2017). This situation occurs in river banks, lakes, beaches, marshes and in regions close to underground water sources.

In Brazil, the quicksand receives a nomenclature of “*areia movediça*” which in literal translation means moving sand. This term is used because the lack of friction between the grains allows the sand to assume the property of the liquid as it becomes movable.

This phenomenon happens when the sand is submitted to a condition of constant ascending flow, in such a way that it undergoes a specific tension, resulting in a soil resistance equal to zero. With that the balance of the grains is broken making the ground unstable (Cavalcante 2006).

In this research a structure capable of simulating the phenomenon of quicksand was developed in a reduced scale to facilitate the understanding of this natural phenomenon. The study can be applied as a didactic form of assimilation of the grain saturation and understanding of how water flow can cause the quicksand phenomenon in sandy soils.

2 Methodology

The methodologies used for the study are quantitative and qualitative. For analysis, data were collected on the sand grains granulometry, permeability coefficient (K) and observed the percentage of immersion (I) during the phenomenon.

The equipment capable of simulating the phenomenon of quicksand was developed to be capable of performing permeability tests on the used soil. The equipment has mechanisms that can control the situation in the occurrence of the quicksand phenomenon and allows the understanding of its occurrence.

To understand and analyze the simulation, it is necessary to know the system variables, the resource used, what processes are executed and what is the simulated event. The variables are the different types of sand and their different permeabilities. The process is a continuous and ascending flow of water. The resource is the path the water will percolate through, in this case, the sand column. The sum of all these components enables simulation and the study of quicksand.

To eliminate one of the variables, a BMA system was developed (system composed of gravel, mesh and sand). This system, regardless of the type of sand used, can allow the permeability to remain in the range of 10^{-2} cm/s with small changes in the millimeter scale. The realization of quicksand simulation with permeability on a scale of 10^{-2} cm/s is a good option since this permeability is one of the most probable for the occurrence of the phenomenon.

This affirmation was deduced by the permeability test and simulation of the effect in the laboratory.

The soil characterization was based on the ABNT NBR 7181/2016 standard and the permeability coefficient was obtained using the equipment developed for the project, based on Caputo (1988), where it states that the permeability coefficient of a soil can be quantified numerically using Darcy's Law expressed by the following equation:

$$K = \frac{Q}{A \times I} \quad (1)$$

where:

- K Coeff. of permeability;
- Q quantity of flow;
- A Sample length;
- I hydraulic gradient.

To prove the efficacy of the simulation, the BMA system was submitted to a continuous and upward flow of water.

3 Description of Equipment and Materials

The equipment was designed for permeability laboratory study. It was constructed with reused material and three types of aquariums that interconnect, Fig. 1, forming a mutual system of tests.

The first aquarium has dimensions of 70 cm × 35 cm × 50 cm and consists essentially of two parts. These parts are separated by a sheet of glass at 50 cm from the left end of the aquarium. The glass sheet thickness is 5 mm and contains a circular cut of 5 cm in diameter at the height of 42 cm.

The first part of the aquarium (1) is intended for the small-scale quicksand simulation test and the second part (2) has the function of reserving excess water during the test.

The second aquarium has dimensions of 25 cm × 20 cm × 20 cm and contains a cut at the bottom of one of its faces intended for the exit of water regulated by a plastic tap. This aquarium is the third module of the equipment (3) and has the function of being a water reservoir, keeping the volume constant since it is always replenished by the second module (2).

The third aquarium has dimensions of 25 cm × 20 cm × 20 cm and contains a hole in the center of its base to allow an upward flow of water. This aquarium is the fourth and last module of the equipment (4) for testing the permeability coefficient (K).

All aquariums are made of glass, supported by a device made of reused school desks.

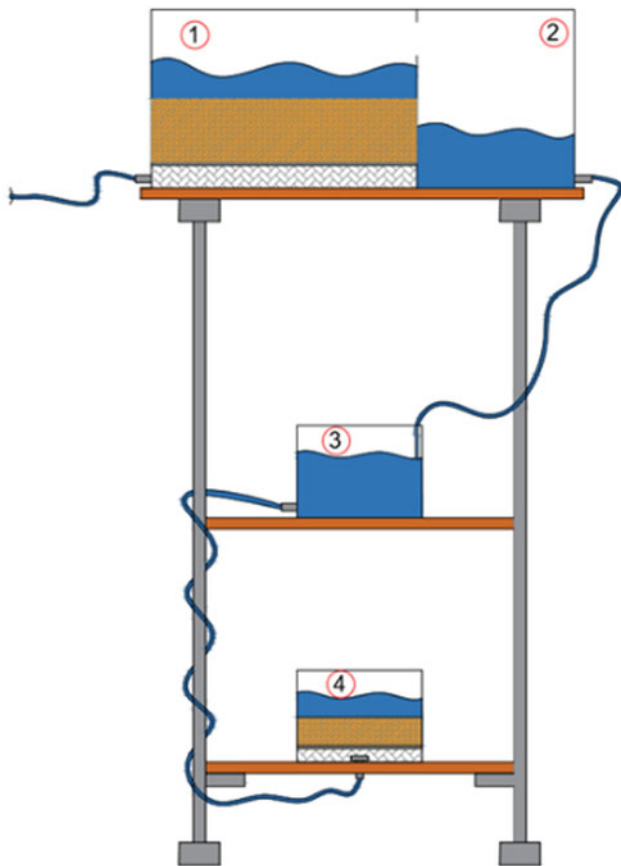


Fig. 1 2D diagram of the equipment, consisting of an aquarium for simulation of the small-scale quicksand phenomenon (1–2), a water aquarium (3) and an aquarium for the permeability test (4)

3.1 Geodrenant Mesh

For the execution of the permeability test and the simulation, a Bidim Geodrenant mesh was used to prevent the passage of sand and allow only the passage of the fluid.

The use of the mesh is justified for two reasons, the container used for the permeability test has an upstream water inlet located in the center of its base, thus the water flow created a larger flow section than in the other regions, the mesh allowed a flow homogeneity at all points of the container. The second reason is that the sand is a fine granular material that in direct contact with the water inlet could clog the passage. The use of the mesh prevented the direct contact between the sand and the passage of water.

The arrangement of materials in the equipment, as shown in Fig. 2, was: gravel 1, the geodrenant mesh, and sand, which was the studied variable.



Fig. 2 Layout of materials

4 Results

The results found coincide with the expected physical properties and the BMA system maintained the permeability constant in all the simulations.

4.1 Soil Characterization

For the soil characterization, 150 kg of sand were acquired to carry out all the tests proposed by the research. Using the ABNT NBR 7181: 2016 the entire sample of sand studied was washed, dried, and sifted, separating the grains by their granulometry.

Figure 3 shows in percentages the amount of each type of sand contained in the lot, where it is perceived that in the region where the study was applied, the average sand grain size is prevalent.

4.2 Permeability Coefficient (K)

After developing the BMA system, the tests were carried out to determine the permeability coefficient using the equipment developed during the research.

The equipment acts as a permeameter of constant load, where there are two reservoirs where in one reservoir the water is kept constant and percolates the BMA system that is allocated in the second reservoir. After this process the permeability coefficient (K) was determined.

Fig. 3 Classification of sand samples

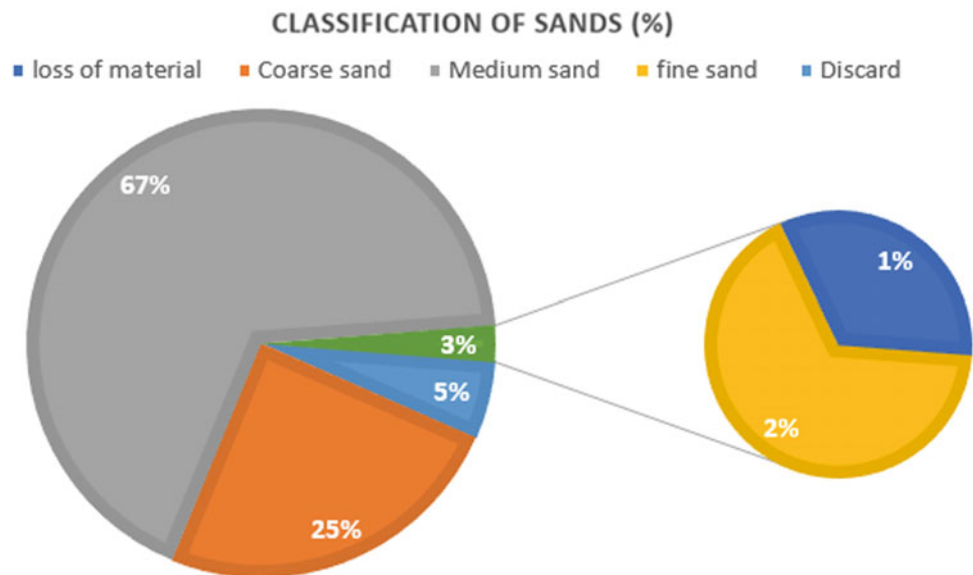


Table 1 The permeability of the BMA system

Sand	K (cm/s)
Coarse	1.18×10^{-2}
Medium	1.05×10^{-2}
Fine	1.00×10^{-2}
System average	1.08×10^{-2}

With the values presented in Table 1, the efficiency of the BMA system is proven, since it can keep permeability at the same intensity regardless of the type of sand.

4.3 Simulation of the Phenomenon

The small-scale quicksand phenomenon carried out in the laboratory was efficient in presenting the situation in a didactic way. The specimen subjected to the phenomenon was submerged with the application of the upward flow of water. This has proved that sand particles in a constant flow saturated environment lose contact with each other and behave like a fluid.

Figure 4 shows the moment when the water begins to saturate the sand grains.



Fig. 4 Apparatus for carrying out the quicksand phenomenon

5 Conclusion

The developed equipment demonstrated a good performance for use as didactic assistance on a permeability study.

The permeability of the BMA system may not interfere with the sands permeability, since the permeability of the system is considerably constant and does not differ on a large scale with the sands studied.

The tests proved that the quicksand phenomenon occurs only with constant water flow because it prevents the saturated particles from maintaining contact.

References

- ASSOCIAÇÃO BRASILEIRA DE NORMAS TÉCNICAS. NBR 6502: Rochas e solos. Rio de Janeiro (1995)
- ASSOCIAÇÃO BRASILEIRA DE NORMAS TÉCNICAS. NBR 7381: Solo- Análise Granulométrica. Rio de Janeiro (2016)
- Caputo, H.P.: Mecânica dos solos e suas aplicações, vol. 1, 6th edn., p. 71. ver. e ampl., Rio de Janeiro, BR (1988)
- de Cabral, G.: Areia Movediça. Mundo educação. <http://mundoeducacao.bol.uol.com.br/curiosidades/areia-movedica.htm>. Last accessed 2017/04/05
- de Campos, I.: Conheça os três tipos principais de solo: areia, silte e argila. Fórum da Construção. <http://www.forumdaconstrucao.com.br/conteudo.php?a=9&Cod=59>. Last accessed 2017/04/05
- de Cavalcante, E.: Mecânica dos Solos 2- Notas de Aula (2006). <https://goo.gl/oN0F1X>. Last accessed 2017/04/05
- de Freitas, E.: Areia Movediça. Brasil Escola. <http://brasilecola.uol.com.br/geografia/areiamovedica.htm>. Last accessed 2017/04/05
- LNCS Homepage: <http://www.springer.com/lncs>. Last accessed 2016/11/21

Fault-Landslide Interactions: Examples from the 2016 M7.8 ‘Kaikōura’, New Zealand, Earthquake

Clark Fenton, Mark Gray, Natalie Hyland, and James Smith

Abstract

The surface rupture generated by the 14th November 2016 M7.8 ‘Kaikōura’ earthquake ruptured multiple faults over a distance of approximately 200 km. The southern extent of the rupture in northern Canterbury displays a remarkable complexity of rupture style, geometry and surface expression. Much of the surface trace is closely associated with a number of large, complex mechanism coseismic landslides. The spatial proximity of landslides and fault rupture through a region of elevated topography has resulted in areas where the determination of the origin of surface deformation features becomes difficult. The identification of primary fault rupture is vital for surface rupture hazard determination, especially for the development of fault avoidance and setback zones. We present the results of detailed field investigations showing the relationships between primary and secondary surface faulting and areas of slope failure. The geomorphological characteristics of each deformation mechanism are discussed, and approaches to developing criteria for distinguishing the origin of upland surface deformation are presented.

1 Introduction

The 14th November 2016 M7.8 ‘Kaikōura’ earthquake produced over 200 km of surface faulting (Fig. 1) on a number of linked structures extending from close to Waiiau in North Canterbury through the Leader-Conway catchment, continuing offshore south of Kaikōura and through Marlborough and finally offshore into the Cook Strait (Stirling et al. 2017). In addition to the surface faulting extensive landsliding was triggered across the entire region, extending from the Hurunui District in North Canterbury to Cape Campbell in Marlborough (Dellow et al. 2017). Many of these landslides, especially large volume failures, were closely associated with the fault rupture. The observed complex movement styles in a number of these failures were controlled by fault-related bedrock structure.

In this paper we examine a number of landslides along the southern part of the rupture through the Hurunui District of Northern Canterbury. The relationship between bedrock structure, including fault geometry, and the ensuing style of landsliding is investigated.

2 Earthquake-Triggered Landslides

The M7.8 ‘Kaikōura’ earthquake initiated about 5 km west of the town of Waiiau in North Canterbury at a depth of 14.1 km. The rupture then propagated in a unidirectional manner towards the north and east. The rupture involved a number of faults (Fig. 1) with differing activities: some were previously recognized active faults with a broad range of slip rates and recurrence intervals (Stirling et al. 2017) while others were previously unmapped or not recognized as active structures. The rupture generated ground shaking (PGA) in excess of 1.0 g horizontal and up to 2.7 g vertical (Bradley et al. 2017). This ground shaking triggered tens of thousands of landslides over a 10⁴ km² region of North Canterbury and Marlborough (Dellow et al. 2017). These

C. Fenton (✉) · M. Gray · N. Hyland · J. Smith
Department of Geological Sciences, University of Canterbury,
Christchurch, New Zealand
e-mail: clark.fenton@canterbury.ac.nz

M. Gray
e-mail: mrg77@uclive.ac.nz

N. Hyland
e-mail: natalie.hyland@pg.canterbury.ac.nz

J. Smith
e-mail: jas351@uclive.ac.nz

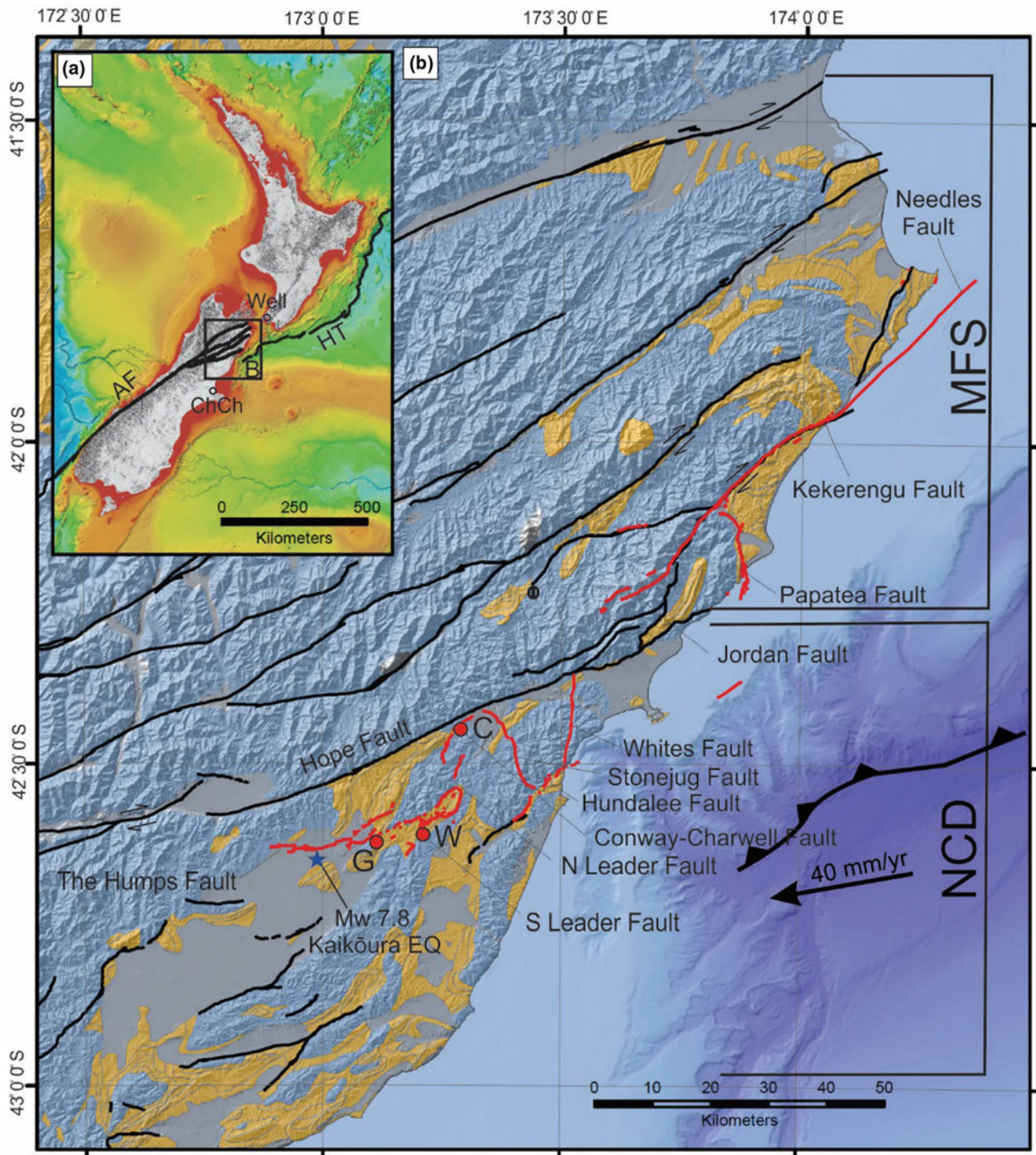


Fig. 1 Surface fault ruptures of the M7.8 Kaikōura earthquake shown in red. Other major active faults shown in black. Locations of landslide study areas discussed in text marked by red circles. C Conway; G Glenbourne; W Woodchester

range from minor rockfalls, soil debris flows, slumps, and rotational failures, to complex rock slope failures and mobile rock avalanches. The greatest frequency of landsliding was observed within a 3500 km² region surrounding the fault rupture (Dellow et al. 2017). Most of the earthquake affected

region is underlain by Torlesse Group greywacke. These rocks constitute the ‘basement’ of much of South Island. These materials are extensively tectonised and as such are of variable bedding geometry but are universally highly fractured. The cover rocks over much of the region are a mix of

volcanic and poorly-cemented marine sediments of Neogene age. The former comprise a sequence of basaltic eruptive facies as well as volcanoclastic deposits. These materials are often deeply weathered and covered by a thick residual soil/colluvial sequence. The latter include the Eocene Amuri Limestone, the Oligocene Motunau Formation and Early to Middle Miocene Waima Formation. These are found in a series of uplifted and inverted basin remnants. Through much of North Canterbury this sequence comprises claystones, siltstones, sandstones and limestones. The clastic

units all exhibit slaking, often disintegrating within seconds on contact with water. The limestones show variable bedding thickness and cementation.

As well as being associated with a region of high ground shaking, a significant number of landslides show close spatial association with the fault rupture, indicating that surface and near-surface fault displacement played a part in slope failure initiation and in determining the geometry and mechanism of failure (Fig. 2). Three examples of fault-controlled slope failure are discussed in the following sections.

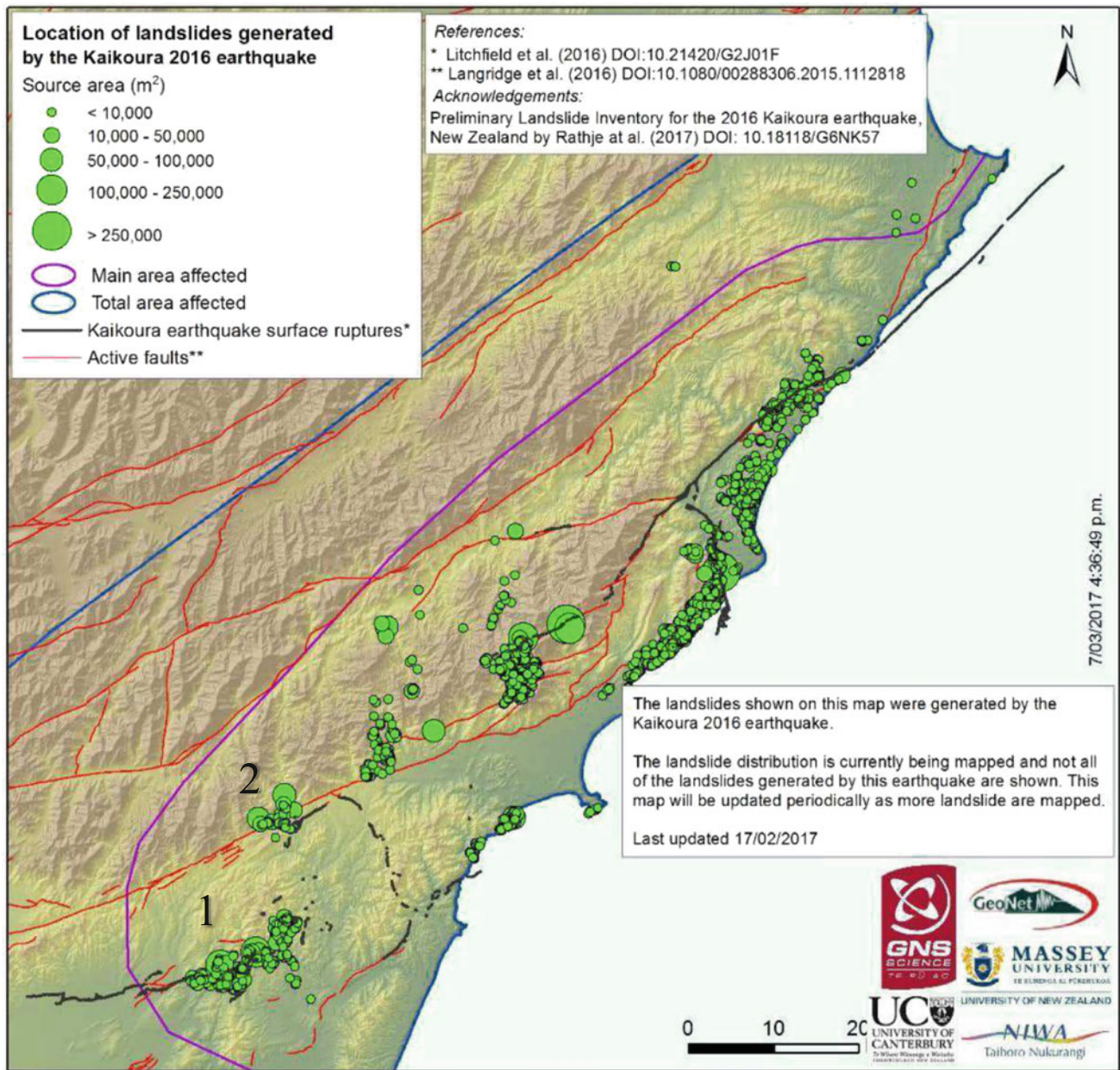


Fig. 2 Distribution of landslides from the M 7.8 Kaikōura earthquake (from Dellow et al. 2017). Note the proximity of the landslide clusters to the surface ruptures (shown in black). The landslides discussed in

this paper are located in the cluster of landslides around the Humps and Leader faults (1) and at the junction between the North Leader and Conway-Charwell faults (2)

2.1 Woodchester Station

Woodchester Station is the locus of some of the most complex faulting along the Kaikōura surface rupture trace. Three major fault structures, the WSW-ENE Emu Plain-Humps fault connects with the NNE South Leader and NE Mount Stewart/North Leader fault forming a triple junction (Fig. 3). This produces a broad complex zone of faulting across a zone over 1 km in width. The faults cross a variety of terrain from rolling hills, steeper mountain slopes and broad uplifted outwash terraces. The underlying bedrock is a mix of Torlesse basement and Tertiary basin fill, all overlain by Pleistocene and Quaternary fluvial gravels, sands and colluvium.

2.1.1 Mount Stewart/Lake Rebekah Landslide

The range front immediately north of the Leader River is the location of one of the larger, more spectacular landslides triggered by the earthquake. A southern spur of Mount Stewart failed, with the resulting slide mass blocking the Leader River creating the landslide-dammed Lake Rebekah.

The Mount Stewart Slide (Fig. 3) shows a complex movement geometry, involving planar sliding, rotation, toppling, and chaotic debris flow activity. The toe of the landslide is marked by a curvilinear thrust fault, with up-to-the-north displacement of up to 1.5 m and right-lateral displacement of 0.5 m. The landslide headscarp is coincident with the basin bounding fault marking the contact between the Torlesse basement and the Tertiary basin fill. This fault can be traced to the northeast as an up-to-the-north thrust fault with ~4 m of vertical offset. These surface rupture traces are broadly coincident the previously mapped Woodchester fault.

According to eyewitness accounts, the Mount Stewart landslide occurred coincidentally with the earthquake main shock (D. & R. Kelly, pers. comm. 2017). Extensive raveling and rockfall continued from the initiation of the failure up to the present day. The v-notch gully between the headscarp and the main slide mass is now filled with extensive rockfall debris. The magnitude of rockfall activity is linked to local precipitation (D. & R. Kelly, pers. comm. 2017).

The lower section of the slide mass comprises a mix of Tertiary marine rocks weathered Torlesse and Torlesse-derived colluvium. The former failed as a series of discrete blocks, bounded by fracture and bedding plane discontinuities. A subsequently wet winter has resulted in this material slaking and being remobilized in places as debris flows.

The geometry for the slide mass is controlled by the interaction of the surface-rupturing fault planes, bedding within the Torlesse basement, and the regional tectonically-controlled joint sets. The main headscarp is formed by the intersection of the Mount Stewart/

Woodchester fault structure and the local bedding attitude in the Torlesse. From the geomorphology of the intact blocks within the main slide mass it appears that there is little or no overall rotation. Thus the basal slip plane is inferred to be a planar surface allowing predominantly translation. The toe of the slide mass is coincident with the thrust fault running parallel to the Leader River (Fig. 3). The toe of the slide is a chaotic blocky zone within the Greta Siltstone and weathered Torlesse greywacke. The disaggregated nature of this part of the landslide is a function of the poor rock mass quality (highly fractures, thinly bedded, and weakly bonded) of the siltstone. The weathered greywacke shows similar rock mass quality. The thrust fault at the toe of the landslide is coincident with a broader bedrock fault zone. The recent rupture uses a combination of the bedrock fault and layer-parallel slip to develop the observed curvilinear geometry. Recently exposed bedrock exposures, created by a series of outburst floods as Lake Rebekah and a lower 'stilling basin' lake have overtopped and down cut through the slide mass, show the fault zone to be a series of steeply dipping planes and cataclastic zones striking approximately 070°. This is flanked by fractures with spacing of 0.5–2.0 m.

2.1.2 Leader River Terrace Landslides

The terrace margin along the southern side of the Leader River shows evidence of ongoing slope instability. Several generations of landslides are evident from the 'bite mark' edge of the terrace margin (Fig. 3). At the western end of the terrace the Kaikōura earthquake has triggered renewed movement on a planar block slide, creating a head scarp up to 4 m high. This scarp is fronted by a series of open fissures and a small graben-like structure. This linear scarp is approximately parallel to the Mount Stewart thrust fault, but truncates several WNW-trending fault traces crossing the Woodchester terrace surface (Fig. 3). A series of uphill facing scraps on the downslope part of the slope indicates sacking or toppling failure. The headscarp was an existing feature, marked by a prominent step in the terrace surface (D. Kelly, pers. comm., 2017). The western margin of the slide is bounded by the main trace of the Humps fault as it extends west from Woodchester (Fig. 3).

2.1.3 Eastern Stanton River Tributary Landslides

South of Woodchester, the South Leader Fault runs north-south and crosses an area of undulating topography (Fig. 3). This section of the fault rupture displays predominantly dip-slip behavior, with a mix of reverse and normal offset. The former also include a component of left-lateral displacement, as would be expected by the regional tectonics. The latter is a manifestation of hanging wall deformation above a blind reverse fault. This deformation creates a broad damage zone, with the amount of displacement varying from

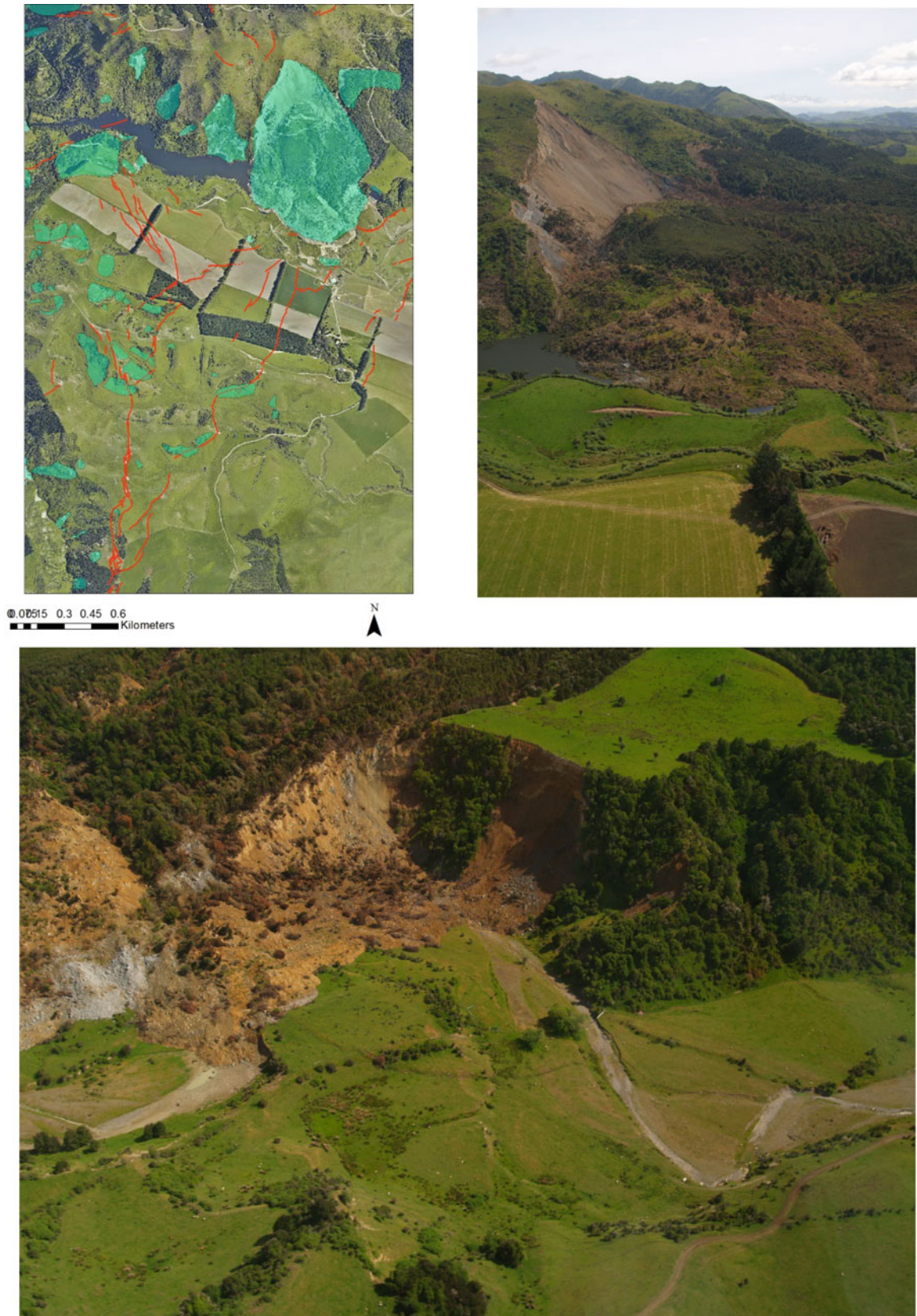


Fig. 3 Landslides and surface rupturing faults at Woodchester Station, Hurunui District. Top Left: Orthophoto showing the faults (red) and major landslides (green). The Mount Stewart landslide that dammed the Leader River forming Lake Rebekah is the largest slide mass. Top

Right: The headscarp of the Mount Stewart Landslide. Lower: Toe of the Mount Stewart Landslide. Note the curvilinear reverse surface rupture disappearing into the slide mass center-left

as much as 3.5 m to less than 0.1 m on individual fault traces. In addition, the displacement on individual traces varies significantly along strike. This section of the fault runs through an extensive zone of slope movement. In a number of areas it becomes difficult to distinguish fault related ground deformation from ground disturbance resulting from slope movement. As well as issues for fault location, this also raises uncertainty in the determination of fault slip at any one location. The location of fault traces is important for local planning regulations in New Zealand (Kerr et al. 2003).

The linking faults between the northern end of the South Leader fault and the Woodchester Terrace fault traces traverse an area of undulating topography where most slopes are affected by shallow landslides occurring at the colluvium-bedrock contact. The morphology of many of these slides mimic the fault related features noted elsewhere. In particular the toe regions of these slope failures display ground deformation that is difficult to distinguish from low angle reverse faulting (Cotton 1999).

The largest fault trace along the South Leader fault, the 3.5 m high 'Waiiau Wall' terminates at its northern end as a series of fault splays, forming a damage zone up to 100 m wide. This is coincident with a zone of shallow slope movement on a south-facing hillside. At this location it is not clear whether the observed surface deformation is reflective of differential movement within a shallow landslide, or whether the fault has ruptured through and reactivated an existing landslide.

To the South, the South Leader fault trace drops into an eastern tributary of the Stanton River. This north-south trending valley has steep sides incised into the softer Tertiary marine cover rocks. The valley walls have been affected by a large number of slope failures, including rotational failures, large volume rockfalls and slumps (complex failure mechanism or failure mechanism not clear). To date mapping of the fault trace along this section of the fault has been problematic, as the suspected fault trace location along the valley floor is coincident with the toes of several landslides. The reverse and reverse-oblique displacement along this section of the fault produces similar ground deformation to the contractional toe regions of many of these landslides

2.2 Glenbourne Farm Landslides

At Glenbourne Farm the ENE Emu Plain-Humps fault moves from the subdued topography of the northern part of the Amuri Plain to the upland of The Humps (Fig. 4). The fault changes from being predominantly right-lateral strike-slip to reverse, north side up. This is coincident with a subtle fault bend. At this point the fault zone increases in width and, combined with the local topography, indicates that Glenbourne is the locus of a releasing fault bend. At this

location the fault zone is approximately 1.1 km wide. This is also the locus of extensive landsliding. In this area there is a mix of incipient slope failure (open fissures, and rockfall/toppling) in an area with evidence for past slope movement (hummocky ground; debris fans). The open fissures are coincident with or parallel the local surface-rupturing fault trends. The mechanism of landsliding at this location has not been investigated in detail, however the straight map traces of the fissures across areas of irregular topography indicates that the detachment planes are steep to vertical and planar in nature. It is inferred that the extensive localized fracturing of the bedrock within the area as a result of the fault geometry leads to a relatively disaggregated, weak rock mass, which coupled with the sudden steepening of the topography, results in enhanced landsliding.

2.3 Conway-Charwell Fault Landslides

Immediately to the west of the Conway River, the NE North Leader fault connects with the Conway-Charwell fault. This ENE fault rupture segment extends for about 4 km and shows predominantly reverse (up to 1.7 m up-to-the-north) displacement with a subordinate right-lateral component. This fault trace runs parallel to the main trace of the Hope fault, the major right-lateral plate boundary fault in the region. Although there was no recognized displacement on the Hope fault at this location, the Conway-Charwell fault dips steeply to the northwest, and therefore likely merges with the Hope fault at a relatively shallow depth. Where the Hope and Conway-Charwell faults cross the Conway River a series of landslides have been triggered in both bedrock and the overlying outwash gravels (Fig. 5). As the fault crosses the river the mapped traces indicate a narrow left-step in the fault geometry. On the western bank of the river a planar slump failure has detached along one of the main traces of the Hope fault (Fig. 5). The headscarp is a planar detachment trending ENE. Along the east bank of the surface rupture on the Conway-Charwell fault acts as a detachment for a series of planar slides and topples within the terrace gravels and the underlying Torlesse bedrock. Movement on these slopes has given rise to accentuated vertical expression along a number of fault traces.

3 Fault Control on Landslide Geometry and Landslide/Fault Recognition

From this preliminary investigation of landslides related to the Kaikōura earthquake it is clear that bedrock geometry controls the mechanism and extent of deeper-seated landslides. The discontinuity geometry is a function of the tectonic history, and in the near fault environment, the

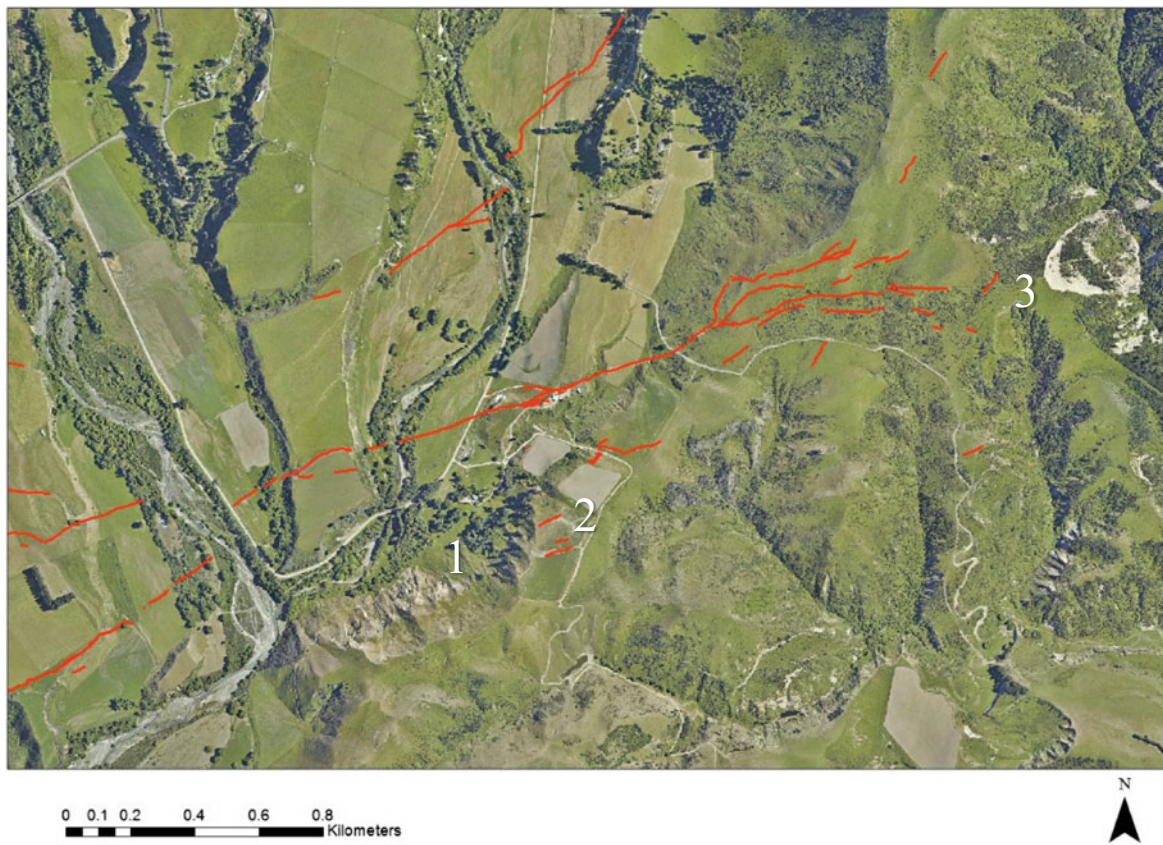


Fig. 4 Landslides and surface rupturing faults at Glenbourne Farm, Hurunui District. Top: Orthophoto showing the fault rupture (red). Areas of major slope movement are numbered. 1: incipient failure, open fissuring and dilated rock mass. Fissures subparallel to the fault traces.

2: shallow failure at the bedrock-colluvium contact bounded by fault traces. 3: deep-seated rotational failure bounded by surface fault traces. Bottom: View looking NE across Glenbourne showing reactivated landslide in the foreground

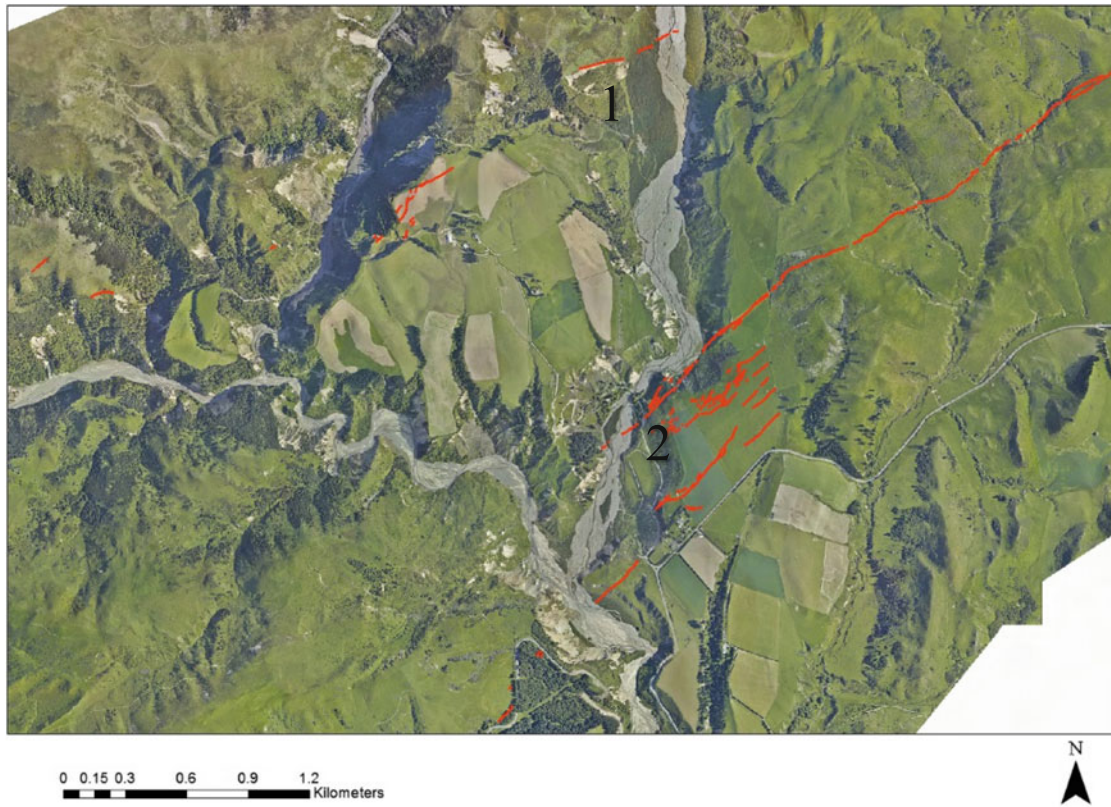


Fig. 5 Landslides and surface rupturing faults at Conway Station. Top: Orthophoto showing the fault rupture (red). Areas of major slope movement are numbered. 1: The Cloudy Range landslide detached along a trace of the Hope fault. No surface faulting was found on the

Hope fault at this location. 2: broad complex zone of landsliding coincident with a prominent left step in the Conway-Charwell fault. Bottom: View looking SW across the Conway river to the Cloudy Range landslide. The headscarp is a trace of the Hope fault

frequency and geometry of fault-related discontinuities are the predominant controlling features. In immediate near-fault locations, within the surface faulting damage zone, the main fault rupture plane acts as a slip plane or releasing structure.

In other areas, the bedrock fault propagates through overlying colluvial and fluvial materials and controls the extent and style of shallower soil slope failures. In these areas it can be difficult to distinguish between fault-related and landslide-induced ground deformation. Although the criteria of Cotton (1999) can be useful for distinguishing between the two, the complex nature of faulting though much of the region, especially in fault linking regions such as Woodchester where there may be a mix of both dip-slip and lateral fault movement, often partitioned onto adjacent fault traces, makes this somewhat problematic. The failure to distinguish between the two can lead to misidentification of hazards, and the potential to misrepresent tectonic strain. This has implications for local hazard planning (fault avoidance zones) and seismic hazard source characterization and modelling.

4 Conclusions

The Kaikōura earthquake triggered a multitude of landslides over an extensive region of the upper South Island New Zealand. In the immediate vicinity of the fault rupture it is noted that the primary fault rupture, the broader fault damage zone, and a number of fault related discontinuities are involved in the slip surfaces or other releasing structures in a number of earthquake-triggered landslides. These include first-time and reactivated failures. The former are mainly in bedrock while the latter are predominantly soil slope failures occurring at rock head. The close spatial association of many landslides with the surface rupture leads to difficulty in accurately distinguishing the contribution of fault deformation from ground disruption resulting from slope movement. This has implications for fault hazard mitigation in terms of determining fault avoidance zones and also in fault characterization for seismic hazard modelling. The proximity of many of the larger landslides to the 2016 surface fault rupture (Dellow et al. 2017) will also bear careful examination. Parametric studies investigating fault-landslide distance and the influence on other landslide parameters including geometry, including depth to slip plane, and landslide magnitude-frequency relationships will hopefully lead to

greater understanding of the hazard posed by earthquake-triggered landsliding in alpine terrain.

Acknowledgements The field data for this study is part of the Kaikōura earthquake response effort involving a large team of postgraduate students and researchers from the Department of Geological Sciences, University of Canterbury. Narges Khajavi has been generous with her time and knowledge of all things tectonic and geospatial. The many farmers and landowners across North Canterbury have been extremely supportive and generous in allowing us access to their property. David and Rebekah Kelly at Woodchester Station and Grant and Cheryl Barbara at Glenbourne are especially thanked for allowing extended access during a period of protracted adversity.

References

- Bradley, B.A., Razafindrakoto, H.N.T., Ahsan Nazer, M.: Strong ground motion observations of engineering interest from the 14th November 2016 Mw 7.8 Kaikōura, New Zealand earthquake. *Bull. NZ Soc. Earthq. Eng.* **50**(2), 85–93 (2017)
- Cotton, W.: Faults aren't always what they're cracked up to be. In: Hanson, K.L., Kelson, K.I., Angell, M.A., Lettis, W.R. (eds.) *Techniques for Identifying Faults and Determining Their Origins*, U.S. Nuclear Regulatory Commission NUREG Report NUREG/CR-5503, pp. A-27–A-50 (1999)
- Dellow, S., Massey, C., Cox, S., Archibald, G., Begg, J., Bruce, Z., Carey, J., Davidson, J., Della Pasqua, F., Glassey, P., Hill, M., Jones, K., Lyndsell, B., Lukovic, B., McColl, S., Rattenbury, M., Read, S., Rosser, B., Singeisen, C., Townsend, D., Villamor, P., Villeneuve, M., Godt, J., Jibson, R., Allstadt, K., Rengers, F., Wartman, J., Rathje, E., Sitar, N., Adda, A.-Z., Manousakis, J., Little, M.: Landslides caused by the 14 November 2016 Mw 7.8 Kaikōura earthquake and the immediate response. *Bull. NZ Soc. Earthq. Eng.* **50**(2), 106–116 (2017)
- Kerr, J., Nathan, S., Van Dissen, R., Webb, P., Brunson, D., King, A.: Planning for development of land on or close to active faults: a guideline to assist resource management planners in New Zealand. Client report 2002/124 Rep., 67 p. Institute of Geological & Nuclear Sciences (2003)
- Stirling, M.W., Litchfield, N.J., Villamor, P., Van Dissen, R.J., Nicol, A., Pettinga, J., Barnes, P., Langridge, R.M., Little, T., Barrell, D.J.A., Mountjoy, J., Ries, W.F., Rowland, J., Fenton, C., Hamling, I., Asher, C., Barrier, A., Benson, A., Bischoff, A., Borella, J., Carne, R., Cochran, U.A., Cockroft, M., Cox, S.C., Duke, G., Fenton, F., Gasston, C., Grimshaw, C., Hale, D., Hall, B., Hao, K.X., Hatem, A., Hemphill-Haley, M., Heron, D.W., Howarth, J., Juniper, Z., Kane, T., Kearsse, J., Khajavi, N., Lamarche, G., Lawson, S., Lukovic, B., Madugo, C., Manousakis, I., McColl, S., Noble, D., Pedley, K., Sauer, K., Stahl, T., Strong, D.T., Townsend, D.B., Toy, V., Villeneuve, M., Wandres, A., Williams, J., Woelz, S., Zinke, R.: The Mw 7.8 2016 Kaikōura earthquake: Surface fault rupture and seismic hazard context. *Bull. NZ Soc. Earthq. Eng.* **50**(2), 73–84 (2017)

Part II
Land Subsidence

Revealing Sinkholes of Karst-Suffosion Origin in Moscow

Irina Kozliakova, Aleksandr Anikeev, Olga Eremina,
and Natalia Ustinova

Abstract

Nearly thirty ground collapses were registered in the northwestern district of Moscow in 1960–1970s. These catastrophic phenomena were triggered by the intense technogenic intake of groundwater from the Carboniferous aquifer, which caused the downward migration of Quaternary sand to the underlying karstified limestone of Carboniferous age. Since those years, the northwestern district of Moscow has been considered to be particularly prone to karst-suffosion phenomena. IEG RAS has collected a substantial database on sinkholes of different origin that occurred in Moscow since the early 20th century. Using this database, we attempted to identify sinkholes of karst-suffosion origin in other districts of Moscow. Our research procedure included the following stages: analysis of engineering geological conditions around the sinkholes using the borehole data obtained in different years and stored in the IEG RAS database; calculation of possible sinkhole diameter using the original computational models; comparison of calculated to actual sinkhole diameters. This approach permitted us to identify the collapses in the historical center of Moscow as of karst-suffosion origin. This unexpected conclusion contradicts with the former boundaries of regions showing the different degree of karst-suffosion hazard outlined on engineering geological maps earlier.

Keywords

Karstic sinkholes • Karst and suffosion
Collapses and surface subsidence • Urban areas

1 Introduction. Collapses and Ground Subsidence in Moscow

Cases of collapses and ground subsidence in Moscow are the manifestation of suffosion process, which develops in the water-saturated sand lying at the top of the geological cross-section. The downward suffosional transportation of sand may arise from both technogenic and natural reasons: it may develop at the contact between the walls of improperly sealed subsurface facilities and a ground massif (technogenic suffosion); it may also go along natural fissures into karst cavities in the underlying limestone (the so-called karst-suffosion process). At the preliminary stage of sinkhole development, the decompaction zone forms in sand. This zone may stay in the massif for a long time until some external factors disturb its equilibrium to make the massif unstable. The intense water percolation upon snow melting and heavy rains is one of such factors. Most of ground deformations are known to happen in Moscow in spring and summer.

Human-induced (technogenic) suffosion disturbs a loose soil structure in a relatively small ground volume, i.e., in the immediate vicinity of the subsurface engineering facility; whereas the natural karst-suffosion process spreads over the entire sandy-clayey massif covering a karst cavity or a karstified zone in the limestone massif. It appears rather difficult to tell karst-induced collapses in the area of covered karst from the collapses of other kind. However, it is very important to outline the zones of intensified karst-suffosion in the city in order to assess the risk of probable economic loss and to set special requirements and constraints on the urban territory use.

I. Kozliakova (✉) · A. Anikeev · O. Eremina · N. Ustinova
Sergeev Institute of Environmental Geoscience RAS, Ulansky
Lane 13, Moscow, Russia
e-mail: sci-council@geoenvironment.ru

2 The Registered Cases of Karst-Suffosion in Moscow

In 1960–1970s, about 30 large collapses happened in the northwest of Moscow. Some of them resulted in deformations and ruining of buildings. Many researchers (Anikeev 2002; Khomenko et al. 1986; Kozliakova et al. 2015; Kutepov and Kozhevnikova 1989; Kutepov et al. 2011) studied these collapses comprehensively. Numerous boreholes were drilled through the sandy-clayey horizons overlying the karstified Carboniferous limestone massif to penetrate the latter for more than 10 m. The composition, state, and properties of rocks were studied in detail. Several generations of river erosion influenced the geological features at the sites subjected to karstic collapses, i.e., preJurassic, preQuaternary and modern river networks are superposed at these sites (Fig. 1). The buried surface of

karstified terrigenous-carbonate Carboniferous deposits is very rugged, and the stratigraphy and lithology of the overlying Meso-Cenozoic sandy-clayey horizons vary significantly by the depth and the strike.

These collapses are considered to result from the intensified karst-suffosion due to the intense technogenic water intake from the Carboniferous aquifer. In general, karst-suffosion process involves the destruction of impermeable Jurassic clay dividing the Quaternary groundwater aquifer from the confined Carboniferous aquifer under the impact of hydrodynamic pressure and the inflow of sand to the underlying karstic limestone. In the areas with no Jurassic clay divide (where the sand layers overlie the limestone massif immediately), the sand is washed out directly to karstic cavities and fractures.

Since 1970s, the assessment of karst-suffosion hazard has become an obligatory requirement upon civil construction in

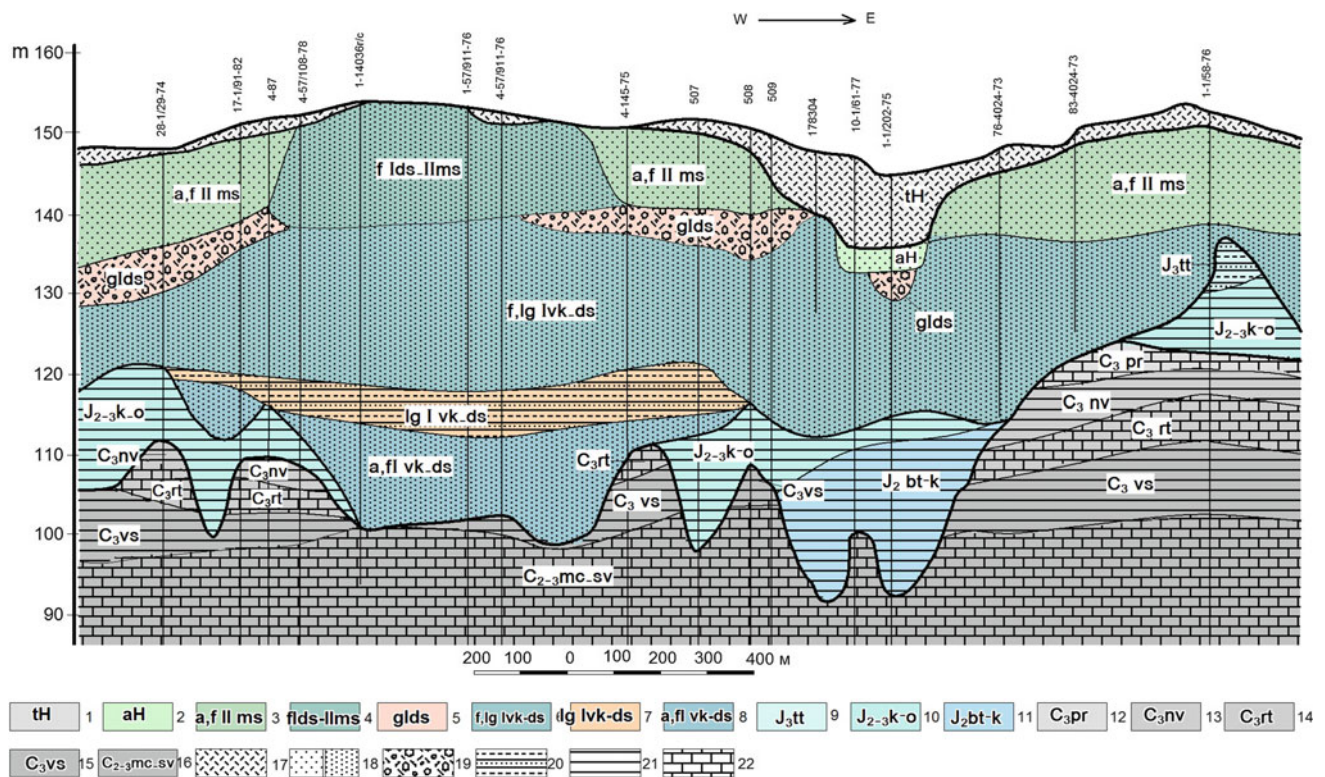


Fig. 1 Geological cross-section in the northwest of Moscow. Holocene: 1—technogenic deposits; 2—alluvial deposits of river channel and flood-plain; Middle Neopleistocene: 3—alluvial-fluvioglacial deposits of the 3rd terrace above the floodplain (Khodynskaya terrace); interglacial deposits of Donskoi-Moskovskii horizons: 4—fluvioglacial deposits of Donskoi horizon; 5—glacial deposits of Donskoi horizon; 6—fluvioglacial and lacustrine-glacial deposits; 7—lacustrine-glacial deposits; 8—alluvial and fluvioglacial deposits. Jurassic system. Upper series: 9—Tithonian stage; Middle-Upper series undivided: 10—

Callovian and Oxfordian stages. Middle series: 11—Bathonian and Callovian stages undivided. Carboniferous system. Upper series. Kasimovian stage. Dorogomilovskii horizon: 12—Perkhorovskii massif; Khamovnicheskii horizon: 13—Neverovskii massif; 14—Ratimirovskii horizon; 15—Voskresenskii massif; Middle and Lower series undivided: 16—Moscovian stage and Suvorovskii horizon. Lithology: 17—fill; 18—sand; 19—loam with gravel; 20—interbedding sandy loam, loam and sand; 21—clay and loam; 22—limestone

Moscow. In 1984, “The guide on projecting buildings and engineering structures in the Moscow districts prone to karst and suffosion” was published (GlavAPU 1984). This Guide sets three main criteria of the karst-suffosion hazard: (1) the registered cases of actual collapses and ground subsidence, (2) the thickness of impermeable clay layer less than 10 m (or its absence), and (3) the gradient of the downward seepage of groundwater through the impermeable clay divide more than 3 (dimensionless value). The mathematical methods for calculating the probable diameters of possible karst-suffosion sinkholes are developed by Russian experts (Anikeev 2002, 2006, 2012; Khomenko et al. 1986).

In 1987, a large sinkhole was registered in the Tukhachevskii street in the northwest of Moscow. It was drilled by boreholes in detail and it was identified to be of karst-suffosion origin. However, this sinkhole was the last one studied and known to be induced by the presence of karstic limestone deposits in Moscow. Since then, although ground collapses happened regularly not only in the northwestern district but also in other regions of Moscow, they were not studied by engineering geologists.

3 Karst-Suffosion Hazard

Three categories of karst-suffosion hazard are distinguished in Moscow: (1) hazardous category covers areas, where the collapses of karst-suffosion genesis are registered; (2) potentially hazardous category outlines regions, where no collapses are registered but they are possible; and (3) regions of nonhazardous category, where collapses are almost excluded. Within these regions of non-hazardous category, the karstified carbonate rocks are separated from the overlying sand by a clay layer thicker than 10 m. The maps of karst-suffosion hazard show the distribution of three categories of karst-suffosion hazard by the Moscow territory. Different researchers built the maps of this kind to a scale 1:50,000 and smaller (Osipov and Medvedev 1997). In 2009, we compiled the large-scale map of karst-suffosion hazard (a scale of 1:10,000) for the whole Moscow territory on the basis of processing a huge amount of archive borehole data. In this map, the regions of hazardous category cover about 1% of the entire city territory, and that of potentially hazardous category, 16% (Kutepov et al. 2011).

Most researchers, who come across the problem of assessing the hazard of karst-related collapses in Moscow, ask the question: “Why did these collapses happen only in the northwest of the city and why did not they happen






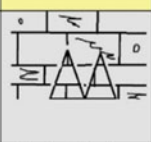

anymore after 1987?” However, the most probable explanation of this paradox is that the sinkholes were not studied any longer after 1987. In order to resume the normal operation of urban facilities, the municipal services have to backfill quickly the newly formed sinkholes. Sinkholes were not analyzed in 1990s–2000s because of the lacking city budget, since drilling deep boreholes (which could penetrate the karstified Carboniferous massif) as well as geophysical survey, etc., are rather costly measures. However, the researchers at the Sergeev Institute of Environmental Geoscience RAS (IEG RAS) have compiled a digital computer database of spatially linked boreholes supplemented by the scanned copies of original borehole records. This database helps us to obtain comprehensive information about the geological structure of the collapsing site without carrying out any special field investigations and observations. We have also collected many data about sinkholes starting from the beginning of the 20th century until nowadays. This allows us to perform the retrospective analysis of some collapse sites in order to classify their genesis.

4 Cases of Karst-Suffosion Collapses

We tried to recognize the cases of karst-suffosion sinkholes in the Moscow districts, which are regarded as potentially hazardous areas. This research included the following steps: (1) study of engineering geological conditions around the collapse proceeding from the analysis of the nearest boreholes of different years stored in the geoinformational database at IEG RAS; (2) calculation of the probable diameter of karst-suffosion sinkhole using special models; (3) comparison of the calculated to the actual sinkhole diameter.

We investigated 23 collapses that happened in the Moscow center in 2011–2015 and that were not induced by any obvious technogenic reasons. In nine cases, we managed to get the reliable engineering geological data from the neighbor archive boreholes. For these sinkholes, the effective diameters were calculated using the mathematical models developed by Dr. A. V. Anikeev for the coherent and incoherent soils overlying the weak rock massif (Anikeev 2006, 2012). In five cases, the calculated diameters almost coincided with the actual sizes of sinkholes. Taking into account that asphalt pavement prevents the natural development of the karst-suffosion process and usually reduces the diameter of the surface sinkhole (as compared to that of the cavity beneath the roadbed pavement), we adopted up to

Fig. 2 Summary geological column of the collapse site in the Balchug street (November 27, 2014), compiled by the archive data

Age		Thickness, m	Lithology
tH		3,0	Brown sandy loam, with admixture of sand and fragments of concrete, bricks, and wood chips, compressed, wet
		1,0	Brownish dark gray loam, with admixture of sand, gruss, and wood chips, compressed, wet.
aH		1,0	Yellowish brown sandy loam, with frequent sand interlayers, plastic, wet
		1,0	Dark brown loam with sand interlayers, ferrugination mottles, soft plastic
		6,0	Brown sand of medium particle size, with sandy loam interlayers, gruss and gravel, low dense, water saturated, with phosphorite pebble in the foot of the horizon
C3pr		0,8	Yellowish and light gray limestone, dolomitized, ruined to powder and gruss, with the admixture of Quaternary sand, of low strength, aquiferous
		0,9	Light gray and yellowish limestone, dolomitized, highly fractured, of low strength, aquiferous

30% allowed error for the calculated and actual sinkhole diameters.

In addition to calculation, we have analyzed the lithology in borehole records thoroughly in order to find any signs of suffusion development in the sandy massif. These signs may involve the presence of decompacted zones in a sandy massif or the admixture of Quaternary sand in the filler of karst cavities. See, for example, the case of collapse site in the Balchug street, Moscow (Fig. 2). In addition, a thick layer of technogenous deposits in this site may witness in favor of now backfilled former sinkholes and ground subsidence there. In the roof of carbonate massif of Carboniferous age, limestone is usually disintegrated or highly

fractured. A rock massif contains fragmentary zones of various size (stretching for 1–10 and more m), voids and fractures. The carbonate massif structure is favorable for the possible suffosional inflow of sand there. No large cavities are registered in the carbonate massif.

We found that sinkholes of karst-suffosion origin are associated with the floodplain and the terraces of the Moscow River, where the ancient buried preQuaternary river network is traced (Fig. 2). Natural hydrogeological conditions have been transformed there by engineering water drawdown. As a matter of fact, the engineering geological conditions in this site are very close to those in the northwest of Moscow (Fig. 3).

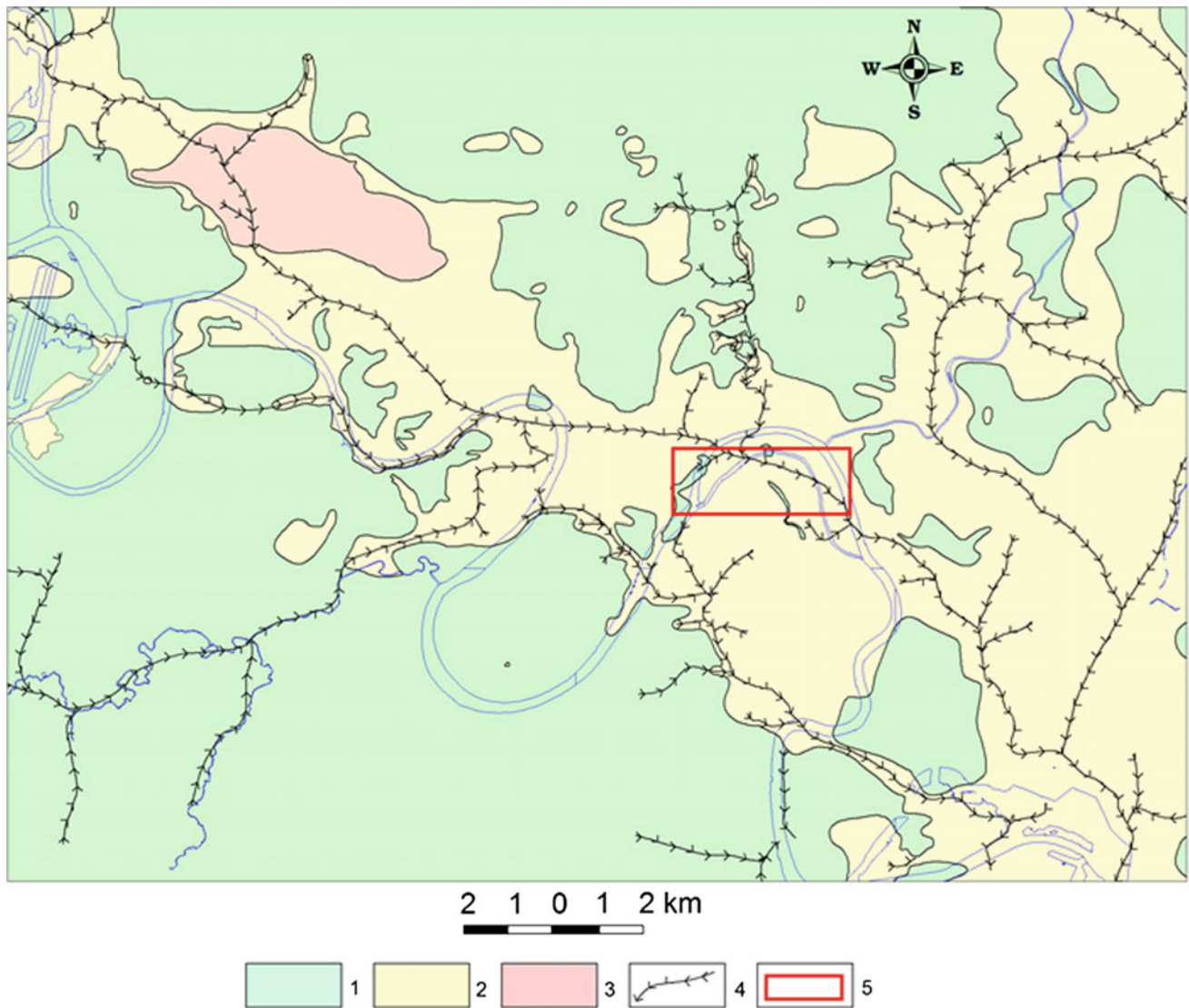


Fig. 3 Fragment of the map of karst-suffosional hazard in Moscow. Designations: hazard categories: 1—nonhazardous, 2—potentially hazardous, 3—hazardous. Other designations: 4—thalwegs of

pre-Quaternary buried river channels; 5—the site of newly registered sinkholes of karst-suffosion genesis

5 Conclusion

The research proved that cases of surface collapses and ground subsidence in Moscow may be successfully investigated using the archive geological data stored in GIS database. Our investigation allowed us to reveal and to outline one more karst-suffosion-prone district in Moscow, in addition to the northwestern district known as hazardous earlier. For experts in assessing geological hazards in Moscow this result may appear to be rather unexpected and even disputable. It impels us to revise the boundaries of hazard categories in the maps, which are used now in engineering

geological survey. Further studies in this direction, for sure, will reveal other sinkholes of karst-suffosion genesis in Moscow.

Acknowledgements This study was supported by the Russian Science Foundation, project no. 16-17-00125.

References

- Anikeev, A.V.: The causes of collapses and local surface subsidence in Moscow. *Geokologiya (Environ. Geosci.)* **4**, 363–374 (2002)
- Anikeev, A.V.: Suffosion. Mechanism and kinematics of free suffosion. *Geokologiya (Environ. Geosci.)* **6**, 544–553 (2006)

- Anikeev, A.V.: Geomechanical aspects of karst-suffosion process. In: Workshop on the Problems in Engineering Karstology, Dzerzhinsk, 4–5 Oct 2012. IGIS Publications, Dzerzhinsk, pp. 72–81 (2012)
- GlavAPU.: The Guide on Projecting Buildings and Engineering Structures in Moscow Districts Prone to Karst and Suffosion, Moscow, Mosgorispolkom, GlavAPU, Mosproekt-1, Mosgor-geotrest, 15p (1984)
- Khomenko, V.P.: Karst-Suffosional Processes and Their Prediction. Moscow, Nauka, 97p (1986)
- Kozliakova, I.V., Kozhevnikova, I.A., Anisimova, N.G.: Collapses and surface subsidence in Moscow. In: Proceedings of Sergeev's Readings (The Annual Session of Scientific Council RAS in Environmental Geoscience, Engineering Geology and Hydrogeology), 23–24 Mar 2015, no. 17. RUDN Publications, Moscow, pp. 259–265 (2015)
- Kutepov, V.M., Kozhevnikova, V.N.: Stability of Karstified Territories. Moscow, Nauka, 151p (1989)
- Kutepov, V.M., Kozliakova, I.V., Anisimova, N.G., Eremina, O.N., Kozhevnikova, I.A.: Assessment of karst and suffosional hazard in the project of large-scale geological mapping of Moscow. *Geoekologiya (Environ. Geosci.)* **3**, 215–226 (2011)
- Osipov, V.I., Medvedev, O.P.: (eds.) Moscow: Geology and The City. Moscow, Moskovskie uchebniki i kartolitografiya, 398p (1997)

Addressing Subsidence in Bangkok, Thailand and Houston, Texas: Scientific Comparisons and Data-Driven Groundwater Policies for Coastal Land-Surface Subsidence

Aranya Fuangswasdi, Surin Worakijthamrong, and Sachin D. Shah

Abstract

Land subsidence in coastal regions of the world is a common occurrence. In large metropolitan areas such as Bangkok, Thailand, and Houston, USA, land subsidence occurs as a direct result of groundwater withdrawals for municipal supply, industrial use, and irrigation that depressurize and dewater aquifers. The impacts of subsidence are exacerbated in both cities because of flat, low-lying topography and the presence of unconsolidated clay layers that exist in the aquifer sediments and are prone to compaction. The compaction of these sediments leads to land-surface subsidence, which increases flooding risk and leads to infrastructure and engineering problems. The aquifers in Bangkok are divided into 8 water-bearing units with the Upper Bangkok aquifer (20–30 m thick) being the principal aquifer. In the Houston region, two primary aquifers, the Chicot and Evangeline aquifers (200 and 500 m thick, respectively), comprise the Gulf Coast aquifer system and are susceptible to compaction, with 111.13 cm (1974–2017) and 47.98 cm (1973–2017) of cumulative compaction recorded at the Addicks and Seabrook extensometers, respectively. In both cases, compaction in the aquifer-systems has occurred for decades as groundwater levels declined. Scientific advancements in data collection, analysis, and communication have helped policymakers implement various management strategies with groundwater use becoming even more crucial as population increases. Both the Thailand Department of Groundwater Resources and U.S. Geological Survey have more than 40 years of subsidence data to compare how data is collected and

analyzed within their respective areas. This paper will illustrate scientific efforts to study subsidence in Bangkok and Houston by correlating data of long-term groundwater withdrawals and cumulative sediment compaction and then comparing resulting policy changes.

Keywords

Subsidence • Aquifer • Compaction • Bangkok • Houston

1 Introduction

Both Bangkok and Houston rank among their respective country's largest metropolitan areas. Permanent subsidence has occurred in both cities following decades of heavy groundwater pumping for agricultural, industrial, and municipal use. Though in different parts of the world, land subsidence is a challenging and costly urban hydrogeological hazard, with both regions addressing the issue differently from both scientific and policy perspectives. In general, the aquifers in Bangkok and Houston are comprised of multiple stratigraphically stacked sequences of clay and sand layers, and as groundwater is withdrawn, the entire aquifer compacts leading to a decrease in land-surface elevation, or subsidence. In coastal areas that have low topographic relief, this can permanently inundate an affected area or make it more flood-prone. Additionally, in inland areas, subsidence also changes preexisting surficial drainage patterns, making these areas susceptible to flooding. However, continued data collection, improvements in scientific techniques, and lessons learned from global cases have improved the understanding of the causes and effects of subsidence, leading to better approaches to construction practices, flood control, and regional policymaking.

A. Fuangswasdi (✉) · S. Worakijthamrong
Department of Groundwater Resources, Ministry of Natural Resources and Environment, Latyao, Chatuchak, Bangkok, 10900, Thailand
e-mail: aranya.f@dgr.mail.go.th

S. D. Shah
U.S. Geological Survey, Texas Water Science Center,
1505 Ferguson Lane, Austin, TX 78754, USA

2 Hydrogeologic Settings

2.1 Bangkok, Thailand

Bangkok is located in the Central plain of Thailand, known as the Lower Chao Phraya Basin (Fig. 1). The basin is comprised of Tertiary clastic sediments with fluvial and deltaic deposits. The Lower Chao Phraya basin is approximately 175 kilometers (km) wide and 200 km long. The surface formation is Holocene marine clay, known as the Bangkok Clay with thicknesses ranging from 20 to 30 meters (m). There are 8 confined sand and gravel aquifers in the basin interbedded with clay layers ranging from 5 to 20 m thick (Fig. 2). Most of the groundwater withdrawals in Bangkok are from three principal aquifers: Phra Pradang (PD), Nakhon Luang (NL) and Nonthaburi (NB) (100, 150 and 200 m below land surface (bls), respectively). Groundwater flows from Ayutthaya in the north through Bangkok to Samut Prakan in the south. Hydraulic properties vary between the PD, NL, and NB aquifers with average transmissivities of about 24, 17.2 and 19.2 m^2/day , respectively and specific storages of about 9.49×10^{-5} (PD), 9.58×10^{-5} (NL), and 2.44×10^{-5} (NB).

2.2 Houston, Texas

The Houston metropolitan area, is located in the southeastern part of coastal Texas in the United States of America, and encompasses about 28,490 square kilometers (km^2) (Fig. 3). The Chicot and Evangeline aquifers are part of the Gulf Coast aquifer system and are composed of unconsolidated and laterally discontinuous deposits of gravel, sand, silt, and clay. The youngest and uppermost aquifer, the Chicot aquifer, consists of Holocene- and Pleistocene-age sediments, and the older, underlying Evangeline aquifer consists of Pliocene- and Miocene-age sediments. The greatest thickness of the stacked sequences of sediments comprising the Chicot and Evangeline aquifers are located along the Gulf Coast and are as thick as about 366 m and about 1097 m, respectively (Fig. 4). The updip limit of the Chicot aquifer crops out closer to the coast than the Evangeline aquifer outcrop. These two aquifers are hydraulically connected without a confining unit separating them, and because of this hydraulic connection, water-level changes that occur in one aquifer can affect water levels in the adjoining aquifer (Kasmarek et al. 2009). Hydraulic properties of the Chicot aquifer do not differ appreciably from the

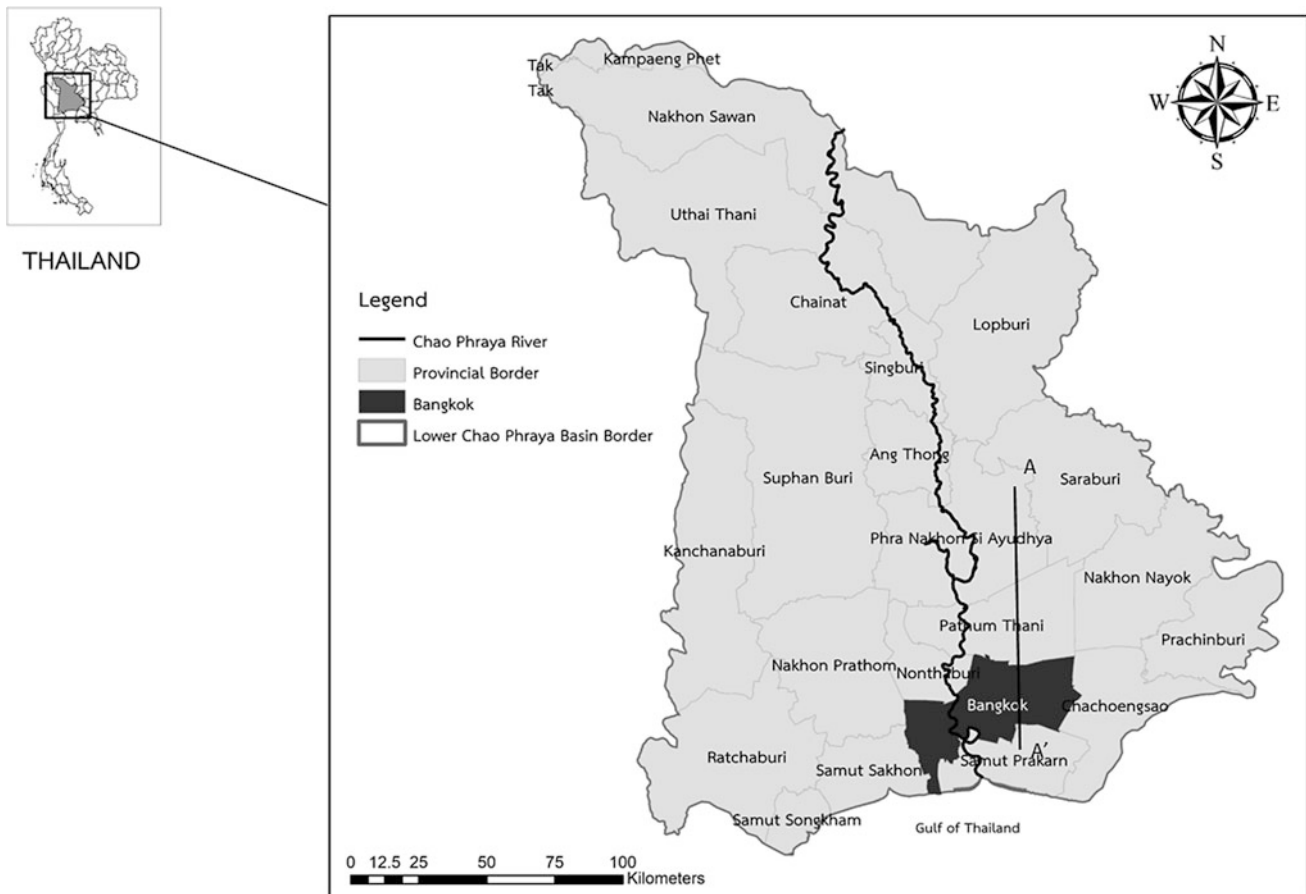


Fig. 1 Location of the Lower Chao Phraya Basin, Bangkok, Thailand

Fig. 2 Hydrogeologic cross-section of the eight aquifer systems (Ayutthaya to Samut Prakan), Bangkok, Thailand (modified from Ramnarong and Buapeng 1992). These depths refer to the approximate bases of each of the different aquifers

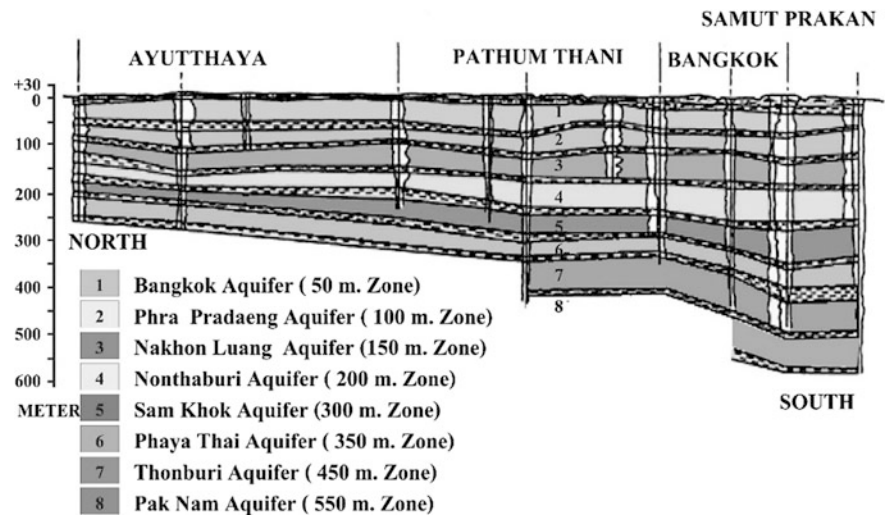
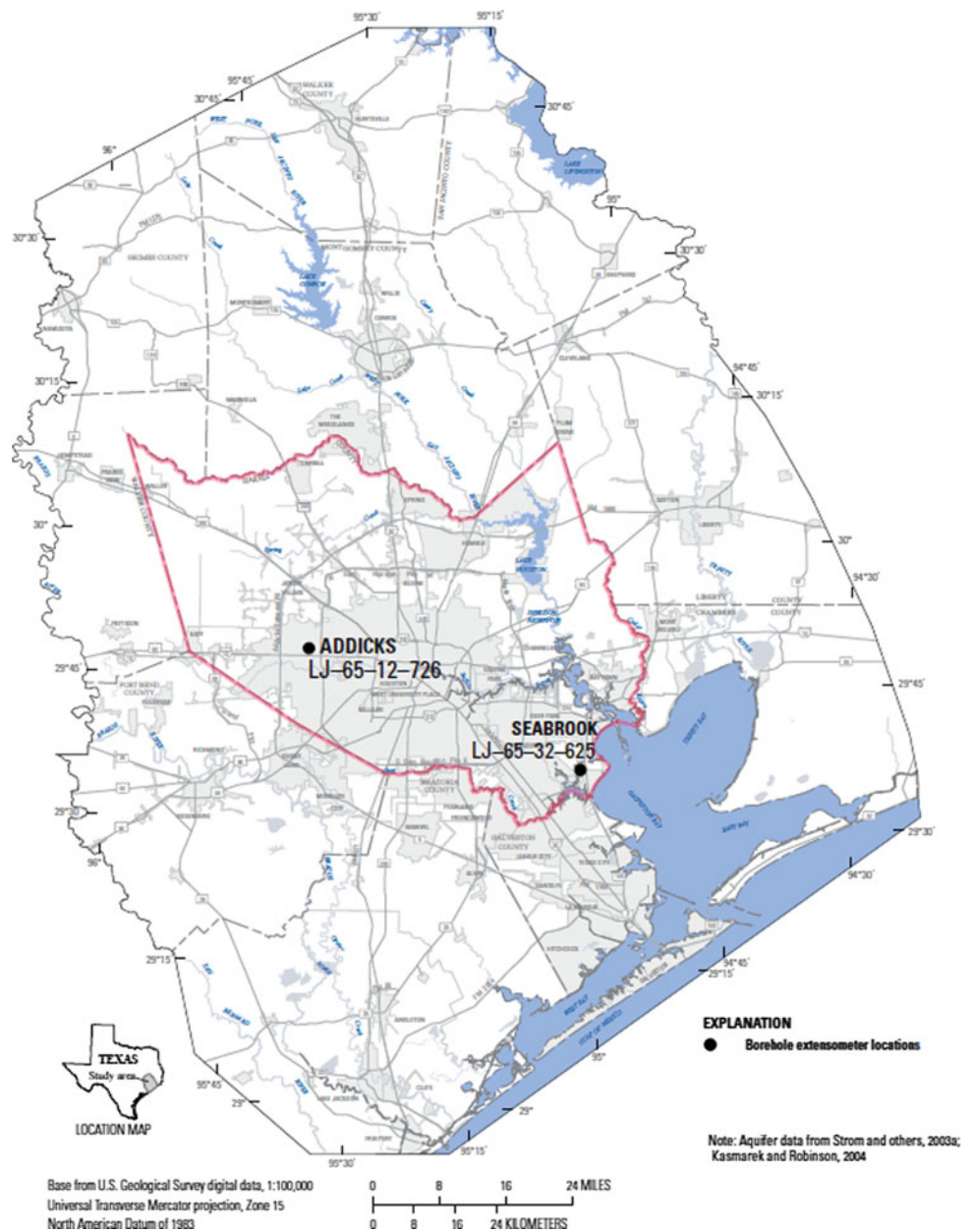


Fig. 3 Location of the Houston metropolitan area, Harris County, Texas, USA



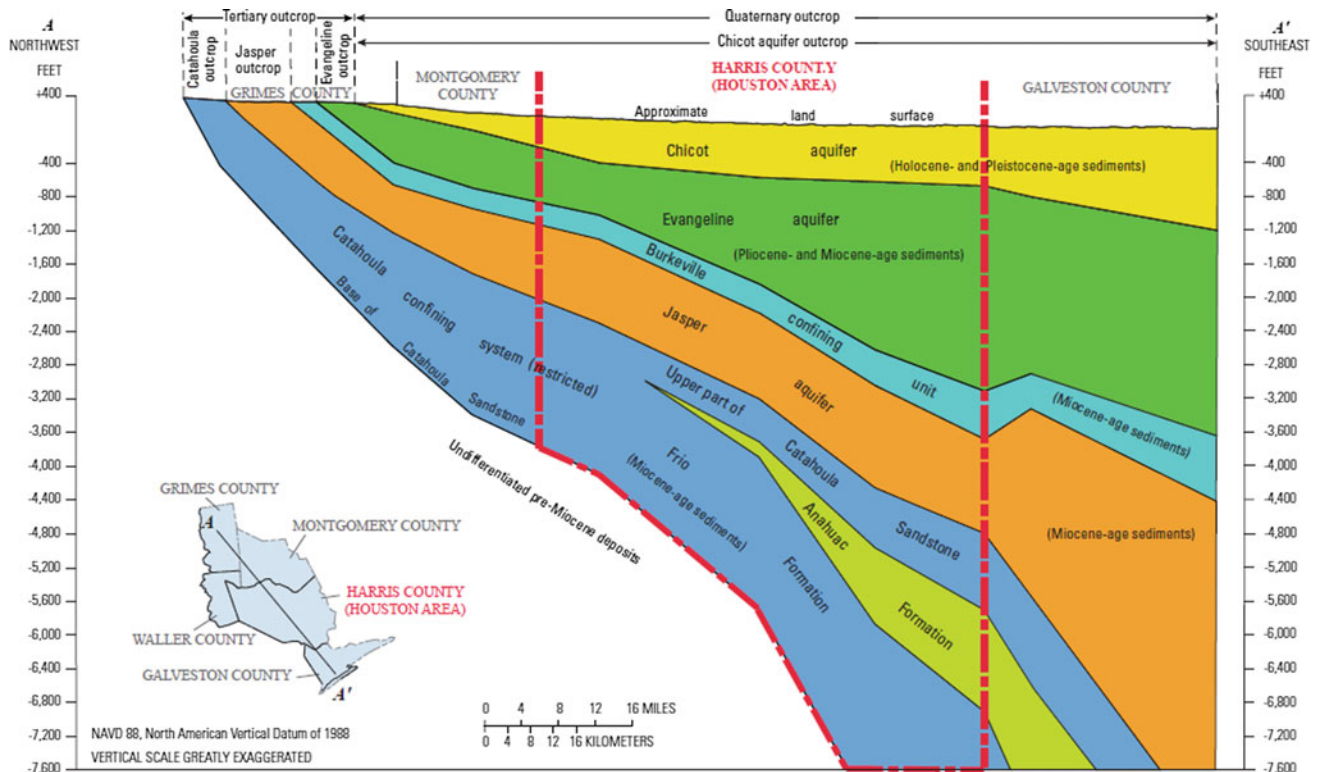


Fig. 4 Hydrogeologic section A–A' of the Gulf Coast aquifer; the area bound in red represents Harris County, which encompasses Houston, Texas (modified from Baker 1979)

hydrogeologically similar Evangeline aquifer. Aquifer-test data estimate that the transmissivity of the Chicot aquifer ranges from 280 to 2300 m²/day, and that the transmissivity of the Evangeline aquifer ranges from 280 to 1400 m²/day.

3 Historical and Current Subsidence and Compaction Issues

3.1 Bangkok, Thailand

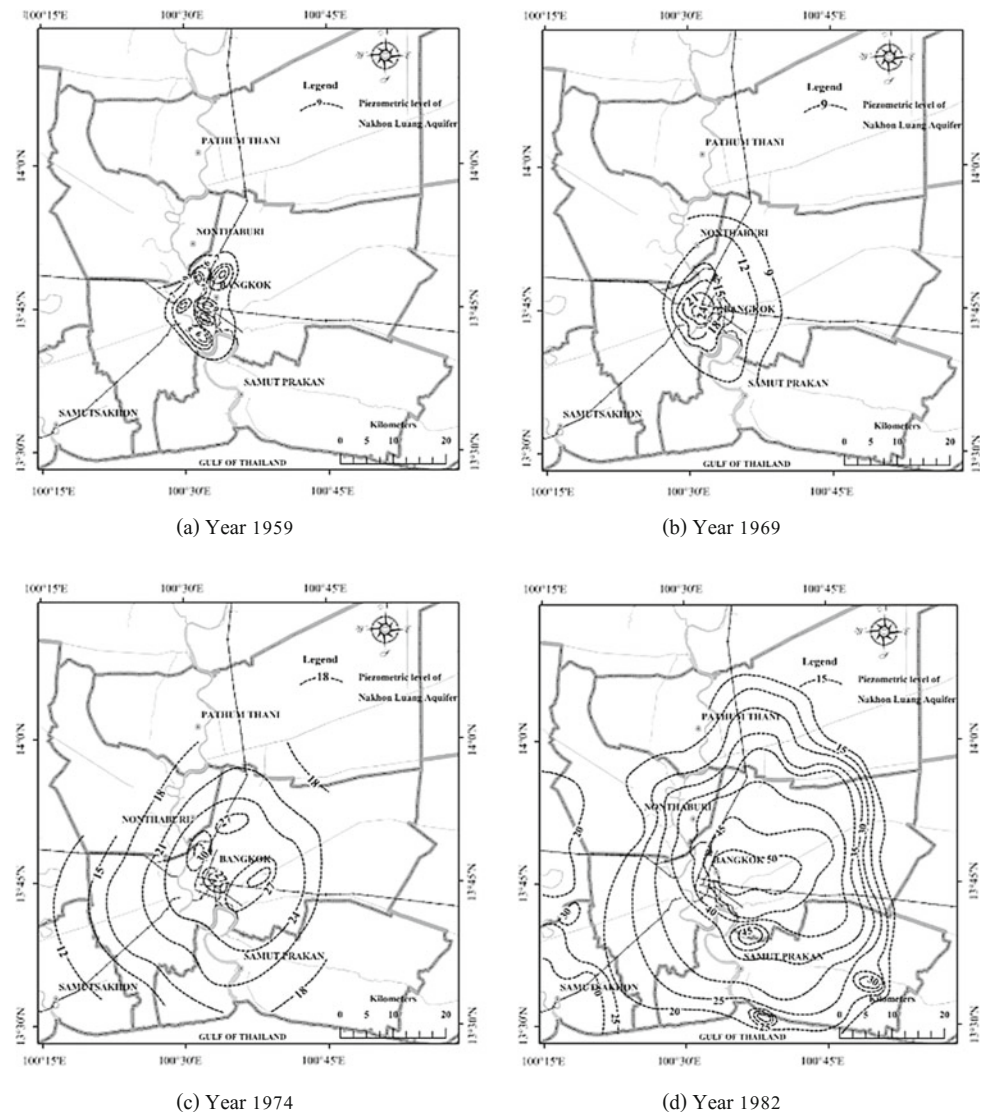
Groundwater development for public supply in Bangkok began in 1954 with extraction of 8360 cubic meters per day (m³/day). By 1982 the withdrawal rate for public supply had increased to 450,000 m³/day. In 1959, water levels were about 4–5 m bls in Eastern Bangkok and 12 m bls in Central Bangkok. After 1967, large drawdowns occurred in Eastern Bangkok, with the lowest water level of 30 m bls occurring in the NL aquifer in Central Bangkok and the eastern suburbs. From 1959 to 1982, water levels in the NL aquifer declined by 50 m in central Bangkok and in the eastern suburbs (Fig. 5).

The Thai Groundwater Act was established in 1977, and the Department of Groundwater Resources (DGR) is tasked with regulating the use of groundwater, protecting natural resources and public health, and alleviating land subsidence.

The main purpose of this law is that groundwater is a public asset, and anyone who wants to drill for and use groundwater must apply for relevant permits from the Director-General of the DGR. In addition, the regulation provides three different types of permits for the following purposes: (1) drilling, (2) groundwater extraction, and (3) discharging water into a well. In 1983, 3 critical zones were established: critical zone 1, with subsidence rates over 10 cm/year, critical zone 2, with subsidence rate between 5 and 10 cm/year, and critical zone 3, with a subsidence rate of less than 5 cm/year.

In 1992, a second revision of the Groundwater Act was enacted to designate areas as where no pumping was allowed within particular critical zones in order to control land-subsidence in the Bangkok metropolitan area. The third revision of the Groundwater Act in 2003, provided DGR the authority to create the Groundwater Development Fund that incorporated groundwater tariffs and conservation taxes. The proceeds from this fund were allocated for groundwater and environmental studies and research. Groundwater tariffs were first introduced in 1984 charging 1–3.5 baht/m³. From 2000 to 2004, areas designated as critical zones received a groundwater tariff increase from 3.5 to 8.5 baht/m³. For larger groundwater users such as factories, the groundwater tariff was higher ranging from 9.5 to 12.50 baht/m³ in 2005 to 17 baht/m³ in 2006.

Fig. 5 Potentiometric surface of the Nakhon Luang aquifer from 1959–2005, Bangkok, Thailand (modified from Lorphensri and Ladawadee 2007)



The 10-year (1978–1988) cumulative subsidence of Bangkok and adjacent vicinities ranged from about 10 to 70 cm, with the greatest subsidence observed in eastern Bangkok. The 27-year (1978–2005) cumulative subsidence ranged from about 10 to 105 cm (Fig. 6). The first cadastral survey of surface elevation in Bangkok was conducted in 1978 by the Royal Thai Survey Department. Subsequent cadastral surveys discovered varying amounts of land subsidence in the area, and in recent years, the rate of subsidence has stabilized.

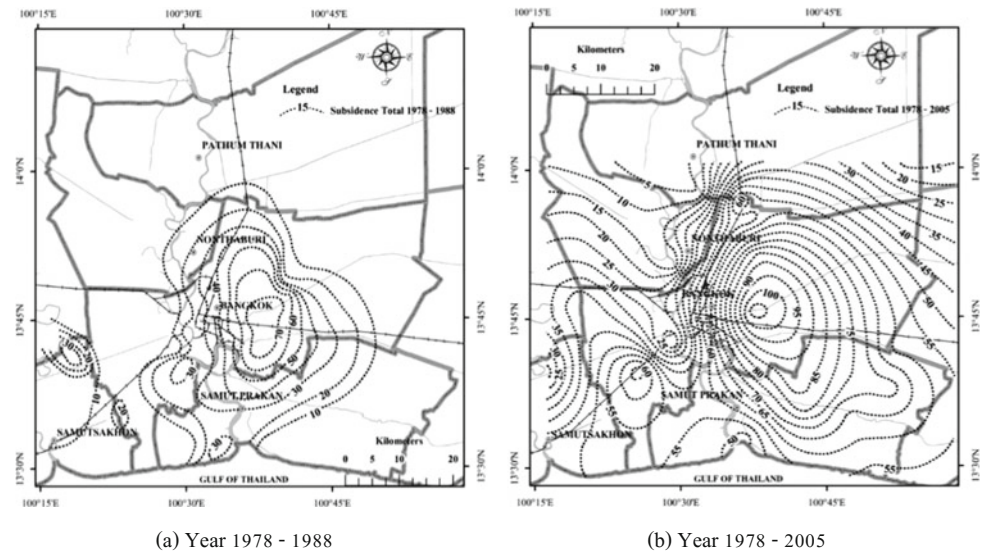
3.2 Houston, Texas, USA

Groundwater withdrawals from wells began in 1891 in the region and has been extensively relied upon for uses such as irrigation, public supply, commercial, and industrial demand. During 1906 to 1943, there was localized

subsidence caused by extraction of oil and gas and groundwater withdrawals for public supply that depressurized and dewatered the sediments in the Chicot and Evangeline aquifers, causing more than 1.0 m of subsidence in some locations (Coplin and Galloway 1999). By 1976, continued reliance on groundwater had increased withdrawals to as much as 1.75 m³/day, and by the mid-1970s, more than 1.8 m of subsidence had occurred in some locations. By 1979, as much as 3.0 m of subsidence had occurred in the southeastern portion of the study area, and about 8290 km² had subsided at least 0.30 m (Kasmarek and Ramage 2017).

Indicators that subsidence was occurring in the study area were realized through time, such as inundation of man-made structures within topographically low lying coastal areas, increased flooding, problems caused by compromised structure foundations, damaged infrastructure, and led to the establishment of the Harris-Galveston Subsidence District

Fig. 6 Cumulative rate of land subsidence from **a** 1978–1988 and **b** 1978–2005 (modified from Lorphensri et al. 2011)



(HGSD) by the 64th Texas State Legislature in 1975. HGSD's directive was to regulate and reduce groundwater withdrawals in Harris and Galveston Counties (Harris-Galveston Subsidence District 2013). Similarly, the Fort Bend Subsidence District was created in 1989 with the same directive as HGSD (Fort Bend Subsidence District 1990).

4 Scientific Data Collection and Water Management Policy Changes

4.1 Bangkok, Thailand

Extensometers and groundwater observation stations have been setup in 750 locations throughout Thailand. Locations of groundwater observation wells in the Lower Central Plain are shown in Fig. 7. The main objective of the extensometers and groundwater observation stations is to collect scientific data and to use these data to respond to many environmental issues, including land subsidence. Six extensometers were established to detect compaction rates in the Bangkok area. The results from these data are used to detect and document land-surface-elevation changes and to determine the relation between water level changes and the rate of subsidence.

Data from Observation Wells

Observation wells were installed by the Department of Mineral Resources in order to measure and monitor the water level in each principal aquifer. The correlation between water level decline and the rate of subsidence from

1978 to 2008 is shown in Fig. 8. The water level in PD aquifer (100-m zone) declined about 3-m with a subsidence rate of about 40 cm (subsidence rate of 9.72 cm/year in 4 years). In 1984, after introducing the tariff of 1 baht/m³, the water level recovered by about 5 m in the PD aquifer, 8 m in the NL aquifer, and 10 m in the NB aquifer. As a result, the total rate of subsidence had decreased from 9.72 to 2.16 cm/year. However, from 1991 to 1998, groundwater demand increased during a period of economic and industrial growth, and water levels continued to decline, in spite of the introduction of a 3.5 baht/m³ tariff increase in 1994. In 2000, after increasing tariffs to 8.5 baht/m³, water levels substantially recovered and the subsidence rate decreased to 1.30 cm/year. Currently (2017), subsidence in the Bangkok area is primarily caused from building loads and seawater encroachment.

4.2 Houston, Texas, USA

Prior to 1975, the USGS started building a groundwater-monitoring network that was mostly located in Harris and Galveston Counties. Subsequently, two initial water-level-altitude maps of the Chicot and Evangeline aquifers were created in 1977 using water-level measurements from similarly screened wells in Harris and Galveston Counties. Initial altitude maps indicated the water-levels ranged from about 76.2 to 91.4 m bls in the Chicot and Evangeline aquifers (Gabrysch 1979), respectively, in parts of the Houston area. After the creation of HGSD in 1975, the USGS began to progressively expand the network to include water wells in the nine adjacent counties.

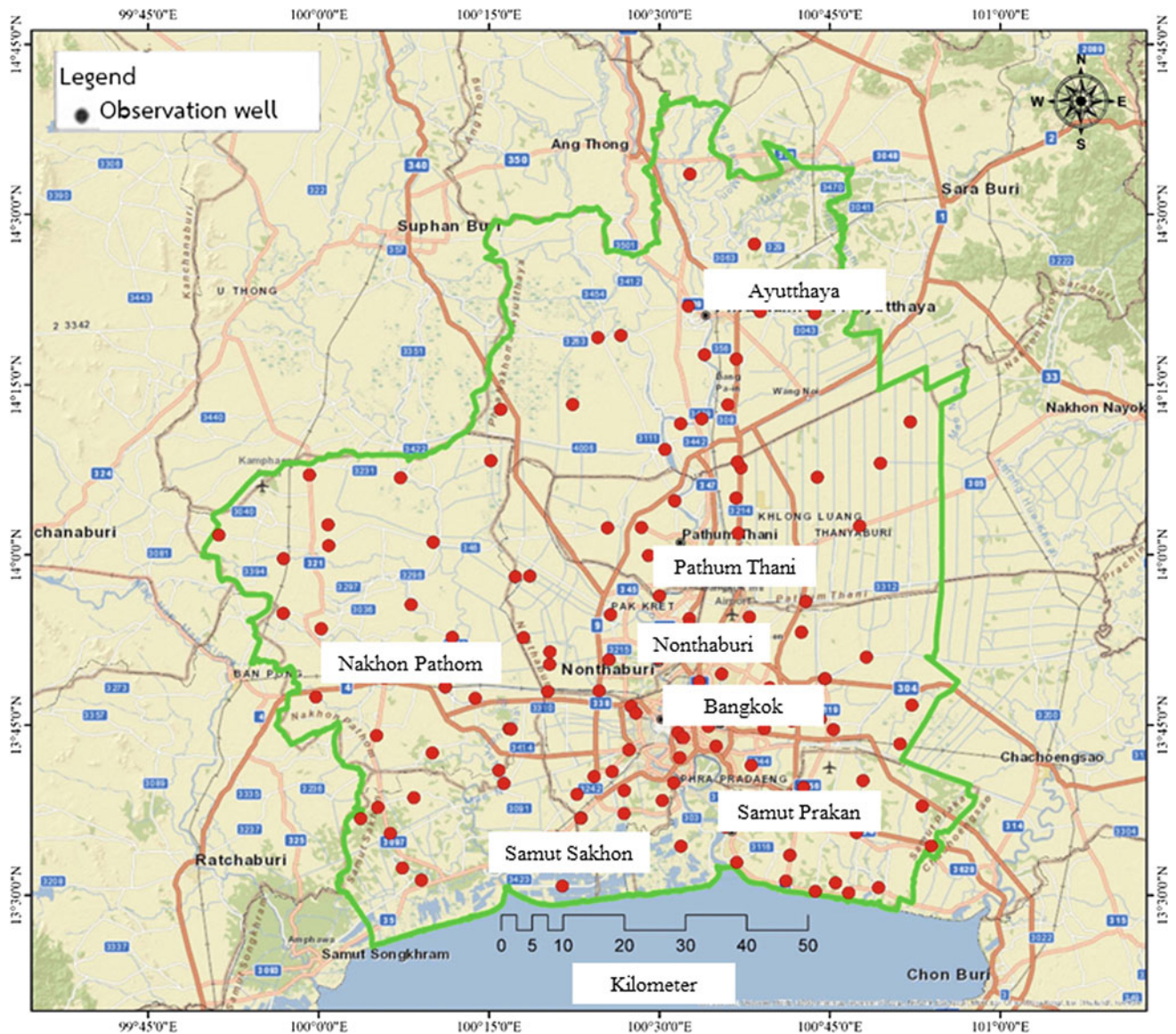


Fig. 7 Locations of groundwater observation wells in the Lower Central Plain, Thailand

After 1975, groundwater withdrawals began to curtail in the southeastern part of Harris and Galveston Counties as mandated by HGSD regulatory policy (Harris-Galveston Subsidence District 2013) and water levels in the aquifers started to recover. Hence, by 2017, water-level altitudes ranged from about 61.0 m bls to about 76.2 m bls in the Chicot and Evangeline aquifers, respectively (Kasmarek and Ramage 2017), and the primary areas having high groundwater withdrawals had geographically moved west where groundwater regulations have yet to be established. Despite massive population growth in Houston, by 2017, water levels had risen as much as 61.0 m in the Chicot aquifer and 73.1 m in the Evangeline aquifer (Kasmarek and Ramage 2017).

Extensometer Observations

From 1973 to 1980, a network of 12 borehole extensometers were installed in Harris County to monitor the occurrence of compaction in areas where groundwater withdrawals were known to be large and development was occurring. In 2017, the long-term cumulative-compaction data show that the rates of compaction have progressively decreased at all 12 extensometers, which correlates with the regulatory curtailment of groundwater withdrawals in the study area. Comparing cumulative compaction data from each of the 12 extensometer sites, the compaction data from the easternmost extensometer in Harris County (Seabrook) was about 47.98 cm, or an average rate of

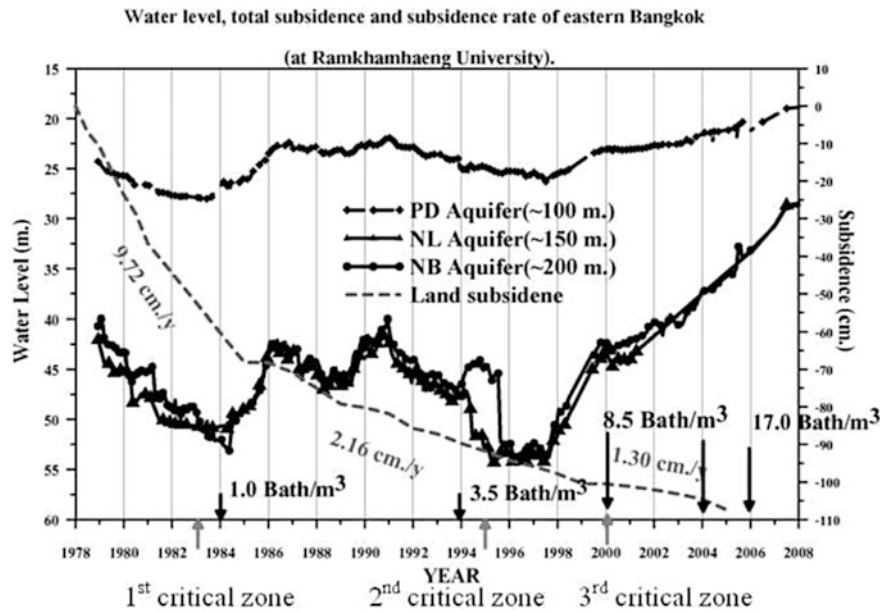


Fig. 8 Relationship between water-level, total land subsidence, and mitigation measures, eastern Bangkok, Thailand (modified from Lorphensri et al. 2011)

about 1.14 cm per year. However, for the westernmost extensometer in Harris County (Addicks), cumulative compaction was about 111 cm, for an average rate of about 2.71 cm per year (Fig. 9). The reason that the compaction value for the Seabrook extensometer is the less than the Addicks extensometer is that the Seabrook site is located in the area where groundwater withdrawals were first curtailed due to a conversion to surface water in the area. Conversely, the Addicks extensometer is located in the area where water use has yet to be completely converted to surface water resources.

5 Discussion and Conclusions

Scientific data collection is essential in shaping groundwater policy and managing water, particularly in areas with widespread subsidence. The Bangkok and Houston areas have long histories of relying on groundwater withdrawals to meet ever-increasing water demands for irrigation, public supply, commercial, and industrial purposes. In Thailand, water levels recorded from hundreds of groundwater observation stations, exhibited up to 30 m of decline in Nakhon Luang aquifer in Central Bangkok and the eastern suburbs during the 1970s. Data from 1978 to 2008, show there is a correlation between water-level decline and the rate of subsidence. Currently (2018), water

levels in the Bangkok region has recovered despite some areas having subsidence rates at about 1.3 cm/year occurring mainly from building loads and sea water encroachment.

Initial altitude maps (1977) in the Houston area indicated that the water levels in the Chicot and Evangeline aquifers had appreciably declined. Temporal variations in compaction rates at 2 extensometers in the Houston area suggest that the rates of compaction were greater when the extensometers were initially installed, but as groundwater withdrawals began to be curtailed, the rate of compaction slowly decreased. However, sustained groundwater withdrawals prior to curtailment and the associated lowering of land-surface elevation, related to the irrecoverable compaction of the stacked fine-grained sediments, altered the original topography in the affected areas, thereby incrementally modifying the gradient of surficial drainage patterns.

It is important to monitor water levels and compaction to build datasets that can be used by regulatory entities to make decisions on groundwater policy. The most current techniques for long-term monitoring of groundwater levels, compaction, and land-surface elevation are necessary to understand how the aquifer system responds to groundwater withdrawals, thereby providing policymakers information needed to implement better management strategies.

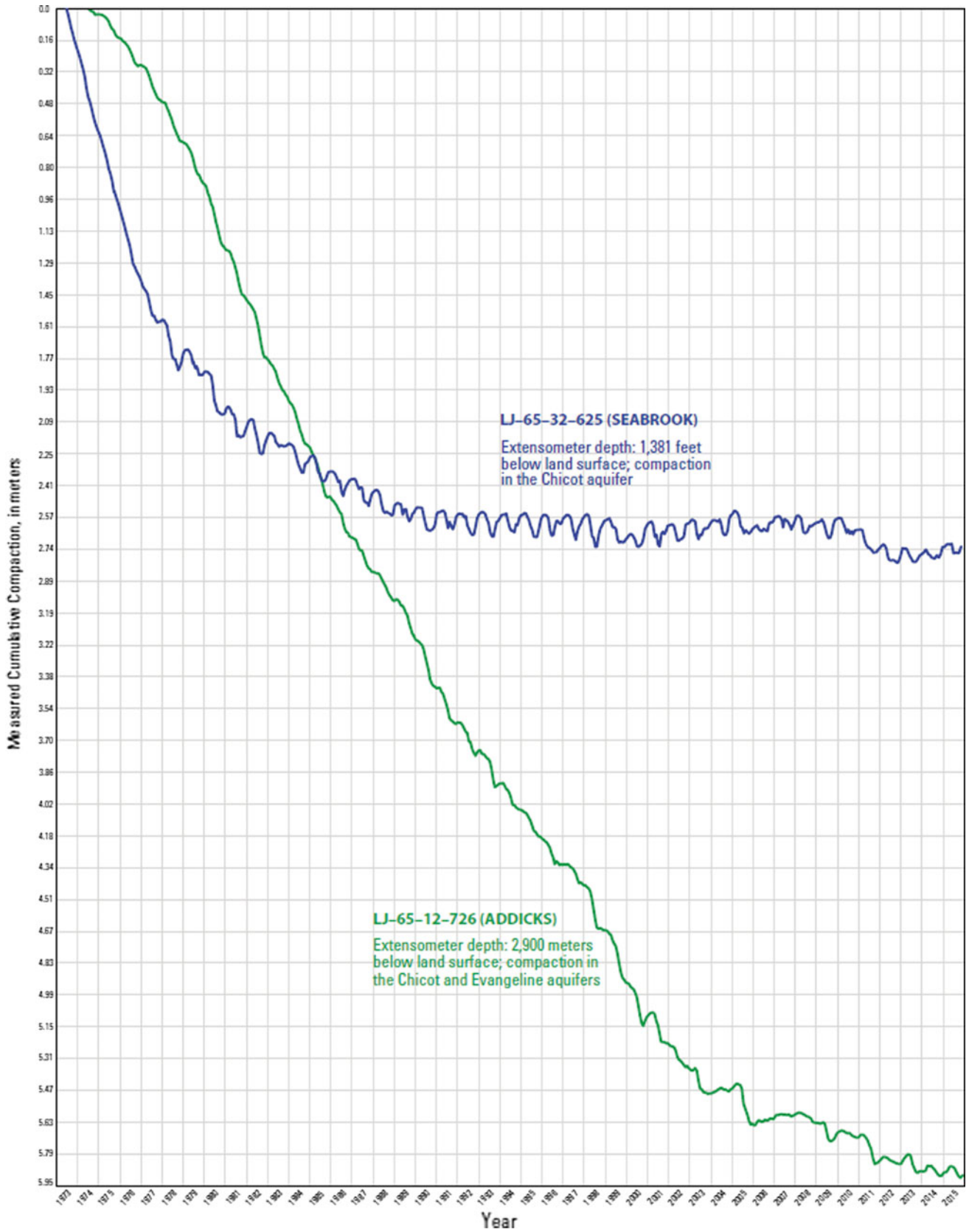


Fig. 9 Cumulative compaction at two borehole extensometer sites in the Harris County

References

- Baker, E.T., Jr., Stratigraphic and hydrogeologic framework of part of the Coastal Plain of Texas: Texas Department of Water Resources Report 236, 43p (1979)
- Coplin, L.S., Galloway, D.: Houston-Galveston, Texas—Managing coastal subsidence. In: Galloway, D., Jones, D.R., Ingebritsen, S. E. (eds.) Land Subsidence in the United States: U.S. Geological Survey Circular 1182, pp. 35–48 (1999)
- Fort Bend Subsidence District.: District Enabling Act (1990). Accessed 29 Sept 2017. <http://fortbendsubsidence.org/documents/>
- Gabrysch, R.K.: Approximate Altitude of Water Levels in Wells in the Chicot and Evangeline Aquifers in the Houston area, Texas, Spring 1977 and Spring 1978. U.S. Geological Survey Open-File Report 79–334, 4 sheets (1979)
- Harris-Galveston Subsidence District.: District Regulatory Plan (2013). Accessed 29 Sept 2017 at <http://hgsubsidence.org/wp-content/uploads/2013/07/HGSD-2013-Regulatory-Plan-with-Amendment.pdf>
- Kasmarek, M.C., Gabrysch, R.K., Johnson, M.R.: Estimated land-surface subsidence in Harris County, Texas, 1915–17 to 2001. U.S. Geological Survey Scientific Investigations Map 3097, 2 sheets 2009. Accessed 2 Oct 2017. <http://pubs.usgs.gov/sim/3097/>
- Kasmarek, M.C., Ramage, J.K.: Water-Level Altitudes 2017 and Water-Level Changes in the Chicot, Evangeline, and Jasper Aquifers and Compaction 1973–2016 in the Chicot and Evangeline Aquifers, Houston-Galveston Region, Texas. U.S. Geological Survey Scientific Investigations Report 2017–5080, 32p (2017). Accessed 29 Sept 2017. <https://doi.org/10.3133/sir20175080>
- Lorphensri, O., Ladawadee, A.: Report to the Prime Minister Office: Groundwater and Land Subsidence Situation in Bangkok and Vicinity (2007)
- Lorphensri, O., Ladawadee, A., Dhammasarn, S.: Review of Groundwater Management and Land Subsidence in Bangkok, Thailand. In: Taniguchi, M. (ed.) Groundwater and Subsurface Environment: Human Impacts in Asian Coastal Cities, Chap. 7, pp. 127–142 (2011)
- Ramnarong, V., Buapeng, S.: Groundwater resources of Bangkok and its vicinity; impact and management. In: Proceeding of a National Conference on “Geologic Resources of Thailand: Potential for Future Development”, Bangkok, Thailand (1992)



Arizona Department of Water Resources Land Subsidence Monitoring Program

Brian D. Conway

Abstract

Land subsidence due to groundwater overdraft has been an ongoing problem in south-central and southern Arizona since the 1940s. The first earth fissure attributed to excessive groundwater withdrawal was discovered in the early 1950s near Picacho, Arizona. In some areas of the State, groundwater level declines of more than 120 m have resulted in extensive land subsidence and earth fissuring. Land subsidence in excess of 5.7 m has been documented in both western metropolitan Phoenix and Eloy, Arizona. The Arizona Department of Water Resources (ADWR) has been monitoring land subsidence throughout Arizona since 1998 using Interferometric Synthetic Aperture Radar (InSAR) Data and Global Navigation Satellite System (GNSS) Data. The ADWR InSAR program has proven to be a critical resource for monitoring land subsidence throughout Arizona and has resulted in the identification of more than 26 individual land subsidence features that cover an area of more than 7300 km². Using InSAR data in conjunction with groundwater level datasets, ADWR is able to monitor land subsidence areas as well as identify areas that may require additional monitoring. The declining groundwater levels in Arizona are both a challenge for future groundwater availability and for mitigating land subsidence. ADWR's InSAR program will continue to be a critical tool for monitoring land subsidence due to excessive groundwater withdrawal.

Keywords

Subsidence • InSAR • Earth fissures • Arizona (USA)
Groundwater management

1 Introduction

Land subsidence due to excessive groundwater overdraft has been an ongoing problem in south-central and southern Arizona. The first documented case of land subsidence was from repeat leveling in 1948 in the Eloy area (Robinson and Peterson 1962). Historical groundwater declines vary by groundwater basin, but in some of the alluvial groundwater basins of south-central and southern Arizona, groundwater declines have exceeded 120 m. The potential problems of land subsidence prompted the Arizona Department of Water Resources (ADWR) to start a land subsidence monitoring program in 1998.

Land subsidence has resulted in extensive earth fissuring, with the first earth fissure attributed to groundwater withdrawal being discovered in the early 1950s near Picacho, Arizona (Carpenter 1999). More than 273 km of earth fissures have been identified and mapped by the Arizona Geological Survey (AZGS 2017). Land subsidence will continue to pose a problem across Arizona as long as groundwater demands exceed natural and/or artificial recharge, or until groundwater levels recover to refill the open pore-spaces in the aquifer, or until the dewatered and open pore-spaces completely compact.

2 Interferometric Synthetic Aperture Radar (InSAR) Data

ADWR began using survey-grade GNSS equipment at the onset of its land subsidence monitoring program in 1998. Shortly after starting the program, ADWR tested a pilot program using interferometric synthetic aperture radar (InSAR) data in 2001. After deeming the pilot InSAR program a success and a proven method in monitoring regional land subsidence, ADWR began developing its own in-house InSAR program in 2002 after being awarded a NASA Earth Sciences grant.

B. D. Conway (✉)
Arizona Department of Water Resources, 1110 W. Washington
St., Suite 310, Phoenix, AZ 85007, USA
e-mail: bdconway@azwater.gov

Since 2002, ADWR has collected more than 140,000 km² of InSAR data throughout Arizona, identifying more than 26 individual land subsidence features that cover an area greater than 7500 km². ADWR has compiled an extensive historical InSAR dataset for the active land subsidence areas in Arizona. Most data sets cover time periods between 1992 to 2000, 2004 to 2010, 2006 to 2011, and 2010 to present, which reflect the time-series for each satellite sensor. ADWR has utilized SAR data from the ERS-1, ERS-2, Envisat, Radarsat-1, Radarsat-2, ALOS-1, ALOS-2, TerraSAR-X, and Sentinel-1 satellites (Fig. 1). ADWR has used the InSAR data to produce more than 400 land subsidence maps that can be accessed and downloaded at this link: <http://www.azwater.gov/AzDWR/Hydrology/Geophysics/LandSubsidenceInArizona.htm>.

The land subsidence maps cover various periods of time for each land subsidence feature and are updated each year. ADWR has also developed an interactive land subsidence map that can be used to view the extent of each land subsidence feature.

ADWR has used InSAR not only for monitoring land subsidence but also seasonal deformation (uplift and

subsidence), natural and artificial recharge events, as a tool for geological mapping and investigations, locating earth fissures, identifying areas where conditions may exist for future earth fissure formation, for dam mitigation and land subsidence modeling, and for monitoring floodplains and changing drainage patterns due to land subsidence. ADWR's InSAR program has produced valuable results and end products that are used not only by ADWR but also other state, county, and local agencies, universities, and private companies for their own research, monitoring, modeling, mitigation, planning and design projects.

3 Land Subsidence

Groundwater pumping in south-central and southern Arizona has been occurring since the early 1900s. Groundwater has been a primary source of water for the municipal, agricultural, industrial, and mining sectors. This groundwater pumping has exceeded the natural recharge for more than half a century, resulting in declining groundwater levels; some groundwater basins have experienced more than

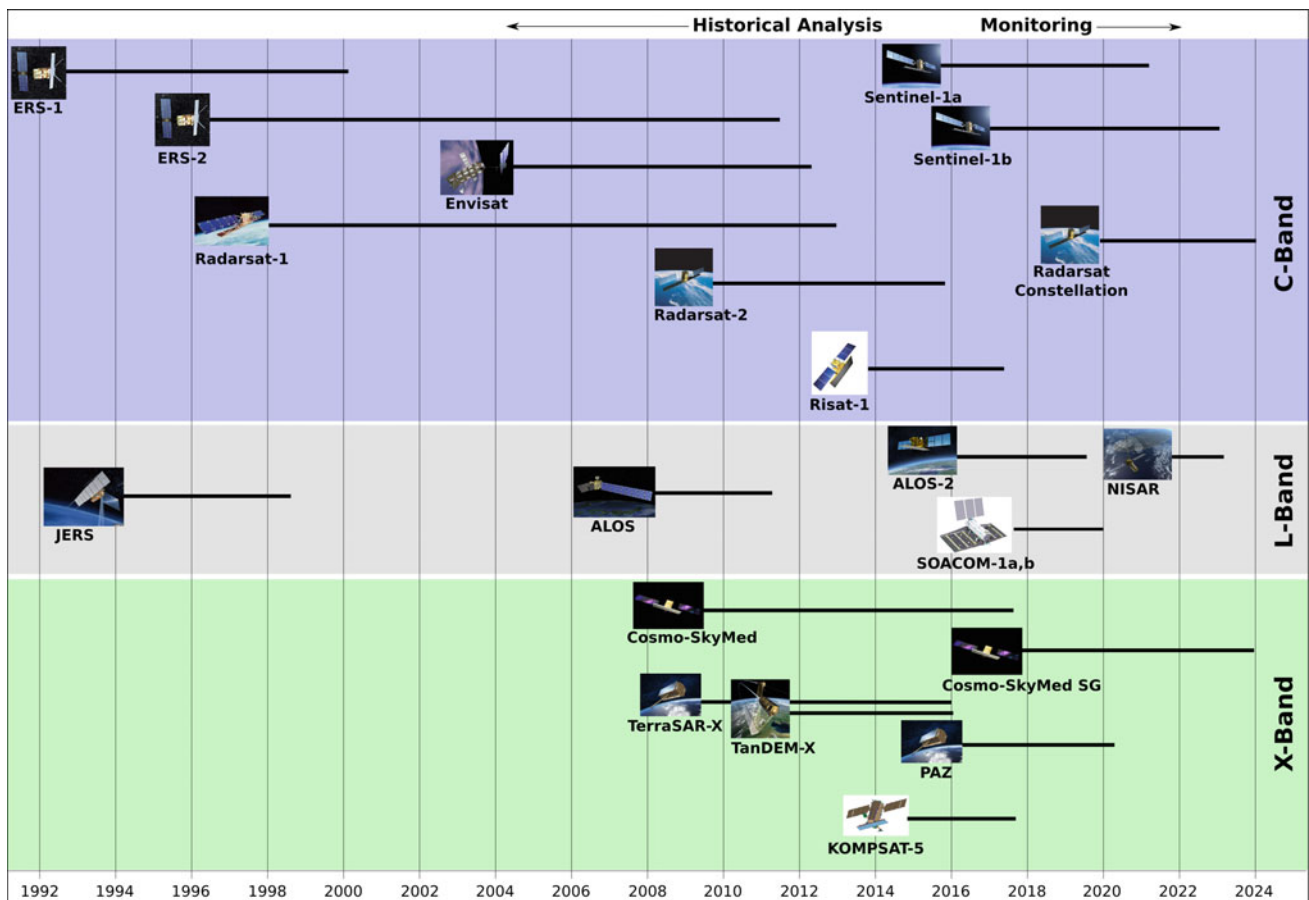


Fig. 1 Chart of past, present, and projected SAR satellite missions Image courtesy UNAVCO

120 m of groundwater decline (ADWR 2017b). These groundwater declines have resulted in regional land subsidence (Fig. 2) with some areas experiencing land subsidence in excess of 5.7 m in the western portion of the Phoenix metropolitan near Luke Air Force Base (Schumann and O'Day 1995) and near the town of Eloy (Schumann and Genualdi 1986).

The construction and completion of the Central Arizona Project canal in the mid-1980s began delivering Colorado

River water to water-users in the Phoenix and Tucson metropolitan areas as well as water to agricultural users in Pinal County (located between Phoenix and Tucson). These surface water deliveries have reduced groundwater demands, resulting in groundwater recovery in many areas. The groundwater recoveries have slowed land subsidence rates in these areas where surface water is being used to replace or supplement groundwater, but residual land subsidence continues to exist. Climate change, drought, and/or a decrease in

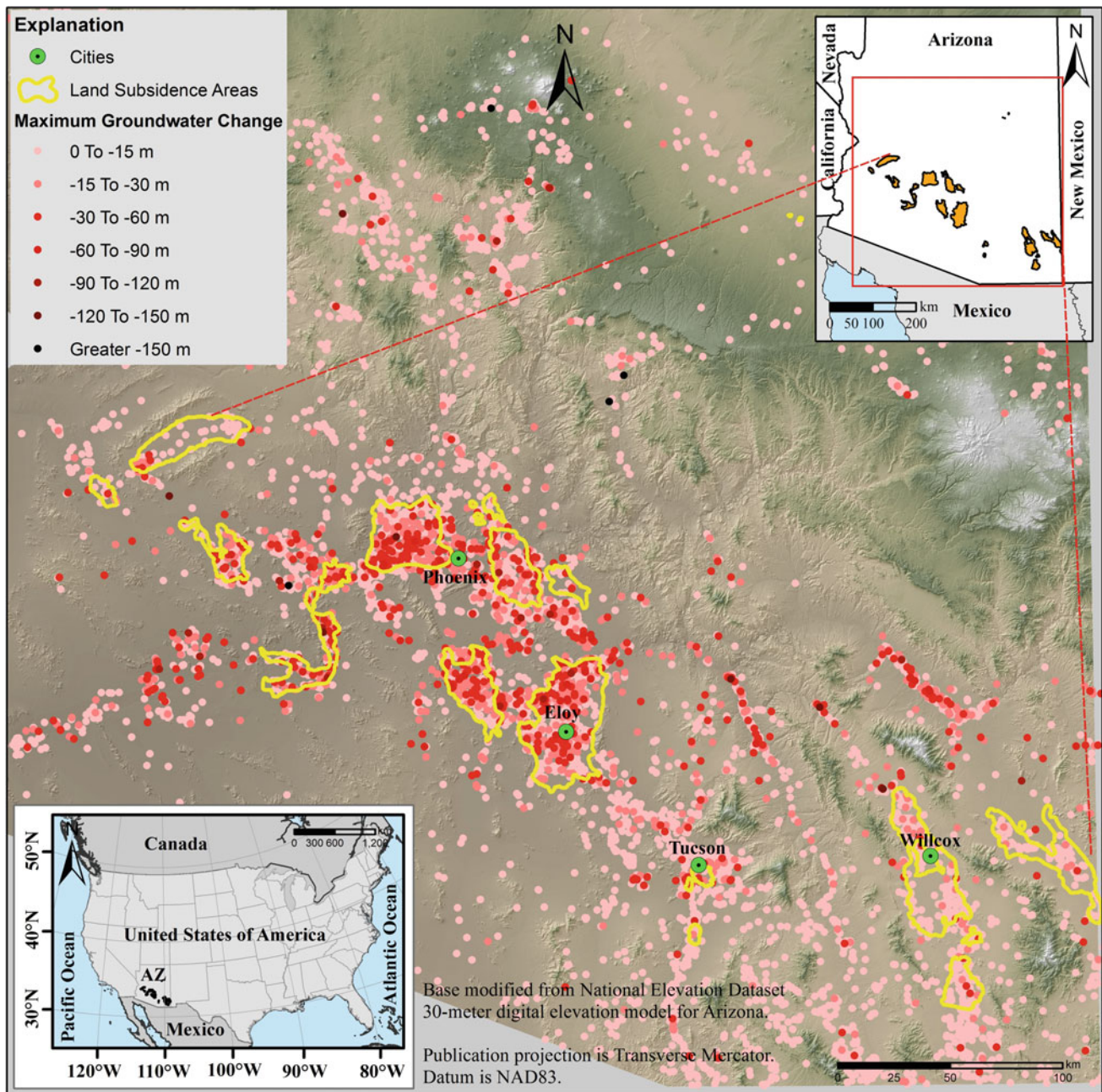


Fig. 2 Land subsidence features in Arizona based on InSAR data and maximum groundwater change from ADWR groundwater sites inventory database (ADWR 2017a, b)

surface water deliveries could cause an increase in groundwater pumping, resulting in renewed land subsidence rates that were present during the pre-1980s era.

Hazards associated with land subsidence include the potential to change natural drainage patterns and floodplains, which has occurred in the McMullen Valley basin and the Eloy sub-basin of central Arizona, and elsewhere (ADWR 2013). Land subsidence causes earth fissures in areas that experience differential compaction. Land subsidence may also affect the hydraulic properties of the aquifer. As the pores become more compressed, it becomes more difficult for water to move through the aquifer, which may reduce transmissivity. Also, compaction of the aquifer results in a loss of storage because pore volume decreases.

4 Earth Fissures

Regional land subsidence has resulted in a large number of earth fissures. Earth fissures are tension cracks that are formed from differential land subsidence occurring near the basin fringes or near shallow bedrock. Earth fissures develop as small hairline cracks in the sub-surface. Some cracks may reach the surface and others may lie hidden just below the surface. Earth fissures are usually identified after large rain events when the hairline crack intercepts surface runoff, causing erosion. The earth fissure opens up, creating what is called a fissure gulley. An earth fissure gulley can be more than 3 m wide and have depths of 10 or more meters (Fig. 3). The Arizona Geological Survey (AZGS) started mapping earth fissures in 2007 and has since mapped more than 273 km of earth fissures throughout Arizona (AZGS 2017). The AZGS has published 26 earth fissure study area maps that display all the earth fissures mapped in each study area. These maps, as well as an online earth fissure viewer and GIS earth fissure shapefiles, can be accessed at this link: <http://www.azgs.gov/efmaps.shtml>. Several of these earth fissures have impacted and damaged pipelines, highways, roads, railways, flood control structures and homes.

5 Land Subsidence in Active Management Areas

The 1980 Arizona Groundwater Act recognized the need to aggressively manage the state's finite groundwater resources to support its growing economy. Areas with heavy reliance on mined groundwater were identified and designated as Active Management Areas (AMAs). The five AMAs (Prescott, Phoenix, Pinal, Tucson and Santa Cruz) are subject to regulation pursuant to the Groundwater Code. Each AMA carries out its programs in a manner consistent with these



Fig. 3 Earth fissure in Pinal County, Arizona that opened in 2016

goals, while considering and incorporating the unique character of each AMA and its water users.

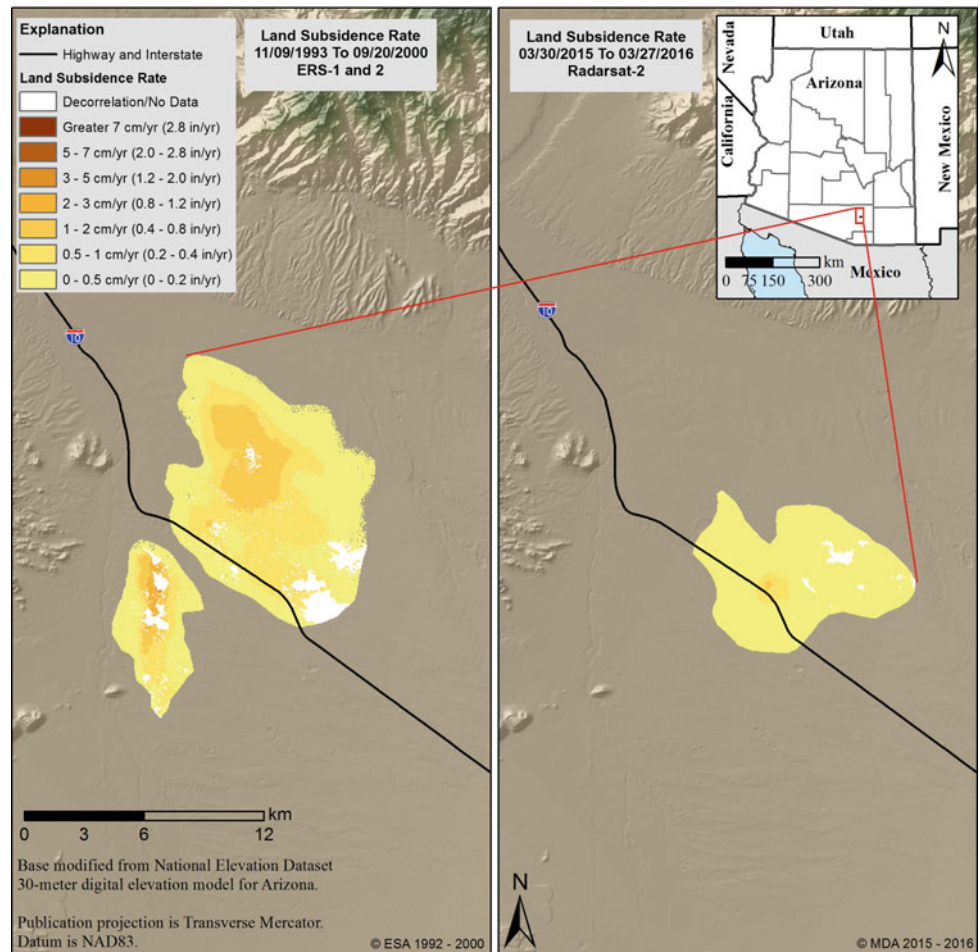
In the Phoenix, Prescott and Tucson AMAs, the primary management goal is safe-yield by the year 2025. Safe-yield is accomplished when no more groundwater is being withdrawn than is being annually replaced.

In the Pinal AMA, where the economy is primarily agricultural, the management goal is to preserve that economy for as long as feasible, while considering the need to preserve groundwater for future non-irrigation uses.

In the Santa Cruz AMA the management goal is to maintain a safe-yield condition in the active management area and to prevent local water tables from experiencing long term declines.

Groundwater levels in the Phoenix, Pinal and Tucson AMAs have been recovering since the early 1990s. This is due to a number of reasons: increase in water-use efficiency; artificial groundwater recharge; using renewable surface water; decrease in agricultural acreage; mandatory conservation programs; 100-year assured water-supply requirements for all new developments; and, groundwater management. The Tucson AMA has seen a significant decrease of almost 90% in land subsidence when comparing the InSAR rates between the 1990s and 2015–2016 (Fig. 4).

Fig. 4 Land subsidence rate comparison between 1993–2000 and 2015–2016 in Tucson AMA (ADWR 2017e, f)



Groundwater pumping in and around these land subsidence features had been reduced and replaced by using recharged surface water, resulting in recovering groundwater levels. The Phoenix AMA has seen decreases between 25 and 50% in land subsidence when comparing InSAR rates between the 1990s and 2015–2016.

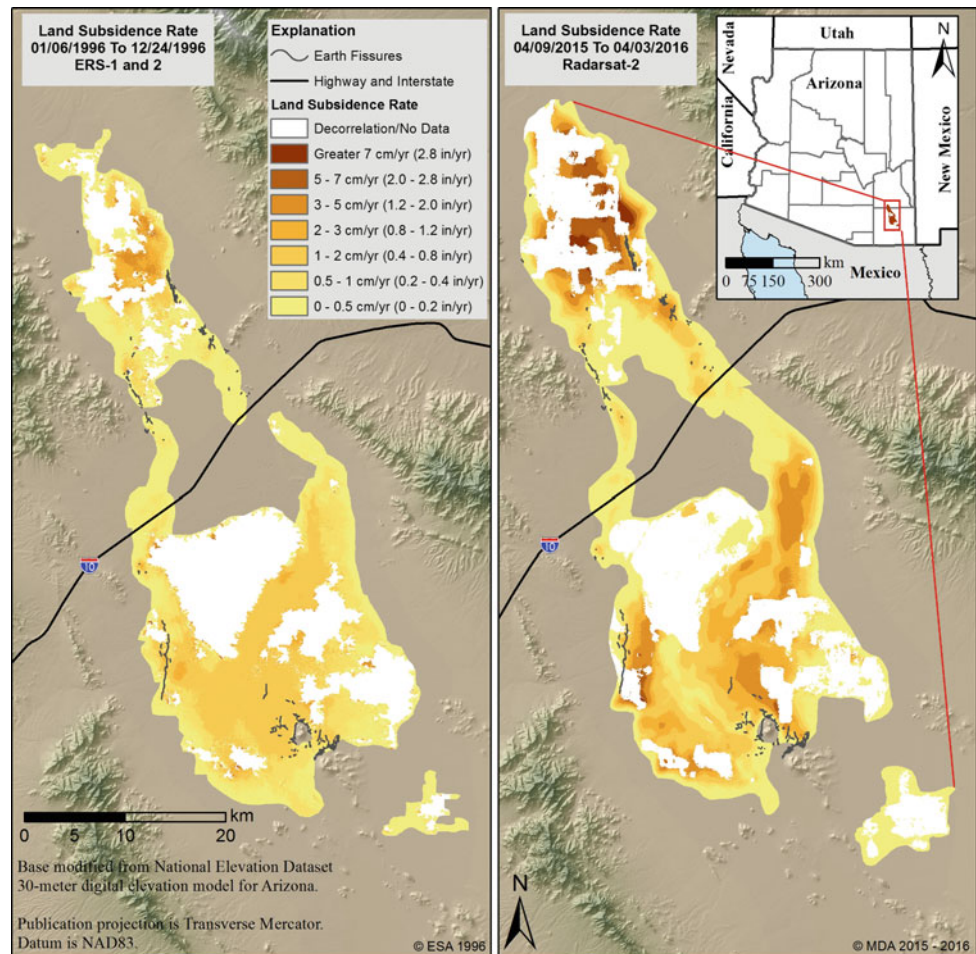
6 Land Subsidence Outside Active Management Areas

The majority of land subsidence areas outside AMAs do not have access to renewable surface water supplies and are not subject to mandatory conservation programs and groundwater management. Two of the land subsidence areas are within two separate Irrigation Non-Expansion Areas (INA):

the Harquahala INA and Douglas INA. INAs have restrictions on increasing the number of irrigated acres.

All the land subsidence areas outside the AMAs have seen an increase in land subsidence when comparing older InSAR data to the more recent InSAR data. The Willcox Groundwater Basin located in southeastern Arizona (and outside an AMA) is a closed groundwater basin. Water-users there currently do not have access to any renewable surface water supplies. The Willcox Basin has seen an increase in agricultural acreage since the 1950s. Groundwater levels have declined as much as 100 m since the 1950s, resulting in land subsidence of more than 1.5 m. There has been a significant increase in land subsidence when comparing the InSAR rates between the 1990s and 2015–2016 (Fig. 5.); rates have increased between 200 and 400%.

Fig. 5 Land subsidence rate comparing between 1996 and 2015–2016 in the Willcox Basin (ADWR 2017c, d)



7 Conclusions

Land subsidence and earth fissures have been a problem in south-central and southern Arizona for more than 50 years and will continue to be a problem into the future. Even though groundwater levels are recovering in many areas where renewable surface water supplies are being used to replace groundwater, residual land subsidence continues. Many of the rural groundwater basins outside AMAs that do not have access to external sources of surface water are experiencing greater groundwater declines and land subsidence rates than those basins that have access to surface water supplies.

There are several factors that could affect groundwater conditions and land subsidence in a groundwater basin. A few of these are climate change, drought, or even wet periods. Wet periods have resulted in groundwater recoveries and even uplift in some areas in 2005 and 2010. The

ongoing drought in Arizona has resulted in some basins receiving decreased surface water deliveries and thereby causing increased groundwater pumping in those particular areas. As a result, land subsidence started to occur in the area where groundwater pumping had increased (to offset decreased surface water supplies) and groundwater levels had declined. This type of situation could repeat itself for those entities that use Colorado River water if a shortage is declared for the Lower Colorado River system at Lake Mead. That would cause Arizona to lose 325,000 acre-feet of water per year of its Colorado River allotment. Groundwater would be used to replace the cuts in the Colorado River water deliveries, and would result in increased pumping and the possible increase in land subsidence or the possible development of new land subsidence features.

All these factors and many others that could affect groundwater conditions and land subsidence are why it is critical to monitor both land subsidence and groundwater conditions throughout Arizona. These data allow

water-planners, hydrologists, policy makers, etc. to research a problem, or develop a water management plan, or make informed decisions because they are using the most recent and comprehensive data that are available.

References

- Arizona Department of Water Resources: Land Subsidence Monitoring Report No. 1 (2013)
- Arizona Department of Water Resources: Active Land Subsidence Areas 05-2017, Shapefile (2017a)
- Arizona Department of Water Resources: Groundwater Sites Inventory (GWSI) Database (2017b)
- Arizona Department of Water Resources: Land Subsidence Rate Map in the Willcox and Kansas Settlement Areas, Cochise County, 01/06/1996 to 12/24/1996 (2017c)
- Arizona Department of Water Resources: Land Subsidence Rate Map in the Willcox and Kansas Settlement Areas, Cochise County, 04/09/2015 to 04/03/2016 (2017d)
- Arizona Department of Water Resources: Land Subsidence Rate Map in the Tucson Metropolitan Area, Pima County, 11/09/1993 to 09/20/2000 (2017e)
- Arizona Department of Water Resources: Land Subsidence Rate Map in the Tucson Metropolitan Area, Pima County, 03/30/2015 to 03/27/2016 (2017f)
- Arizona Geological Survey: Locations of Mapped Earth Fissure Traces in Arizona. Arizona Geological Survey Digital Information (DI-39 v. 01.29.2015), Shapefile (2017)
- Carpenter, M.C.: Part I: South-Central Arizona. In Galloway, D., Jones, D.R., Ingebritsen, S.E. (eds.) Land Subsidence in the United States, circular no. 1182, pp. 65–78. U.S. Geological Survey, Reston, VA (1999)
- Robinson, G. M., and Peterson, D. E.: Notes on Earth Fissures in Southern Arizona: U.S. Geological Survey Circular 466, 7 p. (1962)
- Schumann, H.H., Genualdi, R.B.: Land subsidence, earth fissures, and water-level change in Southern Arizona: Arizona Bureau of Geology and Mineral Technology Map M-23, scale 1:1,000,000 (1986)
- Schumann, H.H., O'Day, C.M.: U.S. Department of the Interior-U.S. Geological Survey-Investigation of Hydrogeology, Land Subsidence, and Earth Fissures, Luke Air Force Base, Arizona-Administrative Report, Tucson, Arizona (1995)

The Pixley Fissure Revisited—Understanding an Old Geohazard to Safeguard New Infrastructure

Michael L. Rucker, Kenneth C. Ferguson, and Danielle Smilovsky

Abstract

The Pixley Fissure is an earth fissure associated with historic land subsidence (more than 12 feet between 1926 and 1970) in the southern (San Joaquin Valley) portion of California's Central Valley. It was the easternmost of three earth fissures discovered after flooding in 1969, and was investigated in 1974 as part of the regional geohazard assessment for a proposed nuclear generating station. Although published results of that investigation are part of the earth fissure literature, characterization was not presented of the adjacent compressible basin alluvium from which groundwater withdrawal caused differential subsidence and the earth fissure. The California High Speed Rail (HSR) is in design through portions of the valley currently undergoing land subsidence at annual rates greater than one foot per year. A better understanding of the geological setting at the Pixley Fissure may provide insight into potential earth fissure mechanisms in the Central Valley that might impact the HSR. Historic oil and gas well geophysical logs are available online; this resource provided several resistivity and spontaneous potential well logs for detailed basin alluvium characterization at depths relevant to subsidence behavior in the Pixley Fissure vicinity. A vertical offset of about 150 feet in the Pleistocene sediments, increasing to 400 feet in the Miocene sediments, is tentatively interpreted to bracket the fissure. It suggests compaction faulting as a mechanism to concentrate subsidence-induced tensile strain, possibly as a hydraulic barrier impacting groundwater extraction from the alluvium, for the fissure development and location. In combination with InSAR and other subsidence monitoring to identify zones of developing tensile strain due to subsidence, available historic geophysical log data may help characterize areas of

possible compaction faulting with potential for earth fissuring, including along the HSR alignment.

Keywords

Earth fissure • Subsidence • Compaction fault
Geophysical logs • High speed rail

1 Introduction

Three earth fissures were identified within the Pixley Subsidence Bowl in the San Joaquin Valley (SJV) of central California in the late 1960s. The most significant of these fissures, named the Pixley Fissure (Fig. 1), was investigated as part of the geohazards assessment for a proposed nuclear power plant; results of that investigation are presented by Guacci (1979). Located on the flank of a groundwater extraction-induced subsidence bowl near Pixley, the surface expression of this earth fissure was reportedly about 0.5 mile long, up to 8 feet wide, and up to 6 feet deep. It was traced in the shallow alluvial soils, using an auger bucket, as a few 1/8 to 3-inch wide subsurface cracks, infilled with sands and silts, to depths greater than 55 feet. No vertical offset was noted at the cracks, and the fissure system was determined to be a tensional feature resulting from differential subsidence. Guacci (1979) included no discussion of the deeper alluvial basin, but referenced Lofgren and Klausing (1969) which described the basin characteristics and presented results from a 730-foot deep corehole and compaction recorder installation located 1.3 miles west of the Pixley Fissure.

Another subsidence-related surface feature observed in the 1970s was the Pond-Poso Creek Fault (PPCF) described by Holzer (1980). Located about 15 miles south of the Pixley Fissure (Fig. 1), this feature exhibited vertical ground displacements up to 1 inch in 4 months, and offsets of nearly 10 inches since groundwater pumping began. This movement was interpreted to be differential subsidence across a fault system that was inferred to be a hydraulic barrier within

M. L. Rucker (✉) · K. C. Ferguson · D. Smilovsky
Wood Plc, Phoenix, USA
e-mail: michael.rucker@woodplc.com

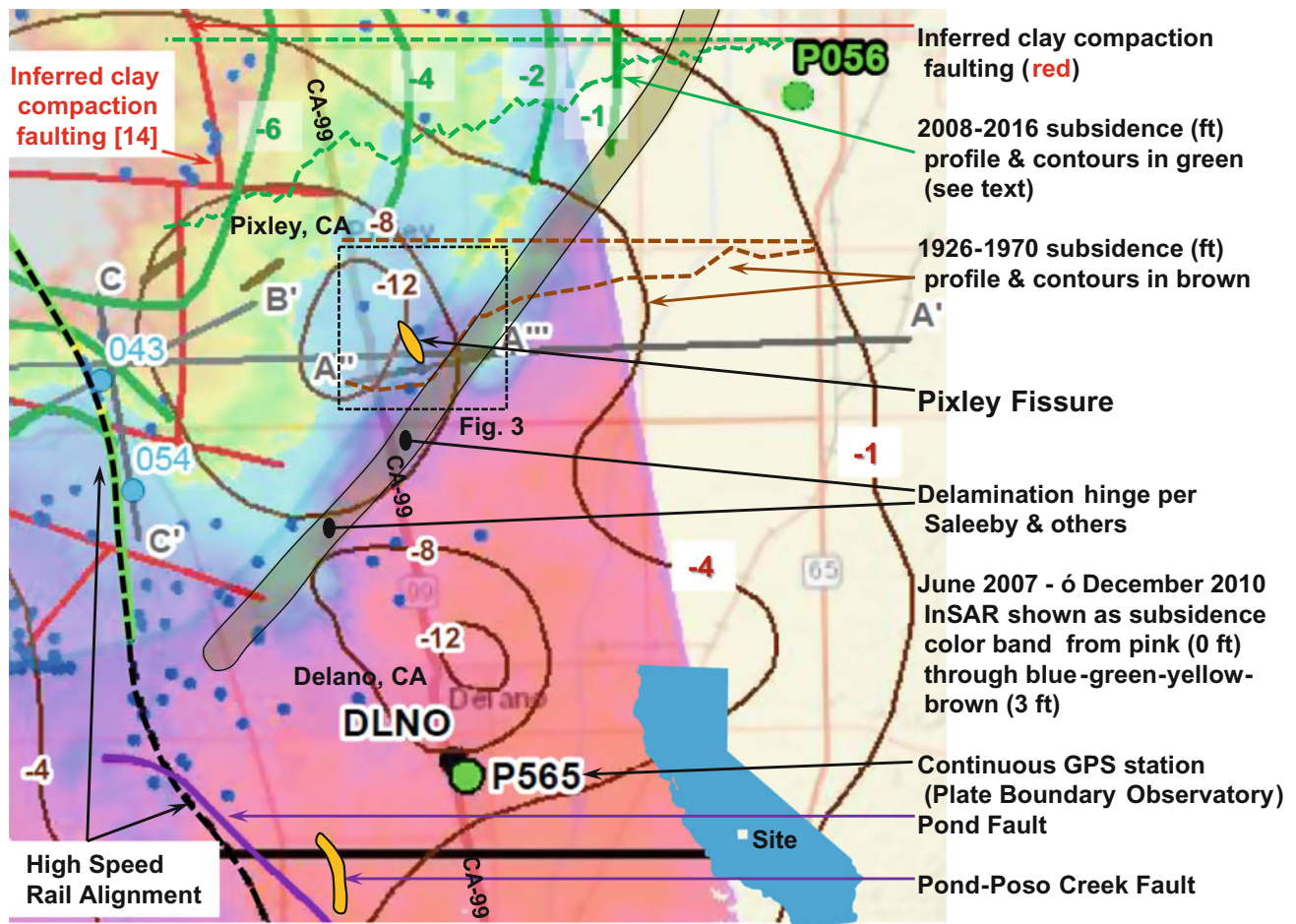


Fig. 1 Pixley Fissure area showing various features and subsidence over different time periods. The HSR alignment is in the western part of the figure area. Inferred clay compaction faulting is from Saleeby and Foster (2004)

the pumped aquifer system (Holzer 1980); historic PPCF movement is as a compaction fault rather than a tectonic fault. Reviewing seismic reflection results across the adjacent Pond Fault (PF), Smith (1983) reported that vertical fault offset is about 250, 100 and 50 feet at depths of 3600, 1760, and 875 feet respectively in the Pleistocene Tulare and underlying Pliocene to Miocene San Joaquin Formations. The California High Speed Rail (HSR) alignment crosses the PF trace northwest of the PPCF.

Subsidence rates in the southern SJV are now being monitored utilizing aircraft- and satellite-based InSAR technology. As interpreted by Farr et al. (2015, 2017), subsidence has accelerated in the last few years, with maximum rates of about 2 feet per year and large areas with rates greater than 1 foot per year in 2015–2016. Differential subsidence is already impacting flood plain geometries and performance of the California Aqueduct (Farr et al. 2017), and if sustained, might induce new earth fissuring. Infrastructure, such as water conveyance systems and the

California High Speed Rail project, could be impacted by differential ground movement or piping erosion from fissuring.

2 Newly Available Information

New technologies have revolutionized the study and characterization of land subsidence since the Pixley Fissure was studied in the 1970s. Subsidence was measured using optical survey re-occupying permanent benchmarks through much of the 20th century (see brown contours and profile in Fig. 1). Current technologies include GPS survey with permanent station capability and satellite-based InSAR with regional area coverage. Figure 1 shows 2008–2016 subsidence contours and profile (in green) generated from a 2008 airborne LiDAR survey compared to a 2016 vehicle-mounted real-time kinetic (RTK) survey conducted on roadways; these relatively imprecise (for subsidence

studies) technologies nevertheless captured large-scale subsidence, with a maximum of nine feet over the 8-year period, through a portion of the SJV.

Information technology advances has also made older information, specifically historic oil and gas well geophysical logs, available online. Scientific studies focusing on aspects of plate tectonics have also provided tantalizing new clues of possibly relevant geologic forces that might be influencing subsidence and earth fissure behavior.

2.1 Historical Geophysical Logs

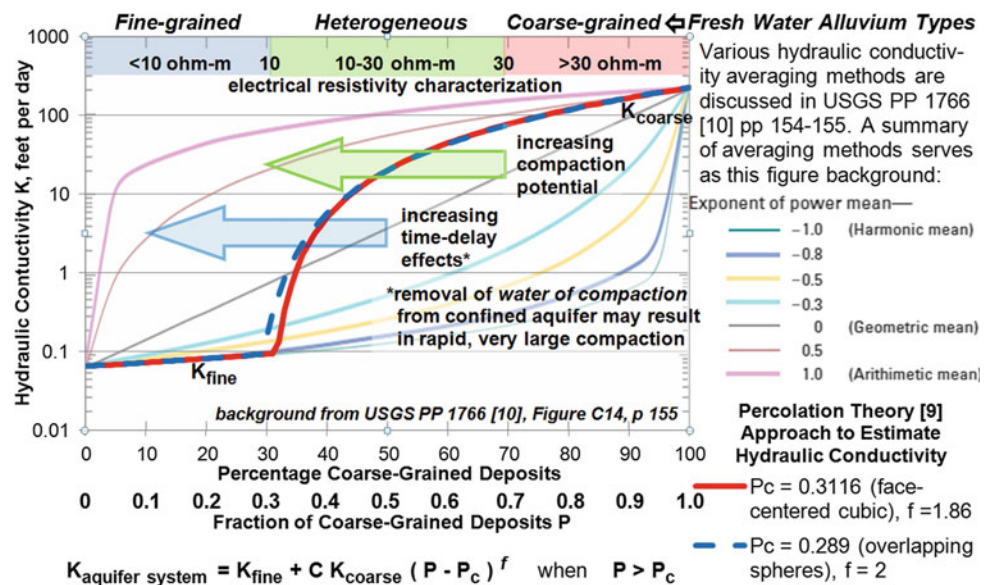
The State of California Department of Conservation Division of Oil, Gas and Geothermal resources (DOGGR) has scanned, and made available online, files of historical geophysical logs (DOGGR 2017). Downhole electrical logs, as described by Miller et al. (Miller et al. 1971) have long been a preferred means of deep alluvial basin characterization as utilized in the classic USGS subsidence studies in the SJV in the 1950s through 1970s. On-line access to these historic geophysical well log files permits evaluation of basin material characteristics and geometries to depths of thousands of feet at vertical resolutions of a few feet where such logs are available.

Alluvial basin materials compaction characteristics control subsidence magnitudes and rates, and electrical well logs provide a practical means to assess these materials. Rucker et al. (2015) describe typical material properties corresponding to fresh water alluvium types that impact subsidence behavior as summarized in Fig. 2 adapted from Faunt (2009). **Fine-grained alluvium**, with low resistivity

typically less than 10 Ωm, is composed primarily of very compressible silts and clays. Having low (less than about 1ft/day) to very low (less than about 0.1 ft/day) permeability, it compresses slowly in natural settings, perhaps over decades to centuries, with time being a function of layer thickness. However, major and rapid compression (and resulting major subsidence) may occur when confined aquifers having significant fine-grained alluvium are pumped. **Coarse-grained alluvium**, with high resistivity typically greater than 25–30 Ωm in fresh water aquifers, is composed primarily of sands and gravels. High energy transport typically results in densification during deposition, so it is relatively incompressible. Compaction tends to be minor, and given its' high permeability (typically greater than about 80 ft/day in Fig. 2), occurs rapidly. **Heterogeneous alluvium** is composed of inter-lensed and/or inter-fingered fine-grained and coarse-grained alluvium. The coarse-grained portions provide drainage to the very compressible fine-grained portions, so that overall moderate to major compaction (resulting in moderate to major subsidence) may occur over periods of years to decades. Heterogeneous alluvium with fresh water has moderate resistivity, typically about 10–25 or 30 Ωm.

Estimated quantitative inter-relationships of alluvium hydraulic conductivity (permeability), measured electrical resistivity, and percentage of coarse-grained materials in the aquifer system are presented in Fig. 2. Utilizing these relationships, borehole electrical logs can be a powerful tool for characterizing aquifer system compaction and resulting land subsidence. Rucker et al. (2015) have used such tools to help assess impacts and mitigation of subsidence on infrastructure. In their experience, typical impacts of sustained subsidence

Fig. 2 Estimating relationships between alluvium hydraulic conductivity, resistivity, and fraction of coarse-grained deposits in a fresh-water aquifer system utilizing concepts of percolation theory (PT) (Rucker et al. 2015). Parameter P_c is the percolation threshold at which exponential behavior change begins, and C is a scaling constant (Sahimi 1994). Background to figure is from Faunt (2009)



rates on infrastructure tend to be minor at less than 0.01 ft/year, may become moderate at about 0.01 to 0.1 ft/year, and have potential to be major when greater than 0.1 ft/year.

2.2 Recent Developments in Understanding Local Plate Tectonics

Saleeby et al. (2012, 2013) have interpreted a ‘delamination hinge’ defining a boundary between tectonic deep subsidence in the Tulare Basin portion of the SJV, and tectonic anomalous uplift or bulging at the adjacent southern Sierra Nevada Range. This hinge is interpreted to be at the top of the upper earth’s mantle at a depth of about 30 km. The approximate location of the southern portion of the hinge (trending north-northeast) is included in Fig. 1. It is reasonable to assume that the geologic material columns adjacent to the sides of the hinge, including compressible basin alluvium forming freshwater aquifer systems, would be in a state of horizontal tension at both the edge of anomalous deep subsidence in the Tulare Basin, and the edge of the Sierra uplift. A state of horizontal tension, and thus reduced geological material confinement, could result in lower material modulus,

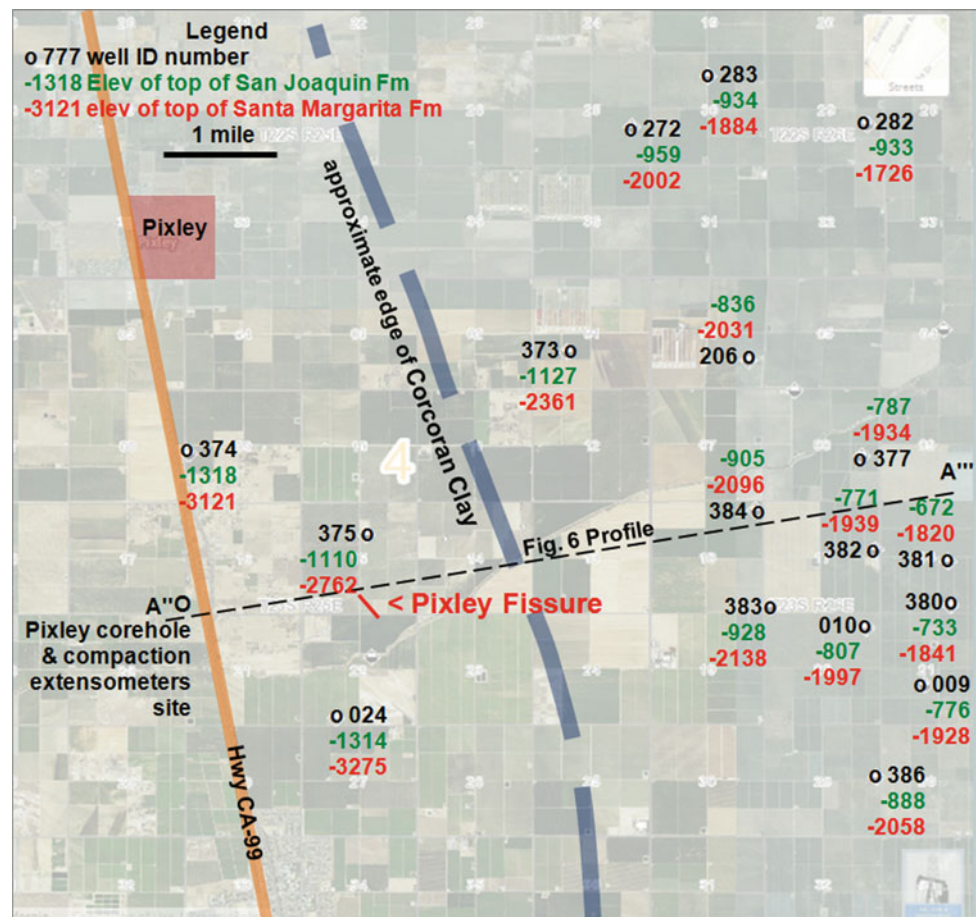
and thus greater compressibility (and resulting greater subsidence), in those aquifer system materials.

This interpreted delamination hinge is located between two localized subsidence bowls that developed prior to 1970 (Lofgren 1969) along Highway CA-99 as shown in Fig. 1. An area of reduced subsidence is located over the interpreted delamination hinge. This subsidence pattern is consistent with increased horizontal tension on either side of the delamination hinge relative to the horizontal stresses over the hinge. Farther to the north, other historic subsidence profiles have increases in subsidence rates starting near the edge of the interpreted hinge. The Pixley Fissure is located near to the approximate hinge edge along the side of the northern subsidence bowl.

3 Refined Local Geology from Geophysical Logs

Scans of historic well logs from the DOGGR website (DOGGR 2017) in the vicinity of the Pixley Fissure were downloaded and reviewed. Locations of wells with relevant and useful logs are shown in Fig. 3. The available

Fig. 3 Tops of San Joaquin (green) and Santa Margarita (red) formation elevations in Pixley Fissure vicinity from oil and gas well geophysical logs (DOGGR 2017). Approximate eastern edge of the Tulare Formation Corcoran Clay Member is also shown



information is primarily electrical resistivity logs, typically 16-inch short normal logs and 64-inch long normal or induction electrical logs, with corresponding spontaneous potential logs. The 16-inch short normal logs generally provide the most useful data (Miller et al. 1971). Substantial information concerning the local stratigraphy and fresh water aquifer is available from these logs.

3.1 Pixley Fissure Local Stratigraphy

Three distinct stratigraphic formations, the Tulare, San Joaquin and Santa Margarita Formations, are relevant to improved understanding of geologic conditions at the Pixley Fissure. Figure 3 summarizes contact elevations between these formations at specific well locations. The Tulare Formation is Pleistocene age basin alluvium that extends to depths of about 700 feet to over 1300 feet in the fissure vicinity. Within the Tulare Formation, the about 0.74 to 0.62 million year old (Ma) Corcoran Clay Member, is a lakebed clay. It is a regional aquifer confining layer to the west that feathers out in the fissure vicinity. The clay was tentatively identified in the Pixley corehole (Lofgren 1969) about 1.3 miles west of the Pixley Fissure, at a depth of about 300 feet. Its approximate extent has been extrapolated to the Pixley Fissure vicinity (Fig. 3). Oil wells penetrating the Corcoran Clay in this area were typically cased to depths of 400–500 feet or more before open hole logging could begin; logs from these wells were blinded to the presence or absence of the Corcoran Clay.

Underlying the Tulare Formation, the San Joaquin Formation represents the youngest marine sediments in the southern SJV. The top of the San Joaquin Formation has been aged to about 2.5 to 3.4 Ma. Its marine clays are anticipated to have lower resistivities, about 2 to 3 Ω m, than overlying Tulare freshwater clays with resistivities of typically 7 or more ohm-meters. However, east of the Pixley Fissure, relatively high resistivities in portions of the logs are consistent with fresh water in the high permeability coarse-grained alluvial units within the San Joaquin Formation. Lofgren and Klausing (1969) noted this deep fresh water to the east of the Pixley Fissure, extending to depths of

nearly 3000 feet, in their (Lofgren and Klausing 1969, Fig. 4) profile of the SJV through the Pixley corehole.

Finally, underlying the San Joaquin Formation, the top of the Santa Margarita Formation at depths of about 2000 feet to over 3000 feet in the Pixley Fissure vicinity, provides another distinct stratigraphic signature with an age of about 7 Ma (Saleeby et al. 2013). A resistivity increase, typically from about 2 to 3 Ω m to about 15 to 20 Ω m, accompanied by a large negative swing in the spontaneous potential, marks the top of the Santa Margarita Formation. Example well log formation contact interpretations are shown in Fig. 4.

3.2 Tulare Formation Stratigraphy

Applying the Fig. 2 resistivity criteria facilitates interpreting fine-grained, heterogeneous and coarse-grained alluvium in the fresh water aquifer system. Details of the alluvial materials composing the Tulare Formation become readily apparent. Several short-normal electrical logs in Fig. 5 have been color coded to depths of 1100 feet to enhance patterns of fine-grained (blue), heterogeneous (green to yellow) and coarse-grained (red) alluvial horizons within part of the fresh water aquifer. Wells 374, 024, 375 and 373 bracket the Pixley Fissure. Their plan view location is shown in Fig. 3 and resistivity well log profiles are shown in Fig. 5.

Measurements (at the short-normal resistivity tool vertical resolution of a few feet) illustrate several Tulare Formation alluvium material characteristics as shown in Fig. 5. First, there is great resistivity variability, and thus alluvium variability, within the vertical profile of each well log. Where logging begins (below a depth of about 500 feet), multiple fine-grained alluvium horizons with thickness ranging from about 20 to 80 feet, and in one instance, nearly 200 feet, are interpreted. Coarse-grained alluvium horizons, with thicknesses ranging from about 20 to 50 feet, are sometimes interspersed between fine-grained horizons. Finally, heterogeneous alluvium horizons fill the remaining vertical alluvium profiles. It appears that the overall alluvial system (below about 500-foot depth) at these wells has a heterogeneous nature as described in Fig. 2.

Fig. 4 Typical geophysical electrical log (DOGGR 2017) signatures for tops of the San Joaquin (left) and Santa Margarita (right) formations

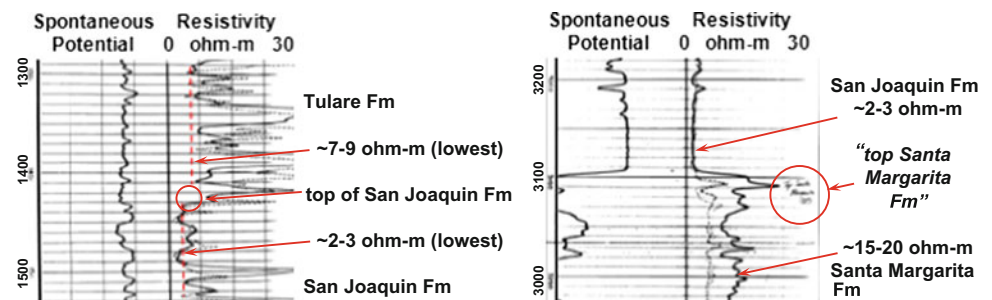
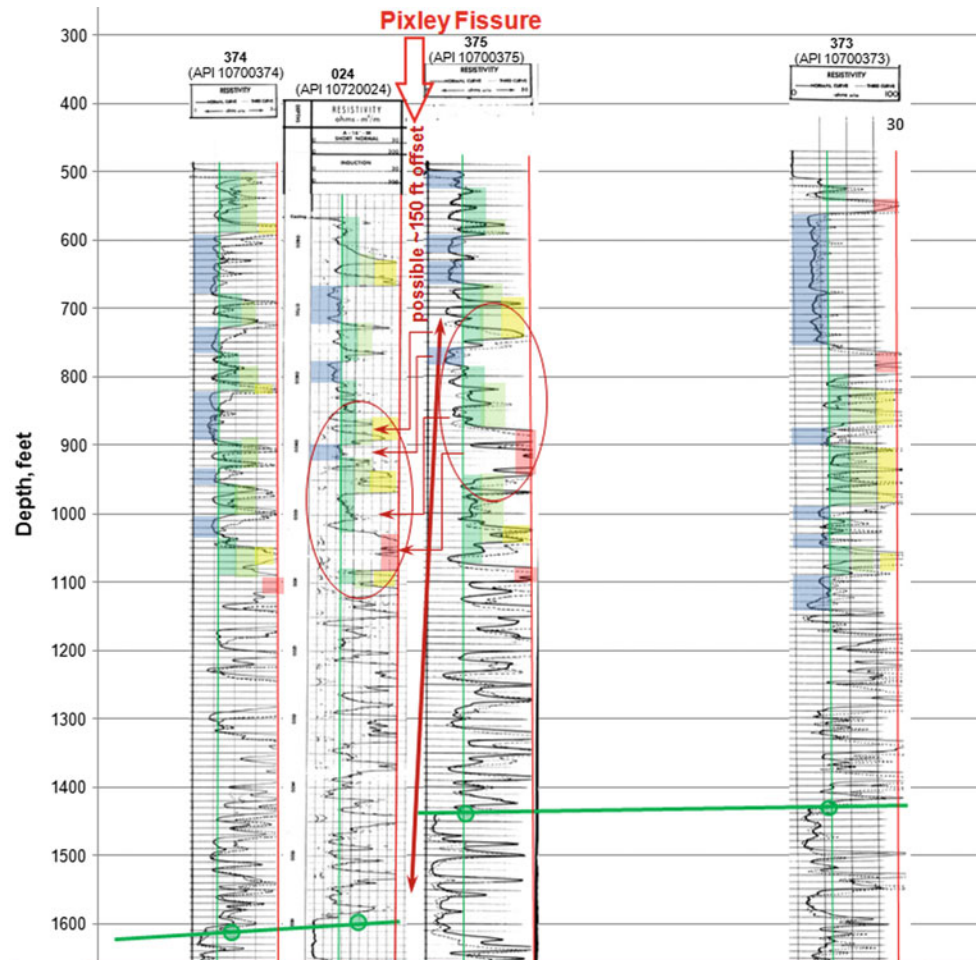


Fig. 5 Well logs (DOGGR 2017) nearest to the Pixley Fissure. Well locations are shown in Fig. 3. Resistivity color coding is similar to Fig. 2. An apparent offset of about 150 ft, downward to the southwest, between Wells 024 and 375, brackets the fissure



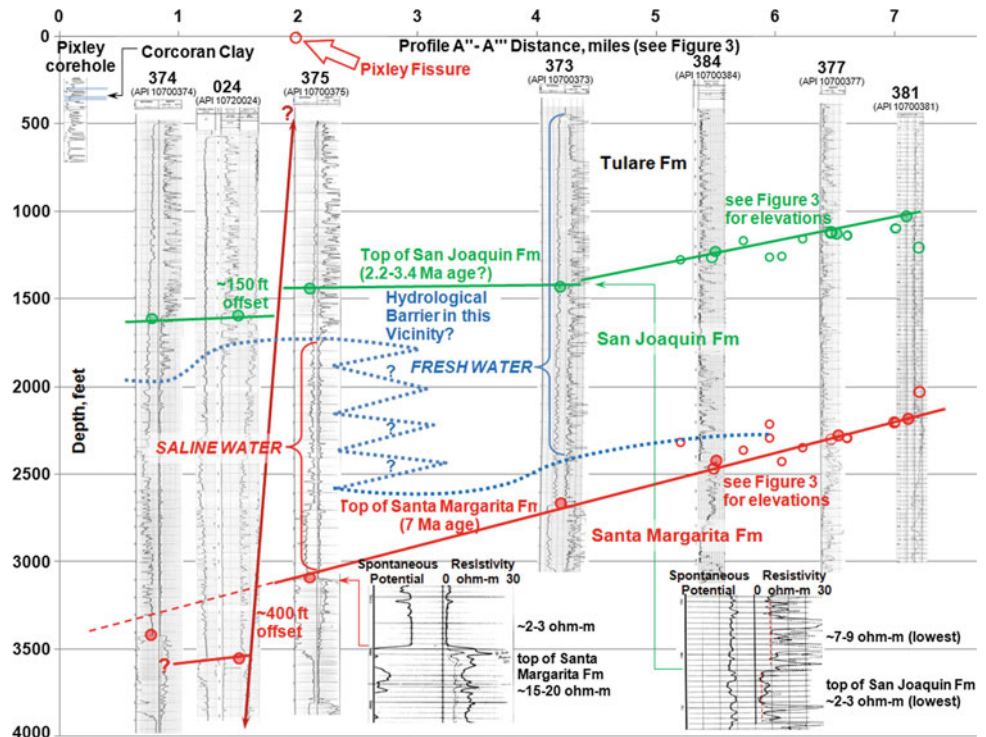
A second aspect of the Tulare Formation alluvium is the formation bottom, interpreted as the lowest depth with fine-grained alluvium resistivities greater than about $7 \Omega\text{m}$, shown in Fig. 5. Wells 375 and 373 northeast of the Pixley Fissure trend indicate bottom of the Tulare to be at depths of about 1430 to 1440 feet. Wells 374 and 024, west and southwest of the fissure trend, indicate the Tulare bottom to be at depths of about 1600 to 1620 feet. A possible offset of about 150 feet, downward to the southwest, is indicated at the geophysical log signature between the Tulare and underlying San Joaquin Formations.

Finally, patterns of fine-, heterogeneous and coarse-grained alluvium do not match up across the same depths between Wells 024 and 375 bracketing the Pixley Fissure. However, the alluvium pattern about 150 feet deeper in Well 024 does match well with the shallower Well 375 alluvium pattern. This is consistent with an about 150-foot offset downward to the southwest in the near vicinity of the Pixley Fissure.

3.3 Possible Vertical Offset at Top of Santa Margarita Formation

Another vertical offset between Wells 024 and 375 may be interpreted at depth below 3000 feet. As shown in Fig. 6, an offset of about 400 feet to the southwest is indicated from interpretations of the top of the Santa Margarita Formation (dated to about 7 Ma). This offset is about 2.7 times greater than the offset at the top of the San Joaquin Formation. Assuming a uniform vertical displacement rate over time, a 400-foot offset over 7 million years is consistent with a 150-foot offset over 2.6 million years. These offset rates are consistent with compaction faulting with tectonic origin similar to the PPCF (Holzer 1980) described in the introduction, and indicate potential for a hydrological barrier in the fissure vicinity (Fig. 6). Differential subsidence around the Pixley Subsidence Bowl likely generated horizontal strains capable of initiating earth fissuring. These strains may have been concentrated at the Pixley Fissure location due to

Fig. 6 Interpreted local geologic profile to 4000 ft depth in the Pixley Fissure vicinity. Well locations are shown in Fig. 3. Pixley Fissure and vertical offset zone is between Wells 024 and 375 (DOGGR 2017). Fresh and saline water aquifer system zones are shown, and a potential hydrological barrier is queried



the basin material offset and resulting hydrological barrier within the alluvium.

4 Conclusions

Where relevant historical oil and gas well geophysical logs are available for deep site characterization, more detailed subsidence-related geohazard evaluations have become practical. Geophysical log information in the Pixley Fissure area indicates a possible vertical offset, perhaps at least a compaction fault or deeper tectonic fault, in the fissure vicinity. Deep subsurface vertical offsets at the Pixley Fissure are comparable to and larger than vertical offsets interpreted at the PPCF located 15 miles to the south. The PPCF is likely a hydrological barrier (Holzer 1980) within the local fresh water aquifer system. Similarly, the offset at the Pixley Fissure might also act as a hydrologic barrier as implied by differences in fresh water aquifer depths in the area. Groundwater pumping near such a barrier could increase the likelihood of concentrating differential subsidence and initiating earth fissuring.

Characterization for earth fissure potential at new infrastructure, such as the California High Speed Rail alignment, would benefit from understanding potential vertical offsets and hydrological barriers within the basin alluvium. The HSR alignment crosses the PF trace and inferred clay

compaction (Saleeby and Foster 2004) faulting (Fig. 1). Effective subsidence monitoring can provide early warning of future differential subsidence impacts on HSR and other infrastructure that may need maintenance or mitigation.

References

- DOGGR: California DOGGR: California Department of Conservation, Division of Oil, Gas and Geothermal Resources Website. <https://secure.conservation.ca.gov/WellSearch/>. Accessed 29 Oct 2017
- Farr, T.G., Jones, C.E., Liu, Z.: Progress Report, Subsidence in the Central Valley, California, submitted to CA DWR, California. Available at: <http://www.nasa.gov/jpl/nasa-california-causing-valley-land-to-sink> (2015)
- Farr, T.G., Jones, C.E., Liu, Z.: Progress Report, Subsidence in California, March 2015–September 2016. Jet Propulsion Laboratory, California Institute of Technology (2017)
- Faunt, C.C. (ed.): Groundwater Availability of the Central Valley Aquifer, California. Geological Survey Professional Paper 1766 (2009)
- Guacci, G.: The Pixley Fissure, San Joaquin Valley, California. In: Saxena, S.K. (ed.) International Conference on Evaluation and Prediction of Subsidence held at Casino Hotel, Pensacola Beach, Florida, ASCE Engineering Foundations Conferences, pp. 303–319 (1979)
- Holzer, T.L.: Faulting caused by groundwater level declines. *Water Resour. Res.* **16**(6), 1065–1070 (1980)
- Lofgren, B.E., Klausning, R.L.: Land Subsidence due to Ground-Water Withdrawal, Tulare-Wasco Area, California. Geological Survey Professional Paper 437-B (1969)

- Miller, R.E., Green, J.H., Davis, G.H.: Geology of the Compacting Deposits in the Los Banos-Kettleman City Subsidence Area, California. Geological Survey Professional Paper 497-E (1971)
- Rucker, M.L., Ferguson, K.C., Panda, B.B.: Subsidence characterization and modeling for engineered structures in Arizona. *Proc. IAHS* **372**, 361–366 (2015)
- Smith, T.C.: Pond Fault, Northern Kern County. California Division of Mines and Geology Fault Evaluation Report FER-144 (1983)
- Sahimi, M.: Applications of Percolation Theory, 1st edn. Taylor & Francis, Bristol, Pennsylvania (1994)
- Saleeby, J., Le Pourhiet, L., Saleeby, Z., Gurnis, M.: Epeirogenic transients related to mantle lithosphere removal in the southern Sierra Nevada region, California, Part I implications of thermo-mechanical modeling. *Geosphere* **8**(6), 1286–1309 (2012)
- Saleeby, J., Foster, Z.: Topographic response to mantle lithospheric removal, southern Sierra Nevada region. *Calif. Geol.* **32**, 245–248 (2004). <https://doi.org/10.1130/G19958.1>
- Saleeby, J., Saleeby, Z., Le Pourhiet, L.: Epeirogenic transients related to mantle lithosphere removal in the southern Sierra Nevada region, California, Part II, implications of rock uplift and basin subsidence relations. *Geosphere* **9**(3), 394–425 (2013)

Mitigation Strategies and Engineering Solutions for Infrastructure at Risk from Earth Fissures

Kenneth C. Fergason and Michael L. Rucker

Abstract

Land subsidence can severely impact infrastructure and alter existing floodplain designations by changing ground elevation, ground slope (gradient), and through the development of ground cracks, known as earth fissures, that can erode into large gullies. Mitigation strategies and engineering solutions for infrastructure at risk from earth fissures are not widely available in existing literature, however many examples exist. Guidance on mitigation strategies intending to reduce the level of risk associated with the infrastructure exposed to earth fissure hazards has been developed for several sites in Arizona. The options are intentionally flexible so that the owner and design team can develop solutions that conform to the risk tolerance of stakeholders. The guidance is as follows:

- High Hazard Areas (earth fissures known to be present). Avoidance and/or significant engineered mitigation solutions.
- Moderate Hazard Areas (earth fissures could be present or develop in the future). Consider avoidance or implement engineered mitigation efforts such as structural elements and/or subsidence and earth fissure monitoring.
- Low Hazard Areas (earth fissures unlikely to be present or to develop in the future). Typical safety monitoring and maintenance for the infrastructure type.

Additionally, engineering solutions have been designed and constructed throughout the Southwestern USA. These engineering solutions depend on the consequence of failure for the infrastructure at risk due to earth fissuring. Solutions include a variety of design goals, such as prevention of catastrophic failure, reduction of maintenance needs, and monitoring the hazard. Constructed engineering solutions include monitoring

instrumentation, surface water diversion, cut-off walls, geotextile encapsulating aggregate ‘burrito’ wrap, structurally reinforced embankments, geotextile reinforcement of engineered fill, reinforced concrete lining, rip-rap lining, geotextile liners, use of controlled low-strength material backfill, and hybrid methods combining multiple approaches mentioned above.

Keywords

Land subsidence • Earth fissure • Mitigation

1 Introduction

Land subsidence can severely impact infrastructure and alter existing flood-plain designations by changing ground elevation, ground slope (gradient), and through the development of ground cracks, known as earth fissures, that can erode into large gullies. Mitigation strategies and engineering solutions for infrastructure at risk from earth fissures are not widely available in existing literature, however many examples exist. The purpose of this paper is to summarize some mitigation examples and offer guidance to mitigation strategies where earth fissuring poses a potential hazard due to earth fissures exists. The authors were directly involved in investigation and design for many of the examples presented in this paper, however other examples are discussed. A brief discussion of the land subsidence phenomenon and earth fissures that can result from land subsidence is included below.

1.1 Land Subsidence

Land subsidence due to groundwater withdrawal is caused by lowering the groundwater elevation in a column of unconsolidated material, increasing the effective stress. This

K. C. Fergason (✉) · M. L. Rucker
Wood Plc, Phoenix, AZ 85034, USA
e-mail: ken.fergason@woodplc.com

change in effective stress results in increased loading on the material column. If that column consists of granular materials, typically sands and gravels, compression below the initial water level is typically minor and takes place rapidly. Until granular particle contact points are changed by compression, at least some of the compression can be recovered elastically if water levels rise and effective stress decreases. Inelastic compression results from particle slipping or crushing; that portion of compression will not elastically rebound. If the material column contains a significant fraction of fine-grained materials, typically silts and clays, consolidation of the material below the initial water level may be relatively significant. The time frame of that consolidation is a function of the material permeability, where lower permeability increases consolidation time. Consolidation is further a function of the distance to higher permeability zones where excess pore pressure is relieved by draining water from the compressible fine, and especially clay-rich materials. Greater distances to such permeable drainage zones increases consolidation time. Although consolidation can be modeled (using modulus) as an elastic phenomenon, rebound from a decrease in loading (water level recovery) is a small fraction of the initial consolidation.

Multiple tools, some in use for many years and some available only in the last decade, are needed to effectively characterize local subsidence. Understanding of groundwater level changes, the driving mechanism for subsidence, often requires long-term water-level databases to document historic changes. Direct subsidence measurement has been and is accomplished by survey methods using historic baseline data with repeat surveys at specific locations. Recently, satellite-based repeat-pass synthetic aperture radar interferometry (InSAR) can measure subsidence across entire alluvial basins. When available, historic well log data provides limited information concerning basin lithology and geometry. In a few cases, detailed profiles of basin alluvium lithology can be interpreted from downhole geophysical logging of wells through basin alluvium. Historic well pump test and other data provide further hydrogeologic information. Gravity, seismic, and deep resistivity methods are useful for depth to bedrock and basin geometry characterization. Deep resistivity soundings are especially useful to characterize and estimate basin alluvium modulus and permeability parameters, and thus subsidence characteristics. Guidelines for characterizing land subsidence are published in both Arizona and Utah, providing a basic approach for land subsidence and earth fissure investigations (Arizona Land Subsidence Interest Group 2011; Lund 2016).

1.2 Earth Fissures

Where differential rates and magnitudes of land subsidence occur over relatively short distances, horizontal strains can become sufficient to cause earth fissuring. Jachens and Holzer (1979, 1982) evaluated threshold tensile strains to initiate fissuring based on studies of the Eloy Casa Grande area of Central Arizona. These studies included precise leveling and geophysical surveys, and comparisons with other cases of fissuring due to groundwater withdrawal. They concluded that at local basin scales with minimum benchmark spacing at fractions of a mile, most fissuring occurred at horizontal tensile strains in the range of about 0.02–0.06%. This compares with the threshold strains, measured at shorter-distance project station engineering scales, for cracking of compacted clay zones in dam embankments (or compacted clay liners) of about 0.1–0.3% (Leonards and Narain 1963; Covarrubais 1969).

The first recorded observance of earth fissuring in the Southwestern USA was in 1927 near the town of Picacho, Arizona (Leonard 1929). Since that time, eleven subsiding Central Arizona regions within the Basin and Range province have been identified, all with suspected or verified earth fissures (Fellows 1999; Poland 1981; Holzer and Davis 1981). Subsequent benchmark studies were undertaken to evaluate the distribution and mechanisms of fissuring (Jachens and Holzer 1979; Holzer 1980, 1981; Laney et al. 1978; Larson and Péwé 1986). Additional subsiding basins where earth fissures have been identified occur California, Nevada, Southern Utah, New Mexico, and Texas (Galloway et al. 1999; Borchers and Carpenter 2014).

Earth fissures overlying alluvial aquifers suffering large groundwater decline are likely associated with a process termed generalized differential compaction (Carpenter 1994). At least one of three mechanisms are likely at play to form fissures: (1) bending of a plate above a horizontal discontinuity in compressibility (Lee and Shen 1969), (2) dislocation theory representing a tensile crack (Carpenter 1994) and (3) vertical propagation of tensile strain caused by draping of the alluvium over a horizontal discontinuity in compressibility (Haneberg 1992). Given these probable mechanisms, fissures commonly develop along subsiding basin perimeters, often in apparent association with buried or protruding bedrock highs, suspected mountain-front faults or distinct facies changes in the alluvial section.

Fissures often first manifest at the surface as subtle hairline cracks, or as alignments of small potholes. These features are commonly modified by burrowing animals.



Fig. 1 Examples of earth fissures. Beginning clockwise from the top left: (1) un-eroded incipient earth fissure in bottom of trench excavation at powerline FRS in Central, Arizona, (2) fresh earth fissure gully at Siphon Draw Wash Basin in Central Arizona, (3) earth fissure with

vertical deformation in Southern Utah, (4) large earth fissure gully in Southern Nevada, (5) mature and partially in-filled earth fissure gully including dumped tires in Central Arizona, and (6) mature, in-filled earth fissure gully at McMicken Dam in Central Arizona

Overland surface water flow is then intercepted, and the surface manifestation of the fissure grows as piping erosion and material caving occur during runoff events. Figure 1 shows several examples of earth fissures.

2 Guidance

Guidance on mitigation strategies intending to reduce the level of risk associated with the infrastructure exposed to earth fissure hazards has been developed for several sites in Arizona and California. Recommended options are intentionally flexible so that the owner and design team can develop solutions that conform to the public safety requirements and stakeholder risk tolerance. The guidance is as follows:

- High Hazard Areas (earth fissures known to be present). Avoidance and/or significant engineered mitigation solutions.
- Moderate Hazard Areas (earth fissures could be present or develop in the future). Consider avoidance or implement engineered mitigation efforts such as structural elements and/or subsidence and earth fissure monitoring.
- Low Hazard Areas (earth fissures unlikely to be present or to develop in the future). Typical safety monitoring and maintenance for the infrastructure type.

A strategy of avoidance is most often recommended in areas where earth fissure hazards are present. However, in some situations avoidance is not possible, or avoidance of an earth fissure is spatially constrained. Earth fissuring could still present a future hazard if existing fissures were to grow or if new fissures were to develop. In these cases some form of remediation is needed to reduce the risk posed by the earth fissure hazard.

3 Mitigation Strategies

Engineering solutions have been designed and constructed throughout the Southwestern USA where earth fissuring is considered to be a potential hazard. These engineering solutions are dependent on the consequence of failure for the infrastructure at risk and include design goals, such as prevention of catastrophic failure, reduction of maintenance needs, and monitoring of the hazard. Typically, multiple remedial strategies are utilized to meet these goals.

Additional strategic considerations discussed below include whether a known earth fissure is in direct contact with the planned infrastructure, if the planned infrastructure is located near an area where earth fissuring is present, or that potential for earth fissuring to develop in the future has been determined. Remediation strategies will vary depending on the proximity in space and time of the planned infrastructure and existing or potential earth fissuring.

The life cycle of earth fissures is not well understood, particularly in the case of surficial deformation. For example, an existing earth fissure could be undergoing active and measurable surface deformation, while another earth fissure could be dormant with no active or measurable deformation occurring, but with a potential for future deformation to occur. Once groundwater decline has stopped and resulting subsidence ceased, an earth fissure could have no active or measurable surface deformation and be considered ‘extinct’ or ‘relic’; unless future groundwater decline occurs, it is reasonable to assume that there is little or no potential for future deformation to occur. Remediation strategies and the perceived risk to infrastructure will be different for each of those scenarios, and considerable investigative effort may be necessary to determine which scenario is most applicable.

3.1 Monitoring

Although monitoring is often not thought to be mitigation, it is arguably the most important and widespread remedial method used for earth fissures. Monitoring reduces the risk an earth fissure could pose to infrastructure by repeated observation allowing for additional action to be undertaken if or when activity associated with an earth fissure threatens the monitored infrastructure. Methods include monitoring the land subsidence (survey, InSAR, groundwater levels, etc.) that causes earth fissures, and direct monitoring of earth fissures (mapping, visual observation, ground displacement measurements, etc.). Monitoring methods currently utilized in the Southwestern USA include conventional practices and proven, instrumented in-ground sensing systems. Conventional techniques include repeat optical levelling and GPS surveys, ground reconnaissance, photo-geological analysis, groundwater monitoring, and tape-extensometers. Advanced techniques include the processing and interpretation of differential interferograms of repeat-pass, satellite-based synthetic aperture radar data (InSAR), and as-needed in specific situations, borehole tiltmeters, microseismic arrays, excavation of monitoring trenches, quartz tubes, and time-domain reflectometry (TDR) (Ferguson et al. 2015).

Examples of infrastructure projects that have active earth fissure monitoring projects include several flood control district projects in Central Arizona including McMicken Dam (Rucker 2008; Ferguson et al. 2013; Rucker et al. 2013), Vineyard Road, White Tanks No. 3, and Powerline Flood Retarding Structures (FRS), and Siphon Draw Wash Basin (Ferguson and Rucker 2018). Monitored industrial ponds include the Arizona Electric Power Cooperative (AEP) Apache Generating Station (Keaton et al. 1998) and brine ponds at a natural gas storage facility. Additionally, fissuring is monitored at a facility in Chino, California (Carpenter 2015), and at a mine in northern Nevada.

3.2 Surface Water Diversion

Typically the biggest risk posed to infrastructure from earth fissuring relates to potentially destructive (piping) erosion of near-surface soils at an earth fissure. Therefore one of the most common mitigation strategies is to limit or prevent surface water from entering into an earth fissure. Several strategies exist to achieve this, including simple backfill of an earth fissure and creation of positive drainage away from the earth fissure (backfill methods are discussed in further detail in Sect. 3.8). Other methods include creating diversion structures upstream of earth fissures. Many of the other remediation strategies discussed in this paper are variations of the basic concept of prevention of erosion by limiting surface and subsurface water flow. Most remedial strategies for earth fissure hazards involve some form of surface-water drainage control.

Examples of infrastructure where surface water diversion mitigations are utilized include the Central Arizona Project (CAP) Canal in Central Arizona where known earth fissures were backfilled with local materials and left with positive drainage, essentially forming a small embankment where there was once an earth fissure. For the Powerline FRS in Central Arizona, a new section of FRS was constructed to both avoid an encroaching earth fissure and to limit surface flow to that earth fissure’s location.

3.3 Cut-Off Walls

Cut-off walls and related strategies are designed to limit water flow and flow velocity through an earth fissure below the ground surface, limiting the ability for piping erosion to occur. This strategy involves constructing a cut-off wall from the surface to a more competent soil layer at depth. Driven piles have been utilized as well, though not extensively as driven piles often have constructability issues in arid-land soils.

Cut-off walls have been utilized at several sites in the Southwest USA, including the Hunt Highway in Central Arizona, White Tanks FRS No. 3 in Central Arizona, Siphon Draw Wash Basin in Central Arizona (Ferguson and Rucker 2018), I-80 in Northern Nevada, the CAP Canal in Central Arizona (driven piles), and a mine site in Northern Nevada.

3.4 Geotextile Encapsulating Aggregate ‘Burrito’ Wrap

The design goal of a geotextile encapsulating aggregate ‘burrito’ wrap is to limit erosion of an earth fissure while allowing some water to slowly flow through. This concept is similar in nature to aggregate filter drains utilized to stop cracking in embankments. This method is typified by excavation of an earth fissure, placement of a geotextile

fabric, and encapsulation of aggregate backfill with the fabric. This method has been utilized in Southeastern Arizona where an earth fissure crosses a busy county roadway in Cochise County. This mitigation has not alleviated ongoing vertical deformation of the earth fissure, but has prevented large-scale piping erosion at the fissure under the roadway in an area of flash flooding and potential catastrophic failure of the roadway. Similar designs have been recommended for roadways in Maricopa County, Arizona.

3.5 Structurally Reinforced Embankments

In areas where dams, FRSs, levees, and other embankments are potentially at risk from earth fissuring, structural reinforcement is a mitigation strategy that has been employed. Structural reinforcement can be achieved through several methods, including geotextiles, concrete, soil cement, and others. Generally the intent of the structural reinforcement is to prevent catastrophic failure of the embankment were an earth fissure to cause piping erosion of the foundation.

Locations where structurally reinforced of embankments have been utilized include McMicken Dam and White Tanks FRS No. 3 in Central Arizona.

3.6 Seepage Blanket

Another mitigation strategy to limit potential erosive forces in an earth fissure include methods for lengthening the seepage path within the earth fissure system. At McMicken Dam in Central Arizona, this was achieved with a soil cement apron that extended upstream of the embankment.

3.7 Reinforced Concrete and Other Liners

Where channels, basins, or other water transport/storage facilities face a potential hazard from earth fissures, a commonly utilized remedial strategy is to line the facility. Risk of failure of the infrastructure is realized by limiting water from the system entering the earth fissure and from reinforcement of the structure if the earth fissure causes erosion in the foundation.

Reinforced concrete lining is the most common approach employed and examples of its utilization include the CAP canal in Central and Southern Arizona, Dysart Drain in Central Arizona, Meridian Channel in Central Arizona, and drainage channels along several highways including I-10 in Southern Arizona and SR 202L in Central Arizona.

Other liner methods for channels and basins include HDPE liners, often in combination with rip-rap support. Examples where HDPE liners have been utilized include the Siphon Draw Wash Basin in Central Arizona (Fig. 2) (Ferguson and Rucker 2018) and the AEPCO Apache Generating Station in Southeastern Arizona. Additionally, at the SR 303L highway in Central Arizona, the mitigation design incorporated a geogrid filtration barrier (Neely 2011).

3.8 Backfill

Excavation and backfill of an earth fissure is one of the most basic mitigation strategies utilized. This method often mitigates existing erosion from the earth fissure and limits the potential for future erosion with backfill that is more resistant to erosion. These methods are often quick and economic though it is generally not a long-lasting mitigation unless combined with other methods.

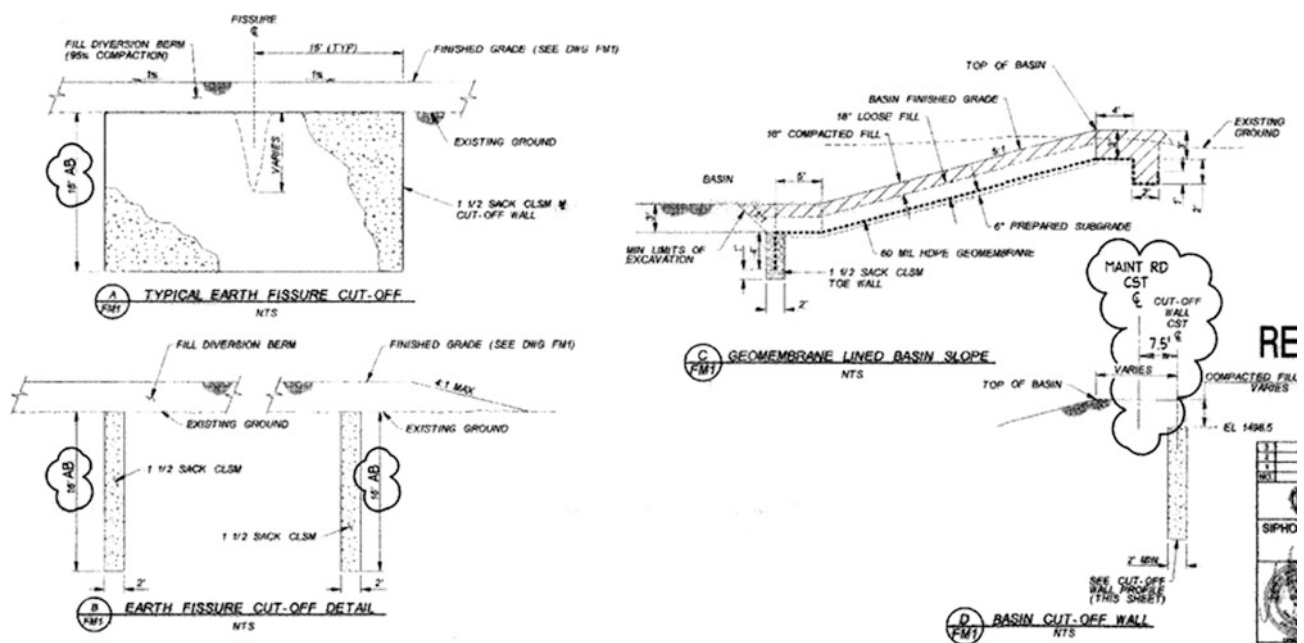


Fig. 2 Design drawings for cut-off wall and geomembrane liner at Siphon Draw Wash Basin in Central Arizona (Ferguson and Rucker 2018)

Engineered Fill. Backfilling an earth fissure with compacted fill is one approach often utilized. This approach limits but does not eliminate the potential for future erosion to occur in an earth fissure and is often utilized in areas with lower traffic roadways, residential and other small-scale developments. An example of this includes the intersection of Meridian and Baseline Roads in Central Arizona.

Geotextile Reinforcement. Geotextile reinforcement of an earth fissure is a common way to limit deformation, and is a simpler version of the approach described in Sect. 3.4. Single or multiple layers of reinforcement can be utilized. Examples of geotextile reinforcement include the intersection of Baseline and Meridian Roads, the SR 202L and SR 303L (Neely 2011) in Central Arizona, and I-10 in Southern Arizona.

Cement Reinforcement. Backfill with materials such as a concrete slurry, controlled low-strength material, soil cement, or other materials that are strengthened with cementing agents can be utilized. This method has been utilized by electric utilities where earth fissures are present near access roadways for powerline corridors and in the vicinity of transmission tower foundations.

Aggregate. Erosion potential can potentially be limited by utilizing aggregate and other ‘filter’ backfill materials.

Sand Bags. Sand bags can provide a quick and economic backfill material that can reduce the potential for erosion along an earth fissure. This approach can be especially useful as an emergency or other rapid response during a runoff event as a temporary remediation until a more robust solution can be implemented.

Geo-foam. Geo-foam backfill materials can provide a quick and economic backfill material that can reduce the potential for erosion along an earth fissure. The authors are not aware of any locations where this method has been utilized specifically to mitigate an earth fissure, however it could be a viable method to consider.

References

- Arizona Land Subsidence Interest Group: Suggested Guidelines for Investigating Land-Subsidence and Earth Fissure Hazards in Arizona. Arizona Geological Survey Contributed Report CR-11-D (2011)
- Borchers, J.W., Carpenter, M.: Land subsidence from groundwater use in California. Prepared by Luhdorff & Scalmanini Consulting Engineers. Prepared for the CA Water Plan Update 2013, vol. 4 Reference Guide (2014)
- Carpenter, M.C.: Continuous monitoring of an earth fissure in Chino, California, USA—a management tool. Proc. IAHS **372**, 291–296 (2015)
- Carpenter, M.C.: Deformation across and near earth fissures: measurement techniques and results. U.S. Geological Survey Subsidence Interest Group Conference, Edwards Air Force Base, Antelope Valley, California, November 18–19, 1992: Abstracts and Summary. Open-file Report 94–532 (1994)
- Covarrubais, S.W.: Cracking of earth and rock-fill dams: a theoretical investigation by means of the finite element method. Harvard Soil Mechanics Series No. 82. 163 p. Harvard University Press, Cambridge, MA (1969)
- Fellows, L.D.: Groundwater pumping causes Arizona to Sink. *Ariz. Geol.* **29**(3), 1–5 (1999)
- Fergason, K.C., Rucker, M.L., Greenslade, M.D.: Investigative procedures for assessing earth fissure risk for dams and levees, United States Society on Dams, 33rd Annual Meeting and Conference, Phoenix, AZ, 11–15 Feb 2013
- Fergason, K.C., Rucker, M.L., Panda, B.: Methods for monitoring land subsidence and earth fissures in the Western USA. In: Proceedings IAHS, 372, Proceedings of the Ninth International Symposium on Land Subsidence, Nagoya, Japan, November 15–19, pp. 361–366 (2015)
- Fergason, K.F., Rucker, M.L.: Earth Fissures and Infrastructure: A Case History at the Siphon Draw Detention Basin, Central Arizona. IAEG/AEG Annual Meeting Proceedings, San Francisco, CA, 2018—Volume 5: Geologic Hazards: Earthquakes, Land Subsidence, Coastal Hazards, and Emergency Response, Volume 5—IAEG-AEG_2018, 032, v1 (2018)
- Galloway, D.L., Jones, D.R., Ingebritsen, S.E.: Land subsidence in the United States, U.S. Geological Survey Circular 1182, 177 p. (1999)
- Haneberg, W.C.: Drape folding of compressible elastic layers, I. analytical solutions for vertical uplift. *J. Struct. Geol.* **15** (1992)
- Holzer, T.L., Davis, S.N.: Earth fissures caused by ground-water level declines, Sonoran and Mojave deserts. *Geol. Soc. Am. Abs. Prog.* **13**(2), 61–62 (1981)
- Holzer, T.L.: Preconsolidated stress of aquifer systems in areas of induced land subsidence. *Water Resour. Res.* **17**(1) (1981)
- Holzer, T.L.: Reconnaissance maps of earth fissures and land subsidence, Bowie and Willcox Areas, Arizona. U.S. Geological Survey Miscellaneous Field Studies Map MF-1156 (1980)
- Jachens, R.C., Holzer, T.L.: Differential compaction mechanisms for earth fissures near casa grande. *Ariz. Geol. Soc. Am. Bull.* **93**, 998–1012 (1982)
- Jachens, R.C., Holzer, T.L.: Geophysical Investigations of Ground Failure Related to Groundwater Withdrawal, Picacho Basin, Arizona in Groundwater, vol. 17, no. 6. pp. 574–585
- Keaton, J.R., Rucker, M.L., Cheng, S.S.: Geomechanical analysis of an earth fissure induced by ground-water withdrawal for design of a proposed ash and sludge impoundment, Southeastern Arizona. In Land Subsidence Case Studies and Current Research: Proceedings of the Dr. Joseph F. Poland Symposium on Land Subsidence, Edited by Borchers, J.W., Special Publication No. 8, Association of Engineering Geologists, Star Publishing Company, Belmont, California, pp. 217–226, (1998)
- Laney, R.L., Raymond, R.H., Winikka, C.C.: Maps Showing Water Declines, Land Subsidence, and Earth Fissures in South-Central Arizona. U.S. Geological Survey Water Resources Investigations Open-file Report 78–83 (1978)
- Larson, M.K., Péwé, T.L.: Origin of Land Subsidence and Earth Fissuring, Northeast Phoenix, Arizona. *Bull. Assoc. Eng. Geol.* **XXIII**(2), 139–165 (1986)
- Lee, K.L., Shen, C.K.: Horizontal movements related to subsidence. *J. Soil Mech. Found. Div. ASCE* **95**(SM1), 139–166 (1969)
- Leonard, R.J.: An earth fissure in Southern Arizona. *J. Geol.* **37**(8), 765–774 (1929)
- Leonards, G.A., Narain, J.: Flexibility and cracking of earth dams. *ASCE J. Soil Mech. Found Div.* **89**(SM2), Pt. 1, pp. 47–98 (1963)
- Lund, W.R.: Guidelines for evaluating land-subsidence and earth-fissure hazards in Utah. In Bowman, S.D., Lund, W.R. (eds.) Guidelines for investigating geologic hazards and preparing engineering-geology reports, with a suggested approach to geologic-hazard ordinances in Utah: Utah Geological Survey Circular 122, pp. 93–110

- Neely, S.D.: Identification and Mitigation of an Earth Fissure. Arizona State Route 303L; Glendale Avenue to Peoria Avenue Segment, Phoenix, Arizona. Prepared for the 62nd Highway Geology Symposium, July 2011
- Poland, T.F.: Subsidence in the United States due to groundwater withdrawal. *J. Irrig. Drain. Div. ASCE* **107**(2), 115–135 (1981)
- Rucker, M.L., Ferguson, K.C., Greenslade, M.D., Hansen, L.A.: Characterization of Subsidence Impacting Flood Control Dams and Levees, United States Society on Dams, 33rd Annual Meeting and Conference, Phoenix, AZ, 11–15 Feb 2013
- Rucker, M.L., Greenslade, M.D., Weeks, R.E., Ferguson, K.C., Panda, B.B.: Geophysical and remote sensing characterization to mitigate McMicken Dam. In: Reddy, K.R., Khire, M.V., Alshwabkeh, A.N. (eds.) *GeoCongress 2008: Geosustainability and Geohazard Mitigation (GSP 178)*, pp. 207–214. American Society of Civil Engineers (2008)

Earth Fissures and Infrastructure: A Case History at the Siphon Draw Detention Basin, Central Arizona

Kenneth C. Fergason and Michael L. Rucker

Abstract

Land subsidence can severely impact infrastructure and alter existing floodplain designations by changing ground elevation, ground slope (gradient), and sometimes through the development of ground cracks, known as earth fissures, that can erode into large gullies. Due to the alteration of surface water flow, ground elevation, and ground cracking that can undermine foundations, subsidence poses a particularly high risk to water conveyance, flood control, and other linear infrastructure. The Siphon Draw Wash (SDW) Detention Basin in Apache Junction, Arizona provides a unique opportunity to observe the impact of an actively propagating earth fissure. Earth fissures were first identified in the area in the 1990s. In the mid-2000s, plans were developed to construct a basin and channel to provide flood control along Siphon Draw Wash. A series of land subsidence and earth fissure investigations were performed as part of the design process for the SDW Detention Basin. During investigations, the nearby Southwestern Earth Fissure (SWEF) extended over 200 feet overnight following a rain event. Later during the investigation a trench located at the termination of the fissure extension was flooded by another rain event. The SWEF extension terminated just upstream of the boundary of the basin. The need for a basin for flood control purposes at this location required that fissure mitigation measures be implemented. Mitigation strategies included constructing 2 16-foot deep by 2-foot wide by 30-foot long slurry cut-off walls along the fissure extension and placing an embankment over the fissure extension, to help prevent propagation of the fissure into the basin. In addition, cut-off walls and geomembrane liner were constructed along the southwest embankment of the basin, to help prevent the fissure from moving further southwest toward residential areas, in the event that the fissure propagates into the basin.

Construction of the SDW Detention Basin and Meridian Channel was completed in 2010. An annual monitoring program has been implemented that includes evaluation of satellite-based interferometric synthetic-aperture radar (InSAR), real-time kinematic GPS survey, analysis of high-resolution aerial imagery, and annual ground inspection.

Keywords

Land subsidence • Earth fissure • Mitigation

1 Introduction

Land subsidence can severely impact infrastructure and alter existing flood-plain designations by changing ground elevation, ground slope (gradient), and causing the development of ground cracks known as earth fissures. The Siphon Draw Wash (SDW) Detention Basin and Meridian Channel system provides a unique opportunity to observe how earth fissures interact with infrastructure. The project was constructed in close proximity to an actively propagating earth fissure designated the Southwestern Earth Fissure (SWEF). Mitigations were included in the basin and channel design, including an annual monitoring system that has allowed the system to be observed since construction in 2010.

The SDW Detention Basin is part of the larger SDW Drainage Improvement Project, which is owned and operated by the Flood Control District of Maricopa County (FCDMC). Other notable stake-holders in the project include the Arizona Department of State Lands and the City of Mesa. The SDW Drainage Improvements Project consists of the two components: (1) SDW Detention Basin and (2) Inlet Structure and Meridian Channel. These improvements are located approximately 1.5 miles west of the Powerline and Vineyard Road Flood Retarding Structures (FRS), and northeast of the intersection of Meridian and Elliott Roads, in the City of Apache Junction and in unincorporated

K. C. Fergason (✉) · M. L. Rucker
Wood Plc, Phoenix, AZ 85034, USA
e-mail: ken.fergason@woodplc.com

Maricopa County, Arizona. The SDW Detention Basin is an earth-lined basin with tall-pot trees planted around the basin perimeter and on the slopes, and is hydroseeded with native vegetation. The basin intercepts flood flows from the north and detains flows from Siphon Draw Wash, and outlets back to the wash. Cut-off walls constructed of controlled low strength material (CLSM), along with a buried geomembrane liner, were installed along the basin's western and southern sides to mitigate potential impacts of earth fissures that could potentially develop within the basin. Cut-off walls were also installed at the ends of the visible portion of a known earth fissure at the northeastern portion of the basin. That fissure was then backfilled. The Meridian Channel is an incised, concrete-lined channel that runs east of the Meridian Road alignment from the north end of Meridian Road to West Guadalupe Road. The Meridian Channel conveys flood flows from the north and outlets to the SDW Basin. A brief discussion of the land subsidence phenomenon and earth fissures that can result from land subsidence is included below.

1.1 Land Subsidence

Land subsidence due to groundwater withdrawal is caused by lowering the groundwater elevation in a column of alluvial basin material, which increases the effective stress within that column. This increase in effective stress results in an increase in loading on the material column. If that column consists of granular materials, typically sands and gravels, compression of the material below the initial water level is typically minor and takes place rapidly. Until granular particle contact points are changed by compression, at least some of the compression can be recovered elastically if water levels rise and effective stress decreases. Compression that results from particle slipping or crushing will tend to have much less elastic rebound. If the material column contains a significant fraction of fine-grained materials, typically silts and clays, consolidation of the material below the initial water level may be relatively significant, yet take place slowly. The time frame of the consolidation is a function of the materials' permeability, where lower permeability increases consolidation time. Consolidation is further a function of the distance to higher permeability zones which relieve the excess pore pressure by draining water from clay-rich materials. Greater distances to such permeable drainage zones increases consolidation time. Although consolidation increases can be modeled as an elastic phenomenon, rebound of the consolidation is typically not recoverable with a decrease in loading.

Multiple tools, some in use for many years and some available only in the last decade, are needed to effectively

characterize local subsidence. Characterization of groundwater level changes, the driving mechanism for subsidence, requires long-term water-level databases to document historic changes. Direct subsidence measurement has been and is accomplished using survey methods with historic baseline data with repeat surveys at specific locations, and recently, satellite-based repeat-pass synthetic aperture radar interferometry (InSAR) that can cover entire alluvial basins. When available, historic well log data provides limited information concerning basin lithology and geometry. Historic well pump test and other well data provide further hydrogeologic information. Gravity, seismic, and deep resistivity methods are useful for depth to bedrock characterization. Deep resistivity soundings are especially useful to characterize and estimate basin alluvium modulus and permeability, and thus subsidence characteristics. Guidelines for characterizing land subsidence have been published in both Arizona and Utah, providing a basic approach for land subsidence and earth fissure investigations (Arizona Land Subsidence Interest Group 2011; Bowman and Lund 2016).

1.2 Earth Fissures

Where differential rates and magnitudes of land subsidence occur over relatively short distances, horizontal strains can become sufficient to cause earth fissuring. Jachens and Holzer (1979, 1982) evaluated threshold tensile strains for fissuring based on studies of the Eloy Casa Grande area of Central Arizona. These studies included precise leveling and geophysical surveys, and comparisons with other cases of fissuring due to groundwater withdrawal. Jachens and Holzer (1982) concluded that, at local basin scales at minimum benchmark spacing at fractions of a mile, most fissuring occurred at horizontal tensile strains in the range of about 0.02–0.06%. This compares with the threshold strains, measured at shorter-distance project station engineering scales, for cracking of compacted clay zones in dam embankments (or compacted clay liners) of about 0.1–0.3% (Leonards and Narain 1963; Covarrubais 1969).

The first recorded observance of earth fissuring in the Southwestern USA was in 1927 near the town of Picacho, Arizona (Leonard 1929). Since that time, eleven subsiding Central Arizona regions within the Basin and Range province have been identified, all with suspected or verified earth fissures (Fellows 1999; Poland 1981; Holzer and Davis 1981). Subsequent benchmark studies were undertaken to evaluate the distribution and mechanisms of fissuring (Jachens and Holzer 1979; Holzer 1980, 1981; Laney et al. 1978; Larson and Péwé 1986). Additional subsiding basins where earth fissures have been identified occur in Southern California, Central California, Nevada, Southern Utah, New

Mexico, and Texas (Galloway et al. 1999; Borchers and Carpenter 2013).

Earth fissures in areas of large groundwater decline in alluvial aquifers are likely associated with a process termed generalized differential compaction (Carpenter 1992). Three mechanisms are likely at play to ultimately form fissures: (1) bending of a plate above a horizontal discontinuity in compressibility (Lee and Shen 1969), (2) dislocation theory representing a tensile crack (Carpenter 1992) and (3) vertical propagation of tensile strain caused by draping of the alluvium over a horizontal discontinuity in compressibility (Haneberg 1992). Due to these probable mechanisms, fissures commonly develop along the perimeter of subsiding basins, often in apparent association with buried or protruding bedrock highs, suspected mountain-front faults or distinct facies changes in the alluvial section.

Fissures often first manifest at the surface as subtle hairline cracks, or as alignments of small potholes, commonly modified by burrowing animals. Overland surface water flow is then intercepted, and the surface manifestation of the fissure grows as piping erosion and material caving occur during runoff events.

Mitigation strategies and engineering solutions for infrastructure at risk from earth fissures are not widely available in existing literature, however Ferguson and Rucker (Ferguson and Rucker 2018) summarize methods employed in the Southwestern USA.

2 Land Subsidence and Earth Fissure Investigations

Land subsidence and earth fissures were recognized to be potential hazards for the design of the SDW Detention Basin and Meridian Channel. In 2006 an initial land subsidence and earth fissure hazard investigation was performed. This was followed by a more comprehensive land subsidence and earth fissure hazard investigation performed as part of the final design for the project in 2007.

2.1 Initial Land Subsidence and Earth Fissure Hazard Investigation

The initial land subsidence and earth fissure hazard investigation consisted of literature and data review, analysis of InSAR, analysis of high-resolution digital aerial imagery, geologic reconnaissance, and an initial delineation of earth fissure risk zones pertaining to the channel and basin.

The data review task of the investigation included review of relevant publications, technical reports, and groundwater data from government sources. It also included review of

previous work performed for the Powerline FRS, located about 1.5 miles east of the project.

InSAR data was acquired, reviewed, and analyzed for the times that were available, allowing for an in-depth recent land subsidence history to be determined. Analysis of high-resolution aerial imagery allowed detailed mapping of known and suspected earth fissures in the project vicinity to be identified and confirmed through geologic reconnaissance.

Results of the investigation were utilized to develop a delineation of earth fissure risk zones to aid in the ongoing design of the project. Additional recommendations were given to specific planned project elements in regard to potential risk from land subsidence and earth fissures, including guidance summarized below. The options were intentionally flexible so that the owner and design team could develop solutions that conformed to the risk tolerance of stakeholders.

- High Hazard Areas (earth fissures known to be present). Avoidance and/or significant engineered remedial solutions.
- Moderate Hazard Areas (earth fissures could be present or develop in the future). Consider avoidance or implement engineered remedial efforts such as structural elements and/or subsidence and earth fissure monitoring.
- Low Hazard Areas (earth fissures unlikely to be present or to develop in the future). Typical safety monitoring and maintenance for the infrastructure type.

2.2 Final Design Land Subsidence and Earth Fissure Hazard Investigation

The purpose of the final design land subsidence and earth fissure investigation was to further refine the delineation of risk developed in the initial investigation, and provide geotechnical information for design of the project elements. The investigation included updates to the previous investigation, completion of seismic refraction profiles to further characterize known earth fissures and their potential extent beyond surficial signs of their presence, and excavation and detailed logging of test trenches. The earth fissure risk delineations were refined, recommendations for future subsidence were included, and recommendations for the instrumentation and monitoring were provided.

During the final investigation field work, a rain event resulted in the extension of the SWEF by approximately 250 feet toward the proposed location of the SDW Detention Basin (Fig. 1). At this location, the SWEF had captured surface runoff upstream of the location of the SDW Detention Basin. This extension was documented to have

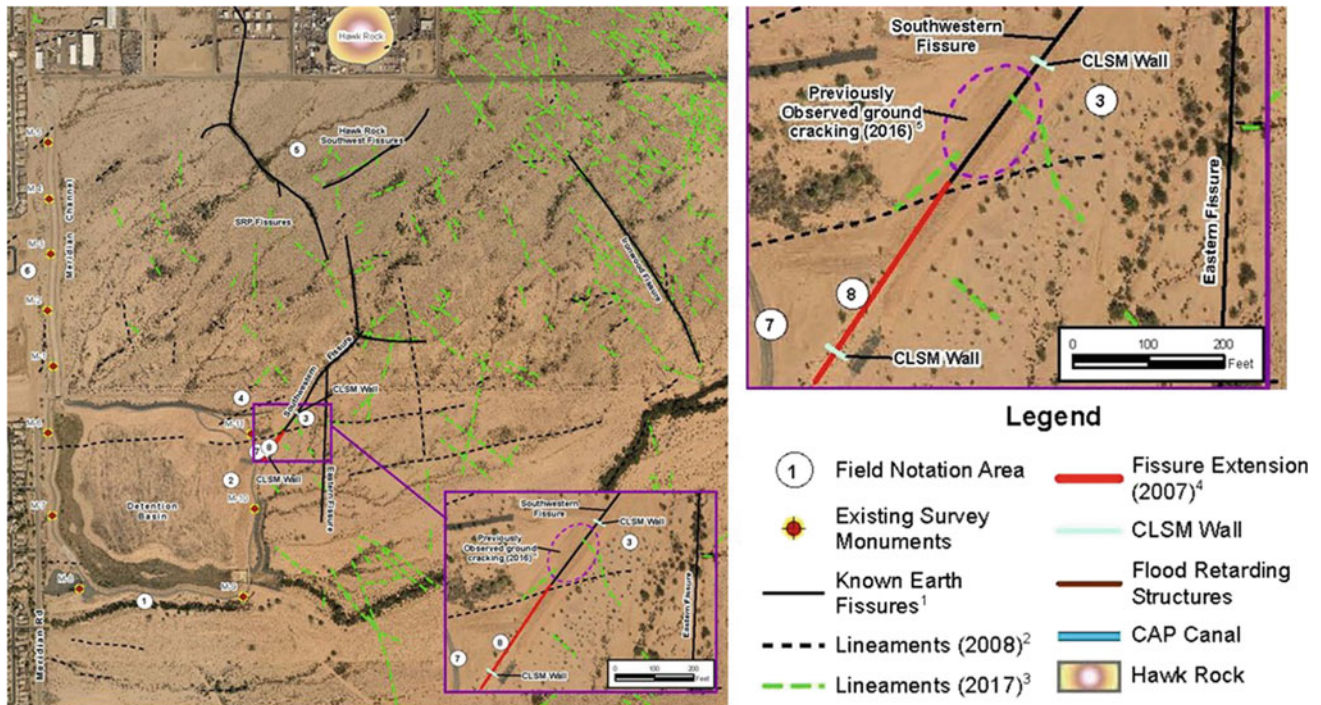


Fig. 1 Project location showing the SDW Detention Basin, Meridian Channel and other project elements including the SWEF

happened during a single rain event that occurred one evening between field visits (Fig. 2). A test trench was excavated at the termination of the newly propagated surface crack. A vertical zone of moist ground was visible on the trend of the propagated fissure. Another rain event flooded the test trench, impacting the ability to create a detailed log of the test trench. It was noted that the trench filled with water and needed to be pumped dry, after the seepage rate was monitored for several hours. This indicated that at the time of that rain event, and shortly after the SWEF had extended approximately 250 feet, no open crack was present at the fissure termination that would allow water to drain from the trench (Fig. 2).

Results of the final investigation were used to adjust the location of the SDW Detention Basin and design mitigation measures. Additionally, recommendations were made for an instrumentation and monitoring system.

3 Land Subsidence and Earth Fissure Mitigation

The SDW Detention Basin was located to avoid having the SWEF within the basin, however, the basin was located in close proximity to the fissure, and the 2007 extension of the SWEF brought it closer to the basin. A Failure Modes and Effects Analysis (FMEA) was performed to analyze potential failure modes of the basin and channel from an earth fissure

and the results were used to develop mitigation strategies to reduce the risk posed from the identified failure modes. Ultimately, five mitigation strategies were incorporated into the design of the SDW Detention Basin and Meridian Channel: (1) construction of a compacted embankment on top of the SWEF extension, (2) construction of 2 CLSM slurry cut-off walls along the SWEF, (3) incorporating a subsurface geomembrane liner and cut-off walls in the bank of the southwestern portion of the SDW Detention Basin, (4) constructing the Meridian Channel with reinforced concrete, and (5) developing an instrumentation and monitoring system.

The construction of the compacted fill embankment on top of the SWEF extension created positive drainage away from the fissure and results in a less erodible backfill of the fissure gully. Since the SWEF upstream of this location captures surface runoff, this is not believed to be a permanent mitigation, but one that will require maintenance through time. One cut-off wall was constructed along the SWEF extension and the second cut-off wall at the termination of the SWEF extension, both under the embankment fill. The cut-off walls are intended to limit subsurface erosion of the fissure by limiting water flow through the system. Figure 3 shows the as-built design of the cut-off walls and geomembrane. The cut-off walls and geomembrane along the southwest slope of the basin is designed to limit erosion from the SWEF should it extend into and through the basin at some point in the future. It is noted that such an event



Fig. 2 View of the SWEF prior to construction of the SDW Detention Basin. The upper 2 images show the extension of the earth fissure that occurred overnight as the result of a rain event. The bottom three photos show the trench at the termination of the SWEF. The left image shows

the trench after excavation. The middle image shows the trench filled with runoff one day later, the image on the right shows the trench after water was pumped out of the trench

should be seen in advance and mitigated through the monitoring program. The geomembrane design is also shown in previous chapter Fig. 2.

4 Monitoring

Monitoring is arguably the most important and widespread remedial method used for earth fissures, though it often not thought of as a remediation. Monitoring of the site is included in the Operation and Maintenance (O&M) Manual for the Project. Monitoring reduces the risk an earth fissure could pose to the SDW Detention Basin and Meridian Channel and downstream residences through repeated observation that allows for additional action to be undertaken if or when additional activity associated with an earth fissure occurs. Methods include monitoring the land subsidence (survey, InSAR, groundwater levels, etc.) that drives earth fissuring, and direct monitoring of earth fissures (mapping, visual observation, ground displacement measurements, etc.). Monitoring methods currently at the project

site include real-time kinematic (RTK) GPS surveys, ground reconnaissance, photo-geological analysis, groundwater monitoring, and the processing and interpretation of differential interferograms of repeat-pass InSAR.

A network of GPS survey monuments has been constructed along the Meridian Channel and the SDW Detention Basin. These survey monuments allow changes in grade that develop due to ongoing differential subsidence to be measured. However, current subsidence rates are sufficiently small that annual surveys have been determined to be unnecessary; the frequency of survey acquisition is currently every 3 years.

Given the structural remedial features present in the design of the SDW Detention Basin and that local subsidence-related stresses appear to be focused at the SWEF, high-resolution aerial imagery is analyzed every 3 years rather than annually. However, analysis of InSAR and ground inspections do occur on an annual basis.

Since monitoring began in 2011, cracking within the embankment fill overlying the SWEF extension has been observed. This surficial cracking does not impact the

operation and integrity of the SDW Detention Basin, and it has been mitigated through ripping and compaction of the embankment area where cracking was observed. It is unclear at this time if this cracking indicates that subsurface erosion has continued to occur along the SWEF extension or if the erosion has progressed beyond one of the cut-off walls. It is noted that no cracking associated with earth fissures has been observed within the SDW Detention Basin, and all indications are that the design is currently functioning as intended. These conditions will continue to be monitored and the FCDMC is currently considering constructing additional cut-off walls.

A rain event that occurred July 23–24, 2017 opened the SWEF northeast of the SDW Basin. This was discovered and reported by the FCDMC maintenance crew. Subsequent evaluation determined that there was no large erosion past the northeast cut-off walls, no erosion along the southwest bank, and no erosion at the channel. It was determined that the northeast cut-off walls appeared to function as designed and it was recommended to back-fill the opened fissure gullies, and rip and compact rilled areas.

References

- Arizona Land Subsidence Interest Group: Suggested Guidelines for Investigating Land-Subsidence and Earth Fissure Hazards in Arizona. Arizona Geological Survey Contributed Report CR-11-D (2011)
- Borchers, J.W., Carpenter, M.: Land subsidence from groundwater use in California. Prepared by Luhdorff & Scalmanini Consulting Engineers. Prepared for the CA Water Plan Update 2013, vol. 4. Reference Guide (2014)
- Bowman, S.D., Lund, W.R. (eds.): Guidelines for investigating geologic hazards and preparing engineering-geology reports, with a suggested approach to geologic-hazard ordinances in Utah. Utah Geological Survey Circular 122 (2016)
- Carpenter, M.C.: Deformation Across and near earth fissures: measurement techniques and results. U.S. Geological Survey Subsidence Interest Group Conference, Edwards Air Force Base, Antelope Valley, California, November 18–19, 1992: Abstracts and Summary. Open-file Report pp. 94–532 (1994)
- Covarrubais, S.W.: Cracking of earth and rock-fill dams: a theoretical investigation by means of the finite element method, 163 p. Harvard Soil Mechanics Series No. 82. Cambridge, MA: Harvard University Press (1969)
- Fellows, L.D.: Groundwater pumping causes Arizona to Sink. *Arizona Geol.* **29**(3), 1–5 (1999)
- Fergason, K.F., Rucker, M.L.: Mitigation strategies and engineering solutions for infrastructure at risk from earth fissures. IAEG/AEG Annual Meeting Proceedings, San Francisco, CA, 2018—vol. 5: Geologic hazards: earthquakes, land subsidence, coastal hazards, and emergency response, vol. 5—IAEG_AEG_2018, 031, v1 (2018)
- Galloway, D.L., Jones, D.R., Ingebritsen, S.E.: Land subsidence in the United States. *U.S. Geol. Surv. Circ.* **1182**, 177 (1999)
- Haneberg, W.C.: Drape folding of compressible elastic layers, I. Analytical solutions for vertical uplift. *J. Struct. Geol.* **15**, 713 (1992)
- Holzer, T.L.: Preconsolidated stress of aquifer systems in areas of induced land subsidence. *Water Resour. Res.* **17**(1), 693 (1981)
- Holzer, T.L., Davis, S.N.: Earth fissures caused by ground-water level declines, Sonoran and Mojave Deserts. *Geol. Soc. Am. Abstr. Programs* **13**(2), 61–62 (1981)
- Holzer, T.L.: Reconnaissance maps of earth fissures and land subsidence, Bowie and Willcox Areas, Arizona. U.S. Geological Survey Miscellaneous Field Studies Map MF-1156 (1980)
- Jachens, R.C., Holzer, T.L.: Geophysical investigations of ground failure related to groundwater withdrawal—Picacho Basin, Arizona. *Groundwater* **17**(6), 574–585 (1979)
- Jachens, R.C., Holzer, T.L.: Differential compaction mechanisms for earth fissures Near Casa Grande, Arizona. *Geol. Soc. Am. Bull.* **93**, 998–1012 (1982)
- Laney, R.L., Raymond, R.H., Winikka, C.C.: Maps showing water declines, land subsidence, and earth fissures in South-Central Arizona. U.S. Geological Survey Water Resources Investigations Open-File Report 78–83 (1978)
- Larson, M.K., Péwé, T.L.: Origin of land subsidence and earth fissuring, northeast Phoenix, Arizona. *Bull. Assoc. Eng. Geol. Environ. Eng. Geosci.* **XXIII**(2), 139–165 (1986)
- Lee, K.L., Shen, C.K.: Horizontal movements related to subsidence. *J. Soil Mech. Found. Div. ASCE* **95**(SM1), 139–166 (1969)
- Leonard, R.J.: An earth fissure in Southern Arizona. *J. Geol.* **37**(8), 765–774 (1929)
- Leonards, G.A., Narain, J.: Flexibility and cracking of earth dams. *ASCE J. Soil Mech. Found. Div.* **89**(2), 47–98 (1963)
- Poland, T.F.: Subsidence in the United States due to groundwater withdrawal. *J. Irrig. Drainage Div ASCE* **107**(2), 115–135 (1981)

Part III
Coastal Hazards

A Coastal Susceptibility Index Assessment of KwaZulu-Natal, East Coast of South Africa

A. Shanganlall, M. Ferentinou, E. Karymbalis, and A. Smith

Abstract

The KwaZulu-Natal coastline on the east coast of South Africa is one of the most densely populated coastlines in Africa and has been subjected to human developments over the last 18 years. In recent years, extreme coastal events, due to a rapidly changing climate have caused much damage along the coast and are predicted to increase in intensity and frequency with the rise in eustatic sea-level. Therefore, assessing the coastal susceptibility in KwaZulu-Natal (KZN) attempts to identify the most sensitive locations along the coast to anticipated sea-level rise and related coastal hazards. This study discusses the application of the Coastal Susceptibility Index, which incorporates and ranks six physical variables, namely: geomorphology, coastal slope, historical shoreline change rate, significant wave height, mean tide range, and relative sea-level rise, to calculate the CSI. This information was displayed based on quartiles, indicating sections of the coastline with a very high, high, moderate or low susceptibility. The majority (34.33%) of the studied KZN is ranked as high susceptibility. More than half the coast (56.72%) is characterized as highly and very highly sensitive, primarily due to the susceptible geological landforms, low lying topography, high erosion rates and a highly significant wave height. The study provides a framework for decision-makers to prioritize coastal zones that require enhanced natural resilience and adopt appropriate management strategies within the study area.

A. Shanganlall · A. Smith
University of KwaZulu Natal, Geological Sciences,
Durban, South Africa

M. Ferentinou (✉)
Civil Engineering Science, University of Johannesburg,
Johannesburg, South Africa
e-mail: mferentinou@uj.ac.za

E. Karymbalis
Department of Geography, Harokopio University of Athens,
Athens, Greece

1 Introduction

The KwaZulu-Natal (KZN) coast is one of the most densely populated coastal areas in Africa and is a popular tourist destination that fuels the South African economy. The coastal environment is highly dynamic and human development poses pressure on coastal systems by creating conflict between the natural coastline processes and anthropogenic use (Davies 2012). This pressure is exacerbated by natural coastal hazards such as seasonal variation (Guastella and Smith 2014), storm surge flooding (Mather 2007), coastal erosion (Smith et al. 2010), tsunamis and the impacts of sea-level rise (Mather et al. 2009; Shaji 2014). Global projections predict a future sea-level rise of 2–9 mm/year by 2100 (Wigley 2001). There is a general consensus that sea level is rising (SLR), the likelihood and intensity of coastal hazards affecting already threatened coastal zone (Davies 2012). In recognition of these risks, identifying sections of the coastline that are more vulnerable is paramount for effective coastal management (Abuodha and Woodroffe 2010). To this end a coastal susceptibility index was estimated.

The Coastal Susceptibility Index (CSI) was proposed by Gornitz (1990) and later modified by Thieler and Hammar-Klose (1999) and used to assess the coasts of the USA, Europe, Brazil, Argentina, India and Canada. The CSI incorporates six physical variables as indicators of a coastlines susceptibility to sea-level rise and assesses the likelihood of physical changes that may occur along the coastline because of this rise (Thieler and Hammar-Klose 1999). These physical variables include geomorphology, coastal slope, the rate of historical shoreline change, significant wave height (H_s), mean tidal range (T_s) and relative sea-level rise (Pendleton et al. 2004). These variables can be grouped into two groups: (1) geological variables (geomorphology, coastal slope and historical shoreline change rate), and (2) physical process variables (H_s , mean tidal range and relative sea-level rise). The CSI scores or ranks the coast

based on its relative degree of susceptibility ranging from very high (5), high (4), moderate (3), low (2), very low (1).

In this study, the term susceptibility is utilized in preference to vulnerability, which is commonly used by the United States Geological Survey (USGS), because the latter term generally requires evaluation of human vulnerability to hazards and considers socio-economic factors such as population size and infrastructure type. Previous research concerning the vulnerability assessment for the coastline of KZN (Palmer et al. 2011) used beach width, dune width, percentage rocky outcrop, distance (width) of vegetation behind the back beach and distance to the 20 m isobaths. Seasonal beach widths can change on a scale of tens of metres (Smith et al. 2014), similarly back beach vegetation widths vary seasonally so the above mentioned parameters were not used in this study. Mixed beaches, such as beaches perched on wave platforms, were not considered. This research through the evaluation of CSI attempts to identify the most sensitive regions along the KZN coastline, in order to guide decision making.

2 Study Area

This research focuses on the southeast part of the sub-tropical coastal zone of KZN with a length of 358 km (Fig. 1). On a macroscale, the coast is generally linear and trends obliquely from the south-east of Port Edward to the northeast of the Mfolozi Municipality (Cooper 1994). Mainly along the KZN south coast, 80% is sandy and the rest rocky outcrops. The coast receives a mean annual rainfall of 845 mm (Palmer et al. 2011). The KZN coastline is high-energy with coarse grained reflective and intermediate beaches (Cooper 1991). Towards the southeastern portion, the coastal geology of KZN comprises of rocky outcrops of predominantly Natal Basement complex interspersed with faulted blocks of Natal Group Sandstones and occasional outcrops of Dwyka Tillite. (Cooper 1991). From the Durban region extending northwards to Mozambique coastal plain, Cenozoic coastal deposits of the Maputaland Group dominate. The geomorphology along the coastline varies in accordance with the underlying geology and the amount of sand within the coastal zone, and the shape that these sand bodies have assumed (Cooper 1991). There are five geomorphological classes that have been proposed by Cooper (1994), each varying in susceptibility: rocky coasts, sand covered rocky coasts, sandy embayment's are prominent in regions situated between rocky headlands and are often backed by coastal vegetated dunes, estuary and linear clastic shoreline.

3 Methodology

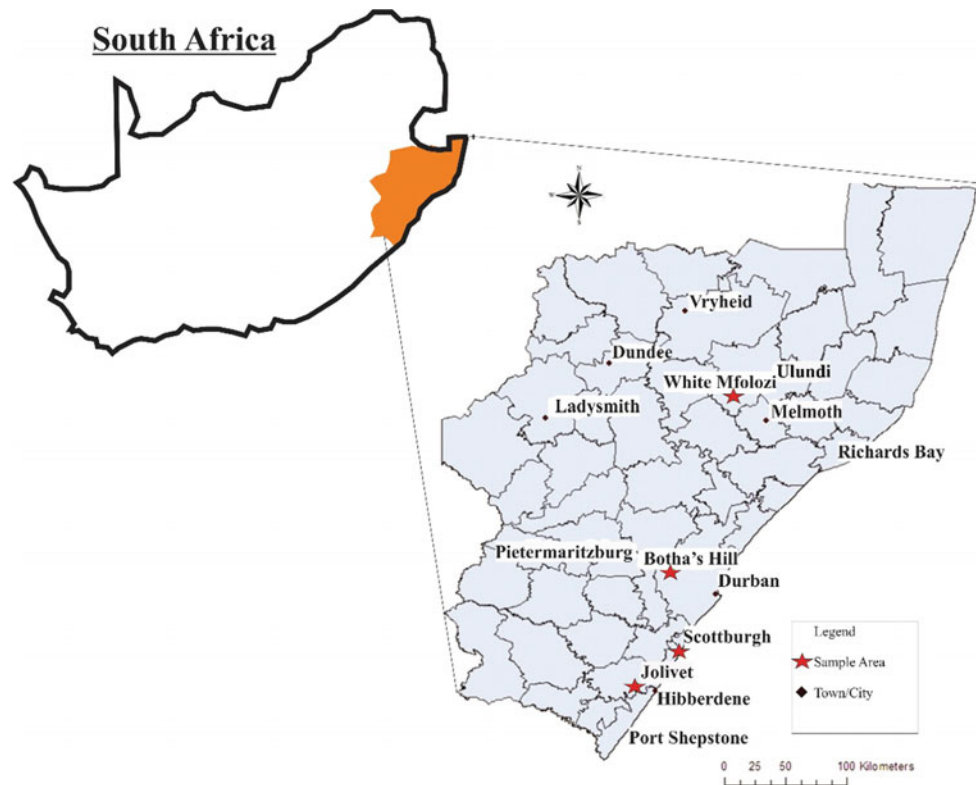
Susceptibility has been defined in this study in terms of semi-quantifiable variables, comprising three geological variables and three physical process variables (Abuodha and Woodroffe 2010). The geological variables include the geomorphology, historical shoreline change rate and the coastal slope (Pendleton et al. 2004). These variables take into consideration the shorelines relative resistance to erosion, long-term erosion and accretion trends, and the coastlines susceptibility to flooding. The physical process variables are the significant wave height, mean tide range, and relative sea-level rise, all of which contribute to the inundation hazards to a specific portion of the coastline over a period ranging from a few hours to centuries (Pendleton et al. 2004). The coastal susceptibility index allows the variables to be attributed in a quantifiable manner so that the relative susceptibility of the coastline to future sea-level rise can be expressed.

The 358 km coastline of KZN has been divided into different sections based on the variations in geomorphology, historical shoreline change rate and the coastal slope. Each of the parameters comprises 5 susceptibility classes, with each class been allocated a susceptibility index value: ranging from 1 to 5 (very low to high susceptibility).

The physical process variables were ranked and mapped as single susceptibility index values for the entire coastline based on published literature and the susceptibility classes used were consistent with Gornitz (1990), Thieler and Hammar-Klose (1999). The parameters incorporated in the CS index are dynamic and the data derived for each variable was from numerous sources. Data was acquired from ortho-rectified 1:50,000 topographic maps from the National Geospatial Institute, orthophoto maps (1:10,000), published literature (Cooper 1994; Mather 2007; Corbella and Stretch 2012), Google Earth Imagery, and Digital Elevation Models ArcGIS., provided a platform for the geospatial database development.

3.1 Geological Variables

Geomorphology: The coastal susceptibility index assesses the geomorphic susceptibility of the coastal landforms to hazards including tsunami's, storm surge flooding and wave erosion (Shaji 2014). The most erodible features (linear clastic shorelines) are subjected to a greater risk and are more sensitive than least erodible landforms (rocky shoreline). Therefore, geomorphology is ranked quantitatively in accordance to the strength of the coastal landforms as well

Fig. 1 Locality Map

the rock types (Karymbalis et al. 2012). The classification of the various geomorphological classes was undertaken by visual assessment on Google Earth, interpretation of the geomorphological classes described by Cooper (1994), as well as field geomorphological mapping that was undertaken in regions of Hibberdene, Scottburgh, Amanzitoti, and Isipingo. The methodology employed to accomplish the geomorphology mapping was undertaken by first constructing a polyline on Google Earth Imagery by digitizing the high-watermark (HWM) in the timeframe of 2014. The different landforms identified and mapped were classified according to the geomorphology classes proposed by Cooper (1994) (Table 1). Linear clastic shorelines are directly exposed to coastal hazards and therefore are the most sensitive with a ranking of 5. In contrast, rocky coastlines are stable and capable of withstanding impacts of coastal hazards, hence they are the least sensitive geomorphological class and allocated a susceptibility index value of 1. Wave platforms overlain by sand are considered to be of very high susceptibility (Smith et al. 2007 for an account of the 2007 high swell event) and allocated a susceptibility index of 5. Estuaries are allocated a ranking of 4 which is classified as a high susceptibility (Table 1).

Coastal Slope: Locations having a gentle to moderate coastal slopes are more susceptible to flooding and experience greater penetration of sea-water when there is any rise in sea-level which will inundate larger extents of land.

Any land loss to inundation is a function of slope, therefore shorelines having a gentle slope are considered highly sensitive whereas areas having a steep slopes are areas of lower susceptibility (Shaji 2014). The coastal slope was computed at every 1 km interval by measuring the distance between the 20 m contour line and the 2014 digitized shoreline. The elevation difference of 20 m was divided by the measured difference at each interval and multiplied by one hundred. Areas recording a coastal slope of greater than 35.28% were assigned a very low susceptibility index of 1, whereas areas with a coastal slope of lower than 8.13% were characterized as a very high susceptibility and allocated a susceptibility index of 5. The coastline exhibiting a slope of between 35 and 22% and considered to be of low susceptibility (2), whereas coastal zones having a slope of moderate susceptibility (3) are those categorized in the range of 22–14%, and a high susceptibility (4) classifies the range of 14–8% (Table 1).

Historical Shoreline Change Rate: The shoreline erosion and accretion rates for the coastline of KZN were calculated using the digitized shorelines in the time frames 2005, 2009 (topographic, orthorectified), and 2014 which were obtained by constructing polylines on the high water mark on Google Earth Imagery and orthophoto maps. This time frame includes the 2007 storm event that resulted in damage to private and public infrastructure within ± 400 km of the coastline (Smith et al. 2007). Historical shoreline

Table 1 Coastal susceptibility index classes for ranking the variables for the KZN coastline

Susceptibility	Very Low (1)	Low (2)	Moderate (3)	High (4)	Very High (5)
Coastal susceptibility index classes for the geomorphology variable and the length (in km and %) of each susceptibility class of the KZN coastline					
Geomorphology	Rocky Coastline	Rock sand	overlain by Embayment	River mouth-influenced embayment	Linear Clastic Shoreline
Length (%)	31.0	21.1	26.0	18.9	3.0
Length (km)	110.4	75.7	93.2	67.6	10.8
Coastal susceptibility index classes for the coastal slope variable and the length (in km and %) of each susceptibility class of the KZN coastline					
Coastal Slope (%)	>35.4	35.4-22.8	22.8-14.2	14.2-8.1	<8.1
Length (%)	4.9	14.60	20.5	31.4	28.8
Length (km)	17.4	52.3	73.5	112.4	103.0
Coastal susceptibility index classes for the historical shoreline change variable and the length (in km and %) of each susceptibility class of the KZN coastline.					
Shoreline Erosion/Accretion (m/yr.)	>0.07	0.07-0.02	0.02--0.03	-0.03-- -0.07	<-0.07
Length (%)	22.2	21.4	17.8	20.00	19.0
Length (km)	79.0	76.3	63.2	69.8	67.7
Coastal susceptibility index classes for the significant wave height variable of the KZN coastline					
Significant Wave Height (m)	<0.6	0.6-0.9	0.9-1.1	1.1-1.2	>1.2
Coastal susceptibility index classes for the mean tide range the KZN coastline					
Mean tide range (m)	>2.1	1.6-2.0	1.1-1.5	0.6-1.0	0.0-0.5
Coastal susceptibility index classes for the relative sea-level rise variable KZN coastline					
Relative Sea-Level Rise (mm/yr.)	<1.8	1.8-2.5	2.5-3.0	3.0-3.4	>3.4

change rates (m/year) were calculated at 1 km intervals (transects) along the coast using the Digital Shoreline Analysis System (DSAS) software, Thieler et al. (2009). The resultant values were normalized against the shape length so that accretion and erosion rates assessed in this investigation were consistent with the study by Copper (1994) for the time period of 1934–1989. The rate-of-change statistics documented in this study was reported as the End Point Rate indicator (EPR). The End Point Rate is calculated by dividing the distance of the shoreline movement by the time elapsed between the youngest (2014) and oldest (2005) shoreline. The positive values of the EPR are representative of accretion and the negative values are indicative of erosion. Shoreline changes for KZN fall within the (Table 1) erosion and accretion rates of -0.07 m/year to $+0.08$ m/year respectively. Areas experiencing erosion rates of <-0.07 m/year were regarded as very highly susceptibility and allocated an index value of 5, those that were eroding at rates of between -0.07 and -0.03 m/year were considered highly susceptible regions (4), moderately susceptible (3) areas were categorized in the range of -0.03 to

0.017 m/year Accretion rates of 0.017 – 0.07 m/year are classified as low susceptibility, whereas those with historical shoreline change rates of greater than 0.07 m/year were assigned a very low susceptibility index value of 1.

3.2 Physical Variables

Significant Wave Height: By definition, the significant wave height is the square root of the wave energy, which indicates the erosion capacity (Karymbalis et al. 2012). The significant height is used as a substitution for the wave energy which influences the coastal sediment transport and plays a significant role in modifying the shoreline. The increase in wave energy is result of an increase in wave height, and as a consequence there is an increase in erosion and inundation along the shoreline resulting in land loss (Pendleton et al. 2004). Therefore, the susceptibility of the coastline is directly proportional to the wave height. For the coastline under discussion, the significant wave height was analyzed from previous investigations carried out by

Corbella and Stretch (2012) whose research aimed to analyze and review 18 years of wave data of the KZN. The investigation established the average significant wave height for the entire east coast of South Africa as 1.68 m and this value was employed in this investigation in order to allow for consistency and comparison with the extensive research performed by other scientists. The data reviewed and analyzed was for the time period of 1992–2009 with various wave recording instruments used at different wave depths. These historical instruments included Waverider (a spherical accelerometer buoy that calculates the wave height and wave direction from accelerations) and the ADCP (located on the ocean floor and uses sonar to measure wave heights). Wave datasets were derived from the Durban and Richards Bay locations. Corbella and Stretch (2012) found that the wave data from Richard Bay has a strong correlation with Durban's data, therefore the significant wave height for the KZN coastline is an average of the significant wave heights of these locations. As a result, a value of 1.65 m is mapped as a single susceptibility value for the entire coastline. We have found that direction is also very important within bays.

Mean Tidal Height: The mean tidal height will influence both inundation and erosion hazards (Karymbalis et al. 2012). The tidal heights for the east coast of Southern African, which includes KZN, are modest and can be characterized by mean spring tidal heights of 1.8–2 m (Cooper 2001). Thus the entire KZN coastline is microtidal. The ranking of susceptibility of coasts with regards to the mean tide range has been viewed differently by different scientists. Gornitz (1990), considers a large mean tide range as highly sensitive whereas a low tidal range has a low susceptibility. The rationale is based on the concept that a large tidal range is related to strong tidal currents that influence a coastlines behavior and this is applied mainly to macrotidal coasts. In contrast, Thieler and Hammar-Klose (1999), Pendleton et al (2004) advocate that a large tidal range is ranked as a low susceptibility. Cooper (1991) suggests that on a wave-dominated coastline such as this a microtidal regime is considered to be of high susceptibility as wave attack is concentrated within a narrow zone. The coastal susceptibility classes used in this study to rank the mean tide range were consistent with that proposed by Abuodha and Woodroffe (2010) for the southeast coast of Australia and corresponds to the assigned vulnerability index for the mean tide range provided Musekiwa et al. (2015) for all South African coastlines.

Relative Sea-Level Rise: The relative sea-level rise value employed in the coastal susceptibility mapping in this project was based on the extensive research performed in Durban and surrounding regions by Mather (2007). The sea-level rise was established by the use of the Durban tidal gauges and changes in barometric pressures, which were

supplied by South African Navy Hydrographic Office and South African Weather Service respectively, for the time period 1970–2003 (Mather 2007). A linear and non-linear analysis was performed on monthly sea-levels (Fig. 4.12). Based on the comparisons of these two methods, Mather (2007) found that the linear rate of sea-level rise of 2.7 ± 0.05 mm/year for Durban and surrounding regions would be the most valid. This SLR Trend was employed in research performed by other authors when assessing sea-level changes in Durban and other locations along the east coast of KZN; some of which include works by Mather and Stretch (2012). Therefore, for this particular scientific study, the relative sea-level rise of 2.7 ± 0.05 mm/year was adopted for the entire coastline of KZN because it allows for comparison and consistency with other research of the executed in the in the study. The relative sea-level rise for the coastline under investigation is classified into only one of these susceptibility ranges, which was 2.5–3.0 mm/year and is categorized as a moderated susceptibility and has a rating of 3.

3.3 Coastal Susceptibility Index

The CSI was calculated using the conventional six variables and applying the formula:

$$CSI = \sqrt{\frac{a \times b \times c \times d \times e \times f}{6}} \quad (1)$$

where, a = geomorphology, b = historical shoreline change rate, c = coastal slope, d = significant wave height, e = mean tide range, and f = relative sea-level rise. For this research, an unweighted product model was adopted whereby the relative importance of each variable on the overall calculation was considered equal (Abuodha and Woodroffe 2010). The data for each coastal section was processed by assigning specific susceptibility ratings in the attribute table for each of the 6 variables. The “raster approach” was adopted by converting the input parameters into raster grids in order to compute the CSI. The resulting output CSI was derived as a raster grid, where the index values were divided into four quartiles such that the discrete index value cells were ranked in terms of their magnitude. The lowest quartile (25th percentile) is representative of the least sensitive areas, those values below the median value were displayed as moderate susceptibility, and the high and very high susceptibility categories were discriminated at the 75th percentile. This method is comparable and consistent with that employed (Thieler and Hammar-Klose 1999; Pendleton et al. 2004) and Australian coast (Abuodha and Woodroffe 2010).

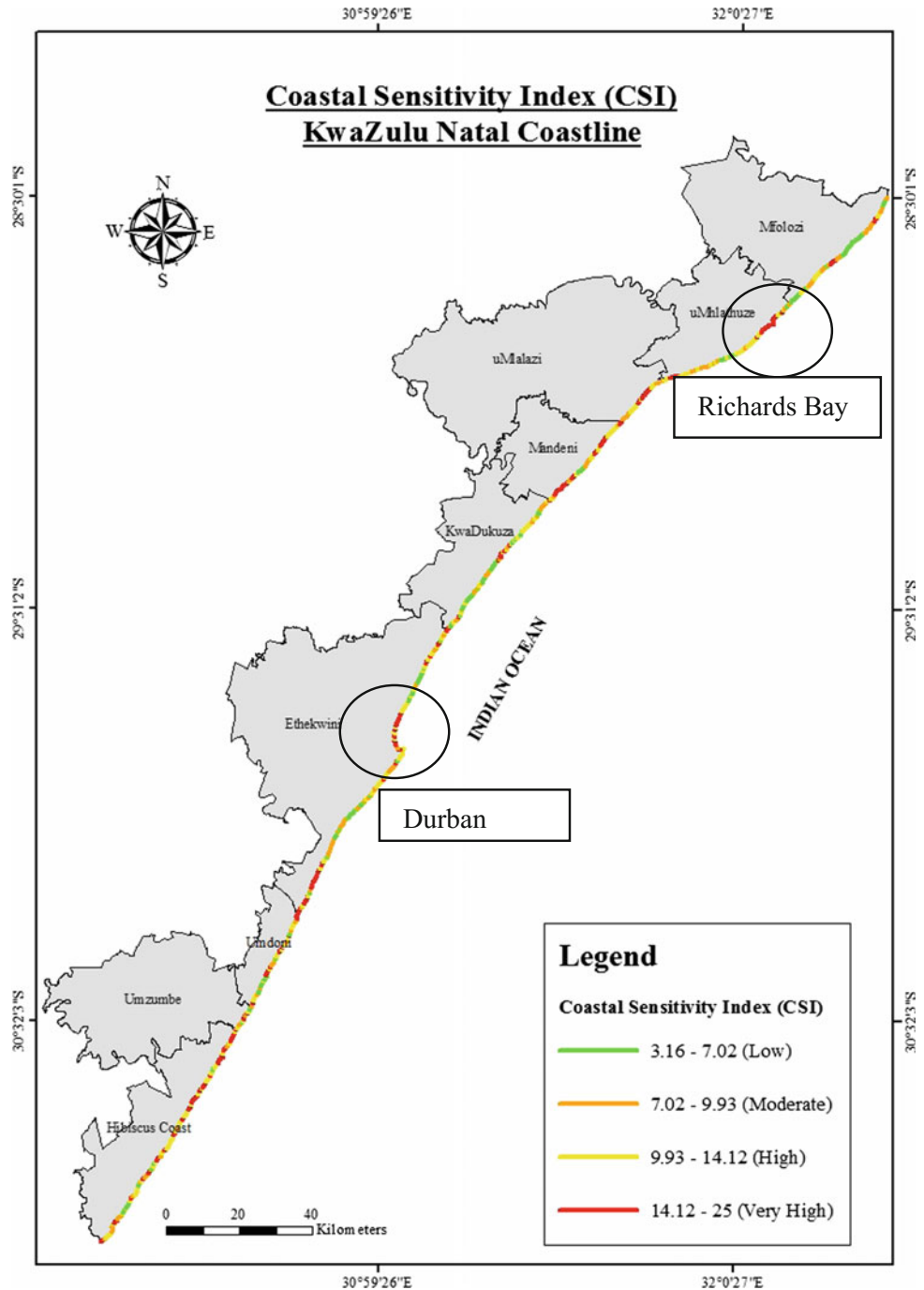
4 Results

4.1 Coastal Susceptibility Index

Figure 2, indicates the susceptibility ranking of various segments of the coast based on the categorization of the CSI values into four classes by applying the “quartile” classification method. The CSI values along the KZN coastline range between 3.16 and 25. CSI values ranging between

9.93 and 25, are classified as high to very high susceptibility areas. From this map, it is seen that majority of the coastline experiences a high susceptibility. The least susceptibility (3.16–7.02) regions are located mainly towards the northern portion of the KZN coast and are considered stable. Susceptibility classification maps of Durban and Richards Bay respectively, they are regarded as ‘hot spots’ areas along the coastline because they have undergone the most disturbance due to human development such as construction of harbors

Fig. 2 Classification of KZN coastline according to the (CSI) values



and resulting dune damage (Cooper 2001). The region surrounding the Durban harbor is classified as high susceptibility 9.93–14.12. In contrast, low susceptibility categories are located towards the south of the Durban Harbor and are considered more stable regions. The Richards Bay region which is classified as high and very high susceptibility because the CSI index values are ≥ 0.12 and is considered one of the most disturbed or susceptible regions of the KZN coastline.

5 Discussion—Conclusion

By employing the six physical variables commonly utilized by the USGS, the coastal susceptibility for KZN was determined. These variables were evaluated individually, then combined to give an overall assessment. Although the CSI is not a complete estimation of susceptibility, it provides a relative index (Palmer et al. 2011). Given that KZN coastline has experienced significant erosion in the past due to extreme storm events (such as that experienced in March 2007) it is expected that these events may be repeated and experienced again, resulting in locations with high CSI values to be greatest at risk (Palmer et al. 2011).

Regions experiencing a low to moderate susceptibility may be attributed to the geomorphology type of rocky coastlines and rock overlain by sand, steep coastal slopes, and the occurrence of accretion. Such susceptibility classes constitute 17.54 and 25.75% of the coastline respectively. The high and very high susceptibility categories are located as stretches of coast, starting from Margate, and occupy 34.33 and 22.39% of the entire coastline respectively. Such areas have undergone high and very high erosion with rates that are greater than -0.07 m/year, are occupied by gentle coastal slopes and geomorphology types of either river mouth-influenced embayment or linear clastic shorelines; and the entire KZN coast is influenced by a large significant wave height.

Overall, the most influential variables in the CSI assessment for KZN are the geomorphology, coastal slope, and significant wave height. Majority of the coastline classified as high susceptibility and this corresponds to the vulnerability assessment performed by Musekiwa et al. (2015). Palmer et al. (2011) ranked majority of the KZN coast as moderately sensitive (68%), however when the analysis included the historical shoreline erosion data into the vulnerability assessment, majority of the coastline was classified as a high susceptibility (58%) and this correlates with the results of this study. In the vulnerability assessment performed by Palmer et al. (2011) for the study area, the historical shoreline change rates were used as indicators to validate the KZN coast data. This is viewed on the grounds that the variable is not so much a physical attribute but rather

a response of the coast to the interactions between coastal processes and structures (Abuodha and Woodroffe 2010).

Research shows that coastal hazard such as the March 2007 storm event will continue and may become more severe with the ongoing climate change, resulting in the areas classified as high and very high susceptibility facing the greatest risk (Mather and Stretch 2012).


References

- Abuodha, P.A.O., Woodroffe, C.D.: Assessing vulnerability to sea-level rise using a coastal susceptibility index: a case study from southeast Australia. *J. Coast Conser.* **14**, 189–205 (2010)
- Cooper, J.A.G.: Shoreline changes on the Natal coast: Mkomazi River mouth to Tugela River mouth. *Natal Town Reg. Plann. Comm. Rep.* **77**, 12–48 (1991)
- Cooper, J.A.G.: Shoreline changes on the Natal coast: Mtamvuna River mouth to the Mkomazi River mouth. *Natal Town and Regional Planning Commission Report 79, The Town & Regional Planning Commission, P/B 9038, Pietermaritzburg, 3200* (1994)
- Cooper, J.A.G.: Geomorphological variability among microtidal estuaries from the wave-dominated South African coast. *Geomorphology* **40**, 99–122 (2001)
- Corbella, S., Stretch, D.D.: Coastal defenses on the KwaZulu-Natal coast of South Africa: a review with particular reference to geotextiles. *Tech. Paper J. South Afr. Inst. Civil Eng.* **54**(2), 57–63 (2012)
- Davies, W.T.R.: Applying a coastal vulnerability index (CVI) to the Westfjords, Iceland: a preliminary assessment. *MSc Thesis, University of Akureyi* (2012)
- Gornitz, V.: Vulnerability of the east coast, USA to future sea level rise. *J. Coast Res.* **1**(9), 201–237 (1990)
- Guastella, L.A., Smith, A.M.: Coastal dynamics on a soft coastline from serendipitous webcams: KwaZulu-Natal, South Africa. *Coast. Shelf Sci.* **150**, 76–85 (2014)
- Karymbalis, E., Chalkias, C., Chalkias, G., Grigoropoulou, E., Manthos, G., Ferentinou, M.: Assessment of the susceptibility of the southern coast of the Gulf of Corinth (Peloponnese, Greece) to sea-level rise. *Central Eur. J. Geosci.* **4**(4), 561–570 (2012)
- Mather, A.A.: Linear and nonlinear sea-level changes at Durban, South Africa. *South Afr. J. Sci.* **103**(509–5), 11 (2007)
- Mather, A.A., Garland, G.G., Stretch, D.D.: Southern African sea levels: corrections, influences and trends. *Afr. J. Mar. Sci.* **31**(2), 145–146 (2009)
- Mather, A.A., Stretch, D.D.: A Perspective on Sea Level Rise and Coastal Storm Surge from Southern and Eastern Africa: a Case Study near Durban, South Africa. *J. Water* **4**, 237–250 (2012)
- Musekiwa, C., Cawthra, H.C., Unterner, M., van Zyl, F.W.: An Assessment of coastal vulnerability for South African Coast. *South Afr. J. Geomat.* **4**(2), 123–135 (2015)
- Palmer, B.J., Van der Elst, R., Mackay, F., Mather, A.A., Smith, A.M., Bundy, S.C., Thackeray, Z., Leuci, R., Parak, O.: Preliminary coastal vulnerability assessment for KwaZulu-Natal, South Africa. *J. Coast. Res. Spec.* **64**, 1390–1395 (2011)
- Pendleton, E.A., Thieler, E.R., Williams, S.J.: Coastal vulnerability assessment of cape hattaras national seashore (CAHA) to sea-level rise. *USGS Open File Report 2004–1064*. Available from <http://pubs.usgs.gov/of/2004/1064/images/pdf/caha.pdf> (2004). Accessed on February 2015
- Shaji, J.: Coastal susceptibility assessment for Thiruvananthapuram, west coast of India. *J. Nat. Hazards* **73**, 1369–1392 (2014)

- Smith, A.M., Guastella, L.A., Bundy, S.C., Mather, A.A.: Combined marine storm and Saros spring high tide erosion events along the KwaZulu-Natal coast in March 2007. *S Afr J Sci* **103**, 274–276 (2007)
- Smith, A.M., Mather, A.A., Bundy, S.C., Cooper, J.A.G., Guastella, L.A., Ramsay, P.J., Theron, A.: Contrasting styles of swell-driven coastal erosion: examples from KwaZulu-Natal, South Africa. *Geol. Mag.* **147**(6), 940–953 (2010)
- Smith, A.M., Guastella, L.A., Botes, Z.A., Bundy, S.C., Mather, A.A.: Forecasting cyclic coastal erosion on a multi-annual to multi-decadal scale: southeast African coast. *Estuar. Coast. Shelf Sci.* **150**, 86–91 (2014)
- Thieler, E.R., Hammar-Klose, E.S.: National assessment of coastal vulnerability to sea level rise: preliminary results for the U.S. Atlanta coast. USGS, Open File Report 99–593. Available via <http://pubs.usgs.gov/of/1999/of99-593/index.html> (1999). Accessed on February 2015
- Thieler, E.R., Himmelstoss, E.A., Zichichi, J.L., Ergul, A.: Digital Shoreline Analysis System (DSAS) version 4.0—An ArcGIS extension for calculating shoreline change, U.S.G.S Open-File Report 2008-1278. *current version 4.3 (2009)
- Wigley, R.: Geohazards in coastal areas. Council Geosci. Rep. Number **2011–0066**, 1–9 (2001)

Part IV
Emergency Response

Emergency Warning of Landslide Natural Hazard Using Nearly Real-Time Monitoring Data

Zbigniew Bednarczyk 

Abstract

This paper discusses the monitoring systems used by the author to monitor ground deformations in relation to groundwater and rainfall conditions at natural and opencast mine slopes. Selected case monitoring locations were located in the flysch Carpathian Mountains and at the Belchatow Opencast Mine. Monitoring instrumentation includes on-line shape-accelerated arrays, in-place inclinometers, pore pressure transducers and rainfall gauges. These systems were used to determine the depth, rate, direction of displacements and the pore pressure response in selected slopes. The internal geological and external triggers of landslides are very complex and diverse in Carpathian flysch natural slopes and clayey mine slopes in Belchatow mine (which is the largest excavation in Europe). These factors, usually make predicting landslide activation time precisely, nearly impossible. Therefore an effective identification of the main triggers requires a multitude of integrated variables. Identification of movement acceleration in relation to pore pressure and rainfall data could be very important. In prior research, the existence of the strong relationship between observed displacements, pore pressure, and rainfall data has been investigated. The ground movement and pore pressurous monitoring data were found to be critical for identifying approaching hazardous conditions. These data could also be useful for taking proactive risk mitigation measures. However, identification of the complex triggers is usually difficult.

Keywords

Landslides • Landslide monitoring • Landslide triggers

1 Introduction

Landslides are one of the most frequent natural hazards. Their activation or reactivation causes high economic losses every year (Petley 2012). In Poland, most of the natural landslides (over 90%) are recognized in the Carpathians. Up to this time, over 60,000 landslides were mapped in the web-based SOPO landslide database (Grabowski et al. 2008). Other human-induced mass movements were also observed. Some are reported every year in Polish opencast mines. In Belchatow, the largest opencast mine in Europe between the period of 1977–1988, 238 landslides were reported, 80 on fixed slopes and 158 on the west exploitive slopes (Hochman 2000). Warning of landslide hazard usually requires identification of several complex internal and external triggers, that is difficult using only field inspection and mapping. These data include landslide location, approximate depth and main geomorphologic features. However, the possibility of identifying landslide activation is still a difficult challenge on natural, as well as artificial, slopes (Bednarczyk 2012, 2017). Its more accurate recognition requires usage of comprehensive and expensive core impregnated boreholes, geophysical scanning, laboratory tests and different types of individually dedicated monitoring measurements. These investigation methods allow detecting slip surfaces and the depths, ranges and directions of slide movement. Different types of systems for different types of measurements could be used for surface displacement monitoring. Most often it is standard geodesy. However, GPS, robotized total station or satellite remote sensing could deliver more data. Other methods, such as extensometers, inclinometers or optosensors could also measure ground displacements, while others could recognize groundwater conditions. Many different early warning systems are based on surface displacements, which deliver precise surface monitoring data and cover large areas. However, inclinometer measurements could detect landslide activation in selected locations earlier and more precisely. Numerous

Z. Bednarczyk (✉)
Poltegor-Institute, Institute of Opencast Mining, Parkowa 25,
51-616 Wrocław, Poland
e-mail: zbyszbed@gmail.com

landslide parameters can now be monitored through real-time or nearly real-time in situ instrumentation. Many different multiple sensors could provide accurate meteorological, ground displacement, groundwater and pore pressure measurements with individually defined collection intervals. To safeguard the important infrastructure, machines and roads located on natural or mine slopes these results could be processed and interpreted by early warning systems. The potential activation time could be estimated by studying the evolution of the slope deformation and other related parameters such as groundwater level depths, pore pressure or rainfall variations over time. These measurements could be processed and interpreted in early warning systems. Presented are examples that represent the first attempts of the usage of on-line nearly real-time monitoring measurements in Poland for identification of landslide activation. Research areas locations are presented in Fig. 1.

Landslide early warning systems could be very useful in emergency scenarios. In Poland general procedures for such installations are still lacking. Landslide activation studies in the Polish Carpathians were mainly based on rainfall measurements connected with field inspections or conventional inclinometer measurement (Starkel 1997, 2011; Gill and Dlugosz 2006). The new on-line measurements could pose a new opportunities for early warning of landslide hazard in selected locations. Data are collected in different time intervals varied from 10 to 360 min depending on the parameter and then compared. Access to the data is very quick but possible only with the same small delay that means that it is in nearly real-time (but not in a real-time).

In Polish opencast mines, warning is usually based on geodesy or inclinometer measurements and field inspection.

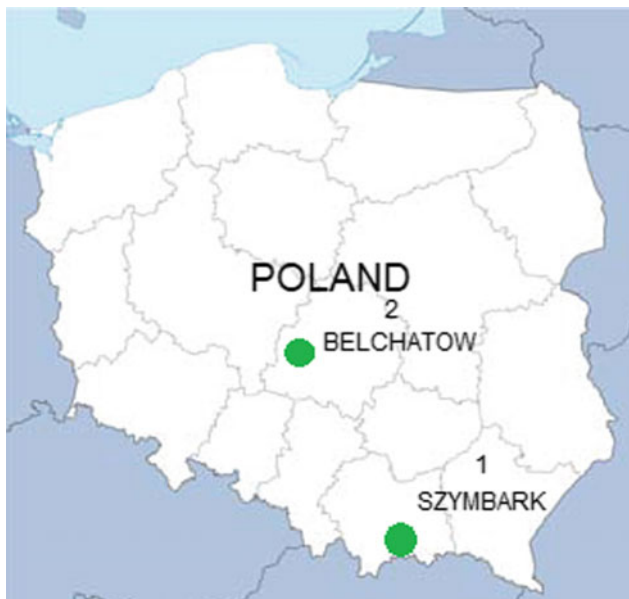


Fig. 1 Locations of two on-line systems



Fig. 2 On-line system in Belchatow Mine

The first nearly real-time system was installed by the author in the Carpathian Mountains near the city of Gorlice in May 2010 as a part of the EU Innovative Economy project. It included three inclinometer field stations to depths of 12–16 m and a weather station. The second nearly real-time inclinometer warning was installed in the Belchatow opencast mine in December 2016 (Fig. 2). That system was installed to a depth of 100 m. Proper calibration of monitoring devices required individually dedicated site investigation and monitoring methods. In this paper monitoring methods in two selected sites and their advantages and limitations are described.

2 On-Line Monitoring System in the Carpathians

2.1 Location and Engineering Geology Conditions

A nearly real-time monitoring system was installed near the village of Szymbark on the east slopes of the Bystrzanka

River Valley in southeast Poland. The Szymbark-Szalowa road is affected by 15 landslides. These pose a serious threat to the public road in the Bystrzanka River Valley connecting 4 villages. The investigated area was localized between two main geomorphology units of the Beskidy Mountains (Beskid Niski Mts.) and Carpathian Foreland (Gorlickie Foothills—Luzna Valley) at an altitude of 440–585.3 m a.s.l. Mass movements, with depths of 9–15 m, had areas ranging from 0.37 to 0.6 km². Flysch layers dip consequent to the slope inclination and are cut by many faults. Various lithological complexes of differing weathering resistance are represented on the slopes. Investigated slopes are underlain predominately by Eocene shale interbedded with thin layers of sandstone with many cracks and joints. The geological structure of the ridges is represented by Inceramowe layers built from average strength sandstone-shale layers and very low strength variegated shales. More resistant Magura sandstones on the main ridges of the Beskid Niski Mts., constitute about 30% of the area. Saturated claystones and sandstones sometimes are covered by weathering zones. Claystones in some parts had mechanical parameters characteristic for weak cohesive soils. Sandstones usually occurred as thin layers with differing degrees of diagenesis. The sandstones represented more permeable strata between clayey layers. These permeable strata allowed water infiltration and seepage. Movements were reactivated in wet periods many times. Landslide depths varied from 2 to 18 m. Bedrock layers had a consequent inclination (Fig. 3). On the basis of the types of movements and the materials involved, the observed slope processes could be defined as rock-soil slides (Cruden and Varnes 1996, Turner and Schuster 1996). Movements occurred on the slopes with inclinations from 15° to 35°.

2.2 Description of Installed Instrumentation

The instrumentation installed in May 2010 consists of the following measuring devices:

- two automatic groundwater level and pore pressure monitoring stations P1 and P2 at depths of 10 and 11 m respectively using piezoelectric sensor type with temperature sensor, in the measuring range of 1.5 Bar and a resolution of 0.025%.
- three ground movement inclinometer systems: (a) one in-place M1 inclinometer at depths of 7–10 m with a sensor type of three single-axis IP sensors, every segment of 1 m in length, multiplexing, inclinometer casing diameters of 70 mm with a measuring range of $\pm 10^\circ$. (b) two Shape Accelerated Arrays M1 and M2, with a sensor type of 3D MEMS inclinometer, consisting of 24–32 rigid segments, each 500 mm in length, arrays of 24 and 32 tilt sensors, with sampling depths of M1-12 m and M2-16 m with a measuring range of $\pm 45^\circ$.
- meteorological station W, with a barometer, rain gauge, temperature sensor, humidity sensor

Monitoring data were transferred by the cellular network to a web server that collected all the measurements. These were shared by authorized users from any computer connected to the Internet. Data could be edited in the form of graphs or exported as text files. The operation of the system was not affected by the data transmission method. The system was powered by a rechargeable 12 V battery and solar panels. This minimized the costs of administration and data management. In order to avoid accidental

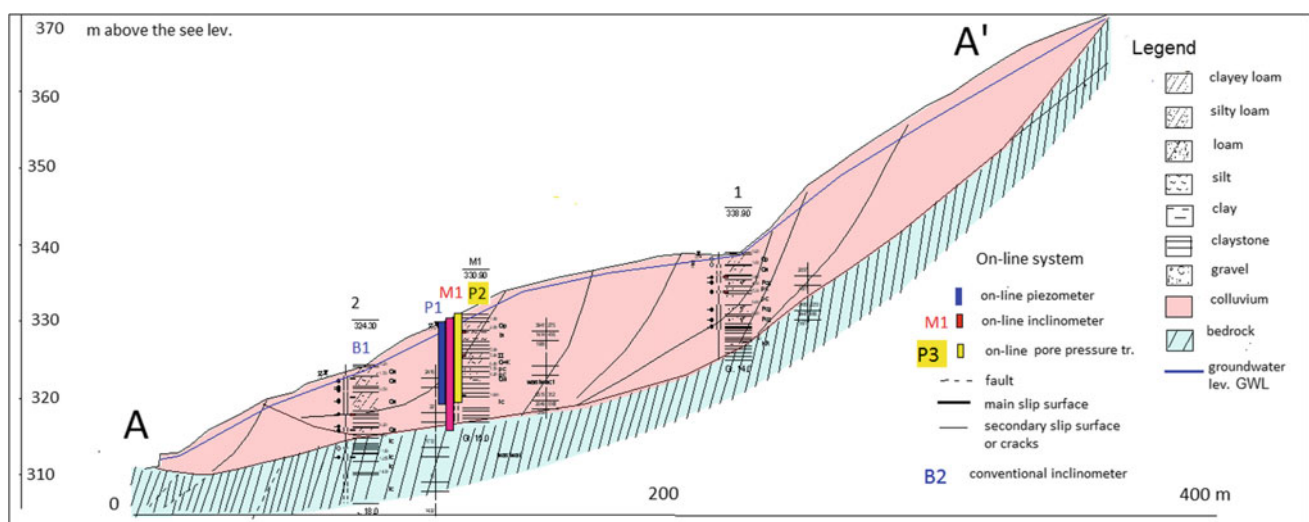


Fig. 3 Geological cross-section, Szymbark landslide, with monitoring instrumentation

loss of data the system provided continuous on-line control of the power supply and GSM signal strength.

2.3 Monitoring Results

Registered displacements, groundwater, and the rainfall data were collected continuously since May 2010. Data acquisition was in real or nearly real-time in the intervals from 10–60 min to 360 min depending on the selected options. After intensive precipitation in May–June 2010 and June 2011, the rates of deformation accelerated to over 11 cm in a few days time. Measurements showed that after intensive rainfall some parts of the slopes were activated, despite the partial remediation works. The data provided by nearly real-time monitoring permitted a better understanding of geodynamical processes that occurred on the slopes. The total displacements in the direction of the slope inclination at M3 Field Station, during first 40 months reached values of 33–54 mm. They occurred to a depth of 12 m (Fig. 4). However, the fastest movements were identified at depths of 0–7 m. The occurrences of displacements that varied in both, direction and depth, indicated the presence of several active slip surfaces related to slope morphology, lithology, geotechnical conditions and stabilization work performed. The largest acceleration of movements occurred after the intensive rainfalls in May–June 2010 and June 2011. The registered pore pressure varied between 39–62 kPa. Pore pressures varied over 100% from 48.6 to 98.9 kPa. The highest pore pressure variations were observed in May–July 2010 and June–September 2011 (Fig. 5). On-line measurements of rainfall, air temperature, and air humidity collected data in 10-min intervals. The average annual rainfall during nine years of observation was 833.7 mm. The lowest annual

precipitation was 303 mm in 2012. Very high yearly rainfall of 1115.4 mm was registered in 2010. In May–June 2010, heavy rainfall of 464.2 mm caused landslide reactivation. At that time, some parts of the drainage ditches in the landslide zone and along with Geobrugg nets near the road were damaged. Very high rainfalls of over 300 mm also occurred in July 2011. The monitoring allowed the measurement of record precipitation including 100 mm of rainfall over a 3 h period occurred on 3 June 2010. Precise determination of precipitation totals needed to determine saturation of the ground and identification of movement activation time were difficult. At times during the rainy season a few instances of rapid increase and decrease of pore pressure were observed. The automated inclinometer monitoring data showed that deformations grew continuously except for the short periods with no movements in the winter of 2010/2011 and in the winter of 2011/2012. The largest deformations were registered during May–September 2010 (14 mm) and July–September 2011 (12 mm). This corresponds well to the greatest sum of monthly rainfalls recorded in May 2010 (210.3 mm), June 2010 (255.0 mm) and July 2011 (302.8 mm). Sometimes in the rainy season, a few cycles of intensive pore pressure increase occurred. Usually, the largest amount of displacement was observed 48 h after initial pore pressure growth up to nearly 100 kPa and saturation levels exceeded over 50%. It was difficult to predict these relations at the start of the investigation. Preliminary alert conditions implemented from previous experience as a 100 mm daily rainfall and 30 mm daily displacement were defined. However, besides 100 mm daily rainfall in May 2010 these values were not detected. Obtained data were shared with Gorlice Road Administration and helped them with risk management and control of the effectiveness of partial remediation techniques. It seems that more

Fig. 4 Hourly rainfall [mm], CPPD [kPa] and total deformation [mm], Szymbark landslide

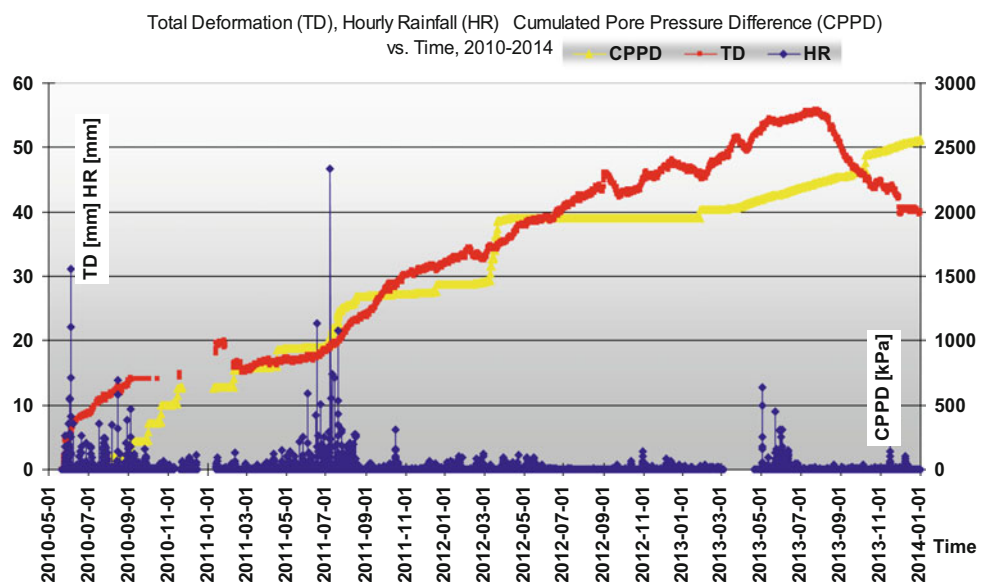
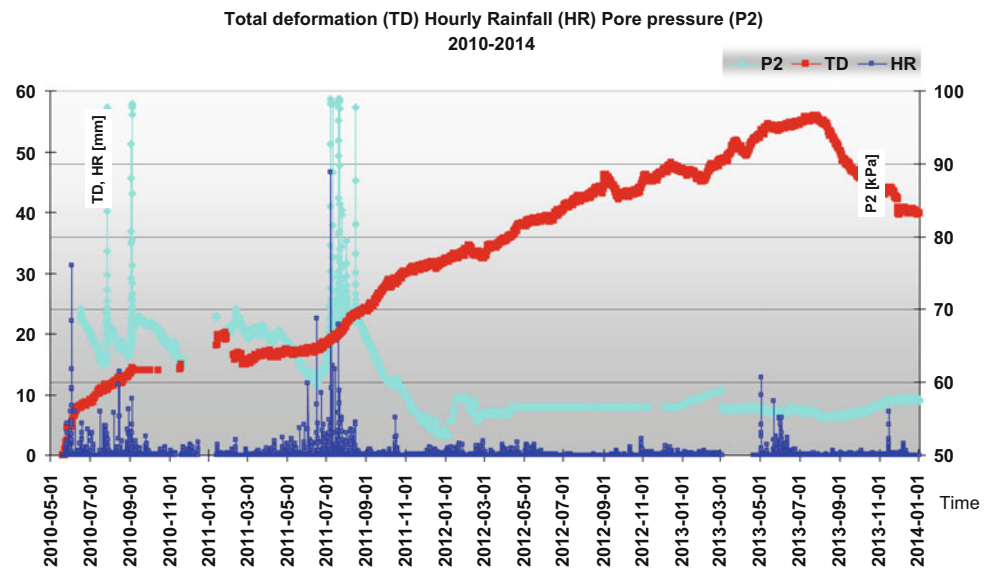


Fig. 5 Hourly rainfalls [mm], pore pressure [kPa] and total deform [mm], Szymbark landslide



comprehensive early warning values could be obtained by identification of ground movement activation in conjunction with pore pressure variations up to 100%. Further detailed analyses are in progress. These should deliver more comprehensive data for detailed analysis using semi-empirical forecasting methods.

3 On-Line Monitoring System in the Belchatow Opencast Mine

3.1 Location and Engineering Geology Conditions

The mine is situated in central Poland 12 km SW from the city of Belchatow. It is located in the tectonic Kleszczow rift, formed in Mesozoic limestones and marls, and filled by Neogene deposits. Mesozoic blocks are separated along faults and dislocations. The thickness of the Neogene deposits within the rift is 150–310 m. These deposits are 5–15 times thicker within the rift than similar deposits located outside of the rift. The main lignite seam is 20–60 m thick. The mine consists of two operational fields—Belchatow and Szczercow. These are separated by a salt dome at Debina. Most of the movements were activated on structural and paleo-landslide surfaces at the southern slope of the pit, near a deep, secondary ditch structure displaying the greatest thickness of lignite. The north slope of this mine exposes Quaternary clayey deposits with unfavourable geotechnical parameters. This slope posed numerous risks to conveyor belts transportation systems and power supply lines in the past. The main landslide-prone structural surfaces are contacts between the Quaternary and Neogene deposits, and the contact between the Neogene clays and the

main lignite deposit. Others landslide-prone surfaces are faults, cracks, tectonic and glaciotectionic surfaces, low strength soils and varved Neogene clays. A significant risk to mining is due to landslides observed as a natural consequence of the complexity of the geological structure of the lignite deposit and overlaying sediments. Landslides had volumes of a few hundred cubic meters to as much as 3,500,000 cubic meters, with displacements from a few millimetres to several meters over a 24 h period (Rybicki 1996). At the investigated west slope of Belchatow field, eight risk areas were recognized at the contact zone of the salt dome and the pit.

3.2 Description of Installed Instrumentation

The instrumentation was installed in December 2016. A borehole 132 mm in diameter was drilled to the depth of 100 m at the northern part of the west slope at level of +42 m a.s.l in the contact zone of the salt dome (Figs. 6 and 7). Instrumentation included innovative Shape Accelerated Arrays. The system of 200 ground displacement sensors located every 0.5 m, extended to a depth of 100 m is built from rigid segments and includes 3 magnetometers for rotational control. One segment included 3 tilt sensors, measuring a range of $\pm 45^\circ$, with an accuracy of 0.02 mm/m an admissible error of joints of ± 0.250 . Every octet (8 segments) is equipped with a ground temperature sensor. The maximum range of equipment depends on the speed and depth of movements, usually no more than 500 mm. The system is waterproof up to 980 kPa. It was additionally equipped with a VW pore pressure sensor located at a depth of 30 m. The field station included a recorder and GPRS data transmission devices powered by a solar panel. The GPRS



Fig. 6 Landslide at level +42 a.s.l, west slope of Belchatow Mine

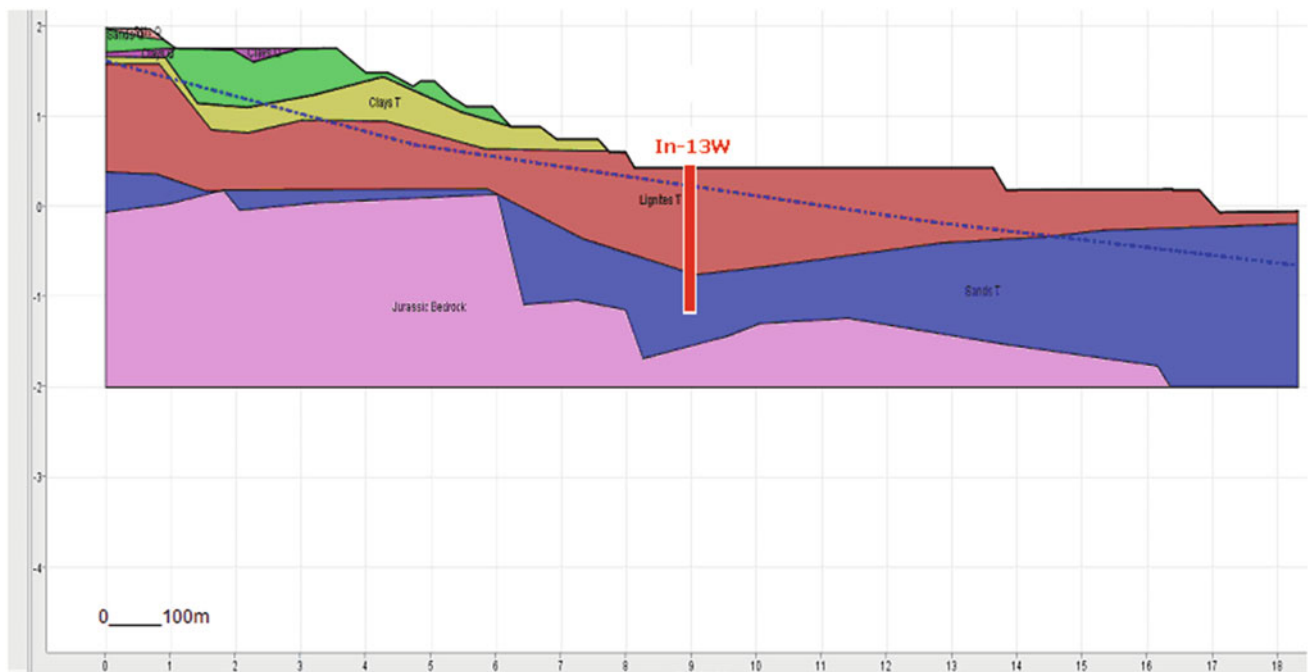


Fig. 7 Geological cross-section, Belchatow Mine with monitoring instrumentation

data are registered every 6 h and available online from 19 December 2016.

3.3 Monitoring Results

Presented monitoring measurements were collected over a 280 day period from 19 December 2016 till 4 October 2017. The largest magnitude of displacements were observed in the

first 40 days of measurements (Jan–Feb 2017) when they reached 70 mm from 210 to 255 days (Aug–Sept 2017) when the displacements increased another 40 mm (Fig. 8). The largest shear strain in the direction of slope inclination X were recorded at the depth of 45 m (Fig. 9). In the Y direction the largest shear strains were recorded at depths of 45 m and 73 m (Fig. 9a, b). A pore pressure sensor, located at depth of 30 m, registered pore pressures of 258 kPa in December 2016. Acceleration of movements usually

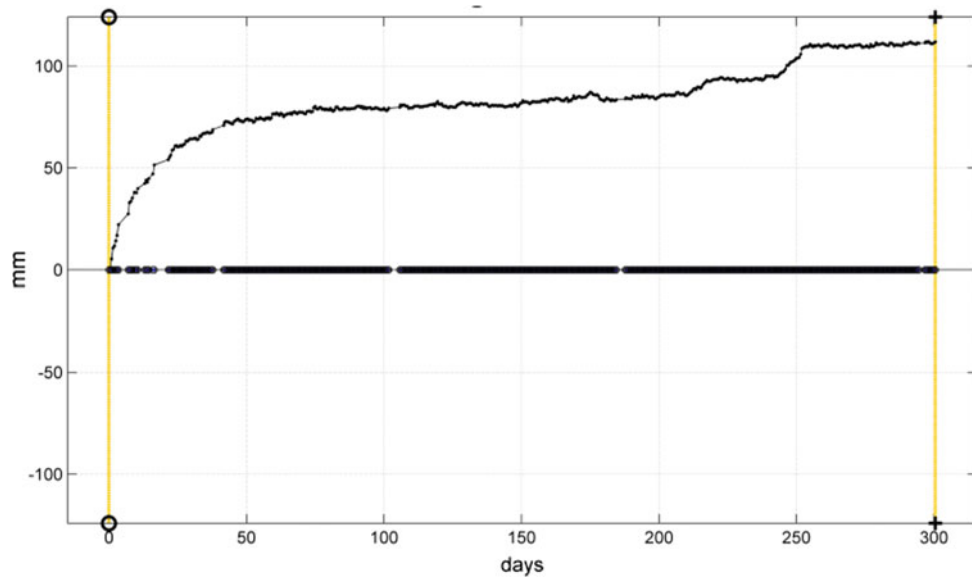


Fig. 8 Monitoring results, magnitude of displacement versus time, Belchatow Mine

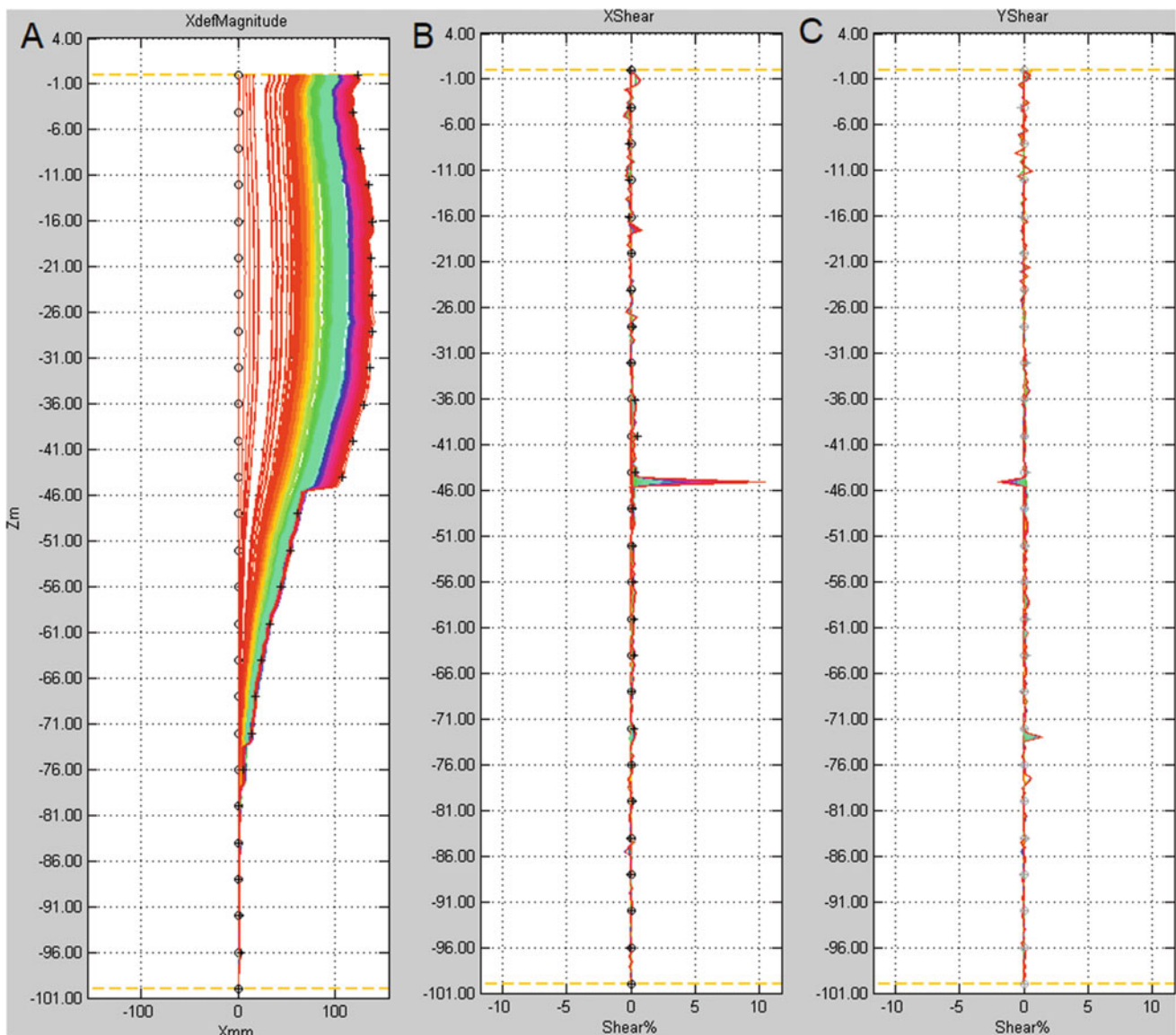
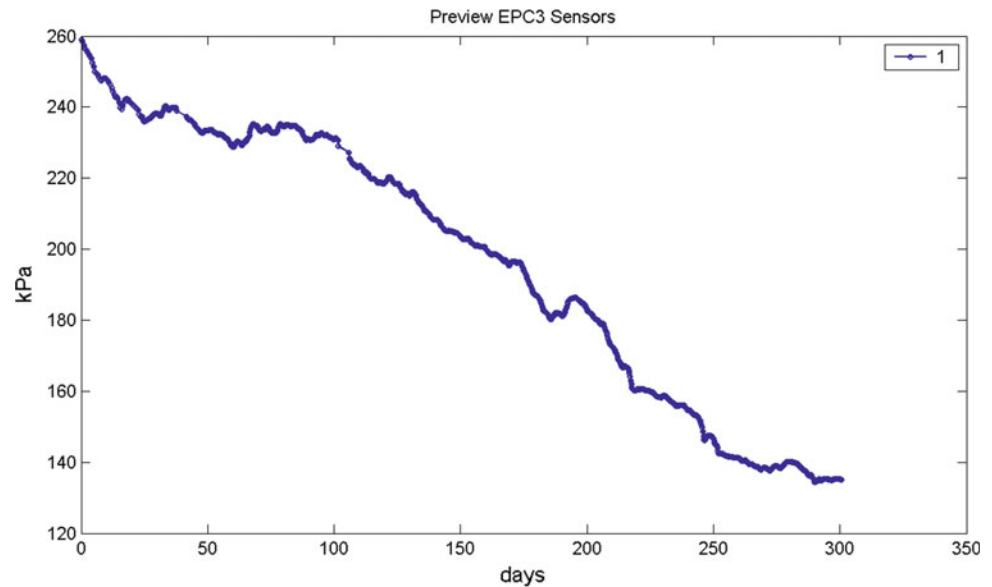


Fig. 9 Monitoring results **a** magnitude of displacement [mm], **b** X shear strain, **c** Y shear strain, Belchatow Mine

Fig. 10 Monitoring results, pore pressure at 30 m depth, Belchatow Mine



occurred after pore pressure drops. After 300 days (October 2017) pore pressure decreased to 139 kPa (Fig. 10). Ground displacements caused uplift of the coal seam, probably by the influence of mining and the salt dome. The early warning alarm trigger was set at 30 mm per day. To the current data this value hasn't been detected. However, displacements are observed to the current date. The total magnitude of the displacements that could be measured by the system is approximately 500 mm. By the end of September 2017, displacements had reached a total of 115 mm.

4 Summary and Conclusions

The implementation of two of the first on-line landslide monitoring and early warning methods in Poland were presented. The system in the Carpathians with 4 field stations and shallow instrumentation up to 16 m depth has been collecting data for a period of over seven years. The second newly installed 100 m deep system in Belchatow mine has been collecting data for a period of 10 months time. Results indicated the occurrence of small ground movements before the significant movements on the surface. Additional important data for the initiation of early warning could be obtained from pore pressure monitoring. The pore pressure transducer in the Carpathians located at the sliding surface depth detected significant increases of pore pressures of 100%. Twenty four hours after the excess of pore pressure the slide movements usually accelerated. In Belchatow mine interpretation of pore pressure influence was more difficult to discern. The pore pressure dropped more than 120 kPa, probably due to stress relaxation (caused by mining activity) and the mine water pumping system. However, movement acceleration usually occurred after significant excess

amounts of pore pressure. The on-line system in Belchatow detected deep movements 235 m below the natural terrain level. It was probably caused by the influence of mining and salt dome structure. This data should help the mine owner better recognize the risks for exploitation and for the improvement of west slope stability. The research allowed testing of new equipment and provided new geotechnical data. More advanced analysis of obtained results is in progress and should deliver more comprehensive data for the early warning system.

Acknowledgements The author would like to acknowledge the European Investment Bank for financing within the SOPO Landslide Counteraction Project. Installation of the first on-line monitoring in Polish Carpathians couldn't be possible without the EU Innovative Economy Project UDA-POIG.01.03.01-00-043/08 financed by the European Agency for Regional Development. Thanks are extended to the EU Euracoal Agency and the Polish Ministry of Science and Higher Education for the financing of the Slopes RFCR-CT-2015-00001 project, the PGE GIEKSA Company, the Gorlice Local Road District Administration, the Polish Academy of Science Research Station in Szymbark and the Carpathian Branch of Polish Geological Survey (PGI). I would like to thank them for their involvement and help in the presented research.

References

- Bednarczyk, Z.: Geotechnical modelling and monitoring as a basis for stabilization works at two landslide areas in Polish Carpathians. In: Proceedings of 11th International and 2nd North American Symposium on Landslides, Canadian Geotechnical Society, pp. 1419–1425. Taylor & Francis: London (2012)
- Bednarczyk, Z.: Landslide monitoring and counteraction technologies in polish lignite opencast mines. *Advancing Culture of Living with Landslides*, Springer 5, 33–43 (2017)
- Cruden, D.M., Varnes, D.J.: Landslides types and processes. In: Turner, A.K., Schuster, R.L. (eds.) *Landslides—Investigation and*

- Mitigation, vol. 247, pp. 36–75. National Academy Press, Transportation Research Board Spec. Report, Washington D.C. (1996)
- Gil, E., Dlugosz, M.: Threshold values of rainfalls triggering selected deep-seated landslides in Polish Flysch Carpathians. *Stud. Geo. Carpatho-Balc.* **40**, 21–43 (2006)
- Grabowski, et al.: Instrukcja opracowania map osuwisk i terenow zagrożonych (Instruction landslide maps and risk areas in Poland) Polish Geological Institute, Copyright of Ministerstwo Środowiska, Warsaw, pp. 1–92. in Polish (2008)
- Hochman, A., Kopalnia Węgla Brunatnego Belchatow, od przedsiębiorstwa państwowego do spółki akcyjnej. in Polish (2000)
- Petley, D.: Global patterns of loss of life from landslides. *Geology* **40**, 927–930 (2012)
- Rybicki, S.: Zjawiska osuwiskowe w krajowych kopalniach węgla brunatnego, ich skala, charakter i uwarunkowania. *Problemy Geotechniczne*. Wydawnictwo Politechniki Krakowskiej, 157–164. in Polish (1996)
- Starkel, L.: Geomorphology role of extreme rainfalls in the Polish Carpathians. *Studia Geom. Carpatho—Balcanica* **30**, 21–38 (1996)
- Turner, A.K., Schuster, R.L.: Landslides investigation and mitigation. National Research Council Transportation Research Board Special Report 247, Washington DC, p. 673 (1996)

Flood Hazard Evaluation in Mzab Valley (Ghardaia—Algeria)

Omar Mimouni, Amira Merchichi, Ghani Cheikh Lounis, Bachir Taleb, and El Hadi Tahalaitit

Abstract

Ghardaïa city is located about 600 km south of Algiers, in the northern Sahara, at an average altitude of 600 m. It is part of the Saharan desert plateau called Hamada, underlain by hard, brown to black limestones of Cretaceous age. The city extension is oriented toward the wadi Mzab which makes it vulnerable to flooding. In this work, we will present a hydroclimatic area overview, a flooding risk study in this arid zone, determine the vulnerability of the city from flooding and propose solutions to avoid such phenomenon. Recently a dam was proposed and built. We describe the characteristics as well as the reasons for the dam location choice.

Keywords

Ghardaïa • Saharan desert • Vulnerability
Flooding • Risk • Arid zone • Prevention

Mzab valley extends at a distance of 20 km length and 2.5 km width. It covers a surface of 50 km² and is located in the 5000 km² watershed enclosure (Bensmail and Hamouti 2010). The Mzab valley is located in a rocky plateau, desertic or Hamada shaped by brown and blackish hard limestones of upper cretaceous age and appears as a vast rocky area of 200–800 m height slightly inclined from West to East with a 3% slope. The topographic surface is strongly eroded by a network of watercourses called Chebka, of which main wadis are wadi Mzab, wadi Metlili, wadi Se-seb, wadi N'sa and wadi Zeghir. The valley draws large meanders of 1–2 km with a depth of 80–90 m. The topographic surface of the plateau is made of outcropping rocks explaining runoff of the slightest rain and lack of vegetation (Medejeraba 2009).

1 Introduction

1.1 Geographic Location

Ghardaia province is located in the center part of northern Algerian Sahara. It is located 632 km south of Algiers, at an average altitude of 600 m. The province covers a surface of 86,560 km² (Bensmail and Hamouti 2010). Its population is estimated to reach 370,020 inhabitants (2022). The province regroups 13 communes within 9 dairas and the Mzab valley covers 4 communes which are: Bounoura, El Atteuf, Ghardaïa and Daya (AMENHYD 2009). The Mzab wadi starts at the confluence of two great tributaries: Hameur wadi from North West and Labiod wadi from the west (Fig. 1).

O. Mimouni (✉) · A. Merchichi · G. C. Lounis · B. Taleb
E. H. Tahalaitit
LGGIP Laboratory, FSTGAT, USTHB, BP 32 El Alia 16111,
Bab Ezzouar, Algiers, Algeria
e-mail: omimouni2000@yahoo.fr

1.2 Lithology of Mzab Valley

The wadi bed is made of quaternary alluvium and sands. The turonian limestones constitute its surface overlaying cenomano-fracasian marls and clays (Fig. 2).

1.3 Climatology

According to data from the national agency of hydraulic resource (ANRH) and the Noumrat Ghardaia station, the climatic characteristics of the Mzab region are:

The rainfall pattern of the studied region is irregular. It is characterized by a dry and hot period (April–September) and a mild period (October–March) characterized by short duration torrential rainfalls. The rainfall amount is low, the mean annual recorded rainfall is in the order of 81.1 mm (ANRH 2010).

Minimum temperatures, 7 °C, were recorded in January and February; Maximum temperatures, 41 °C, were recorded in July and August. The region has a mean annual temperature of 22.4 °C (ONM 2010).

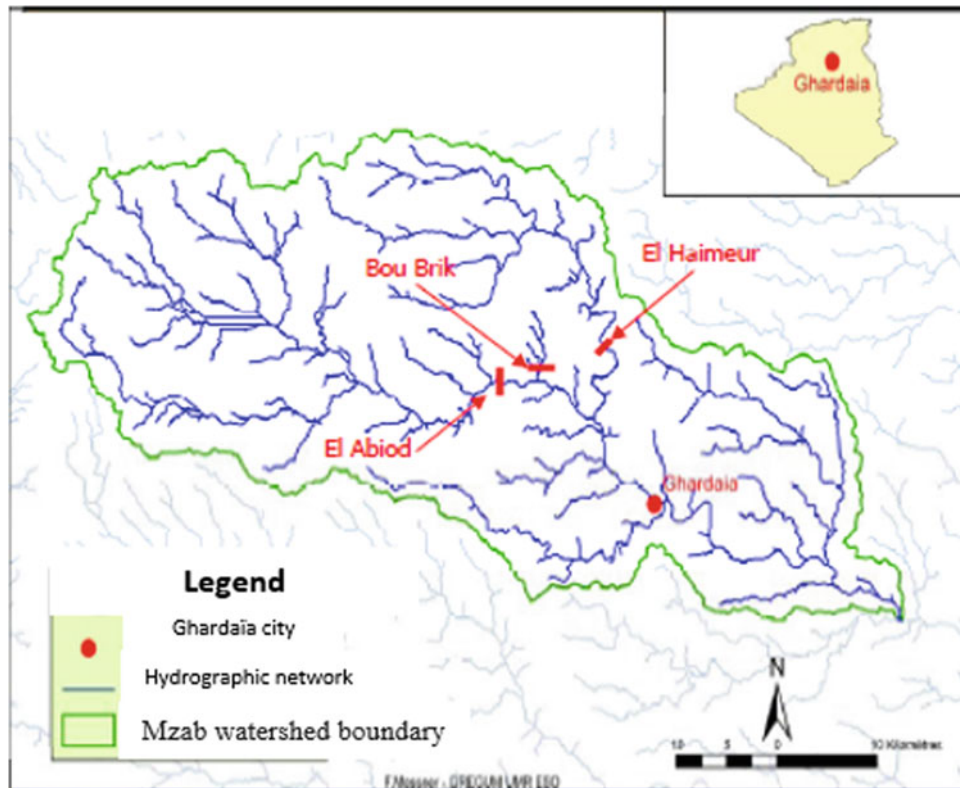


Fig. 1 Geographic location of study area (Djellouli Tabet 2010)

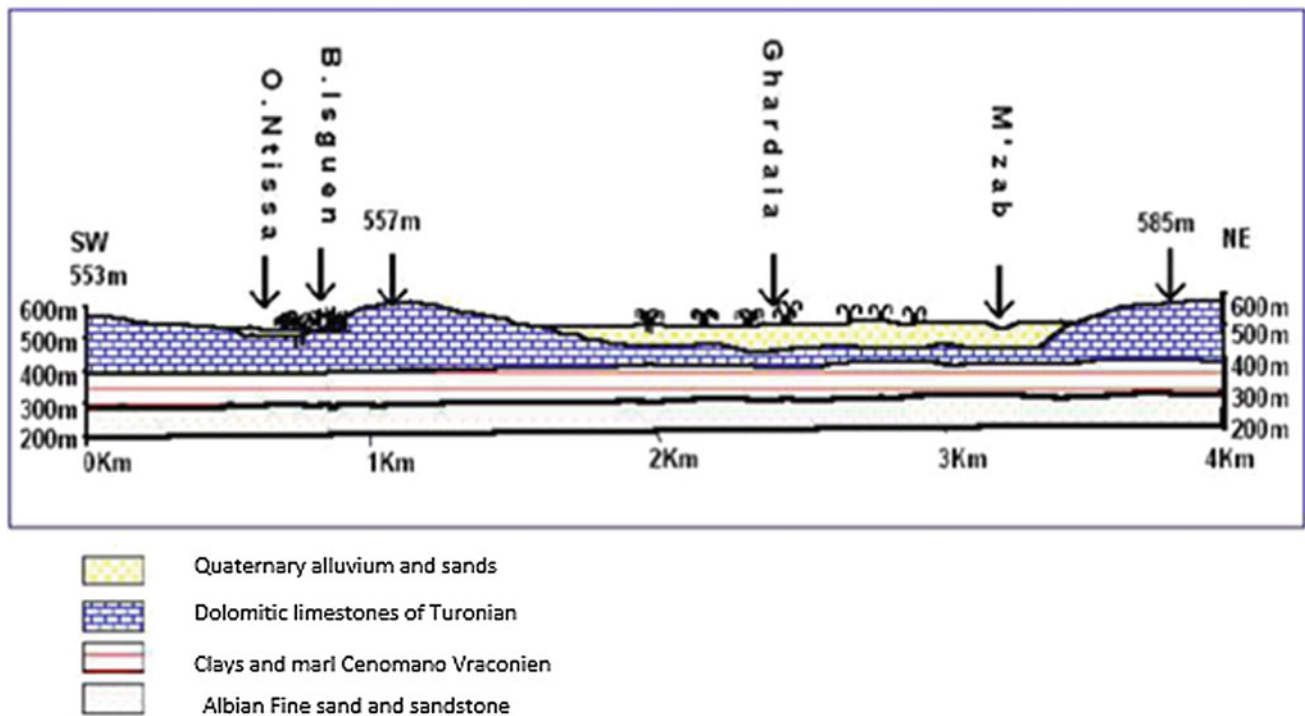


Fig. 2 Schematic geological section of Mzab valley (Medejeraba 2009)

Analysis of rainfall data.

Adjustment of rainfall at Ghardaia meteorological station data for a long observation series (1990–2010) is realized by HYDROLAB software. This software allows the adjustments to the most frequent laws used in Hydrology: Gauss Law (to calculate mean monthly and annual flows, monthly and annual rainfall); Galton Law (mean monthly and annual flows, monthly and annual rainfall, flood pics and daily flows); and the Gumbel Law (evaluation of return period for major rainy events).

Gumbel Law is written as (Pigeon 2005; Lamarre 2008):

$$F(x) = \exp(\exp(-u)) \text{ with } u = \text{reduced Gumbel variable} = (x - a)/b \quad (1)$$

a and t b correspond to position and scale parameters of F(x) graph.

$$fx = e^{-e[-\alpha(x-x_0)]} \quad (2)$$

F(x) = fréquence to non overtake = FND = F.et α , x_0 = adjustment coefficients.

The parameters (adjustment coefficients) of this law, (x_0) et (α) are given by formulas:

$$1/\alpha = 0.78 s \quad (3)$$

where s = standard deviation of maximum daily rainfall sample (x).

$$x_0 = \bar{x} - (0.577/\alpha) \text{ ou } \bar{x} = \text{average of } x \text{ serie.} \quad (4)$$

The estimation of the value that could reach the studied value for a given probability can be done either by a straight reading on a Gumbel probability (Fig. 3) paper or by calculation using formula:

$$x = \frac{1}{\alpha y} + x_0. \text{ (Equation of theoretical right)} \quad (5)$$

With $y = -[\ln(-\ln(f(x)))] =$ reduced Gumbel variable (Table 1).

For the Mzab watershed, exceptional theoretical daily maximum precipitations (more than 39 mm/day) adjust to Gumbel law for different return periods (P10, P50, P100). These rains can generate an important flow which may provoke exceptional floods.

1.4 Urbanisation and Settings

Population Valley: 160, 000 hab. Ksours Sites: 50, 000 hab.
Population Density Valley: 42 hab/ha. Ksours: 746 hab/ha (BG 2001).

Land occupation (Fig. 4) is varied and consists mainly of dry and irrigated crops, tree crops, palm groves, forests, bare land, buildings and Ksours.

2 Evaluation of Flood Risk

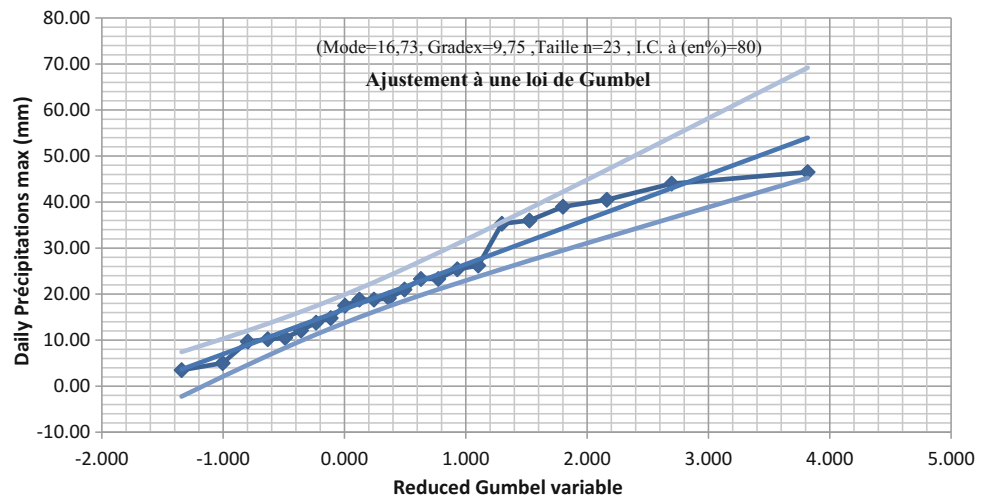
2.1 Historic of M’Zab Valley Floods

Floods recorded in archives of the region were tabulated in Table 2 as follow (Bensmail and Hamouti 2010, BG 2001):

Table 1 Maximum daily rainfall for different return periods adjusted to Gumbel law

Return period (years)	P 10	P 50	P 100
Fréquency	0.9	0.98	0.99
Ghardaia station	39.676	46.903	63.169

Fig. 3 Adjustment to Gumbel law for Ghardaia station



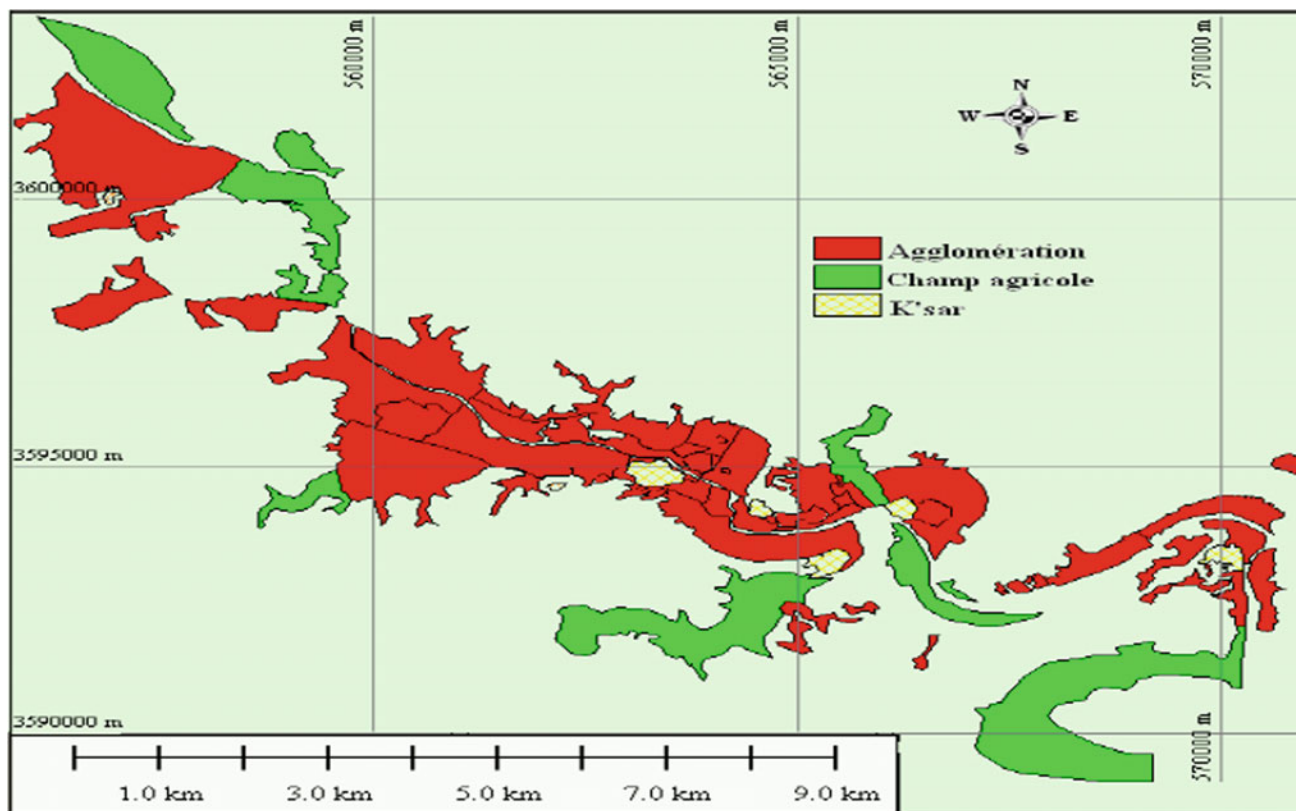


Fig. 4 Land cover map in the Mzab valley (2008)

Table 2 Monthly distribution of important floods from 1909 to 2008

Month	Flood years										Frequency
Sep	1901	1903	1929	1946	1948	1950	1951	1953	1994		9
Oct	1909	1943	1950	1951	1984	1995	2008				7
Nov	1932	1933	1938								3
Dec	1913	1932	1943								3
Jan	1946										1
Feb	1906	1914	1939	1943	1944						5
Mar	1925	1949	1943	1944	1949	1951	1953				7
Apr	1908	1935	1938	1941	1943	1946	1947	1949	1952	1997	10
May	1921	1923	1931	1941	1990						5
Jun	1942	1991	2004								3
July	1951	1953									2

October 1st, 2008 floods

An exceptional flood with a maximum discharge of $1200 \text{ m}^3/\text{s}$ reached Sebkhet Sefioune located at more than 180 km South of Ghardaïa. At Metlili, we registered a 6 m height whereas downstream it exceeded 8 m. The reasons

for this flood are due to a collapse of a hill reservoir built in 2005 at the wadi Laadhira 20 km from Ghardaïa chief town. In fact, heavy rains have caused water accumulation in 2 km (Figs. 5 and 6). The water pressure provoked a 70 m break in the reservoir dam and the onslaught of nearly $900 \text{ m}^3/\text{s}$ on Ghardaïa city (Alli Azouaou 2009) (Table 3).

Fig. 5 Broken dam of El Haimeur



Fig. 6 Flooding M'zab wadi (oct 2008)



Table 3 Precipitations from September 28 to October 1st compared to mean monthly and annual values

Stations	Rainfall cumul (mm)	Monthly mean rainfall (mm)	Monthly index (mm)	Annual rainfall (mm)	Annual index (mm)
Ghardaïa ANRH	79.7	16.77	4.75	83.84	0.95
ONM	47.27	14.58	3.24	82.04	0.58

Monthly and annual indexes reached very high values mainly in the Ghardaïa ANRH station.

2.2 Hazard Evaluation

It is noticeable that most damaged infrastructure are buildings constructed on bed embankments and sometimes inside bed wadis. We notice also that rainfall drainage networks do not exist in some areas (Fig. 7).

During the flood, many houses located in the Daya Ben Dahoua commune, agricultural lands and roads were damaged (Fig. 8).

Hazard Classification in Mزاب valley

The study zone is separated in three classes: strong, moderate and weak hazard:

Strong hazard: Corresponds to one of the three cases below:

- Frequent flooding (return period less than 10 years);
- Submersion height over one meter during the referential flood (referential flood is the strongest known flood)

- Water velocity exceeds referential flood velocity by more than 1 m/s.

Moderate hazard: Area flooded by at least two historical floods.

Weak hazard: Area flooded by only one flood.

To construct the hazard map we considered the October 1st 2008 which we separated in three hazard classes. We then considered three classes, strong, moderate and weak. This classification is made after measuring water heights during this flood and after PDAU classification, (Head plan of urban planning) (Table 4).

These classes are mentioned in Table 5 (Fig. 9).

2.3 Vulnérabilité Evaluation

Vulnerability is the predisposition to be flooded. It is accentuated by some aspects that favor:

- Anarchic urbanization and occupation of the wadi beds.
- Lack of maintenance of wadis and swales.
- Human activity sometimes harmful.

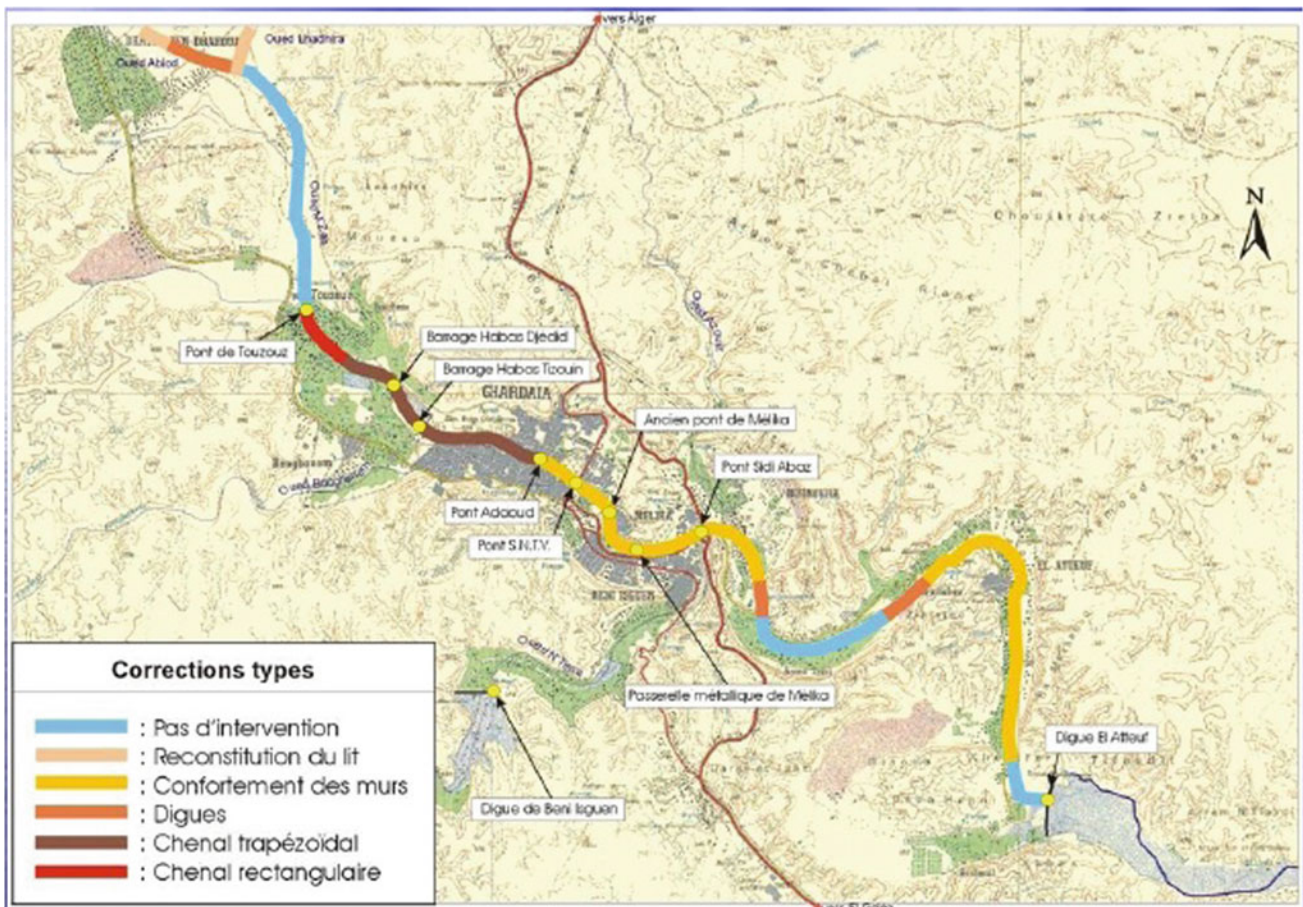


Fig. 7 Location of Mزاب wadi land use in urban areas (Djellouli Tabet 2010)



Fig. 8 01 October 2008 flood (<http://observers.france24.com/fr/2008>)

Table 4 Hazard classification according to water height

Type of hazard	Water height (m)
Weak hazard	0 to 0.5
Moderate hazard	0.5 to 1
Strong hazard	>1

Table 5 Vulnerability classification

Agricultural vulnerability	Urban vulnerability	Agricultural vulnerability
Wasteland + bare land	1	
Palm grove	2	
Habitat + palm grove	3	
Leisure infrastructure		1
Cemetery		1
Collective and semi collective habitat		2
Individual habitat		3
Mixed habitat (commerce or service)		4
Commerce and equipment		5
Aeroport		5
Industrial zone		6

It seemed appropriate to identify two kinds of vulnerabilities:

- Urban vulnerability includes all other tenure types.
- Agricultural vulnerability, which includes palm groves, agriculture and wastelands that are very vulnerable because, by definition, they are land that is not used.

We assign a reference to each type of soil occupation according to a scale starting from 01 for a weaker vulnerability to 06 for a stronger vulnerability (Cheikh Lounis et al. 2013; Mimouni et al. 2009).

Vulnerability classes show the diffusion from upstream to downstream of high vulnerability sectors according to the soil occupation variation during the 30 years reference (Fig. 10).

2.4 Flood Risk in Mzab Valley

It is necessary to compare agricultural and urban vulnerability with hazard classification. In order to construct a risk map, we selected GIS application (software Arc GIS mapping) (Saley et al. 2003) (Tables 6 and 7).

In the flood zones, urbanized lands of high vulnerability are evolving, therefore the risk increases with land use change (Fig. 11). In fact, the risk is a consequence of increasing urbanization in the Mzab valley.

Zones classified with high flooding risk are those where risk values are 3, 4 and 5.

2.5 Study of El Haimeur Clipper Dam Feasibility

After these serious floods, investment programs to restore damaged infrastructure were instituted. The idea to build the El Haimeur dam was a response to the needs reducing floods and containing increasing Laadhira wadi flows in dry seasons.

The body of the dam will be made by alluvium, compacted layer by layer. A key anchor at 4 m depth reduces

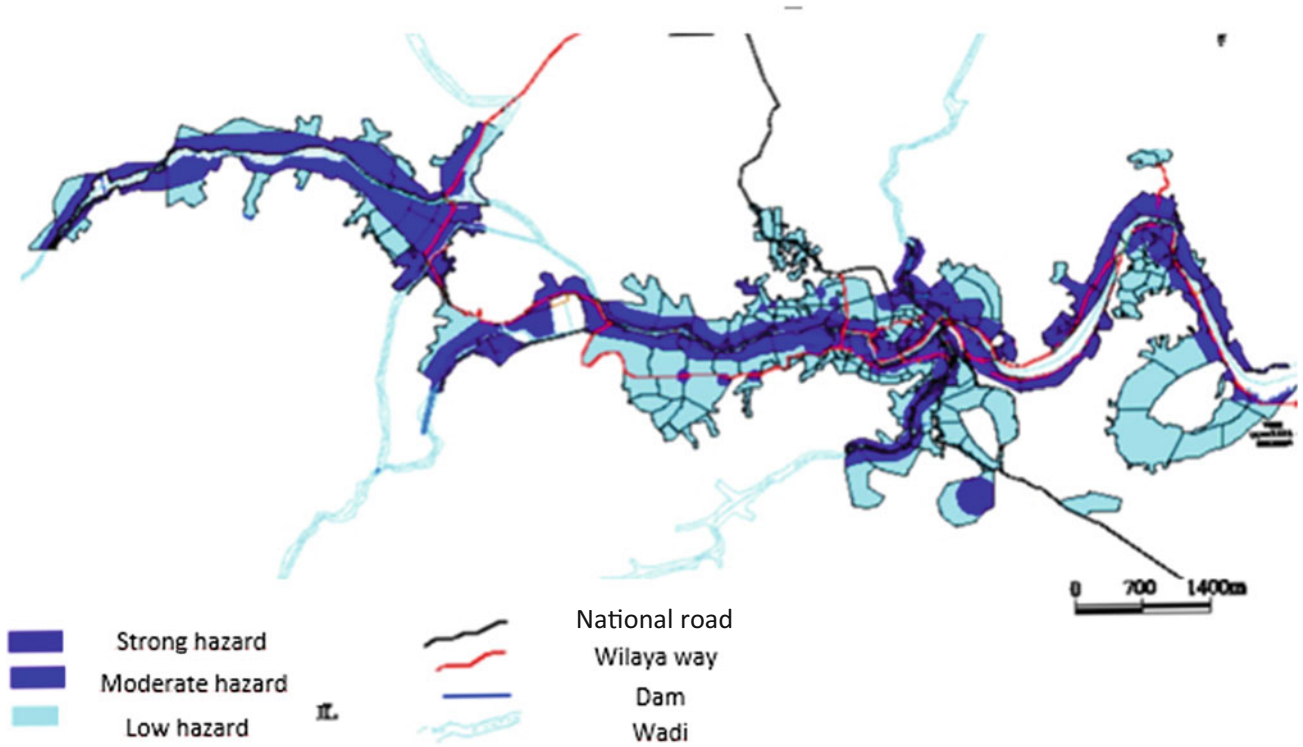


Fig. 9 Flood hazard in Mzab valley

Fig. 10 Evaluation of urban and agricultural vulnerability in the Mzab valley

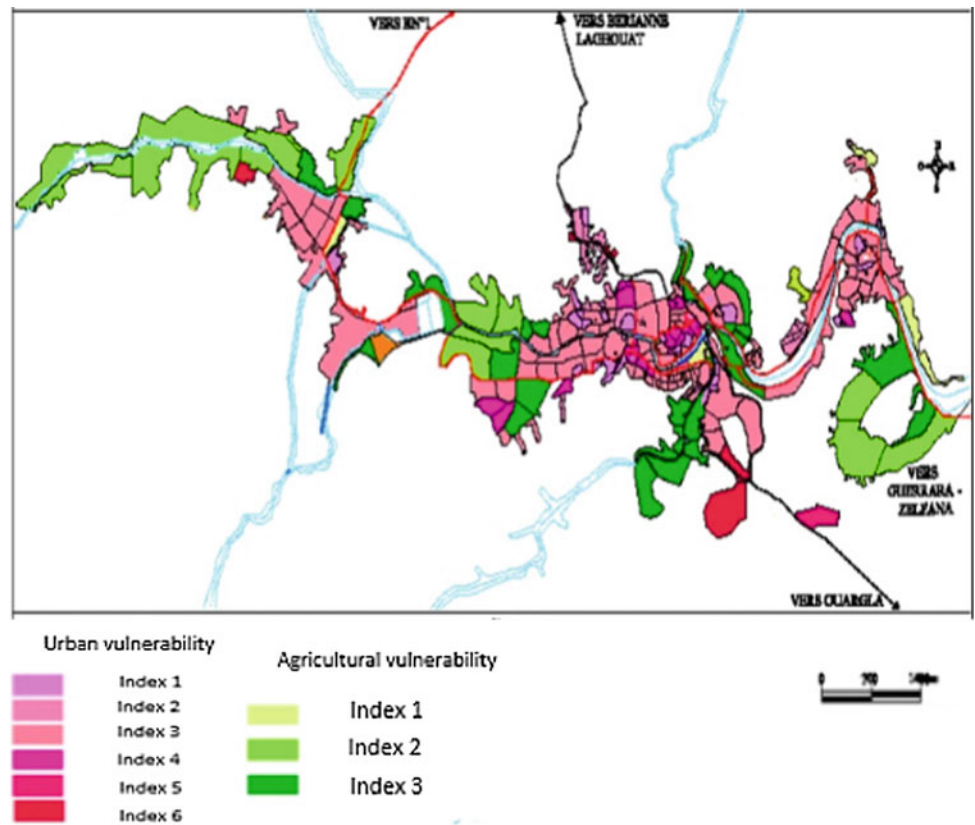


Table 6 Agricultural risk classification

	Agricultural vulnerability level 1	Agricultural vulnerability level 2	Agricultural vulnerability level 3
Hazard 1	1	1	2
Hazard 2	1	2	3
Hazard 3	2	3	3

Table 7 Urban risk classification

	Level 1	Level 2	Level 3	Level 4	Level 5	Level 6
Hazard 1	1	1	2	3	4	5
Hazard 2	1	2	3	4	4	5
Hazard 3	2	3	3	4	5	5

water flow through the foundation and lengthens the filtration path. It will be built with compacted wadi alluvium. A sloping drain and a drain mats will allow evacuation of infiltration waters outside the dam. The dam embankment

will be protected from erosion with a Rip-Rap (30/850) upstream and rockfills (10/300) downstream. An upstream drainage trench will dissipate pore pressure in the foundation.

The upstream face will be equipped with a berm at a 552.2 m with a width of 4 m. Its first role is as a cofferdam to protect the second phase of dam construction from the decennial flood. It will play an important role during the riprap installation in the upstream dam.

Dimensions of maximal section are presented as follow (BG 2001):

Main retention characteristics

- Height of normal retention: 555.8 NGA
- Area of normal level retention: 200 ha
- Capacity to normal retention: 7.2 Mm³
- Cutting Edge: 4.8 Mm³
- PHEE height: 557.9 NGA
- Area of retention at PHEE level: 250 ha (Fig. 12; Table 8).

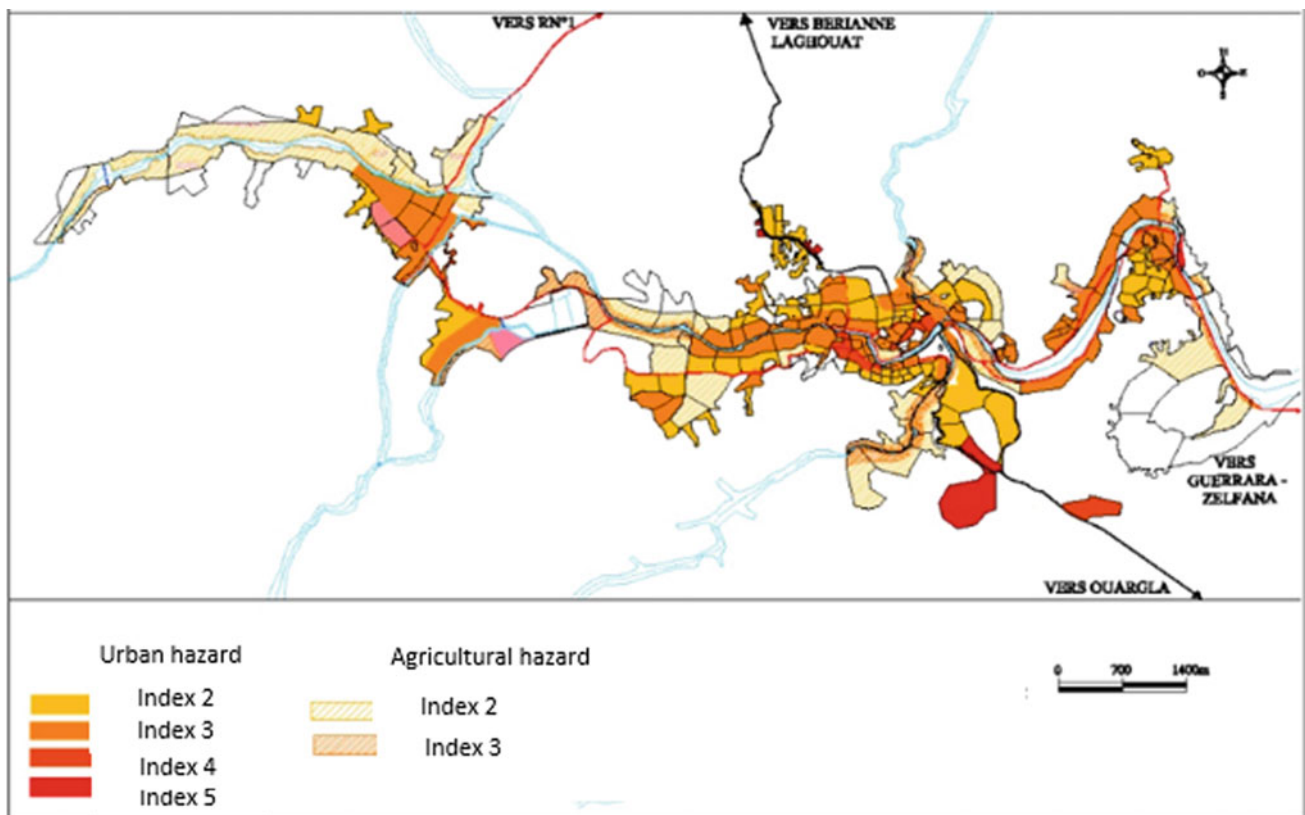


Fig. 11 Risk flooding map in Mzab valley (PDAU Mzab valley)

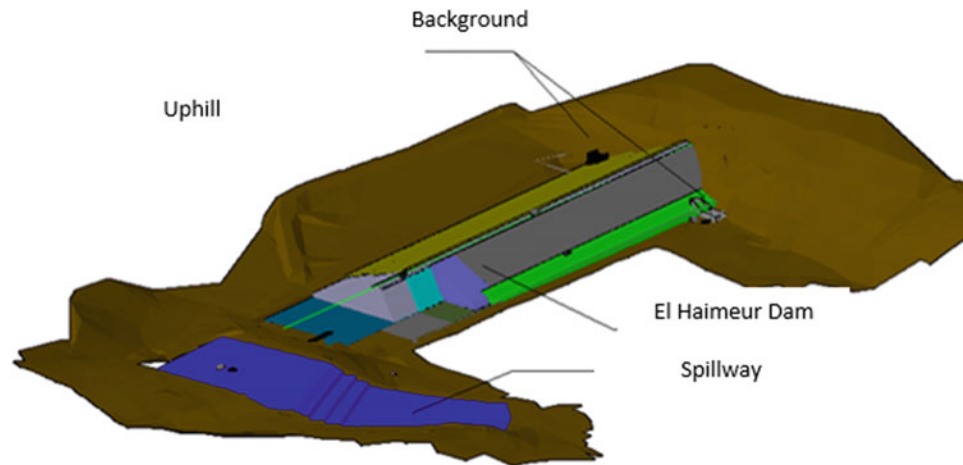


Fig. 12 Overview of El Haimeur dam

Table 8 Characteristics of water level fluctuations (case of a centennial flood)

	Upward		Downward		
	Time (h)	Average speed (m/s)	Time (h)	Average speed (m/s)	Peak speed (m/s)
El Haimmeur	15	2.2×10^{-4}	117	1.8×10^{-5}	2.7×10^{-5}

3 Conclusions

Despite its arid climate the Mzab valley is subject to important floods that can be very severe and very harmful to the population, infrastructure as well as agriculture.

Accelerating urbanization in Mzab valley enhanced soil sealing by building and infrastructure, increase surface runoff and flood occurrence. Human and economic losses due to floods are not solely due to the intensity of a flood, but also the effect of the increase in the vulnerability factor.

The most recent floods in Mzab valley revealed serious problems, linked to the risk management. Thus, increasing population and concentration of activities in the valley, makes the urban environment a major challenge.

References

<http://observers.france24.com/fr/20081010-ville-ghardaia-ensevelie-boue-inondations>

- AMENHYD.: Document RN110-4063 (Volume géologie et géotechnique, volume fondation, volume stabilité, Algeria (2009)
- ANRH.: *Annuaire hydrogéologiques*, Agence Nationale des Ressources Hydrauliques, Ministry of Equipment and Spatial Planning, Algiers (2010)

Alli Azouaou, F.: *Simulation de la crue d'Octobre 2008 dans la commune de Ghar-daia*, engineering memory. Polytechnic National School, Algiers (2009)

BG.: *L'étude avant-projet détaillé des ouvrages de rétention El Abiod*, RN115-4063, Algeria (2001)

Bensmail, L., Hamouti, S.: *Développement urbain face au risque d'inondation, cas de la vallée de Mzab*, engineering memory. USTHB, Algiers (2010)

Cheikh Lounis, G., Chatelain, J. L., Mimouni Omar., Machane, D., Hellel, M., Bel-hai, D., Doukhi, M., Sadou, O.: *Assesment of flood risk in the Kniss wadi catchment in urban area*. In: *National Geological Service Bulletin*, vol. 24, pp. 59–70. Algiers (2013)

Djellouli Tabet, Y., Sioussiou, R.: *Le bassin versant du M'Zab, région méditerranéenne hyperaride, ressources en eau, risques et gestion*, Maine le Mans university (2010)

Lamarre, D.: *Les risque climatiques*, Edition belin, Paris

Medejeraba, A.: *Les inondations catastrophiques du mois d'Octobre 2008 à Ghardaia*. *Geographia Technica*, Algeria (2009)

Mimouni, O., Mesbah, M., Berrahel, M., Merouane, A.: *Etude géologique et géo-technique de problèmes d'inondabilité dans la région d'Alger*. In: *Exemple l'Oued El Harrach*, vol. 20, pp. 109–126, *National Geological Service Bulletin*, Algiers (2009)

ONM.: *Weather Data* (2010)

Pigeon, P.: *Géographie critique des risques*. *Economica*, coll. *Géographie*, p. 217 (2005) ISBN: 2- 7178-5028-7

Saley, M., Kouame, F., Penven, M.J., Biemi, J., Boyassoro K. H.: *Cartographie des zones à risque d'inondation dans la région semi-montagneuse à l'Ouest de la Côte d'Ivoire*, *Contribution of DEMs and satellite imagery*. *Remote Sens. Rev.* **5**(1-2-3), 53–67 (2003)

Assessment of Landslides Triggered by Earthquakes Based on the Combination of Peak Ground Motion and Critical Acceleration Analysis

Chen Xiaoli and Liu Chunguo

Abstract

There is a need for landslide susceptibility models that can be used to quickly predict the locations of earthquake-triggered landslides after large seismic events. As a triggering factor, peak ground acceleration (PGA), which is a measurement of the magnitude of seismic ground motion, has a close relationship with the landslides occurrences and usually is used as an indicator in the assessment of landslides hazards. However, the landslides triggered by the 2014 Ludian earthquake, Yunnan, China show an exception. Different from other events, the landslides exhibit a particular pattern of spatial distribution. They did not occur along a fault or structural zone linearly, instead being relatively concentrated in several locations southeast and west of the epicenter. The usually used factors for landslides assessment such as earthquake magnitude, the distance to epicenter or faults as well as PGA cannot give a reasonable explanation to this phenomenon. Considering the physical mechanism of earthquake triggered landslides, a slope performance during a shaking event mainly depends on two parts: one is the stability of itself, which can be represented by critical acceleration obtained by Newmark method model analysis, and the other is the trigger intensity, which can be measured by PGA. Thus, for a given PGA, whether or not a landslide occurs depends on not only the PGA, but also the stability of the slope itself. Based on these, we use the Newmark's method model to analysis critical acceleration in the landslides affected area during the

Ludian earthquake, and find that the results can make it explicable for the particular distribution patter.

Keywords

Earthquake-triggered landslides • Peak ground acceleration • Slope stability • Critical acceleration • Newmark model

1 Introduction

Earthquake-triggered landslides can increase greatly the destructive impact of earthquakes in mountainous areas. Sometimes a great loss of lives and properties caused by landslides even exceeds the losses caused by the earthquake itself, as it is shown by the 2008 Wenchuan earthquake. For effective mitigation of the disaster, quickly knowing where the most landslides damaged places are located is important for the rescuing managing strategy (Bommer et al. 2002). However, relatively less attention has been focused on rapid response assessments associated with coseismic landslides.

As a triggering factor, peak ground acceleration (PGA), which is a measurement of the magnitude of seismic ground motion, is closely correlated with landslide occurrence (Harp and Jibson 1996; Keefer 1984; Sato et al. 2007; Meunier et al. 2007; Dai et al. 2011; Qi et al. 2010), and it is often used as an index to predict where landslides are likely to occur during an earthquake event. However, some case studies show different phenomena that there exist places with larger PGA but less landslides, such as the 2014 Ludian, Yunnan, China, earthquake (Mw 6.1).

In this paper, we apply a simplified Newmark method to address the issue above. The critical acceleration which can be obtained by the Newmark method is used as an index to portray slope stability in the study area. Then, combined with the peak ground acceleration distribution map caused by the 2014 Ludian earthquake, we conduct the assessment of coseismic landslide hazard and compare the results with the actual landslides.

C. Xiaoli (✉)
Key Lab of Active Tectonics and Volcano, Institute of Geology,
Earthquake Administration China, Beijing, 100029, China
e-mail: chenxl@ies.ac.cn

L. Chunguo
China Earthquake Networks Center, Beijing, 100045, China

2 Data and Methodology

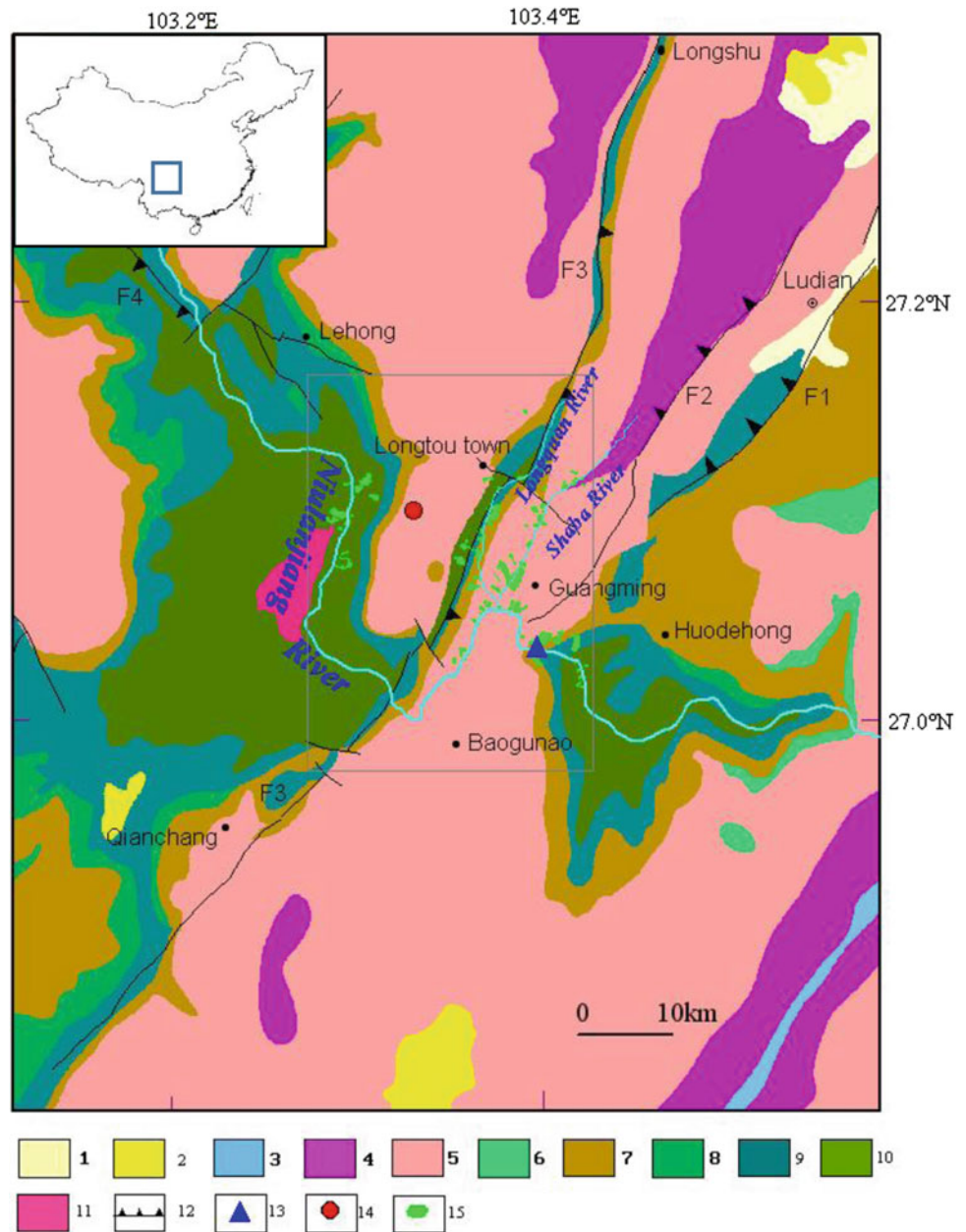
2.1 Landslides Triggered by the 2014 Ludian Mw6.1 Earthquake

The 2014 Ludian Mw6.1 earthquake occurred in south-western China, the southeastern margin of the Tibetan plateau (Fig. 1). Most high mountains in this region trend in NE–SW direction, along which tectonic uplift and river incision have resulted in great topographical relief. There

exist numerous V-shaped river valleys with steep, somewhere even nearly vertical, slopes on either side of the rivers.

Pre- and post-earthquake satellite images and air photos showed that at least 1024 landslides larger than 100 m² were triggered by the 2014 Ludian earthquake, which occupied a total area of 5.19 km² (Xu et al. 2014). The majority of them occur at the river reaches with cliffs, while few landslides occurred near the epicenter or in areas to the north and south. Field investigations showed that they were dominated by shallow slope failures and rock or soil slides, with size of a

Fig. 1 Geologic map of the Ludian seismic area (modified from China Geological Survey (CGS), Regional geological map of Sichuan province (1:200,000), 2001). Box denotes the study area. **Geology:** 1 Quaternary. 2 Neogene. 3 Jurassic. 4 Triassic. 5 Permian. 6 Carboniferous. 7 Devonian. 8 Silurian. 9 Ordovician. 10 Cambrian. 11 Sinian. **Other symbols:** 12 Reverse faults. 13 Seismic dam at Hongshiyuan. 14 Epicenter of Ludian Mw6.1 event. 15 Coseismic landslide. **Fault:** F1- Sayuhe fault. F2- Zhaotong-Ludian fault. F3- Longshu fault. F4- Xiaohe fault



few cubic meters for rock falls and of tens of million cubic meters for rock avalanches (Chen et al. 2015).

2.2 Slope Critical Acceleration

We use the Newmark method to calculate the critical accelerations for the natural slopes (Newmark 1965; Jibson et al. 2000). In this method, the key inputs are local topographic slope and material strength. Here, SRTM 90 m (<http://srtm.csi.cgiar.org/SELECTION/inputCoord.asp>) is used to produce the slope map (Fig. 2). Meanwhile, 1:200,000-scale geologic maps (CGS 2001) of the region is applied to form the basis for assigning material properties (Fig. 1).

When the two datasets are decided, they are combined to yield the critical acceleration grids. For a given shaking level, any two slopes that have the same critical acceleration will behave the same, regardless of how those slopes might

differ in geometry or material properties. The critical acceleration map thus serves as one to delineate slope stability of the study area (Jibson et al. 2000) (Fig. 3).

2.3 Peak Ground Acceleration (PGA)

We prepare the map on distribution of peak ground accelerations based on the ground motions data recorded by seismic stations around the study region. There are 12 seismic stations recorded the ground motions of the 2014 Ludian shock. These seismic stations are mainly distributed in the NE direction. Among these seismic stations, the Longtou town seismic station (labeled 53LLT in Fig. 3) is the only one located near the epicenter, which recorded the highest PGA values: NS, EW and vertical components are 948.5, 704.9, and 503.8 Gal, respectively (Chang et al. 2016). Except that, other seismic stations recorded comparatively lower PGA values less than 0.2 g.

Fig. 2 Map showing the distribution of slope gradients in the Ludian earthquake region

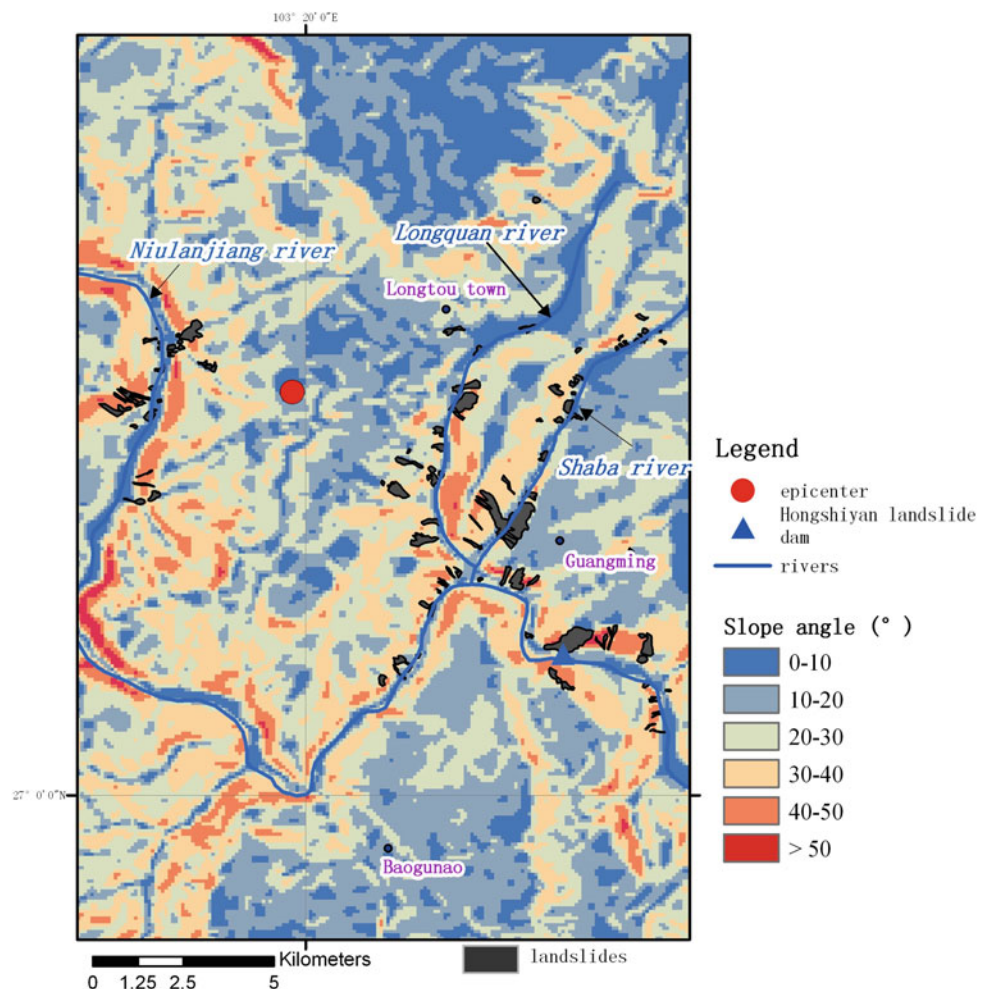
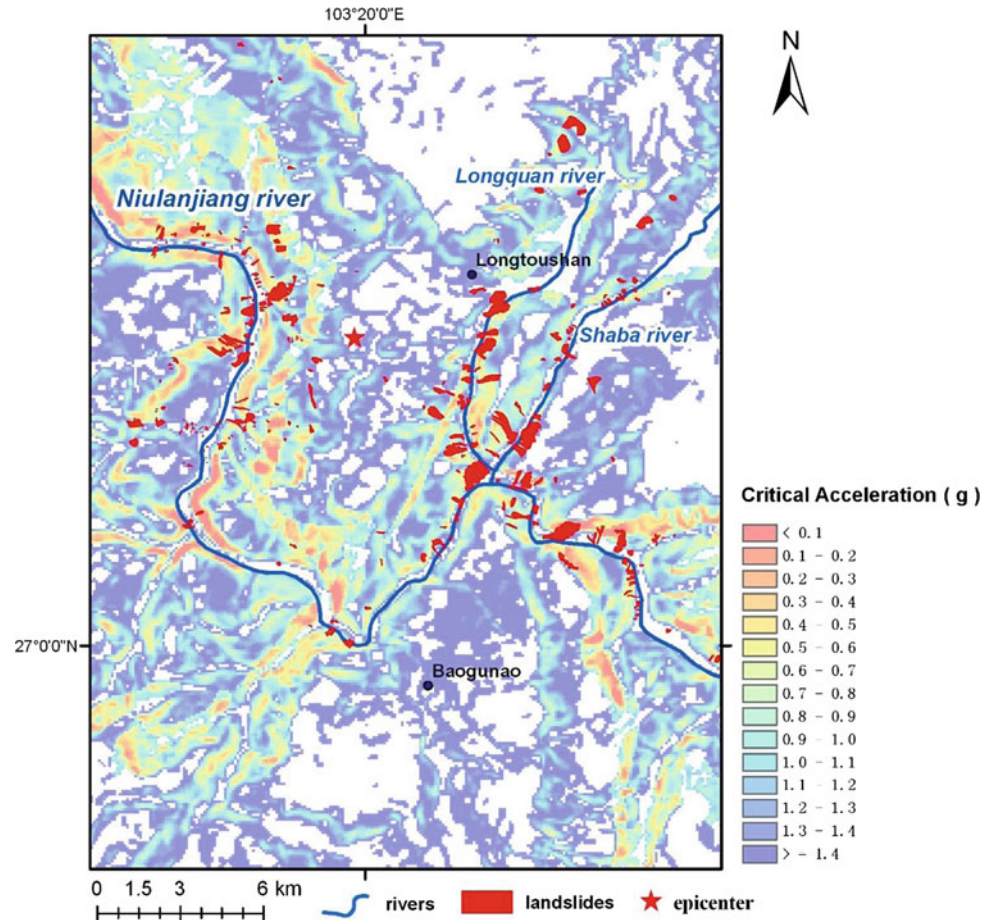


Fig. 3 Map showing the distribution of critical accelerations in the study area



Despite of the uneven distribution of the seismic stations, the distribution map of peak ground acceleration of the study region is generated by applying spatial analyst tools in ArcGIS 9.2 (Fig. 4).

3 Results

Considering the physical mechanism of earthquake-triggered landslides, the behavior of a slope during a shaking event mainly depends on two factors: one is the stability of the slope, the other is the trigger intensity. And it becomes explicable that the places with same PGA may differ much in the landslides occurrence due to the different slopes stabilities.

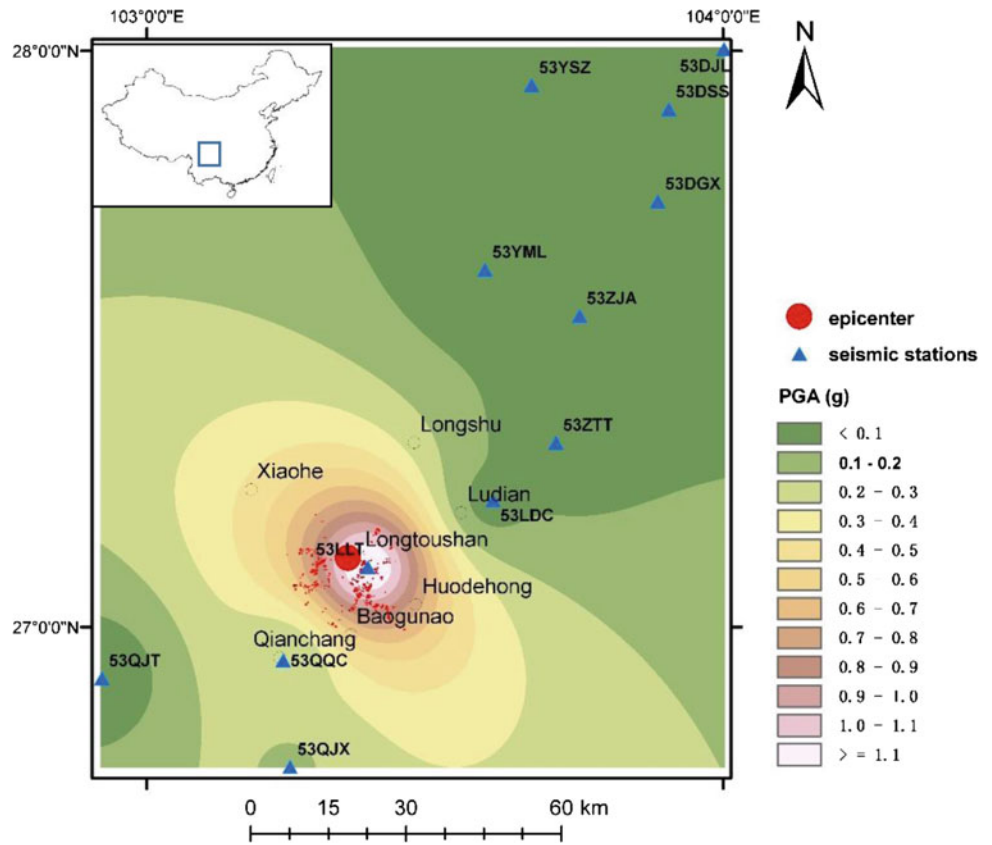
Based on this principle, the assessment of regional co-seismic landslides hazard is conducted by comparing the critical acceleration with PGA value at each computing cell. The results are classified into 5 levels, namely high,

moderate high, moderate, light and very light level, representing different hazardous degrees. Figure 5 shows a map of the predicted landslide hazard zones and the Ludian-earthquake triggered landslides, which demonstrates how well the high and moderate high landslide hazard zones capture what actually happened.

4 Discussion

In this contribution, the method applied here doesn't mean to predict the precise location of every real landslide; instead, it provides information to help identify areas heavily impacted by earthquake-triggered slope failures and assist disaster response activities. More important for rapidly mapping the landslide susceptible areas, this procedure is easy-operation because the required input datasets are few and calculation is simple.

Fig. 4 Map showing the distribution of peak ground acceleration in the Ludian earthquake region

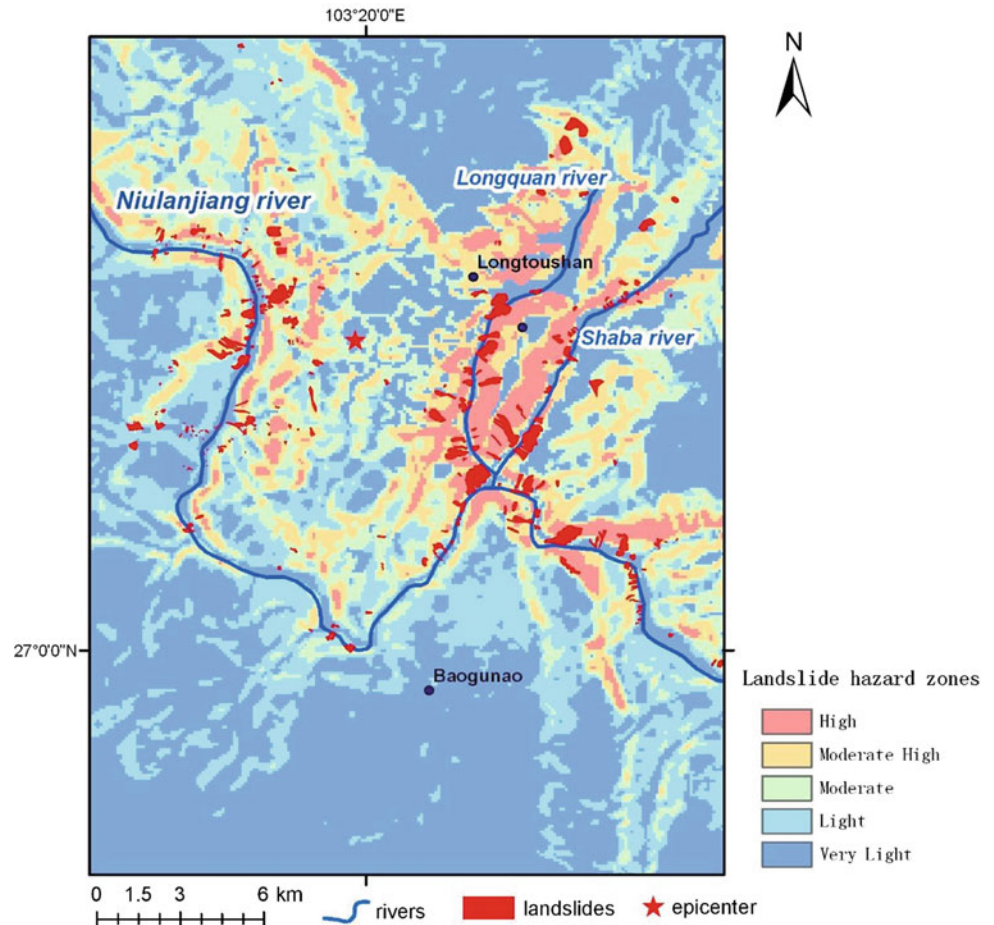


Critical acceleration represented by the slope stability is in general agreement with the distribution of observed landslides, which implies that the distribution of slope stability controls the pattern of landslides to a large extent. Thus, based on critical acceleration analysis, the distribution of landslides can be effectively connected with the distribution of PGA. Comparing with using PGA alone as an index to assess the co-seismic landslides hazard after an earthquake, the method presented in this study, which considers the stability of slopes in advance, has a big advantage of providing a more accurate result by indicating the places most likely to be subjected to landslides. For a given earthquake, slope behavior depends on the comparison

between its stability and the shaking intensity it experiences. If the ground motion doesn't reach the threshold required by slope failures, it will result in few landslides even though the slope is near to the epicenter, which is just what happened in the Ludian earthquake area.

It should be noted that the procedure to generate PGA distribution is a purely mathematic calculation and does not consider the direction of PGA attenuation with respect to the strike-slip fault. The estimated PGA map may not precisely reflect the site PGA, resulting in errors in the predictions. Thus, the method used to obtain a PGA distribution map needs further study in the future.

Fig. 5 Map showing landslide hazard zones and real landslides triggered by the 2014 Ludian earthquake in the study area



5 Conclusions

On the basis of Newmark method, this work maps the slope seismic stability represented by critical accelerations using the data from the Ludian earthquake area. The results show that the distribution of slope stability controls the pattern of co-seismic landslides to a large degree.

The differences between the critical accelerations and PGAs are applied to assess the potential earthquake-triggered landslides. The study region is divided into 5 landslide hazard zones of high, moderate high, moderate, light and very light levels. Comparison shows the resultant landslides hazard zones are in general agreement with distribution of coseismic landslides, indicating effectiveness of the method.

Although this method cannot make a forecast in a rigorous way, it is a far more practical utility for providing the comparatively accurate information about where the most landslide damaged areas may be located, which is important for an emergence preparedness planning.

Acknowledgements This work was supported by the National Natural Science Foundation of China (Grant No. 41572194) and the Basic Scientific Fund of the Institute of Geology, China Earthquake Administration (Grant No. IGCEA1604).

References

- Bommer, J.J., Carlos, E., Rodríguez, C.R.: Earthquake-induced landslides in Central America. *Eng. Geol.* **63**, 189–220 (2002)
- Chang, Z.F., Chen, X.L., An, X.W., Cui, J.W.: Contributing factors to the failure of an unusually large landslide triggered by the 2014 Ludian, Yunnan, China, Ms=6.5 earthquake. *Nat. Hazards Earth Syst. Sci.* **16**: 497–507 (2016)
- Chen, X.L., Zhou, Q., Liu, C.G.: Distribution pattern of coseismic landslides triggered by the 2014 Ludian, Yunnan, China Mw6.1 earthquake: special controlling conditions of local topography. *Landslides* **12**(6), 1159–1168 (2015)
- China Geological Survey (CGS): Regional geological map of Sichuan Province (1:200,000). Geological Press (2001)
- Dai, F.C., Xu, C., Yao, X., Xu, L., Tu, X.B., Gong, Q.M.: Spatial distribution of landslides triggered by the 2008 Ms 8.0 Wenchuan earthquake. *China. J. Asian Earth Sci.* **40**(4), 883–895 (2011)

- Harp, E.L., Jibson, R.W.: Landslides triggered by the 1994 Northridge, California earthquake. *Bull. Seismol. Soc. Am.* **86**(1B), s319–s332 (1996)
- Jibson, R.W., Harp, E.L., Michael, J.A.: A method for producing digital probabilistic seismic landslide. *Eng. Geol.* **58**, 271–289 (2000)
- Keefer, D.K.: Landslides caused by earthquakes. *Geol. Soc. Am. Bull.* **95**(4), 406–421 (1984)
- Meunier, P., Hovius, N., Haines, J.A.: Regional patterns of earthquake-triggered landslides and their relation to ground motion. *Geophys. Res. Lett.* **34**, L20408 (2007). <https://doi.org/10.1029/2007GL031337>
- Newmark, N.M.: Effects of earthquakes on dams and embankments. *Geotechnique* **15**, 139–160 (1965)
- Qi, S.W., Xu, Q., Lan, H.X., Zhang, B., Liu, J.Y.: Spatial distribution analysis of landslides triggered by 2008.5.12 Wenchuan Earthquake. *China. Engineering Geology* **116**, 95–108 (2010)
- Sato, HP., Hasegawa, H., Fujiwara, S., Tobita, M., Koarai, M., Une, H., Iwahashi, J.: Interpretation of landslide distribution triggered by the 2005 Northern Pakistan earthquake using SPOT 5 imagery. *Landslides* **4**(2): 113–122 (2007)
- Xu, C., Xu, X.W., Shen, L.L., Dou, S., Wu, S.E., Tian, Y.Y., Li, X.: Inventory of landslides triggered by the 2014 Ms6.5 Ludian earthquake and its implication on several earthquake parameters. *Seismolog. Geol.* **36**(4), 1186–1203 (2014). (in Chinese)

Rockfall Mitigation Practices in Nepal

Ranjan Kumar Dahal

Abstract

Nepal is an earthquake-prone country and earthquakes in Nepal have been documented since 1255. Earthquake-induced landslides, mainly rockfall and dry debris fall were major geological issues after the 2015 Gorkha Earthquake in central Nepal. Many hydropower projects and roads of central Nepal faced rockfall problems after the earthquake and the damaged areas need extensive support for research and mitigations. As a result, a mitigation plan was initiated in a hydropower project. Detailed investigation has been done to understand the rockfall problems and a suitable remedy for the selected project site was implemented. This paper describes rockfall problems in Nepal and their analysis. It also briefly describes a site modeled for rockfall protection and suggests new technology for rockfall protection systems in the Himalaya.

Keywords

Rockfall • The 2015 Gorkha Earthquake • Nepal • Himalaya

1 Introduction

Varnes (1978) defines rockfall as a fragment of rock detached by sliding, toppling, or falling, that falls along a vertical or sub-vertical cliff, proceeds down slope by bouncing and flying along ballistic trajectories or by rolling on talus or debris slopes. The detachment of rock blocks from the cliff usually follow various natural mechanisms such as freezing and thawing cycles, seismic activities and by anthropogenic activities in the slope such as blasting, and heavy machinery movement (Einstein 1988; McCarroll et al. 1998; Bull et al. 1994; Vidrih et al. 2001; Abebe et al. 2010;

Matsuoka and Sakai 1999; Dorren 2003; Volkwein et al. 2011). In fact, rockfall process is most importantly a slow time-dependent deformation of the slope materials and falling of rock blocks. There is no standard size for rockfalls and they can be of any size. Likewise, rockfalls can occur in all rock types ranging from granite to mudstone.

Nepal is earthquake-prone country and earthquakes in Nepal have been documented since 1255. The recent 2015 Gorkha Earthquake measuring Mw 7.8 occurred at 11:56 AM Nepal Standard Time on 25 April 2015 with an epicenter 77 km northwest of Kathmandu at Barpak village of Gorkha district and killed about 9000 people. Rockfall and dry debris fall were the major earthquake-induced landslides after the 2015 Gorkha Earthquake (Dahal 2015). Rockfall events are serious engineering challenges to infrastructure projects in Nepal—primarily highways and hydropower projects. Until now little progress has been made in mitigating these geodisaster problems in the Himalayas with modern engineering solutions. Geological settings and rock mass properties play vital role for rockfall protection measures. Joints in rock mass and the overall structure on rock slopes are the dominant contributors to rockfall (Dahal et al. 2014). In rockfall, the size of boulder or block can range from small cobbles to large boulders having hundreds of cubic meters in volume, and travel at speeds ranging from a few to tens of meters per second with enormous energy. Annually, Rockfall events cause tremendous damage to life and property in Nepal, especially along highways, settlements and hydropower projects (Dahal 2016).

An initiative has been made in Nepal for rockfall mitigation on slopes adjacent to hydropower projects and road slopes. Two sites were selected for installation of rockfall mitigation systems.

The first site is the Siddhababa area (Figs. 1 and 2) that covers almost 2 km of the Siddhartha Highway of western Nepal, a very famous problematic rockfall site in Nepal. The construction of the Siddhartha Highway was completed in 1971 with the financial aid of the Government of India to connect the Indian boarder town Sunauli with the touristic

R. K. Dahal (✉)
Central Department of Geology, Tribhuvan University, Kirtipur,
Kathmandu, Nepal
e-mail: rkdahal@gmail.com

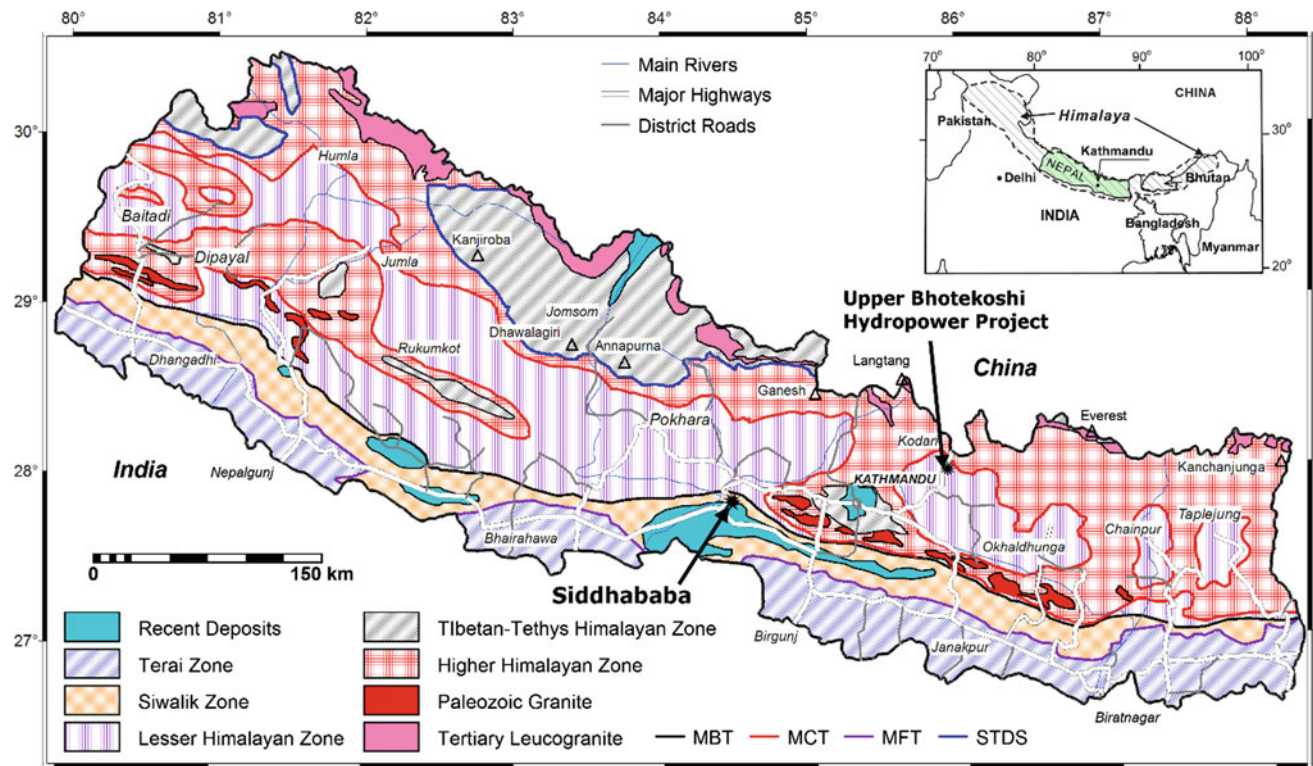


Fig. 1 Geological map of Nepal and location of Siddhababa and Upper Bhotekoshi hydropower project where rockfall mitigation systems were installed

city Pokhara of Nepal. This 180 km long highway passes through relentless bends and curves making it one of the most adventurous roads of Nepal.

Another site (Figs. 1 and 3) is uphill slope of penstocks site of the Upper Bhotekoshi Hydropower Project which was damaged irreparably by rockfall after 2015 Gorkha earthquake. Rockfall mitigation system such as rockfall barriers and gully nets were used to protect penstock site from Rockfall problems.

2 Current Practices and Need of New Technology to Protect from Rockfall

Low cost landslide and roadside slope mitigation practices are well established in Nepal. For protection from rockfalls, landslides and debris flows, measures such as cement stone masonry walls, gabion retaining walls, cascade drainage, bioengineering systems, small fences and upslope catchment

Fig. 2 Model site and surrounding geological settings at the Siddhababa area





Fig. 3 Rockfall problem in Upper Bhotekoshi Hydropower Project after the Gorkha Earthquake

drains are currently used in Nepal. Rock bolting and counterforts are rarely used in Nepal. Among these methods, gabion and stone masonry retaining walls are most often installed. Such protection systems are good for shallow soil slope failure and erosion protection only. They are not suitable for the rockfall protection systems. The flexible gabion wall cannot dissipate the high impact energy of rock fragments and the failure of such protection measures is common on roadside slopes. The current low-cost mitigation practices applied in Nepal for rockfall protection have not been totally successful at all infrastructure development projects, settlements and utilities.

Steep topography at rockfall hazard locations usually precludes the use of low-cost structure measures. Likewise, during monsoon, heavy rainfall always washes out the slope protection structures and so they serve as temporary protection measures only. Failure of low-cost structures increases the damages on roadside slopes and annual construction of new low-cost structures increases the overall cost of the project finally resulting in a great economic loss to the country. Therefore, for a long-term economical solution, a new technology should be adapted for Himalayan geological and geotechnical settings which can perform well for rockfall protection system on slopes.

Many innovative solutions are available for the rockfall protection which are tested in various laboratories and are found to be suitable to mitigate Nepalese rockfall problems. Rockfall barriers are developed to protect infrastructure, utilities, buildings and people from falling rocks and debris. Rockfall barriers can be classified into rigid or flexible and the flexible ones can be installed, with or without retaining ropes. Typical rockfall protection barriers can be installed in run-out or depositional zones, close to the elements at risk. For this purpose, a wide range of tested rockfall protection barriers that differ in the maximum energy level, 100–8000 kJ, and the approved heights, 2.5–9.0 m, are available. Due

to modular construction and variable construction methods, rockfall protection systems can be easily adapted to topographical conditions of Nepal. To verify the performance capabilities of net and rockfall barriers, usually impact tests or crash test are conducted. The normative ETAG 027 (Peila and Ronco 2009) classifies rockfall barriers in eight different energy classes and for each of them there are two different energy levels named as Service Energy Level (in kilojoules) and Maximum Energy Level (in kilojoules). All the rockfall protection systems now available in Nepal are tested at globally certified test sites and approved by many independent institutes.

Because rockfalls are unpredictable and incapable of being analyzed with precision, the concept of a factor of safety is not appropriate. The current approach of rockfall study is to use a rock slope inventory system to predict the Rockfall risk to highway users and then, by means of a computational simulation, to attempt to predict their likely paths in order to make decisions about measures required to mitigate their effects.

Design of protection measures requires data for two basic parameters of Rockfalls—impact energy and trajectory. That is, information is required on the mass and velocity of falls to determine the required energy capacity, and on trajectory paths and impact locations to determine the optimum location and dimensions of the barrier or fence. Development of these design parameters requires the collection of relevant site data, followed by analysis of energies and trajectories and then selection and design of the appropriate protection measure.

3 Siddhababa Model Site

The Siddhababa area that covers 2.1 km of the Siddhartha Highway is famous for most problematic site for rockfall and slope instabilities in Nepal (Fig. 1). This road constructed in 1971 with the financial aid of the Indian Government connects the Indian boarder town Sunauli with Pokhara, famous tourist city of Nepal. This 180 km long highway passes through relentless bends and curves making it one of the adventurous roads of Nepal. Siddhartha Highway is also one of the busiest highways of Nepal with daily traffic volume in Siddhababa area exceeding 3000 vehicles per day. Such high traffic volume increases the vulnerability of the area because the probability of a vehicle getting hit by a falling rock increases with the increase in traffic volume. It is estimated that approximately 75 rockfall events happen in this area every year. Rockfall frequency is highest at the end of monsoon as well as in the winter and spring. During the past three years an average of 10 people per year are killed and about 20 people are injured from rockfall in this area. Apart from the loss of life and property, every year the highway is blocked for long periods of time due to the fallen rocks and

Fig. 4 Model site in Siddhababa. Skilled labors and engineers are installing barriers on left photo and on right photo rock nets installed on hanging sandstone bed



debris, which contributes to further socioeconomic losses in the region. In total, 13 problematic sites for rockfall were identified in the Siddhababa area. Problematic sites were coded as B1 to B13. Out of 13 sites, some part of B8 site was selected for model site installation. In the model site, a rockfall barrier system of 27 m length having maximum

energy level of 1000 kJ is installed along with 120 m² of wire mesh net (Fig. 4). The purpose of model site is to illustrate the function of new technology of rockfall protection system for Nepal. The model site is now performing well and few rock boulders of size up to 1 m³ have been stopped by this barrier.

Fig. 5 Rockfall simulation on trajectory A, Gully 1 without the barriers and with barriers. This helped to understand importance of rockfall barriers in the slope

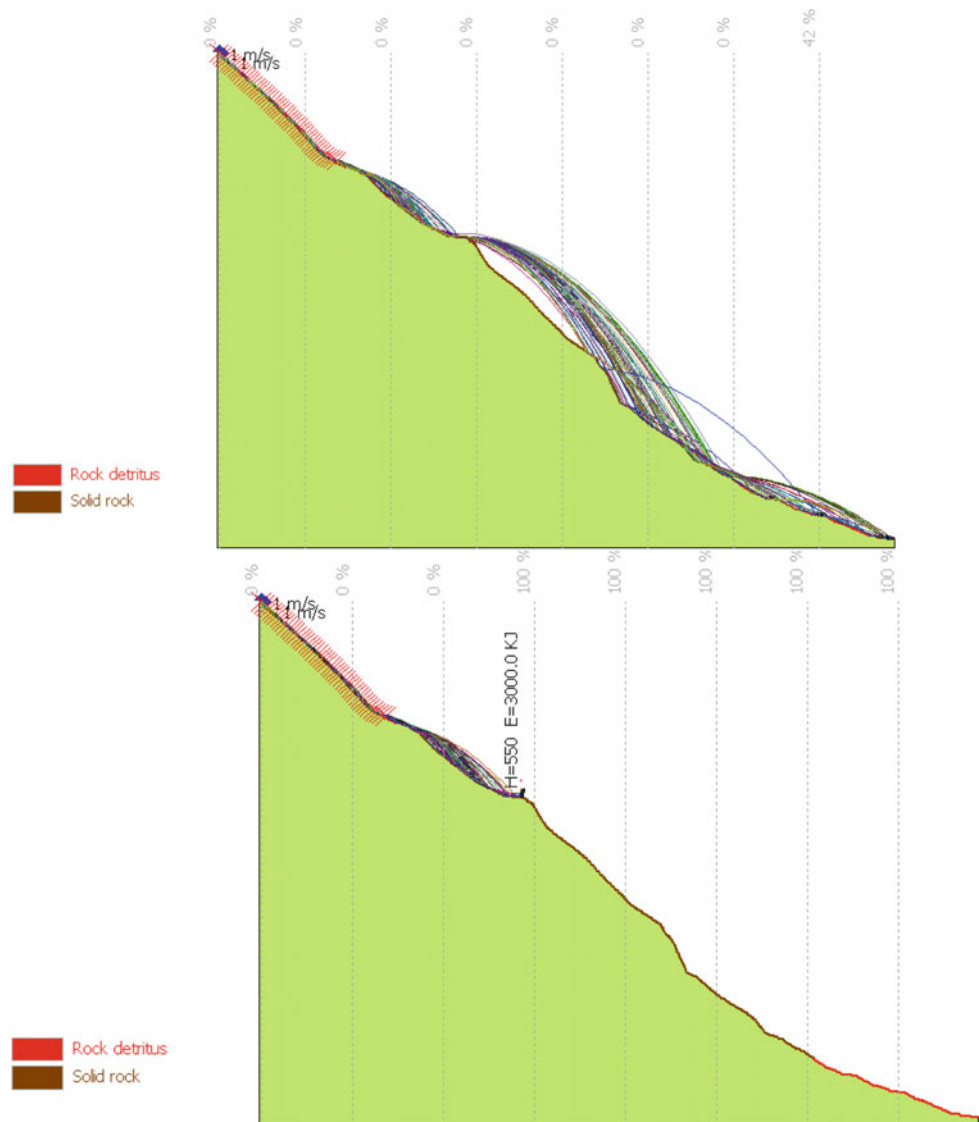


Fig. 6 Already installed rockfall protection barrier on uphill slope of Upper Bhotekoshi Hydropower Project



4 The Upper Bhotekoshi Hydropower Project

The Upper Bhotekoshi Hydropower Project is a run-of-the-river hydropower plant in Sindhupalchowk district, Nepal and it is situated at approximately 105 km northeast of Kathmandu. The Powerhouse site lies at latitude $27^{\circ}54'45''$ N and longitude $85^{\circ}55'28''$ E. It was constructed between 1997 and 2000 and power generation started in January 2001. During 2015 Gorkha Earthquake, considerable damage had been observed in the project site. The penstock pipes were hit by the Rockfall and were irreparably damaged. The rocks are highly fractured quartzite and phyllite of the Lesser Himalayan Zone. To design an effective mitigation barrier at this site, rockfall simulations have been performed (Fig. 5) to understand trajectories and impact locations of rockfalls in the project area. There are drastic changes in rockfall scenarios after installation of rockfall barriers. Simulations suggested to a 3000 kJ system are necessary for optimum protection (Fig. 6).

In total, four rows of flexible barriers approximately 310 m total in length were installed in the area. The rock nets are performing well and already lots of boulders stopped. Rockfall is continuous on the site and more frequent in the gullies. Many rockfalls were seen on the rainy days along with the debris flow through the gullies.

5 Concluding Remarks

This paper describes and discusses new technologies for Rockfall mitigation in the Nepalese slopes. It highlights their importance and installation works. Talking about new technologies is quite easy but implementation is very challenging due to limited resources and limited availability of specialized equipment in Nepal for difficult to access slopes. Installation of rock nets and barriers in the Nepalese slopes suggests that they drastically improve roadside safety and protect hydropower projects in the Nepal Himalaya.

References

- Abebe, B., Dramis, F., Fubelli, G., Umer, M., Asrat, A.: Landslides in the Ethiopian highlands and the rift margins. *J. Afr. Earth Sci.* **56**(4–5), 131–138 (2010)
- Bull, W.B., King, J., Kong, F., Moutoux, F., Phillips, W.M.: Lichen dating of coseismic landslide hazards in alpine mountains. *Geomorphology* **10**, 253–264 (1994)
- Dahal, R.K.: Engineering geological issues after Gorkha earthquake 2015 in Nepal—a preliminary understanding, paper presented in 10th Asian regional conference of IAEG. Kyoto, Japan (2015)
- Dahal, R.K.: Initiatives for rockfall hazard mitigation in Nepal. *Bull. Nepal Geol. Soc.* **33**, 51–56 (2016)
- Dahal, R.K., Bhandary, N.P., Hasegawa, S., Yatabe, R.: Topo-stress based probabilistic model for shallow landslide susceptibility

- zonation in the Nepal Himalaya. *Environ. Earth Sci.* **71**(9), 3879–3892 (2014)
- Dorren, L.K.A.: A review of rockfall mechanics and modelling approaches. *Prog. Phys. Geogr.* **27**(1), 69–87 (2003)
- Einstein, H.H.: Landslide risk assessment procedure. In: 5th International Symposium on Landslides, Balkema, Rotterdam, Lausanne, Switzerland, vol. 2, pp. 1075–1090 (1988)
- Matsuoka, N., Sakai, H.: Rockfall activity from an alpine cliff during thawing periods. *Geomorphology* **28**, 309–328 (1999)
- McCarroll, D., Shakesby, R., Matthews, J.A.: Spatial and temporal pattern of Late Holocene rockfall activity on a Norwegian talus slope: a lichenometric and simulation-modelling approach. *Arct. Alp. Res.* **30**, 51–60 (1998)
- Peila, D., Ronco, C.: Technical note: design of rockfall net fences and the new ETAG 027 European guideline. *Nat. Hazards Earth Syst. Sci.* **9**, 1291–1298 (2009)
- Vidrih, R., Ribicic, M., Suhadolc, P.: Seismogeological effects on rocks during 12 April 1998 upper Soca Territory earthquake (NW Slovenia). *Tectonophysics* **330**, 153–175 (2001)
- Volkwein, A., Schellenberg, K., Labiouse, V., Agliardi, F., Berger, F., Bourrier, F., Dorren, L.K.A., Gerber, W., Jaboyedof, M.: Rockfall characterisation and structural protection—a review. *Nat. Hazards Earth Syst. Sci.* **11**, 2617–2651 (2011)

Internal Erosion in Volcanic Soils—Challenges for Infrastructure Projects in New Zealand

Pedro Martins

Abstract

Internal erosion is a well-documented process in the geotechnical literature. Whilst the process is typically associated with water-retaining structures, it can also occur in natural terrain. Internal erosion and sinkholes have historically posed significant challenges for infrastructure projects in New Zealand. This paper discusses some historical and recent examples of these challenges. Volcanic soils, in particular those associated with pyroclastic environments, such as the central segment of the Taupo Volcanic Zone in the North Island of New Zealand, are particularly prone to internal erosion. The potential risks arising from internal erosion should not be underestimated for projects in volcanic areas, in particular for projects involving water retaining structures and/or stormwater disposal by soakage. A robust design, supported by a detailed geotechnical investigation specifically targeted at identifying internal erosion potential is recommended to better manage these risks.

Keywords

Internal erosion • Sinkhole • Volcanic soils
Infrastructure projects • New Zealand

1 Introduction

Internal erosion is a well-documented process in the geotechnical literature. Whilst the process is typically associated with water-retaining structures, it can also occur in natural terrain. Internal erosion and sinkholes have historically posed significant challenges for infrastructure projects in New Zealand. This paper discusses some historical and recent examples of these challenges.

A large portion of the central North Island of New Zealand is underlain by volcanic soils and rocks derived from the Taupo Volcanic Zone (TVZ). Whilst in the northern and southern segments of the TVZ volcanism occurs mainly as cone-building eruptions of andesite, in the central segment volcanism is dominated by explosive eruptions of rhyolite, with calderas and rift basins infilled with more than 15,000 km³ of air-fall deposits, ignimbrites, and lavas (Wilson et al. 1995; Rowland and Simmons 2012).

2 Theoretical Background—Internal Erosion and Sinkholes

Internal erosion occurs when soil particles from within a volume of soil are carried downstream by seepage flow (Fell et al. 2008). The initiation of internal erosion can occur by four main mechanisms (ICOLD 2013):

- **Concentrated leaks:** where there are pre-existing openings (such as cracks, rootholes or interconnecting voids) through which concentrated flow occurs, the sides of the opening may be eroded by the flowing water. Dispersion, where the clay particles deflocculate and are transported in colloidal state, is also included in the concentrated leaks category under the ICOLD (2013) classification.
- **Backward erosion:** occurs where critically high hydraulic gradients at the toe of a dam erode particles upwards and backwards, often forming small erosion channels or pipes.
- **Contact erosion:** occurs where a coarse soil such as gravel is in contact with a fine soil, and flow parallel to the contact in the coarse soil erodes the fine soil.
- **Suffusion:** occurs when fine particles of soil are transported by seepage flow through the pores of coarser particles.

Where the soils surrounding the zone of internal erosion are competent enough cavities can be formed. As the process

P. Martins (✉)
Beca Ltd., PO Box 903 Tauranga, 3140, New Zealand
e-mail: pedro.martins@beca.com

develops the cavities can reach the ground surface, forming a continuous pipe. At this point, the flow rate, and hence the erosion potential, increases significantly. As the pipe enlarges, the soil cover gets progressively thinner, up to a point where the roof of the pipe collapses, forming a sinkhole.

3 Case Histories of Internal Erosion in the North Island of New Zealand

3.1 Ruahihi Canal Failure (1981)

The Ruahihi canal, in the Bay of Plenty, failed one day after the power scheme being officially opened. *‘Water in the 3350 m long headrace canal, in a matter of about an hour, had scoured a chasm, 500 m long, 100 m wide and 40 m deep’* (Oborn 1988, p. 574). The canal was constructed through volcanic terrain consisting of air-fall and pyroclastic flow deposits and failed due to internal erosion followed by collapse. The failure process started with water seeping through the clay lining, which led to internal erosion and evolved to full collapse of the slopes of the canal (Oborn 1988).

Remedial measures involved extensive earthworks to reshape the canal and significant changes to the lining system. These changes included the construction of an underground drain along the canal invert, the installation of a drainage layer beneath the lining and placement of an impermeable membrane of high density polyethylene (HDPE) (Oborn 1988).

3.2 Wheao Power Scheme Canal Failure (1982)

The headrace canal of the Wheao power scheme, in the Bay of Plenty, failed shortly after being filled for the first time, *‘driving thousands of tonnes of large boulders to engulf the powerhouse’* (Jones 1988, p. 561). The canal was built through volcanic ashes and ignimbrites and failed by internal erosion due to leakage along the interface between the clay lining of the canal and the concrete penstock intake structure (Jones 1988).

Remedial measures included the construction of a new penstock intake structure 125 m upstream of the original location so that it could be founded on more competent and less erodible ignimbrite. Also, a 75 m long transition zone between the clay-lined canal and the new intake structure was built using a flexible concrete lining (Jones 1988).

3.3 Poihipi Reservoir Failure (1996)

The Poihipi reservoir formed a water storage for firefighting purposes at the Poihipi geothermal scheme near Taupo, in the Waikato. Soon after the initial filling, the HDPE lined reservoir breached due to piping through the foundation (Tate

2003). The foundation of the reservoir consisted of tephros of the TVZ, including pumice silts, sands and gravels. The piping process is thought to have started due to leakage through the liner in an area where pipes penetrated the liner for inlets and outlets, and followed an active fault that was present beneath the footprint of the reservoir (Tate 2003).

The main remedial measure implemented was the construction of a new reservoir some 100 m away from the failed one. Key features of this new reservoir included careful design and detailed construction quality control of the pipe penetrations through the lining, and placement of a 1 m thick filter layer beneath the lining (Tate 2003).

4 Recent Cases of Internal Erosion and Their Remedial Solutions

4.1 State Highway 5 Tumunui Sinkhole (2016)

State Highway 5 (SH5) is a regional strategic highway in the central North Island. On 23 June 2016, following 110 mm of rain in 24 h, a section of SH5 at Tumunui, about 18 km south of Rotorua, suffered significant damage due to internal erosion.

4.1.1 Site Investigation, Ground Model and Internal Erosion Process

A site walkover was carried out and it was observed that a 12 m long section of the road, bound by cracks extending across the whole width of the pavement, had dropped about 30 mm (Fig. 1). Aligned with this section, sinkholes had developed in paddocks on both sides of the road. To the west, a 10 m wide sinkhole had extended for more than 100 m, terminating as a natural tunnel into a hill (Fig. 2).

A desk study was completed, followed by a short geotechnical investigation. A cross-section illustrating the ground model for the site is shown in Fig. 3. It was identified that the area is an enclosed depression corresponding to a volcanic vent. From this depression the only possible exit for all water in the catchment is via groundwater flow.

It was concluded that a layer of loose pumiceous sands between 4 and 7 m depth was the main zone where internal erosion was developing. The width of the internal erosion zone was interpreted to be around 12 m, as marked by the cracks on the pavement. Lastly, it was concluded that the internal erosion was well developed under the road and the shallow soils were unable to bridge the voids, therefore creating a risk of road collapse.

4.1.2 Remedial Solution: Concept and Construction

A number of remedial solutions were discussed with the New Zealand Transport Agency. The preferred option was a

Fig. 1 Observed damage to the road. **a** North crack; **b** Detail of the north crack; **c** South cracks, as indicated by the arrows. After Martins and Toan (2017)

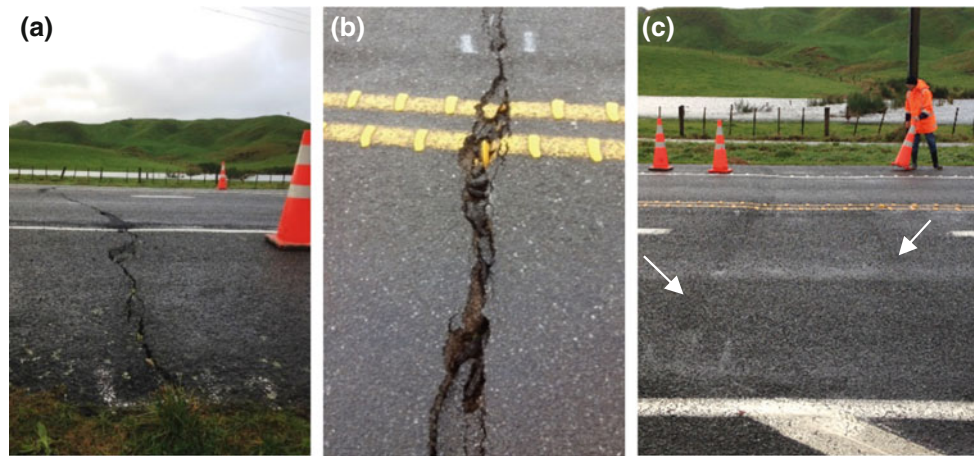


Fig. 2 Sinkholes developed in the adjacent properties. **a** Looking east from the hill towards the road. **b** Looking west from the road towards the hill. After Martins and Toan (2017)

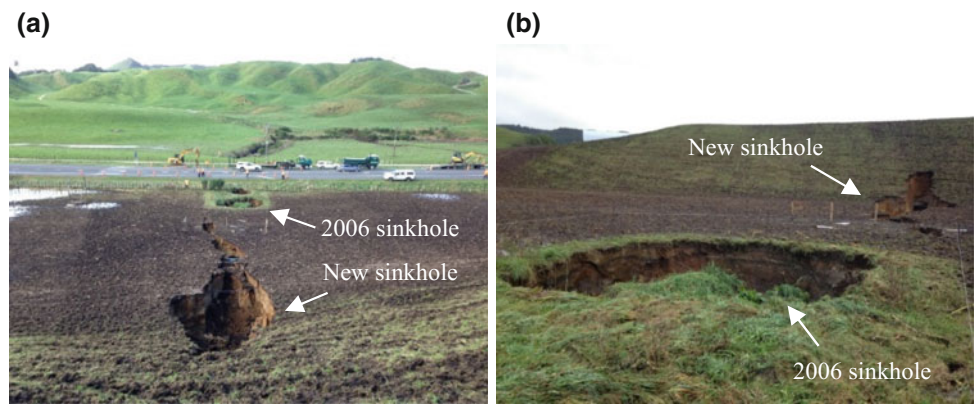
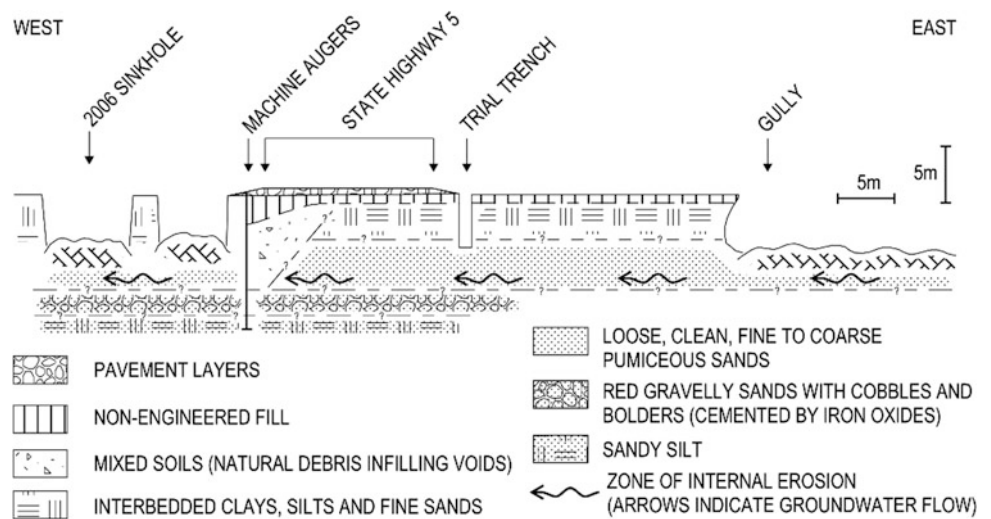


Fig. 3 East-west cross-section illustrating the ground model for the site. After Martins and Toan (2017)



geogrid-reinforced soil raft, capable of spanning the voids whilst providing enough robustness to avoid sudden collapse, should the cavities enlarge as the erosion progresses. The final design of the geogrid-reinforced soil raft was carried out based on BS 8006-1:2010 (British Standards Institution 2010).

During construction, the anticipated ground model was generally confirmed and no significant cavities were

encountered within the excavation to 4 m depth. Some small cavities up to 200 mm long and 20 mm wide were observed along a set of widely spaced subvertical fractures. These subvertical fractures were only observed within the 12 m wide zone delimited by the north and south cracks in the pavement. The north and south cracks themselves were found to be surface traces of the subvertical fractures, and could be traced along the full height of the walls of the



Fig. 4 Sinkhole observed in the playfield of the school. GPR survey underway

excavation. No displacements were observed across any fractures at the site.

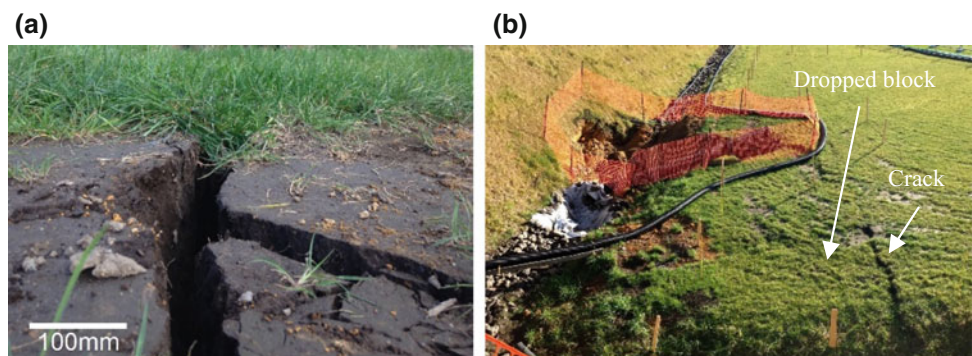
4.2 School Site Playfield Sinkhole (2015)

In 2014 a new school was being constructed at a site in the North Island of New Zealand. The geology of the site consisted mainly of unwelded and variably weathered ignimbrites, overlain by weathered volcanic ashes. Construction of the main buildings and playfields had been completed by early 2015 and nothing unusual occurred at the site in the following dry summer months. However, when the first heavy autumn rains started to fall in the region in May, a sinkhole appeared in one of the playfields.

4.2.1 Site Investigation and Ground Model

A site walkover was carried out and a sinkhole of about 7 m diameter and possibly 3–4 m depth was observed (Fig. 4). Around the sinkhole, across an area of approximately 150 m², cracks up to 90 mm wide had appeared in the playfield (Fig. 5a). Within the cracked area, a block of about 7 × 8 m had dropped approximately 80 mm (Fig. 5b).

Fig. 5 Cracks observed in the area around the sinkhole. **a** 90 mm wide crack; **b** The block to the left of the crack dropped about 80 mm



Following the site walkover, a GPR survey was undertaken in an attempt to identify cavities in the area (Fig. 4). Whilst some potential anomalies were initially identified, subsequent hand augers aimed at ground-truthing the GPR did not find any cavities or soft spots.

It was then decided to proceed with a large test pit to investigate the extent of the collapsed debris and try to identify the base of the internal erosion system. Sub-horizontal cavities up to 100 mm diameter, both open and infilled with material from the upper soils that washed down, were observed to a maximum depth of 5 m. The cavities developed mainly along more sandy pumice layers within the predominantly silty clayey weathered ignimbrite.

4.2.2 Remedial Solution: Concept and Construction

Based on the findings of the test pit excavation, it was decided that the most practical remedial solution was to widen the base of the excavation and install a granular filter with a controlled outlet. The concept was to retain the soil particles, provide a controlled flow path for water that enters the internal erosion area, help drop the groundwater pressures that may build up and reduce the amount of water flowing towards the natural outlets.

Larger cavities were found during the widening of the excavation (Fig. 6), but no change in design was required as the cavities were restricted to shallow depths. A filter layer 800 mm thick was installed at the base of the excavation (Fig. 7), with a coil of drainage (slotted) plastic pipe placed within. A polyethylene pipe was directionally drilled from downstream and connected to the drainage pipe to provide an outlet for the water collected by the system. The excavation was then backfilled with the excavated soils.

5 Conclusions

Volcanic soils, in particular those associated with pyroclastic environments, such as the central segment of the Taupo Volcanic Zone, are especially prone to internal erosion. This can cause significant challenges for infrastructure projects,

Fig. 6 Approximately 1 m diameter cavity observed during construction



Fig. 7 800 mm thick granular filter layer installed at the base of the excavation



as learnt from a number of case histories of failure. The potential risks arising from internal erosion should not be underestimated for projects in volcanic areas, in particular for projects involving water retaining structures and/or stormwater disposal by soakage. A robust design, supported by detailed geotechnical investigation specifically targeted at identifying internal erosion potential is recommended to better understand and manage the risks.

Acknowledgements The author gratefully acknowledges the following institutions: New Zealand Transport Agency and Higgins Group Holdings Ltd for giving permission to publish the results for SH5 Tumunui tomo. The leadership group of the school site for giving permission to publish the results of the work conducted at their site. Beca Ltd. for the institutional support to prepare this paper.

References

- British Standards Institution: BS 8006-1:2010. Code of Practice for Strengthened/Reinforced Soils and Other Fills. British Standards Institution, London (2010)
- Fell, R., Foster, M.A., Cyganiewicz, J., Sills, G., Vroman, N., Davidson, R.: Risk Analysis for Dam Safety: A Unified Method for Estimating Probabilities of Failure of Embankment Dams by Internal erosion and Piping. UNICIV Report No. R 446, Version: Delta, (2) (2008)
- ICOLD: Internal erosion of existing dams, levees and dykes, and their foundations. In: Bridle, R. Fell, R. (eds.) Bulletin 164. Vol. 1: Internal Erosion Processes and Engineering Assessment, 2013. International Commission on Large Dams, Paris (2013)
- Jones, O.T.: Canal Failure on Wheao Power Scheme. In: Proceedings of the 5th Australia-New Zealand Conference on Geomechanics: Prediction Versus Performance, Sydney, pp. 561–566 (1988)
- Martins, P., Toan, D.V.: State Highway 5 Tumunui tomo—a case of road resilience to piping in the Rotorua-Taupo area. In: Proceedings of the 20th New Zealand Geotechnical Society Symposium, Napier (2017)
- Oborn, L.E.: Canal Failure, Ruahiri Hydro Electric Power Scheme, Bay of Plenty, New Zealand. In: Proceedings of the 5th Australia-New Zealand Conference on Geomechanics: Prediction versus Performance, Sydney, pp. 574–584 (1988)
- Rowland, J.V., Simmons, S.F.: Hydrologic, magmatic, and tectonic controls on hydrothermal flow, Taupo Volcanic Zone, New Zealand: implications for the formation of epithermal vein deposits. *Econ. Geol.* **107**(3), 427–457 (2012)
- Tate, D.R.: Piping Failure of the Poihipi Reservoir. In: Proceedings of the 13th New Zealand Geotechnical Society Symposium, Tauranga, pp. 183–192 (2003)
- Wilson, C.J.N., Houghton, B.F., McWilliams, M.O., Lanphere, M.A., Weaver, S.D., Briggs, R.M.: Volcanic and structural evolution of Taupo Volcanic Zone. *N. Z. Rev. J. Volcanol. Geoth. Res.* **68**, 1–28 (1995)

Site-Specific Rockfall Risk Assessments and Rockfall Protection Structure Design Following the 2010/2011 Canterbury Earthquake Sequence

T. I. Mote, M. D. Skinner, M. L. Taylor, and C. Lyons

Abstract

The 2010/2011 Canterbury earthquake sequence triggered wide-spread rockfall, causing fatalities and damage to property and infrastructure. In response, an area-wide rockfall risk assessment was carried out to understand risk and support the recovery process. The risk assessment influenced zoning decisions, insurance pay-outs and property values and has had a significant impact on the disaster risk reduction process. Site-specific assessments were subsequently carried out on individual residential properties to confirm risk and inform rockfall risk reduction design. The characterization of site-specific rockfall source size, probability of detachment and topographic controls on run-out ultimately controlled rockfall protection structure design for residential properties in the Port Hills. Differences between the assessed level of risk to life between the area-wide and site-specific studies were in many cases two orders of magnitude different, lower and higher. This paper demonstrates the enhancement of the area-wide risk assessment with site specific mapping and source characterization to design rockfall protection structures that balance risk reduction, cost, environmental impact, and visual impact. Understanding the advantages and limitations between area-wide and site-specific rockfall assessments is integral to the disaster response, recovery and rebuild process.

Keywords

Rockfall risk • Port Hills • Rockfall protection structure • Canterbury earthquake sequence

1 Introduction

The 2010/2011 Canterbury earthquake sequence triggered wide-spread rockfall, causing fatalities and damage to property and infrastructure. More than 6000 occurrences of rockfall were recorded in the Port Hills suburbs of Christchurch, New Zealand. Five people lost their lives, approximately 65 homes were impacted and many more evacuated as a result of falling rocks (Massey et al. 2011a; 2014). Due to the geology and geomorphology of the area almost every cliff band outcropping in the Port Hills generated rockfalls.

To understand the immediate risk to residents in the Port Hills from rockfall following the earthquakes, a number of hazard mapping and area-wide risk assessments were commissioned. The findings of these assessments provided initial risk zonation across the Port Hills that influenced planning decisions, insurance pay-outs, property valuations and the recovery process.

Subsequent site-specific geotechnics assessments were carried out on individual residential properties to inform rockfall risk reduction design. Design of Rockfall Protection Structure (RPS) followed Christchurch City Council (CCC) Guidelines (CCC 2013).

This paper demonstrates the enhancement of the area-wide risk assessment with site specific mapping and source characterization to design rockfall protection structures that balance risk reduction, cost, environmental impact, and visual impact. Three constructed RPS are presented where risk has been reduced to acceptable levels.

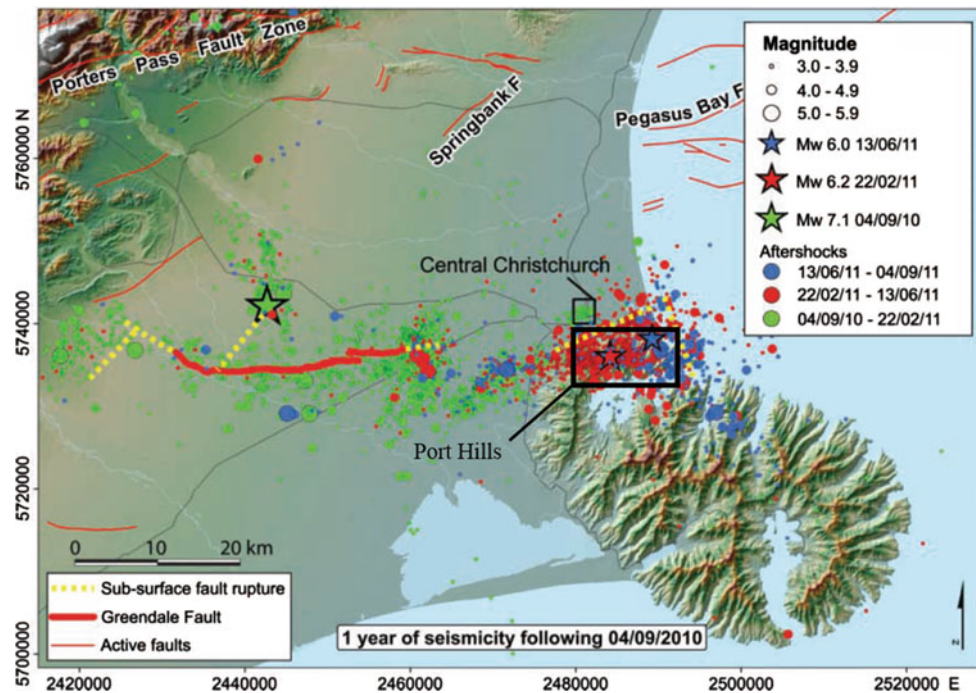
2 Geologic Setting

The Port Hills represents the northern part of the Lyttleton Volcanic Complex. The Lyttleton Volcanic complex is of Miocene age (5–23 Ma) and is comprised of basaltic to trachytic lava flows interbedded with breccia and tuff. The

T. I. Mote (✉) · C. Lyons
Arup, Sydney, Australia
e-mail: tim.mote@arup.com

M. D. Skinner · M. L. Taylor
Arup, Auckland, New Zealand

Fig. 1 The earthquakes of the Canterbury Earthquake sequence (after Cubrinovski 2010)



interbedded lava flows occur in sub-horizontal layers that commonly outcrop in a stepped profile. The volcanic rocks are overlain by younger, Quaternary Aged deposits of loess, a windblown silt deposit commonly greater than 3 m in thickness (Forsyth et al. 2008). It is the volcanic trachyte and basalt cliff lines that present the significant rockfall hazard source.

The Christchurch suburbs of Avoca Valley, Bowenvale, and Heathcote Valley are all located in valleys of the Port Hills, and residential areas extend up the sides of these and other valleys. Rock outcrops are commonly encountered up-slope from residences and infrastructure in these areas.

The Canterbury earthquake sequence was a series of shallow earthquakes that occurred within the vicinity of Christchurch between late 2010 and late 2011 (Fig. 1). The largest event in this sequence was a M7.1 earthquake on September 4, 2010 in Darfield, 30 km away from the Port Hills. A February 22, 2011 M6.2 aftershock earthquake occurred on an unknown fault directly below the Port Hills and resulted in widespread devastation and 181 fatalities (Kaiser et al. 2012). Ground shaking associated with this earthquake was severe, with recorded ground accelerations of up to 2.2 g vertical, and 1.7 g horizontal in the Port Hills. Damage as a result of this earthquake was related to liquefaction, lateral spreading, building collapse and widespread rockfall. The rockfall consisted of a large number of rocks dislodged, falling or rolling down-slope causing fatalities and damage to property and infrastructure. The June 13, 2011 M6.0 aftershock caused more rockfall, although many of the Port Hill properties were vacant at this time awaiting

risk assessment before re-occupancy from the February event. Prior to the 2010/11 earthquake sequence, the risk from rockfall in the Port Hills was not fully appreciated.

3 Area-Wide Hazard Characterization and Risk Assessments

Following the Canterbury Earthquake Sequence a number of area-wide assessments were commissioned to map rockfall, characterize hazard and understand the risk to residents in the Port Hills. The findings of these assessments provided initial risk zonation across the Port Hills that influenced planning decisions, insurance pay-outs, property valuations and the overall disaster risk response. The purpose of the assessments was to make the planning processes simpler and more effective for managing risk.

The Port Hills Geotechnical Group (PHGG) was established as part of the response to the 2010/11 Christchurch earthquakes. One of the many tasks undertaken by the PHGG was mapping the location and size of fallen boulders in the Port Hills. This information was and continues to be extremely valuable, and forms a vital part of regional and site-specific risk assessments.

A major study was completed by New Zealand Geological and Nuclear Sciences (GNS), on behalf of Christchurch City Council (CCC), and presented in a series of reports (Massey et al. 2012a, b, c; Taig et al. 2012; Townsend and Rosser 2012). The GNS study was a quantitative risk estimation method that followed appropriate parts of the

Australian Geotechnical Society framework for landslide risk management (AGS 2007). It set out the principles of assessment of rockfall risk, defined key reference parameters for use in rockfall analyses, presented risk reference maps, and recommended a tolerable risk level for the Port Hills. The highly regarded study was a rigorous peer reviewed risk assessment and provided a basis for all subsequent risk assessments.

The risk assessment methodology considers both rockfalls triggered by earthquakes (taking into account expected changes in seismic activity in the Port Hills region over time), and by other rockfall-triggering events such as rainfall. The recommended tolerable risk level was on the order of 10^{-4} , comparable to the annual individual risk of being killed in a car accident in New Zealand (Taig et al. 2012).

A complementary study was completed by Geovert on behalf of the Canterbury Earthquake Recovery Authority (CERA) (Avery et al. 2012) using 3D rockfall analyses to indicate areas in the Port Hills likely to be influenced by rockfall run-out. The study did not directly present risk levels, but did provide output showing rockfall run-out paths and boulder bounce heights, kinetic energies and velocities. The work was calibrated using boulder roll tests, and by ground-verification site visits.

4 Site-Specific Geotechnical Assessment

CCC (2013) guidelines state that a site-specific geotechnical assessment is required to form the basis of rockfall protection structure design. The site specific geotechnical assessment provides critical input to the risk calculation through characterization of site-specific rockfall source size, probability of detachment and topographic controls on run-out. These inputs ultimately control RPS design in terms of type, size, location, and magnitude of risk reduction.

4.1 Rockfall Source Characterization

In the area-wide assessments potential rockfall sources were considered to be continuous cliff bands across entire valley flanks of any slope steeper than 45° (Avery et al. 2012). While these were readily derived from digital terrain models through automated GIS processing, site-specific mapping shows that these assumptions could not be validated through ground truthing in many areas. For example, the area-wide automated source identification regularly highlighted retaining walls and man-made slopes as source zones.

The site-specific mapping, in many areas, also showed that the upper slopes consisted of a series of discrete sources with soil slopes in-between, rather than a continuous cliff band of rockfall source as assumed in the area-wide assessments (Fig. 2). The identification of discrete sources impacted the risk calculation in two ways: the first was to limit the extent of the source area and provide a credible source for rockfall run-out analysis that allowed consideration of topographic controls, the second was to consider the volume of rockfall source to match the rockfall rate as defined by the area-wide assessments.

4.2 Probability of Detachment

The area-wide assessments estimated a probability of detachment (e.g. likelihood of a rockfall trigger) based on the number of rockfall mapped in the valley by the PHGG. The probability of detachment was calculated by the number of observed boulders/valley length considering the input earthquake ground motions and applied across the valley as a constant.

In contrast, the site-specific geological mapping was able to discern lithology and structural control, evidence of recent voids from rockfall and match lithology of observed rockfall



Fig. 2 Discrete rockfall source outcrops mapped in area identified as continuous cliff bands by the area-wide assessment

below the source areas to compare site-specific rates of rockfall versus area-wide rates.

For example, in Avoca Valley a number of distinct lithologies were found outcropping in the cliff bands. These included blocky trachyte and basalt with flow, brecciated and tabular forms. The blocky trachytic sources were characterized with sub-horizontal and sub-vertical discontinuities at approximately 1 m spacing, creating discrete blocks within the cliff bands. The trachyte outcrops also showed signs of recent block detachment and fresher, less weathered surfaces (Fig. 3, left). In contrast, the basalt flows/breccias showed less evidence of recent rockfall and had a thick cover of lichen implying a reduced probability of detachment (Fig. 3, right). Mapping the rockfall run-out identified that the blocky trachyte sources were the most prevalent sources of rockfall to reach the toe of the slope. If the basalt with flow, brecciated and tabular forms was identified as recent rockfall, it was generally broken into smaller rock (<0.3 m maximum dimension).

4.3 Topographic Controls on Run-Out

The presence of gully or ridge features within a rockfall run-out path can force or direct boulders towards, or away from a property. On many of the slopes in the Port Hills, prominent natural drainage gullies can be shown to clearly control rockfall run-out as observed by concentrations boulder run-out paths. This topographic forcing affects the probability of transport that a rockfall will reach a property and therefore risk.

A local topographical assessment was not completed as part of the GNS study and not considered in the area-wide risk assessment. The influence of topography was modelled by Geovert through the use of 3D rockfall modelling (Avery et al. 2012). This work gives an indication of the likely path of boulders, but did not quantify effect or calculate risk. Figure 4 presents the Geovert model overlain by observed rockfall to demonstrate the topographic controls on a number of properties in Avoca Valley. The blue lines highlight a topographic control forcing rockfall away from the property in red.

Site-specific assessments developed topographic forcing factors for consideration in the risk calculation where mapping showed dispersing or concentrating rockfall relative to a dwelling.

5 Rockfall Protection Structure Design

Following the earthquake, the Canterbury Earthquake Recovery Authority (CERA) zoned residential properties as unacceptable (red-zone) if the long-term annual individual fatality rate at the dwelling was judged to exceed the threshold risk level of 10^{-4} . CCC placed un-inhabitable notices (Section 124—s124) on properties if it was concluded that persons at the dwellings would be at an immediate risk of loss of life by remaining in their properties.

Properties that were red-zoned were given a purchase offer from authorities, equivalent to the 2007 value of the property. Property owners could retain their properties, should the risk to loss of life be demonstrably reduced to



Fig. 3 Blocky trachyte (left) and basalt flow (right) rockfall sources

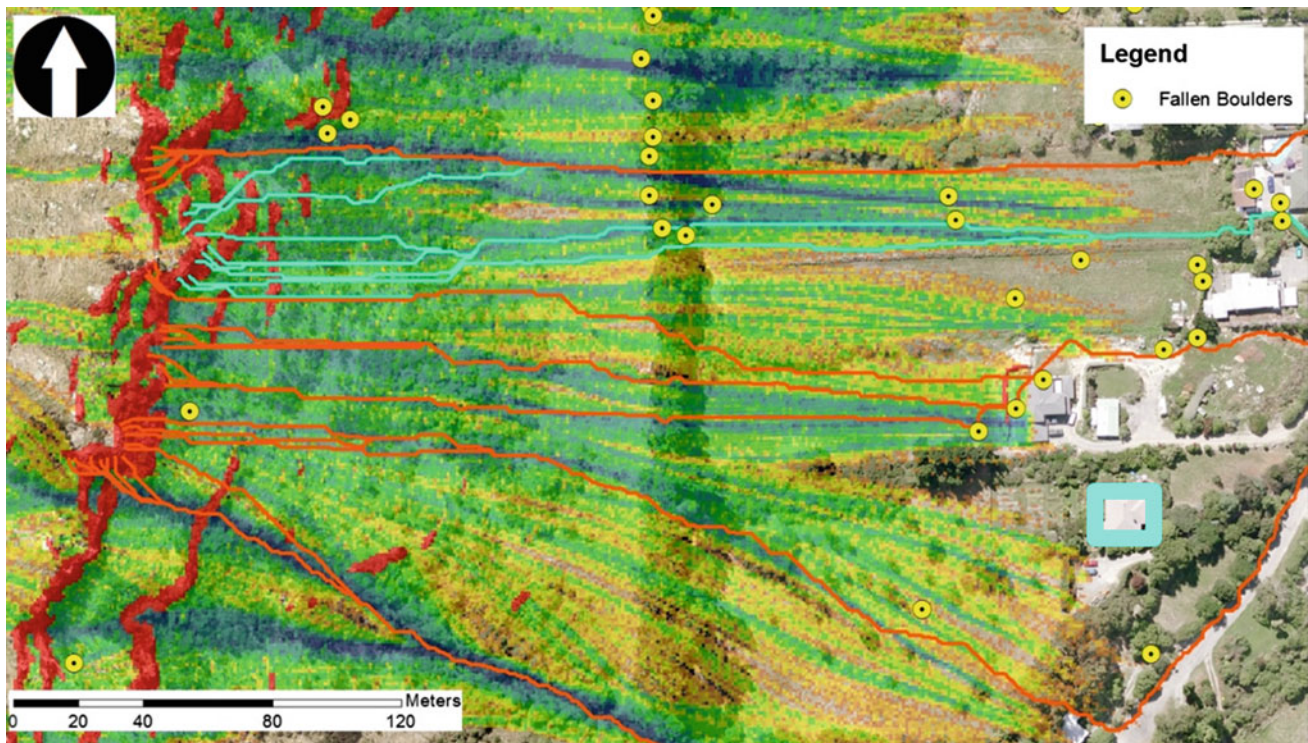


Fig. 4 Rockfall transit modelling highlighting topographic controls forcing potential rockfall away from a property in Avoca Valley (blue box). Red highlights rockfall source zones. Background denotes

modelled rockfall transits with darker colors representing increased modelled rockfall transits. Orange and light green lines denote modelled single rockfall transits

acceptable limits. Authorities offered residents funding to construct an RPS to reduce the risk, in lieu of repurchase. Reductions in risk could be achieved through design and construction of an RPS following CCC Guidelines, options for which included earthen berms, rockfall fences, rock bolting, meshing, terracing of slopes and/or scaling of the source zone.

When implementing rockfall mitigation the aim should be to reduce the risk to as low as reasonably practicable (ALARP), a limit which is most often determined in practice by a balance between risk reduction and cost. The appropriateness of each RPS type is dependent upon site geometry, available space, construction costs, environmental impact and each owner's needs. The site-specific geotechnical assessment formed the basis for the detailed design of the RPS.

Three examples of constructed RPS, driven by site-specific geotechnical assessment are presented below. The examples highlight the enhancement to the area-wide risk assessments that led to a low cost, low maintenance, low environmental and visual impact RPS balanced with risk reduction to appropriate levels.

5.1 Avoca Valley

Immediately following the February 22, 2011 earthquake, many residential properties in Avoca Valley were found to have rockfall risk at unacceptable levels and zoned to have an immediate risk of loss of life. The risk to the properties was driven by the presence of cliff bands rockfall source up-slope and observed rockfall run-out beyond the properties (Fig. 4).

A site-specific geotechnical assessment on an individual property, showed that although the area-wide rockfall rate was high for Avoca Valley, site-specific rates were lower due to the varying source lithologies and topographic controls on run-out. Rockfall modelling also showed the property was far enough down the slope that boulders were close to the end of their run-out paths. The site-specific risk was shown to be two orders of magnitude less than the area-wide risk assessment.

For this location, a terrace RPS was found to provide a reasonably practical reduction of risk (Fig. 5). The terrace included a small berm at its downslope end. Rockfall modelling during the design process demonstrated the



Fig. 5 Terrace and berm RPS on Avoca Valley Road. The image on the right is a Google Earth image of property and terrace upslope

effectiveness of the terrace (without the berm) in reducing the risk to well below the acceptable threshold. The small berm was added to provide practical additional protection.

The owner was informed that a larger berm would reduce the risk at the house to an even lower level, but in balancing the risk with their continued enjoyment of the property, they elected to accept a higher (but still below the acceptable) risk in return for a smaller berm. Other structures (e.g. a rockfall fence or a primary berm) would have been feasible, but the terrace increased the area of flat land, was visually less obtrusive than a berm, and will require less maintenance than the other options.

5.2 Bowenvale

A residential property in Bowenvale was initially assigned a CERA Green-zoning, but this was subsequently revised to Red-zone and deemed to have rockfall risk at unacceptable levels with an immediate risk of loss of life.

The site-specific mapping showed a discrete number of rockfall sources and some topographic control characterizing the hazard above the property (Fig. 6). It was considered technically and economically feasible to remove these discrete source zones. Access to these properties was not difficult and the volume of material was not excessive. An access track and remediation of the track were included in the design.

The rock sources were subsequently removed by milling (cutting) them back to an angle approaching the natural grade (Fig. 7). This treatment rendered the outcrops to be non-credible sources of rockfall, therefore reducing the risk to the properties.

5.3 Heathcote Valley

Following the 2010/2011 Canterbury earthquake sequence, a number of properties in Heathcote Valley were found to have rockfall risk at unacceptable levels and zoned to have an immediate risk of loss of life (Fig. 8).

A site-specific geotechnical assessment of a series of adjacent properties was carried out to characterize the geological conditions, to identify rockfall source zones presenting a hazard, and to undertake analyses to assess the risk of fatalities caused by rockfall across the properties. Mapping showed cliff bands up to 6 m high occur within the upper portion of the slope (Fig. 9), and further isolated rocky outcrops are situated above the cliff on the grassy slope extending towards the crest some 180 m in elevation.

Rockfall triggers to considered earthquakes and rainfall events. The 2016 annual probability of an earthquake occurring was used as the earthquake trigger. This probability considered the influence of aftershocks five years after the 2011 earthquake. The annual risk of rockfall fatality at the properties was calculated to be 10^{-3} and exceeded the tolerable limit. The site-specific risk calculation was consistent with the area-wide risk assessment.

Mitigation was undertaken to reduce the risk to acceptable levels through a reinforced earthen berm RPS immediately above the dwelling.

A design boulder with a 2 m maximum dimension and a volume of $\sim 4.2 \text{ m}^3$ was modeled. This boulder size was derived from field mapping and consistent with GNS during their modelling of rockfall in the Port Hills (Massey et al. 2011a). The results suggested that rockfall impact energies of 2000 kJ would be encountered with a bounce height of around 1.2 m at the berm location. Design of a reinforced

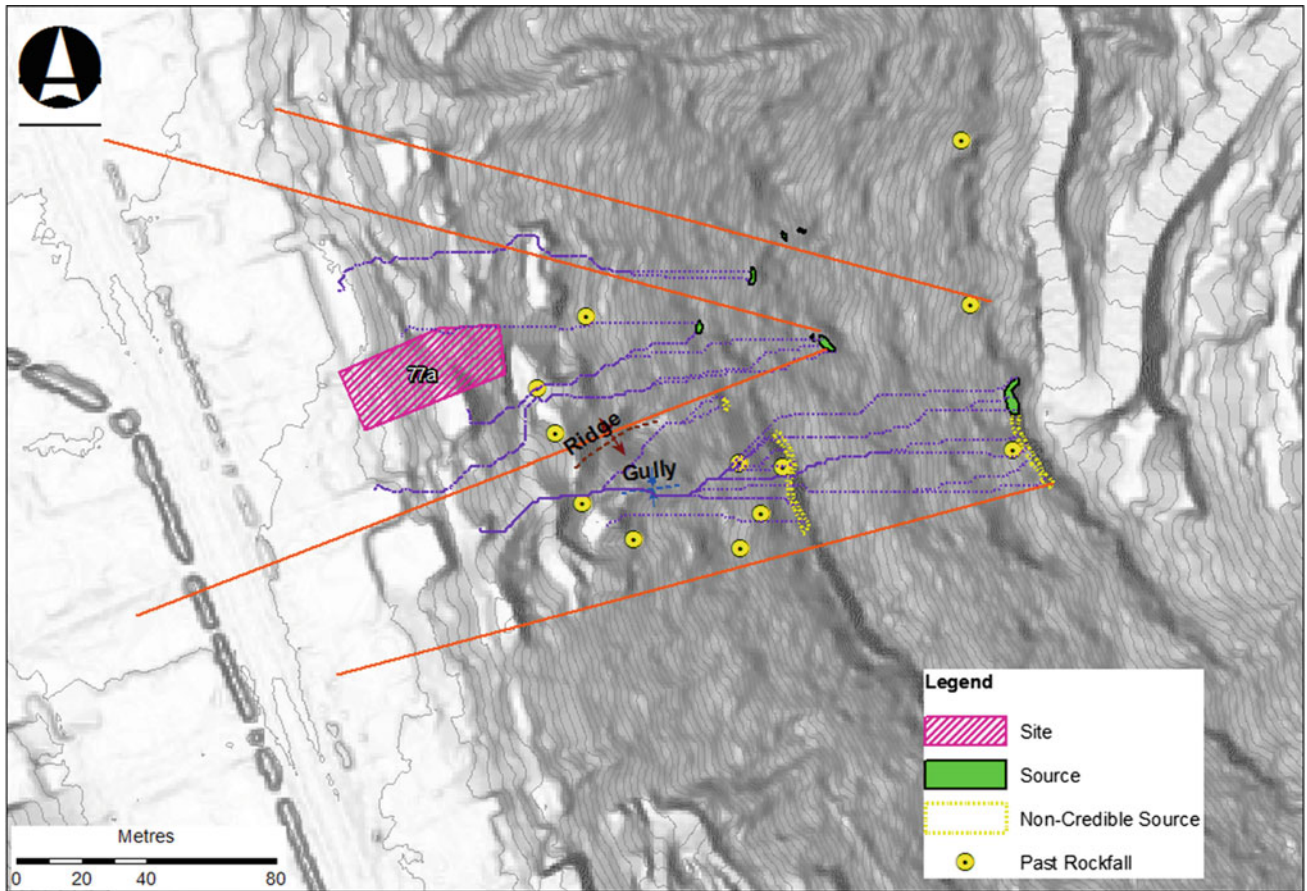


Fig. 6 Rockfall sources and topographic controls on run-out for a property in Bowenvale Valley. Red lines define the extent of rockfall catchment for each source. Purple lines are modelled single rockfall transits from the identified sources



Fig. 7 Discrete rockfall source before (left) and after (right) removal of source

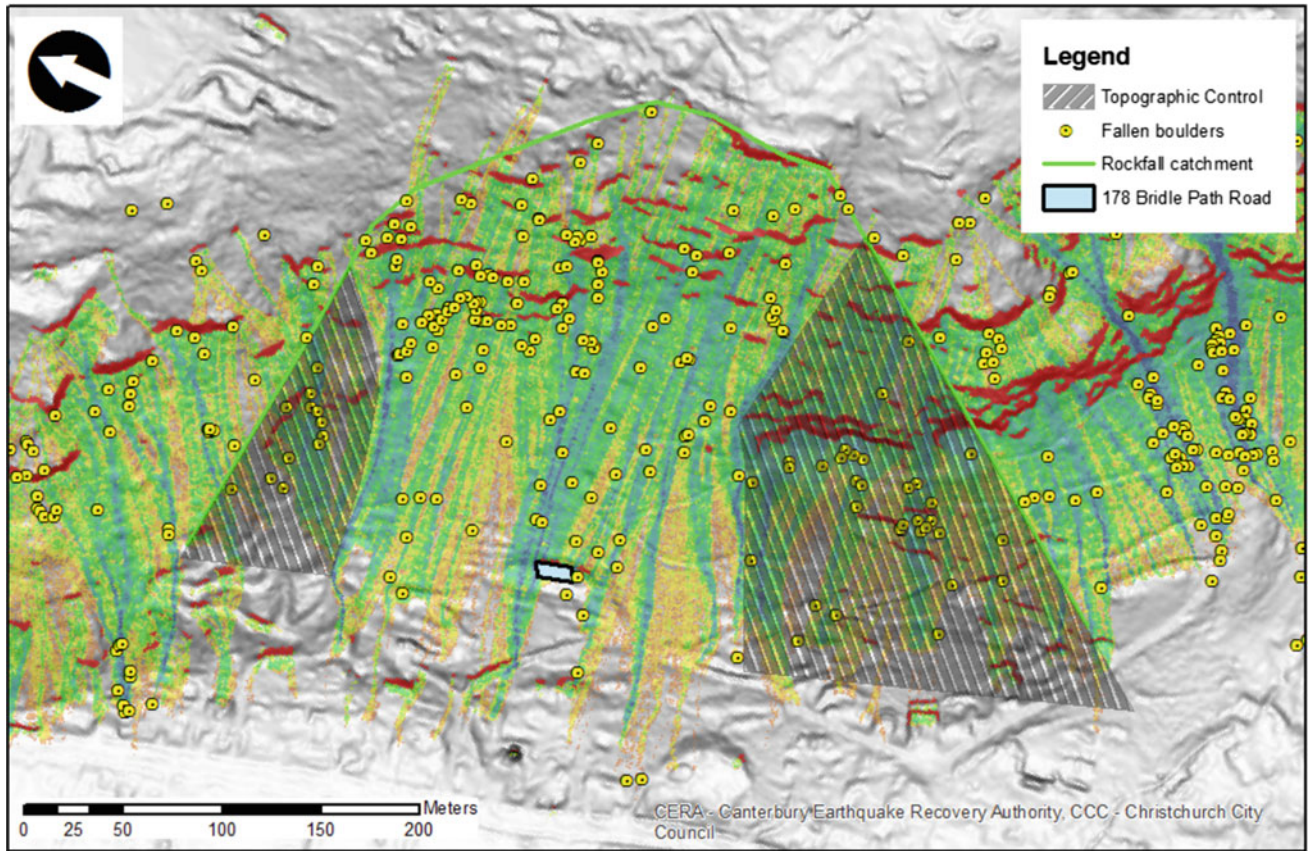


Fig. 8 Rockfall transit modelling, source mapping and observations of fallen boulders. Red areas are rockfall source zones as defined by LiDAR analysis. The hatched areas define where rockfall sources are considered to have a non-credible likelihood of impacting the property at risk



Fig. 9 Photograph of rockfall source cliff bands in Heathcote Valley

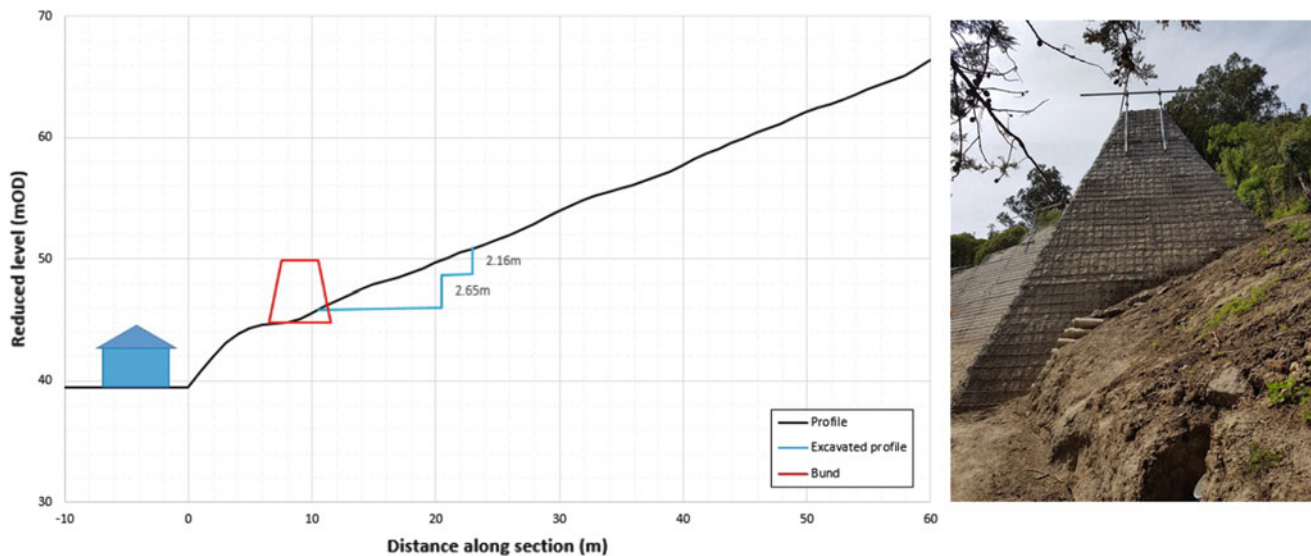


Fig. 10 Design cross-section and construction photograph of rockfall berm

earthen berm followed CCC guidelines and is under construction at the time of this paper (Fig. 10).

6 Conclusions

Area-wide risk assessments are appropriate to define risk and support planning and disaster risk reduction, but one must understand their limitations and uncertainties. Two of the major uncertainties in the area-wide risk assessments are the proportion of boulders that will travel substantial distances downslope; and the assumption that on a given suburban hillside the numbers of passing boulders, and thus the risk of being hit by one, is uniform along the slope and not concentrated at certain localities (Massey et al. 2012). Differences between the assessed level of risk to life between the area-wide and site-specific studies have been found to be up to two orders of magnitude, both lower and higher. Site-specific geotechnical assessments reduce these uncertainties through geologic mapping, characterization of source areas, and assessment of local topographic controls on rockfall run-out.

The characterization of site-specific rockfall source size, probability of detachment and topographic controls on run-out ultimately controlled rockfall protection structure design for residential properties in the Port Hills. The site-specific mapping enhances the area-wide risk assessment to design rockfall protection structures that balance risk reduction, cost, environmental impact, and visual impact. Understanding the advantages and limitations between

area-wide and site-specific rockfall assessments is integral to the disaster response, recovery and rebuild process.

Acknowledgements The authors would like to express thanks to: T. Ging and J. Fitzsimmons (Property Owners), M. and J. Altments (Property Owners), Mark Easton (Opus), I. Wright (CCC), Geotech LTD New Zealand, and James Cox (SMEC).

References

- AGS: Guidelines for Landslide Risk Management. Australian Geomechanics Society (2007)
- Avery, M., Salzman, H., Teen, A.: Port Hills 3D Rockfall Modelling. Christchurch, New Zealand, Geovert (2012)
- Christchurch City Council: Technical Guideline for Rockfall Protection Structures (2013)
- Forsyth, P., Barrell, D., Jongens, R.: Geology of the Christchurch Area. GNS 1:250,000 Map 16 (2008)
- Kaiser, A., Holden, C., Beavan, J., Beetham, D., Benites, R., Celentano, A., Collett, D., et al.: The Mw 6.2 Christchurch earthquake of February 2011: preliminary report. *N. Z. J. Geol. Geophys.* **55**(1), 67–90 (2012)
- Massey, C.I., McSaveney, M.J., Heron, D., Lukovic, B.: Canterbury earthquakes 2010/11 Port Hills slope stability: pilot study for assessing life-safety risk from rockfalls (boulder rolls). GNS Report 2011/311 (2012a)
- Massey, C.I., McSaveney, M.J., Lukovic, B., Heron, D., Ries, W., Moore, A., Carey, J.: Canterbury earthquakes 2010/11 Port Hills slope stability: life-safety risk from rockfalls (boulder rolls) in the Port Hills. GNS Report 2012/123 (2012b)
- Massey, C.I., Gerstenberger, M., McVerry, G., Litchfield, N.: Canterbury earthquakes 2010/11 Port Hills slope stability. Additional assessment of the life-safety risk from rockfalls (boulder rolls). GNS Report 2012/214 (2012c)

- Massey, C.I., McSaveney, M.J., Taig, T., Richards, L., Litchfield, N.J., Rhoades, D.A., McVerry, G.H., Lukovic, B., Heron, D.W., Ries, W., Van Dissen, R.J.: Determining Rockfall Risk in Christchurch Using Rockfalls Triggered by the 2010-2011 Canterbury Earthquake Sequence. *Earthq. Spectra* **30**(1), 155–181 (2014)
- Taig, T., Massey, C., Webb, T.: Canterbury earthquakes Port Hills slope stability: principles and criteria for the assessment of risk from slope instability in the Port Hills, Christchurch. GNS Report 2011/319 (2012)
- Townsend, D.B., Rosser, B.: Canterbury earthquakes 2010/2011 Port Hills slope stability: geomorphology mapping for rockfall risk assessment. GNS Report 2012/15 (2012)

Hazard Risk of Debris/Mud Flow Events in Georgia and Methodological Approaches for Management

Emil Tsereteli, George Gaprindashvili, Merab Gaprindashvili, Nana Bolashvili, and Merab Gongadze

Abstract

Georgia as a typical mountainous region is historically prone to debris/mud flows and flash floods. Thirty percent of the country's territory, more than 70% of settlements, including 15 cities together with the capital (Tbilisi), motorways and railways, international oil and gas pipelines, amelioration and other facilities appear in the hazard area. These disaster events have caused several hundred human deaths. The debris/mud flows formed in the Caucasus highlands are characterized by their heterogeneous nature and devastating characteristics. However, the National Geological Service that at the same time was coincided with a sharp deviation of the debris/mud flow triggering, climatic and meteorological factors, including its negative results, started purposeful studies of these complicated disastrous events in second half of the 20th century. Between 1995–2016 debris/mud flow caused loss of 94 human lives and the direct economic losses reached approx. 350 mln. USD. During this time period up to 3000 debris/mud flow susceptible channels were recorded, catalogued and were assessed according to the morphological and climatic zones and to the engineering-geological formations existing in their space, whereas inside them the following were ranked: geomorphological and genetic characteristics of geological sources which form debris/mud flow events according to the origination of the debris/mud flows' solid components, to the lithology and geodynamic processes which ensure their starting dynamic; According to the springs

nourished by debris/mud flows' water (rainfalls, intense melting of the snow, glaciers and their burned tongues, nourishing by glacier lakes, breakup of the temporally blocked river beds by the glaciers, snow avalanches, landslides and rock avalanches). Two types of specialized 1:500,000 scale maps were composed based on analyses of all these factors: engineering geological conditions for debris/mud flow formation; debris/mud flow hazard zoning map composed per scale of damage, return period, intensity, and risk by municipalities.

Keywords

Georgia • Debrisflow • Methodology • Hazard

1 Introduction

According to the United Nations experts who study natural disasters, economic losses inflicted on planet's population from disasters and more than half of human victims come to debris/mudflows, landslides and floods.

Throughout of human history humankind has been struggled against to such ferocious disaster of nature. Nevertheless, on the overall background of the nowadays scientific and technology development, the risk of this ferocious disaster is not reducing, scientific and technological solutions are still needed to be improved. The clear confirmation of the above mentioned is the Sendai Framework for Disaster Risk Reduction 2015–2030 adopted at the Third UN World Conference held in 2015 (Sendai Framework 2015). Herewith, it is noteworthy that if floods caused by climatic-meteorological factors are entirely associated only with the anomalistic rainwater, the debris/mudflow transformation belongs to the multifactorial geological group's events, the absolute majority of which are transformed into the flashflood mode.

E. Tsereteli · G. Gaprindashvili (✉) · M. Gaprindashvili
Department of Geology, LEPL National Environmental Agency,
Tbilisi, Georgia
e-mail: gaprindashvili.george@gmail.com

E. Tsereteli
e-mail: emiltsereteli@gmail.com

E. Tsereteli · G. Gaprindashvili · N. Bolashvili · M. Gongadze
Vakhushti Bagrationi Institute of Geography, Ivane Javakhishvili
Tbilisi State University, Tbilisi, Georgia

2 Study Area

The Caucasus region, especially Georgia belongs to one of the most vulnerable areas among the mountainous countries due to number of debris/mudflow susceptible drains, heterogeneity of the formation factors, development scales, recurrence of these processes and catastrophic results. Here is revealed all genetic type and kind of debris/mudflow known in geodynamics. Up to 30% of the countries territory, starting from foothill to the highland-alpine-nival zone is located debris/mudflow transformation area (Gaprindashvili et al. 2015). Accordingly, due to the relevant landscape-geomorphological zonality and multi-palette geological structure, composition, physical condition, and characteristics, are transformed flows with sharply different structural-rheological composition, volume, recurrence, and energy. For today, from 5000 debris/mudflow Formation Rivers registered in Caucasus, up to 3000 rivers, which have direct impact on population and infrastructural facilities, are cadastralized in Georgia. However, from 32,258 different rivers (75,500 km of total length and 55 km³ of average annual runoff), 99% are small ones, the length of which is less than 25 km, potentially almost all are prone to debris/mudflow. Also, it should be considered that up to 60% of the population live in small river basins (Gigineishvili 2000; Khmaladze 2009; Bondirev et al. 2007).

It is noteworthy, that in Georgia, studies of disastrous geological processes were conducted episodically until the first half of the 20th century. That is why only 208 debris/mudflow formation rivers had been identified by the 1960 year. Later the database was gradually completed based on studies systematically conducted by LTD “Saq-geologia”, nowadays there are up to 3000 debris/mudflow formation Rivers, which occupy up to 30% of the country’s territory.

Nowadays, 30% of the country’s territory appears at the debris/mudflow hazard risk area, particularly mountainous settlements, including 15 cities together with the capital—Tbilisi (Gaprindashvili et al. 2016). For today, formation Rivers registered 533 debris/mudflow in the area of wired-engineering objects of international importance (Gobechia et al. 2008).

Even under the background conditions of debris/mudflow creation, economic losses vary within 10–20 million dollars, whereas in case of their activation in the extremely sensitive geological environment, exceeds 100 million dollars. For example, in 1977 the debris/mudflow occurred in one river basin located on the territory of Telavi had damaged the city infrastructure and the economic losses amounted 30 million Dollars, whereas on 10–11 August of the same year, heavy rainfall (up to 80 mm) in the upstream of the river Tskhenistskali basin caused extreme debris/mudflow, direct damage amounted 100 million Dollars. In 1982–84 and

1991–92 in the Black Sea coast of Adjara the economic losses inflicted by debris/mudflows amounted 300 million dollars (Gobechia et al. 2008).

In Georgia, in the past and even today significant damage caused by debris/mudflow is often accompanied by human loses. The proof of abovementioned are the catastrophic results caused by multi-scale debris/mudflows occurred in river Tergi basin (segment of Central Caucasus), and up to 210 human death recorded in the upstream of the River Tskhenistskali and river Rioni basins (same segment) since the 1921 year. Over the last 100 years, about 200 people have died in the river Duruji basin (The southern slope of the eastern Caucasus) which is characterized with extremely high activation of debris/mudflow events. The basin represents risk to the population of Kvareli city. In the 1946 year, devastating debris/mudflow event was occurred in river Zhoekvara basin (southern part of the western Caucasus), inundated important coastal part of Gagra, and killed 15 people. The population of Tbilisi and infrastructural facilities were affected dramatically by debris/mudflows occurred from surrounded low mountain rivers and ravines. According to incomplete data, debris/mudflows occurred during last hundred years have killed about 130 people. In Tbilisi, such tragic results were recorded in 1885, 1902, 1922, 1940, 1955, 1972, 1980, 2011 and 2015 years. In 2011–2015 years due to debris/mudflows activated in the city were killed 32 people.

Geo-monitoring studies proved that since last decades of XX century increased activation of debris/mudflow processes is obvious. In extremely sensitive geological environment, this is conditioned by

1. Increased number of debris/mudflow triggering meteorological events on the overall background of climate change;
2. Intensification of earthquakes and significant increase in sloping gravitational processes;
3. Wrongful acts of population, such as cutting forests in the mountainous zone and overgrazing of alpine and subalpine zone meadows; Increase number of erosion-gravitational process by geometrical progression. The clear confirmation of this are statistical characteristics of debris/mudflows recorded during geo-monitoring studies conducted on the territory of Georgia in 1995–2016 years (Table 1).

3 Methodology

Debris/mudflows occurred in Caucasus attracted European researchers’ interest still in the 19th century, mainly they were conducted episodically observations on the occasional

Table 1 Recorded debrisflow/mudflow hazards in Georgia (1995–2016)

Year	Debrisflow event	Economic loss (approximately) mln. USD	Human loss	Year	Debrisflow event	Economic loss (approximately) mln. USD	Human loss
1995	250	41.74	12	2006	63	3.91	–
1996	165	11.74	5	2007	104	5.00	1
1997	335	19.13	7	2008	126	6.52	8
1998	173	8.70	6	2009	193	7.17	3
1999	27	1.96	–	2010	81	2.17	2
2000	23	1.30	–	2011	37	3.91	8
2001	26	11.30	–	2012	88	21.74	5
2002	23	10.00	2	2013	93	Unkn.	–
2003	28	1.74	–	2014	141	65.22	10
2004	258	12.17	2	2015	167	108.70	19
2005	155	3.91	4	2016	208	Unkn.	–

blockade of the only connecting road to Europe in the high mountainous alpine-nival zone of the central Caucasus, by debris/mudflows, as it is evidenced in the bibliography (Gaprindashvili and Gaprindashvili 2014; Vlasov 1969). Despite the enormous negative impact on population and economy of the country, caused by debris/mudflows, in studies of these complicated phenomena were mainly involved hydrologists, almost until the second half of the 20th century.

Heterogeneity of multi-type debris/mudflow events on the territory of Georgia is due to multifactorial natural conditions, including them are the following:

- (1) Geologically construction rocks of the debris/mudflow origination sites and their stimulating solid products with densely different sensitivity to the denudation-erosion processes and their receptor features; As it is known, regarding the classification, in the first two order rivers, debris materials are not formed in the high susceptible denudation-erosive areas, because of small areas. In case of Georgia, in this regard the exception is so called foothills and low and medium mountain zones, where territory are built by molasses materials, which are sensitive to the erosion—denudation processes and occupies a total area of 6.5% of the country.
- (2) In morphological feature, which is expressed in their morphology-morphometric and mechanism of formation of debris/mudflow formation geological product in energetic potential of the slope processes. In sloping gravitational processes it's considered all type of geological processes (rock avalanche, rockfall, landslide), which are directly participating to provide geological product for debrisflow source areas.
- (3) Also, necessary determination factor for debris/mudflow formation is existence of sufficient water in

debrisflow formation origination sites; on the one hand, existence of slope-gravitational and river originated coarse-crashed and clay-sandy material transformative, and on the other hand, high sensitive to erosion-denudation processes, existed in the geological tract. Continental-molasses, glacial and high terraces constructive sediments, which, without preliminary preparation, stipulates the quality of fall and wash down intensity by erosion gravitational processes, also, increase of their “moisture effect” to the displacement critical level and creation-activation of the landslide events.

Prof. Flaishman figurative expression says (Fleishman 1978) “No water no debris/mudflow”, but in morphological and landscape-climatic conditions of different regions, water as a source of debris/mudflow formation is presented with different features.

Based on statistical information analyses and monitoring studies it is identified that among debris/mudflows occurred, the dominant (65–80%) are debris/mudflows which are provoked by prolonged and heavy rains, whereas, debris/mudflows caused by spring extensive snow melting—10% and by landslide processes about 10–30%.

Unfortunately, despite of the fact that debris/mudflows triggered by heavy rain are dominant in Caucasus there were no appropriate analysis until the 70s of the previous century, to determine what amount of precipitation is required to bring geological product, characterized by debris/mudflow formative convergetive features, into cinematic condition and transform this process into extreme dynamic mode.

By processing historical-statistical information, complying regional geo-monitoring studies conducted over the years and analyzing and generalizing these two types of information, in relation with qualitative nature of the geological product, existed in debris/mudflow origination sites,

to define debris/mudflow triggering daily precipitation values for the debris/mudflow creation period (IV–XI months) by using correlative connection of standard method and considering in which morphological-climatic zones are presented.

4 Results and Discussion

In Georgia, It has been identified that the lower bound of the debris/mudflows triggered by heavy rains (30–50 mm in 24 h), starts in origination sites with high geological “sensitivity”, whereas, if the geologic conditions are not creating a favorable environment, flashfloods with ordinary nature are occurred. The debris/mudflows formed in such diapason are mostly characteristic for foothills and lowland territories, which are constructed with tertiary molasses extremely sensitive to erosive-denudational processes and intensely depleted flysch sediments. Their recurrence coefficient (K) averagely varies between 1.90 and 2.64 per year and causes significant damage to the population of the capital and its infrastructure.

In case of daily 50–80 mm rainfall, extreme debris/mudflows are formed in the geologically “sensitive” mountainous river basins, whereas in case of daily 80–100 mm and more rainfall, the catastrophic debris/mudflows are occurred in all debrisflow formation river basins.

According to the incomplete data, during last two century over 800 extreme debris/mudflow had been described with catastrophic results and significant number of victims. It should also be taken into consideration that if until the 70s of the XX century, disastrous debris/mudflow forming rainfalls (80–100 mm) were recorded for Greater Caucasus mountain range, once in 20 years and for Lesser Caucasus once in 40 years, In recent times, significantly increased frequency of rainfalls is noticeable. For example, in the eastern part of the Caucasus, the maximum of these types of rainfalls were recorded three times in 1983 year (87.9; 90.1 and 131.0 mm), once in 1986 and 1988 (156.3 and 156.0 mm). They all had caused catastrophic debris/mudflows on the territory of Great Caucasus.

If we rely on the debris/mudflow forming climate change trend, which was developed by the Caucasus Environmental NGO Network (CENN) for 2020–2050 years, an increased 24-h rainfall is noticed in parameters processed by us.

Analysis of the time and space distribution of the debris/mudflow forming rainfalls conducted on the territory of Georgia demonstrated the fact that their quantitative indicator and frequency in different climatic-morphological zones often do not match each other, moreover, often the Pluviometer size gradients are different not only for various

regions but for the different slopes of the same range. All this must be conditioned by the local orographic conditions of relief. However, there are several cases when the debris/mudflow forming intensive rainfalls simultaneously covered large spaces sharply different from each other with climatic orographic and exposure features. For example, intense heavy rains (3–6 mm/min), provoked disastrous debris/mudflows in the large areas of the Caucasus Range’s both sides in August 24, 1944 and August 17, 1917, which was followed by devastating results (Bondirev et al. 2007).

As noted above, in the complex mechanism of debris/mudflows, the first place takes geological-morphological factor, as the determinant: the types of exo-geodynamic processes providing the geological product of debris/mudflow forming origination sites; their genesis and fractional composition; Structural geological nature, volumes and recurrence criteria of debris/mudflows.

Among debris/mudflow forming exo-dynamic processes the dominants are: physical depletion and gravitational phenomena (bulkstone, rock avalanches), wash out of water accumulative and slope decks, erosion of masses constructed with high “sensitive” molasses sediments, gulling, landslide processes, snow avalanches, cryogenic phenomena.

While discussing, we consider three aspects of Debris/mudflow forming landslide events:

- As a forming factor of the debris/mudflows’ geological product;
- As substantive process for debris/mudflows creation;
- As generator of debris/mudflows which are caused by burst of the landslide blockages.

Thus, the spatial development of exo-dynamic processes in the formation of debris/mudflow forming geological product is mostly obeyed by geological-stratigraphic structure of the territory and morpho-climatic vertical zonality, which changes naturally started from the lowland foothills to the high mountainous Alpine-Nival zone. However, often in relation to the debris/mudflow creation process, genesis of rocks, lithological composition and features have primary importance in formation of debris/mudflow forming geological product and their dependence on climate environment is due to differences between debris/mudflows occurred on the territory of Georgia, such as composition, structural-rheological features, transformed flows and recurrence. Below are the evaluation of some main distinctive features.

Therefore, it is necessary to have the rankings (grouping) in respect of their sustainability criteria for the type of geological formations and rocks placed in the corresponding morphological-climatic zones It was developed criteria for the sustainability of rocks (“geological massifs”) in the

following indicators: Very high sustainable, High sustainable, Medium sustainability; Low sustainability; Very low sustainable.

Below is a classification of the criteria for ensuring the geological product of the mudflow forming nets and the model offers a high level of molar formation in the low and medium morphological zone space mosaic formation in relation to the quality of mudflows. In total, the territory of Georgia is divided into 13 units (Table 2).

Due to complicated natural conditions of Georgia, lack of useful land fund and density of the population, not only large-scale debris/mudflows represents risk to the county, but also their medium and small formations. In this regard, special attention should be paid to the Alazani–Iori watershed anticline ridge constructed with low and medium mountainous Pliocene sediments of eastern Georgia.

Debris/mudflows formed in this geomorphological zone varies from several thousand cubic meters (so-called “Khrami Jetsam”)—to 150–300 thousand cubic meters, in rare cases, it exceeds one million. A good example of this is 2005 year, when rainfall (150 mm) caused formation of debris/mudflows almost in every tributary of the Aragvi Basin, particularly the volume of flow passed in the river Dushetistskali amounted 1.5 million and silted up the important part of the Dusheti city, first floors of the more than two dozen houses, killed one person and damaged infrastructure. At the same period, river Fotikhevi (tributary of the river Aragvi) brought out mudstone masses (300 thousand cubic meters). Debris/mudflow stream height amounted 2.0–2.5 m, as a result, significant territory of the village and motorway of the central Trans Caucasus mountainous range were flooded (Tsereteli et al. 2014, 2015).

Despite of the fact that in most cases vary between 10,000 and 100,000 cubic meters, because they cause enormous damage to the territory and population, most of them are settled on the cones of detritus (among them are cities like Telavi, Sagarejo, Gurjaani) created by debris/mudflows. This zone is ranked as a high-risk category (Ks-0.8-1.0).

Generally, the hilly-knolly and lowland zones of the foothills, constructed by myo-pliocene molasses represent youngest structures formed in the post-inverted phase and

are distinguished with particular “sensitivity” to debris/mudflow processes. During rainstorms, as soon as recorded rainfall reaches 40–50 mm, a positive range of erosion-gravitational processes are created in almost all debris/mudflow formation geological massif and repeated several times during the warm period of the year. For example, according to the Dusheti meteorological station data debris/mudflow transformation at the background level were recorded 4 times in 1924, 1981, 1982 years, 5 times in 1956, 1961, 1975, 1988 years, and 6 times in 1989 year. In total, 125 debris/mudflow passages were recorded (1936–2016 years) in drainage system which passes through molasses strata (forming precipitation range 40–50 mm, average recurrence coefficient per year—2.6); debris/mudflows with medium capacity formed in case of 50–80 m daily precipitation K-1-87, whereas, in case of extreme debris/mudflows (80–100 mm and more)—K-0.26.

Due to extremely complicated geological environment, the capital—Tbilisi occupies special place in terms of debris/mudflow events recurrence frequency and hazard risk, among the lowland area of Georgia. The morphology of the capital is represented in the form of two great folded mountainous systems (Greater and Lesser Caucasus) and the cavity located among the plate of Georgia. It is surrounded by latitude oriented low ranges, constructed with upper Eocene Flysch sediments, extremely “sensitive” to geological processes and Neogene clay-sandstone (Maikop) suites. This is conditioned by sharp asymmetry of erosive gorges, complicated tectonic faults’ thrusts in the monoclinic structures of layers built with produced micro-irrigate folds, and deep hypogenesis process, where, in conditions of soft relief the depleted crust capacity amounts 15–20 m, whereas in the tectonic disturbance zone increases up to 30 m.

Annual average quantity of depletion product in non-softening marl shale located on gravitational slopes, is 0.33–0.39 kg/m², for softening rocks—1.6 kg/m² and 4–5 and 8–11 kg/m² for clay marls. Thus, geological-morphological conditions and climatic-meteorological environment of Tbilisi create all conditions for intense activation of debris/mudflows. There are 50 dry ravines and 12 rivers on the territory of the city, where in case of appropriate debris/mudflow formative heavy

Table 2 Classification of criteria ensuring the geological product of debris/mudflow forming source

1	2	3	4	5	6	7	8		
Morphological-climatic zone	Typography of geological formations and rocks to sustainability of denudation-gravitational and erosive processes	Geological formations and lithological composition of rocks	Criteria for qualitative and quantitative characteristics of rock resistance in geological formations					Average annual index of weathers mass of gravitational downgrade	Dominant exogenic processes in the mudflow formation sources
			Rock solidity Mpa			Softening coefficient			
			In natural conditions	In a watery environment					

Fig. 1 Debrisflow disaster in Dariali (Kazbegi, Georgia)



rains, occur low solidity water flows in the beginning of the drainages with impact from erosive-gravitational processes in the depletion zone. In most cases, low solidity water flows are formed, which are often transformed into flash floods enriched with solid debris. However, there are occasions when landslides also take part in debris/mudflow forming geological product. In such cases, the structural-geological nature of debris/mudflows changes significantly and is transformed into high-solidity stone-muddy or semi-muddy dynamic mode. At the same time, the volume of debris/mudflow streams increases sharply. The classical example of this is debris/mudflows formed on the

northern slope of the Lesser Caucasus (Trialeti anticline), which are created in syncretic synergism of landslide-erosion processes triggering multifactorial agents. In the monoclinic structure of the north side is formed the river Vere basin (with asymmetric morphology), the area of which amounts 196 km², and the depth of the erosion cut in arête zone is 350–400 m (Figs. 1 and 2).

Recently, there is a significant shift in geological disorder in scientific literature, including the threats and hazards of mudflow/debrisflow. Nevertheless there are still significant differences in procedural methodology for the development

Fig. 2 Debrisflow disaster in riv. Vere Basin (Tbilisi)



of regional maps. We believe that this is caused by a different interpretation of the causal linkage of the information derived from the results of the impact of the effects of their enhanced geological phenomena.

We consider that in assessing the risks of the geological disaster and especially mudflows, general strategy should determine risk criteria for assessing and analyzing the obtained information as statistical and statical data.

Assessment of the threats of mudflows, determination of hazardous risks and special mapping related to it is especially difficult for the conditions of the Georgian territory because we are dealing with the extremely complicated relief, lithology, climate et al.

5 Conclusion

Several tens of years of regional character and modal research were needed to obtain relevant information on all of the above-mentioned issues, which were analyzed and disseminated through specialized maps of the country for specialized areas of 1:500,000 scale.

1. Map of Engineering-Geological Conditions of Evaluation of Basic Factors of Debrisflow/Mudflow Development Processes in Georgia 1:500,000 scale.

First of all, the largest area is zoned according to geological formations, where 14 units are separated.

The geomorphological-hypsometric zoning and the geomorphological types of relief prevail in the second large unit are developed on the relevant stratigraphic-lithological substrate. The geomorphological zone is defined as: mountain-hilly zone; Lowland, Low-medium; Medium-highland; High mountain-alpine; High mountain-nival.

For the corresponding morphological zones it is identified by the leading exogenic processes, which are determined by the geological product of Debrisflow forming sources; Lithological composition of geological product; Types of providing water mudflows are established; The dominant genetic types of mudflow; Granulometry of sediments; Volumes of single mudflows (m^3) (maximal, minimum and average) have been established; Return periods and intervals of mudflow events have been established; Geographical location of all estimated objects.

2. Debris/mudflow hazard zoning map composed per scale of damage, return period, intensity, and risk by municipalities.

Based on the generalization and analyzes of the results obtained from the above-mentioned map and the

geomonitoring research of the perennial regional nature and the analyzes of historic-statistical materials, a map of mudflows was developed, where the following indicators are used:

- Proportion of sum of mudflow rivers to the rivers included in this basin and where mudflow processes never was recorded ($k_{sz} n_1/n_2$);
- Proportion of debrisflow sources area to the river basin total area ($k_s z f_{m_1}/F_2$);
- Transformation frequency of debrisflow events in a time unit (k_s-st);
- Maximum volume of single flows of mudflows transformed in the relevant geological environment ($K_s z m^3$ thousand);
- objects that are in the immediate danger area of mudflows, whose area is placed in all residents ($Kz objecta$).

With the total coefficients of the listed indicators 0–1, the territory of Georgia is zoned by damaged by mudflow processes, intensity, activity, activation and hazard risk for population and agricultural infrastructure.

1. Strong high-risk area, risk-ratio $K_n-0.8-0.9$; 2. High risk area: $K_r-0.6-0.8$; 3. Significant danger of mudflows: $K_r-0.5-0.6$; 4. Moderate Hazard Area: $K_r-0.3-0.5$; 5. Limited hazard area $K_r-0.1-0.3$; 6. Low hazard risk area: $K_r-0.01-0.1$; 7. Very low hazard risk area: $K_r->0.001$; 8. Not dangerous hazard risk area $K_r-0.0$.

Acknowledgements The authors would like to thank Department of Geology of National Environmental Agency of Georgia and Vakhusti Bagrationi Institute of Geography for providing various datasets used in this study.

References

- Bondirev, I., Tavartkiladze, A., Tsereteli, E., Mamedov, R., Uzun, A., Lominadze, G.: Geography of catastrophes and risks in the zone of humid subtropics of the Kazakh-Pontic region. Monography, Tbilisi, 357 pp (2007)
- Fleishman, S.: Debrisflow. HydroMet, Petersburg, 311 pp (1978)
- Gigineishvili, G.: Internal waters, monograph, "Geography of Georgia" (Physical Geography), pp. 116–132. "Metsniereba", Tbilisi, Georgia (2000)
- Gaprindashvili, G., Gaprindashvili, M.: Catastrophic debrisflow in Dariali (Georgia) in the year 2014. *J. Nat. Sci.* **7**, 379–389 (2015). <https://doi.org/10.4236/ns.2015.77041>. <http://www.scirp.org/journal/PaperInformation.aspx?PaperID=58225>
- Gaprindashvili, G., Spanu, V., McCall, M.: Participatory methods in the Georgian Caucasus: understanding vulnerability and response to debrisflow hazards. *Int. J. Geosci.* **6**, 666–674 (2015). <https://doi.org/10.4236/ijg.2015.67054>. http://www.scirp.org/Journal/PaperInformation.aspx?PaperID=58168#.VbtpA1gUf_R
- Gaprindashvili, G., Gaprindashvili, M., Tsereteli, E.: Natural disaster in Tbilisi City (Riv. Vere Basin) in the year 2015. *Int. J. Geosci.* **7**,

- 1074–1087 (2016). <http://www.scirp.org/Journal/PaperInformation.aspx?PaperID=70622>
- Gobechia, G., Tsereteli, E., Gobejishvili, R.: Hazard zonation of freshets and mudflow phenomena in Georgia. In: International Symposium on Floods and Modern Methods of Control Measures, pp. 164–172 (2008)
- Khmaladze, G.: Georgian Water Resources. Tbilisi, 73 pp (2009)
- Sendai Framework for Disaster Risk Reduction 2015–2030: United Nations, 37 pp (2015). http://www.preventionweb.net/files/43291_sendaiframeworkfordrren.pdf
- Tsereteli, E., Gaprindashvili, G., Gongadze, M., Bolashvili, N., Lominadze, G., Gaprindashvili, M.: Mudflow phenomena in eastern Georgia (Kakheti region) and their development trends related to climate change. *Int. J. Sci. Res. (IJSR)*, **3**(2), 193–197 (2014). ISSN No 2277 – 8179
- Tsereteli, E., Bolahsvili, N., Gaprindashvili, G., Kurtsikidze, O., Maisuradze, Z.: Debrisflow process development scales and hazard risk for population and engineering-agricultural objects in riv. riv. Tergi, Aragvi and Asa-Arguni. Georgia National Academy of Sciences, Complex Study commission of Mountains, issue “Khevsureti”, pp. 139–167. Tbilisi (2015)
- Vlasov, A.: Debrisflow events in USSR and measures against them, 215 pp. Moscow State University (1969)



Disaster Risk Reduction and Land Use Planning: Opportunities to Improve Practice

J. Garrido and W. S. A. Saunders

Abstract

The Sendai Framework for Action identified land use planning and legislation as a priority action for disaster risk reduction (DRR). Socioeconomic losses associated with natural hazards are increasing, particularly from inappropriate land use. The mechanisms of hazard mapping and structural/non-structural measures to reduce the exposure and vulnerability of elements at risk are outlined in this paper. Concepts and requirements for natural hazard assessments need to be documented and applied to ensure their success. These measures need to be applied at a local level to ensure a more efficient level of risk reduction. Due to financial constraints, councils do not always undertake appropriate hazard mapping; however, they can partner with institutions such as universities to develop hazard and/or risk maps to reduce the costs. Local level decision making is constrained by political and economic pressures, resulting in some natural hazard prone areas being developed. Tools such as explicit civil or administrative responsibilities for risk reduction should be promoted to avoid arbitrary decisions in those areas. Examples showing how DRR can be improved are presented in this paper.

Keywords

Natural hazards • Disaster risk reduction
Land-use planning • Legislation • Local level

1 Introduction

The international research and academic community is raising awareness about how natural hazards are increasing socioeconomic losses related to inappropriate land use, in both developing and developed countries (Scolobig et al. 2012). Disaster Risk Reduction (DRR) through land use planning was identified as a priority action by Sendai Framework for Action. Despite this, most public administrations involved in natural hazards management (i.e. Ministries of Environment, Housing, Civil Works or Civil Defence), are using reactive actions instead of proactive ones. Civil Defence is the clearest example of this (for example Spain, see Garrido 2014). Civil Defence's main objectives are reduction, readiness, response and recovery; the first two are pre-event actions whereas the latter are post-event actions. However, Civil Defence (or emergency management) efforts are focused mainly on response and recovery, in the short (rehabilitation) or long term (reconstruction) (Fig. 1).

Reduction actions should be in place before a natural hazard occurrence, however they are often implemented after the hazard event has occurred. This is because corrective countermeasures are preferred to preventive ones, despite the fact that corrective measures can take longer to implement. Legislation to reduce risk needs to be in place before a hazard event occurs, however, at present it is amended after a natural disaster has happened. DRR is difficult to improve using post-disaster measures.

Land use planning legislation provides the best opportunity to manage natural hazards, along with consistent legislation for other risk reduction methods (e.g. building codes). Legal frameworks for natural hazards are usually related to environmental legislation such as in New Zealand (i.e. Resource Management Act) or Spain (e.g. Environmental Assessment Act), but references to them are found scattered in sectoral laws such as Coastal Act (Spain) or Building Act (New Zealand), and in regulations such as Technical Building Code or Seismic Building Code.

J. Garrido (✉)
Dpto. Ingeniería Civil, Universidad de Granada, Campus de
Fuentenueva s/n, 18071 Granada, Spain
e-mail: jega@ugr.es

W. S. A. Saunders
GNS Science, PO Box 30368 Lower Hutt, 5040, New Zealand

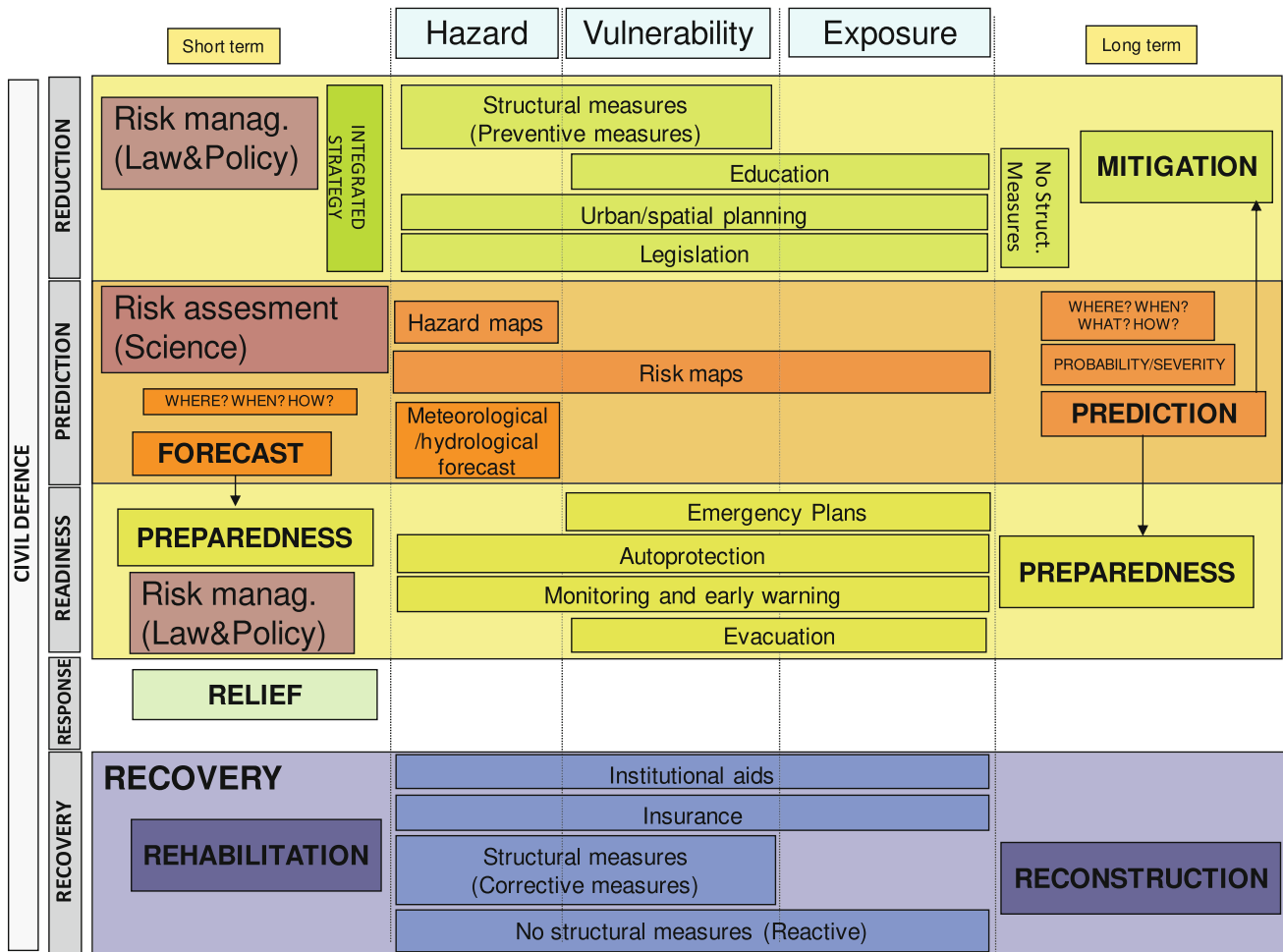


Fig. 1 Relationships between risk factors, risk assessment and risk management (modified from Garrido 2014)

Relationships between different laws, involving different administrations, become a huge challenge in DRR (e.g. Saunders et al. 2007).

Urban planning is the perfect tool for risk reduction, because of the scale required and its ability to assess the exposure of elements at risk. Planning cannot be understood or implemented without legislation, so policies and rules included in District Plans become crucial. If there is mandatory legislation, then liability can be assigned, and the precautionary approach may apply.

2 Risk and Land Use Planning

Risk can be defined as the likelihood and consequence of a hazard. ‘Consequences’ refers to an impact on the natural, economic, built or social environments as a result of a hazard event occurring. The consequences are influenced by the vulnerability of elements at risk, by the exposure of elements at risk to the hazard, and by the characteristics of the hazard.

Risk also considers the likelihood of the hazard occurring, which depends on the type of hazard (Auckland Council 2014). Figure 2 shows the components of risk which are outlined in the following discussion.

Risk management and risk assessment belong to two complementary but opposite worlds, law (which must be certain) and policy versus science (which is inherently

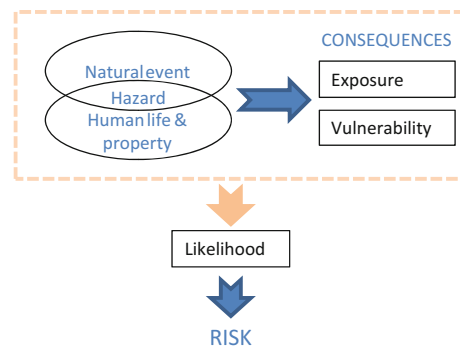


Fig. 2 Components of risk (Auckland Council 2014, p. 5)

uncertain). DRR needs to balance these often competing worlds, and legislation provides the method to establish risk assessment procedures and policies to prioritise proactive measures.

Mapping allows for the identification and location of hazard-prone areas, where built-up areas at risk can be identified, and options for reducing their risk can be addressed. Mitigating risk in already developed urban land by using structural measures is often considered the preferred approach, but changing land use, limiting further development or activities, and/or undertaking managed retreat are more effective tools to reduce risk. All of these options can be identified within District Plans.

While structural measures are usually used to reduce hazard or vulnerability, education is a preferred tool to reduce vulnerability or exposure, while land use planning and legislation can prevent exposure and reduce vulnerability and hazard (Fig. 1). The most economic and efficient tool to reduce risk in developing areas is land use planning through legislation and urban/spatial planning tools. Exposure of planned elements at risk can be assessed, if the hazard has been previously identified and mapped. Examples of elements at risk are provided in Table 1.

While meteorological and hydrological forecasts (i.e. short term), are useful for early warnings and/or evacuation, prediction (i.e. long term) allows risk reduction through prevention and mitigation (Fig. 1). A combination of preventive structural and non-structural measures increases the success rate in DRR. Coordinating risk assessments through hazard and risk maps and risk management practices would improve if legislation established compulsory natural hazards mapping for zoning.

Susceptibility maps (which show where a hazard may occur) and hazard maps (which include the likelihood of an event occurring) are necessary for establishing land use in developing areas. In already developed areas, elements at risk cannot reduce their exposure to the hazard, but vulnerability (through retrofitting measures), and hazard (through countermeasures) can be addressed. Risk maps will allow planning for structural measures and will be useful for civil protection emergency plans. A risk-based approach has been proposed for new developments in New Zealand (Saunders et al. 2013) and Canada (Struik et al. 2015). Cost of risk

maps vs cost of hazard maps is the main constraint for developing risk maps.

However, use of maps already delineated will reduce the mapping cost. Investments in funding natural hazard research to Universities and research centres worldwide are continuing. In the case of New Zealand, the Natural Hazards Research Platform (consisting of GNS Science, NIWA, Auckland, Canterbury and Massey Universities, and Opus plus representatives for a range of central agencies and local government) has invested NZ\$8,710,000 out of a total research budget of NZ\$21,560M for geological hazard models. GNS Science has received NZ\$4,437 million directly for their core services, NZ\$1,142 million came from negotiated contracts (GNS Science, Massey and Lincoln Universities) and around NZ\$3,100 million of investment falls into projects run by GNS, NIWA and Geomarine Ltd through a contestable funding process (Local Government New Zealand 2014). However, to maintain academic impact and credentials, the main project outputs are often conference presentations and papers, and papers published in scientific journals. Unless Council staff have easy access to journals, and have the knowledge and skills to interpret academic papers, they are not in a position to easily use the valuable and accurate peer reviewed information. A legislated portal where funded outputs can be uploaded by the researchers (with acknowledgement of IP) will give better access to the findings and allow for more efficient usability by Council staff. Use of GIS formats will help to update the District Plans natural hazard maps. If legislation states that natural hazards maps/assessments must be updated at specified intervals, and in high/medium risk areas a plan change is mandatory, then planning can take into account the changing state of knowledge.

Civil Defence readiness requires a range of tools such as response plans, early warnings and evacuation planning. The use of risk maps is necessary to design reliable emergency plans and evacuation routes. Maps are useful for Civil Defence as a preparedness tool as well as a proactive action. Whilst improving in New Zealand, there are still opportunities to improve the coordination between District Councils and Civil Defence in Spain. One of these opportunities would be promoting reduction actions such as sharing mapping costs, which would be beneficial to both agencies.

Table 1 Examples of elements at risk from different environments (Auckland Council 2014, p. 16)

Environment	Elements at risk
Built	Commercial, residential and industrial buildings; infrastructures; urban fabric; and community facilities (schools, hospitals, churches, etc.)
Social	Casualties (injuries or deaths of people), community assets and networks, relationships and support systems
Economy	Businesses, jobs, trade and services

3 Legislation

Enforcing legislation is a huge challenge for some States and Regional Councils, particularly those in Spain, Italy and Central America (Garrido 2014). Councils sometimes use legal loopholes to interpret the law and make arbitrary decisions. Legislation must be written as clear and complete as possible and include mechanisms that encourage compliance.

Flooding and seismic hazard legislation in the European Union has recently been updated. For example, the Directive 2007/60/EC on the assessment and management of flood risks requires Member States to undertake hazard and risk mapping which will be used in land use planning. Some considerations for reducing risk in seismic hazard exposed countries have been included in Building Acts through Technical Building Codes or Seismic Building Codes. Seismic hazard maps, invoked by Seismic Building Codes, are usually updated after a destructive earthquake (e.g. Spain after the 2011 Lorca harmful earthquake).

In contrast, legislation about volcanic hazard and landslides is not well developed. Landslides are not often perceived as a ‘big’ hazard because, despite their frequency (comparatively), there are often not large-scale casualties associated with them (e.g. compared to earthquakes). Usually Building Acts, through Technical Building Codes, consider that landslides should be considered in the Geotechnical assessment, but no more specific references are found in the legislation.

On the one hand, undefined legal concepts should be avoided in the legislation in order to reduce Council’s interpretation and discretionary powers. Moreover, terms such as ‘significant risk’ or ‘appropriate scale’ should have clear frameworks to determine what ‘significant’ and ‘appropriate’ is. While the Spanish Land Act establishes that risk-prone areas (probably alluding to hazard), should be classified as ‘greenfields’, no risk levels are established, so zoning in every Council will be different. In Europe, the aforementioned Directive 2007/60/EC establishes different scenarios for flood hazard mapping: low probability, medium probability (likely return period ≥ 100 years) and high probability. While low and high probability are not defined, medium is. Therefore, each Member State can establish whatever return periods that it considers appropriate for low and high probability.

Using return periods, safety factors or Annual Exceedance Probabilities (AEP) for every specific natural hazard would help to establish different hazard/risk levels. In Iceland for example, Regulation 505/2000 on hazard zoning due to snow and landslides, classification and utilisation of hazard zones, and preparation of provisional hazard zoning, uses a hazard line to distinguish acceptable local risk and different hazard zones: A (local risk between 0.3×10^{-4} and

1×10^{-4}), B (local risk between 1×10^{-4} and 3×10^{-4}) and C (local risk between greater than 3×10^{-4}). The different hazard zones can be utilized as shown in Table 2.

The unacceptable areas should be zoned as restricted for development or non-development. Force majeure could be claimed above an unacceptable threshold, while below that threshold responsibility could be established.

A glossary of technical terms included in the legislation is also crucial. Spanish Regional Land Acts include floods, landslides, geological hazards or hydrological hazards in the glossary, but it is not clear if subsidence, sinkholes or settlements should be considered landslides, or which kind of natural hazards are considered in geological and hydrological hazards. Planners have to make an informed guess if they refer to earthquake related hazards and droughts, respectively.

Invoking technical guidelines or standards through legislation makes them legally binding. For example, in New Zealand every District plan uses different methodologies for mapping—methodologies are generally not included in the plans, and are difficult to source. Standardization would benefit mapping processes and provide efficiencies for Councils.

Usually Spanish national or regional legislation on natural hazards and land use is quite general (e.g. not hazard specific), but there are some linkages being established between them in new legislation (for example, the transposition of the Directive 2007/60/EC into the Spanish law). Councils are using resource consents with and policies and rules to diminish the risk for subdivisions and developments in natural hazard prone areas. The balance between Council’s economic and political interests and development is complex, so sometimes Councils transfer risk to land users in high hazard areas instead of avoiding new developments (e.g. allowing development with mitigation measures).

One example of assessment requirements is found in Colombian legislation, where the Decree 1077 of 2015, Regulation Unique Decree of Housing, City and territory (Decreto Único Reglamentario del Sector Vivienda, Ciudad y Territorio) establishes the technical conditions for the assessment of basic reports for landslides, floods and flash floods. Landslide hazard assessments include: inputs (topography, geology), scope (conditioning and triggering factors, type of analysis for urban and rural areas), zoning (high hazard, where all active processes will be included, medium and low hazard), and outcomes (zoning maps for different types of landslides, consequences). Methodologies are explained in a technical report that is easily accessible. A detailed hazard report should be carried out in high and medium hazard areas, while a detailed risk report should be performed in high hazards areas. Detailed studies should include a detailed hazard analysis, vulnerability and risk assessment and mitigation measures proposed.

Table 2 Utilization of different snow and landslides hazard zones in Iceland according to Regulation 505/2000

	Hazard zone A	Hazard zone B	Hazard zone C
New residential and comercial buildings	Allowed		
New cottages for overnight stays in skiing areas	Allowed		
New comercial buildings		Allowed	
New cottages not intended for overnight stays in skiing areas		Allowed	
New individuals and multifamily dwellings with up to four apartments		Allowed	
New schools, day-care centres, hospitals, community centres, multifamily dwellings with more than four apartments	Reinforced		
Additions to schools, day-care centres, hospitals, community centres, multifamily dwellings with more than four apartments		Reinforced	
New structure not expected as a residence of place of employment as a regular basis			Allowed
Residential and comercial building modification if total risk does not increase			Allowed
Safety of people in buildings	Monitoring and evacuation		Permanent protective measures or purchasing
No restrictions if permanent protective measures			

One option to enforce legislation is through personal liability. Some politicians are making planning decisions without considering a precautionary approach. Once liability has been set out according to unacceptable thresholds, establishment of responsibilities becomes easier so any resulting punishment will encourage legal compliance. In Japan, Landslide Prevention Act (1958), the Act for the prevention of disasters caused by steep slope failure (1969) and the Act on sediment disaster countermeasures for sediment disaster prone areas (2005, amended on 2011) include penal provisions (of up to one year) and fines (of up to 500,000 yens). In Iceland, Act 49/1997 on Protective Measures Against Avalanches and Landslides establishes that investigations of suspected criminal action related with personal injuries in settled areas could be carried out in accordance with the Criminal Proceedings Act.

4 Conclusions

Legislation and urban planning should be strengthened to increase their consistency and impact in reducing natural hazards risks. Actions are proposed in this paper to improve DRR, such as land use planning legislation invoking technical guidelines (including glossaries, methodologies or mapping), the avoidance of undefined legal concepts to reduce Council's arbitrary decision making, establishing AEP, determining return periods or factors of safety for

zoning and delimitation of liability and derived punishment from disregarding legislation.

Acknowledgements This research was partially supported by the University of Granada, through a Plan Propio grant, and the Research Group RNM-374 (Andalusian Government, Spain).

References

- Auckland Council: Natural Hazard Risk Communication Toolbox: Natural Hazard Risk Management Action Plan, 49 p. Auckland (2014)
- Garrido, J.: Prevención de riesgos naturales y geotécnicos a través de la legislación sectorial y la ordenación territorial y urbanística. La evaluación ambiental estratégica y los riesgos en la planificación urbanística española (in Spanish). PhD thesis. Universidad de Granada (2014)
- Local Government New Zealand: Managing natural hazard risk in New Zealand—towards more resilient communities, p. 62 (2014)
- Saunders, W.S.A., Forsyth, J., Johnston, D.M., Becker, J.: Strengthening linkages between land-use planning and emergency management in New Zealand. *Aust. J. Emerg. Manage.* **22**(1), 36–43 (2007)
- Saunders, W.S.A., Beban, J.G., Kilvington, M.: Risk-based land use planning for natural hazard risk reduction. GNS Science Miscellaneous Series 67. Lower Hutt (2013)
- Scolobig, A., De Marchi, B., Borga, M.: The missing link between flood risk awareness and preparedness: findings from case studies in an Alpine Region. *Nat. Hazards* **63**, 499 (2012)
- Struik, L.C., Pearce, L.D., Dercole, F., Shoubridge, J., van Zijll de Jong, S., Allan, J.D., Hastings, N.L., Clague, J.J.: Risk-based land-use guide: safe use of land based on hazard risk assessment. Geological Survey of Canada, Open File 7772 (2015)

Author Index

A

Anikeev, Aleksandr, [45](#)

B

Bednarczyk, Zbigniew, [105](#)

Bolashvili, Nana, [155](#)

C

Chunguo, Liu, [125](#)

Conway, Brian D., [61](#)

D

Dahal, Ranjan Kumar, [133](#)

da Silva Feitosa, Jaqueline, [27](#)

da Silva Mendes, Marcus Vinícius Araújo, [27](#)

E

Eremina, Olga, [45](#)

F

Fenton, Clark, [3](#), [33](#)

Ferentinou, M., [95](#)

Ferguson, Kenneth C., [69](#), [77](#), [85](#)

Fuangswasdi, Aranya, [51](#)

G

Gaprindashvili, George, [155](#)

Gaprindashvili, Merab, [155](#)

Garrido, J., [163](#)

Gongadze, Merab, [155](#)

Gray, Mark, [33](#)

Guimarães, Sebastião Geraldo, Júnior, [27](#)

H

Hoare, Blake, [3](#)

Hyland, Natalie, [3](#), [33](#)

K

Karymbalis, E., [95](#)

Kolthoff, Steven H., [13](#)

Kozliakova, Irina, [45](#)

L

Lounis, Ghani Cheikh, [115](#)

Lyons, C., [145](#)

M

Marinos, Vasilis, [21](#)

Martins, Pedro, [139](#)

Merchichi, Amira, [115](#)

Mills, Michael F., [13](#)

Mimouni, Omar, [115](#)

Mote, T. I., [145](#)

P

Papathanassiou, George, [21](#)

R

Rucker, Michael, [69](#), [77](#), [85](#)

S

Saunders, W. S. A., [163](#)

Shah, Sachin D., [51](#)

Shanganlall, A., [95](#)

Shlemon, Roy J., [13](#)

Skinner, M. D., [145](#)
Smilovsky, Danielle, [69](#)
Smith, A., [95](#)
Smith, James, [33](#)

T
Tahalaitit, El Hadi, [115](#)
Taleb, Bachir, [115](#)
Taylor, M. L., [145](#)
Tsereteli, Emil, [155](#)

U
Ustinova, Natalia, [45](#)

V
Valadares, Isabella Magalhães, [27](#)

W
Worakijthamrong, Surin, [51](#)

X
Xiaoli, Chen, [125](#)